Durham University

Durham E-Theses

Depositional architecture and petroleum potential of the Cambro-Ordovician Hawaz Formation, Murzuq Basin, SW Libya.

Tarek Jiuma Alkhalas

How to cite:

Alkhalas, Tarek Jiuma (2006) Depositional architecture and petroleum potential of the Cambro-Ordovician Hawaz Formation, Murzuq Basin, SW Libya. Masters thesis, Durham University.

Use policy

The full-text may be used and/or reproduced, and given to third parties in any format or medium, without prior permission or charge, for personal research or study, educational, or not-for-profit purposes provided that:

- a full bibliographic reference is made to the original source
- a https://etheses.durham.ac.uk/id/eprint/2633/ is made to the metadata record in Durham E-Theses
- the full-text is not changed in any way

The full-text must not be sold in any format or medium without the formal permission of the copyright holders.

Please consult the full Durham E-Theses policy for further details.

Academic Support Office, The Palatine Centre, Durham University, Stockton Road, Durham, DH1 3LE
e-mail: e-theses.admin@durham.ac.uk Tel: +44 0191 334 6107
https://etheses.durham.ac.uk

Depositional Architecture and Petroleum Potential of the Cambro-Ordovician Hawaz Formation, Murzuq Basin, SW Libya.

Tarek Jiuma Alkhalas

Department of Geological Sciences
University of Durham

The copyright of this thesis rests with the author or the university to which it was submitted. No quotation from it, or information derived from it may be published without the prior written consent of the author or university, and any information derived from it should be acknowledged.

A dissertation submitted to the University of Durham in completion of the degree of Master

27 JUL 2006

DECLARATION

I declare that the material contained in this project is the end result of my own work. The work described in this dissertation is entirely that of the author, except where reference is made to previous published or unpublished work, and no part of this dissertation has been previously submitted for a degree at this or any other university.

Tarek Jiuma Alkhalas
Department of Geological Sciences,
University of Durham
August, 2005

ABSTRACT

The Murzuq Basin, SW Libya, contains a sedimentary fill up to 4000 m thick, comprising a marine Palaeozoic section and a continental Mesozoic section. The primary reservoir target in the basin is the Upper Ordovician Mamuniyat Formation, but where this is missing the Middle Ordovician Hawaz Formation is the primary target, as in parts of the study area.

The present study is based on slabbed cores, photographs, core samples, wireline log data and conventional core analysis of the Hawaz siliciclastic sediments. The petrology, textural properties, facies analysis, wireline log response and sequence stratigraphy of the Hawaz Formation suggest that the sandstones are mainly quartz arenites with some arkoses, derived from a similar parent rock, and deposited in shallow marine shoreface and shelf environments. Dynamic interaction between shoreface and shelf along a NW-SE oriented shoreline, probably fed by braided streams and braid delta systems, led to a frequent repetition of depositional facies, within a dominant transgressive setting.

Sequence stratigraphic analysis of the Hawaz Formations shows that it comprises two transgressive systems tracts, two highstand systems tracts and a possible low stand erosion surface, beneath transgressive lower shoreface sediments. The position of the maximum flooding surface between the upper transgressive systems tracts and the succeeding highstand systems tract is controversial. Some authors place it in the upper part of the Hawaz Formation; others place it in the Silurian Tannezuft hot shales. In this study it is located at the base of the Silurian Tannezuft hot shales

Sediment composition, regional facies patterns and sequence stratigraphic analysis suggest that the Hawaz sandstones were derived from a tectonically active, granitic basement source terrain, which was most probably the uplifted Chat/Tikiumit Arch, some 150 km southwest of Concession areas NC115 and NC186. The lower part of the cored succession has the best reservoir properties.

ACKNOWLEDGEMENTS

I must firstly thank my supervisor Dr. Brian R. Turner for supervising the project. I am deeply grateful to Brian for spending many hours reading the manuscript and making valuable comments.

I acknowledge the support of Repsol Oil Operation in providing the funds for the project, special thanks must go to the chairman of ROO Mr Ibrahim K. Sherir for his ongoing support, also to Dr Abdussalam Aziz, Exploration Co-ordinator of Repsol Oil Operations who gave me the opportunity to study in Durham and for providing me with all the data needed for this project. Many thanks also to all the staff of Repsol Oil Operations, particularly the Exploration Department for their support and encouragement, I must thank Dr Sadeg Chnia for his advice in data collection. I would like to take this opportunity to thank my friends for their encouragement and support.

In the department at Durham, I would like to thank Dr Stuart Jones, Dr Dugal Jerram for helping with references and occasional questions. Dave Asbery, Carole Blair, Karen Atkinson and Janice Oakes are thanked for their general helpfulness and friendliness and Dave Stevenson, and Gary Wilkinson for their support and help with the computer.

I am deeply grateful to my father (Juma Alkhalas) and to all my brothers and sisters for their continuous support and encouragement. Finally I am particularly indebted to my family, specially my wife and my children for their patience and support during my study at Durham.

Table of content

DECLARATION ii
ABSTRACT iii
ACKNOWLEDGEMENTS iv
Table of content v
List of Figures x
List of Tables xvi
1. Introduction 1
1.1 Aims of the study 1
1.2 Location map 2
1.3 Methodology and available material 3
1.4 Wireline log data 3
1.5 Stratigraphic succession in the Murzuq Basin 3
1.5.1 Precambrian 6
1.5.2 Infracambrian 7
1.5.2.1 Mourizidie Formation: infracamberian (Algonkian) 7
1.5.3 Cambro-Ordovician 7
1.5.3.1 Hasawnah Formation: Upper Cambrian 8
1.5.3.2 Ash Shabiyat Formation: Lower Ordovician (Tremadocian) 9
1.5.3.3 Hawaz Formation: Middle Ordovician (Llandeilian/ Llanvirnian) 11
1.5.3.4 Melaz Shuqran Formation: Upper Ordovician (Caradocian) 12
1.5.3.5 Tashgart Formation: Upper Ordovician (Caradocian/ Ashgillian) 13
1.5.3.6 Mamuniyat Formation: Upper Ordovician (Ashgillian) 13
1.5.4 Silurian 14
1.5.4.1 Tanezzuft Formation: Lower Silurian (Llandoverian) 14
1.5.4.2 Akakus Formation: Upper Silurian (Wenlockian / Pridolian) 15
1.5.5 Devonian 16
1.5.5.1 Tadrat Formation: Early Devonian (Sigenian) 17
1.5.5.2 Ouan Kasa Formation: Early Devonian (Emsian) 17

1.5.5.3 Awaynat Wanin Formation: Middle-Late Devonian (Couvinian / Strunian) 18
1.5.5.4 Tahara Formation: Late Devonian (Famennian / Strunian) 18
1.5.6 Carboniferous 20
1.5.6.1 Marar Formation: Lower Carboniferous (Tournaisian / Visean) 20
1.5.6.2 Assedjefar Formation: Upper Carboniferous (Namurian) 21
1.5.6.3 Dembaba Formation: Upper Carboniferous (Westphalian) 21
1.5.6.4 Tiguentourine Formation: Upper Carboniferous – Early Permian (Stephanian / Rotliegendes) 22
1.5.7 Hercynian Unconformity 23
1.5.8 Triassic 23
1.5.8.1 Zarzaitine Formation (Post-Tassilian) 24
1.5.9 Jurassic 24
1.5.9.1 Taouratine Formation 24
1.5.10 Cretaceous 26
1.5.10.1 Messak Formation 26
1.5.11 Quaternary 26

2. Texture 27
2.1 Introduction 27
2.2 Different methods of measuring grain-size 27
2.2.1 Sieving 27
2.2.2 Petrographic microscope 28
2.3 Discussion of grain-size parameters 28
2.3.1 Mean grain-size (average grain size) 29
3.3.2 Mode 29
3.3.3 Median 30
3.3.2 Standard deviation (sorting) 30
2.3.5 Skewness 32
2.4 Thin section grain-size analysis of sandstone from wells A1-NC186 and H27-NC115 35
2.5 Interpretation of grain-size parameters 35
2.6 Roundness 43

3. Sedimentology 48
3.1 Introduction 48
3.2 Facies Analysis 48
3.3 Facies models 49
3.4 Sedimentary Facies in the Hawaz Formation 49
3.4.1 Facies (A): Burrowed sandstone facies 49
3.4.1.1 Subfacies (A1): Burrowed and bioturbated fine-grained sandstone subfacies 51
3.4.1.2 Subfacies (A2): Burrowed and bioturbated fine to medium-grained sandstone subfacies 52
3.4.2 Facies (B): Ripple cross-laminated sandstone 54
3.4.3 Facies (C): Cross-bedded sandstone facies 56
3.4.4 Facies (D): Low angle cross-bedded and planar-laminated sandstone facies 59
3.4.5 Facies (E): Heterolithic facies 60
3.4.6 Facies (F): Burrowed heterolithic sandstone facies 63
3.4.7 Facies (G): Burrowed mudstone and sandstone facies 64
3.4.8 Facies (H): Massive sandstone facies 65
3.4.9 Facies (I): Ripple cross-laminated siltstone facies 66
3.5 Facies interpretation 68

4. Petrology and Diagenesis 73
4.1 Introduction 73
4.1.1 Objectives 73
4.1.2 Samples and methods 73
4.2 Compositional analysis 74
4.2.1 Quartz 74
4.2.2 Feldspar 81
4.2.3 Rock fragments 83
4.2.4 Mica 83
4.2.5 Clay minerals 84
4.2.6 Heavy minerals 88
4.2.7 Other constituents 89

4.2.8 Sandstone maturity in the Hawaz Formation 90
4.3 Classification 91
4.4 Provenance 92
4.5 Tectonic setting of the Hawaz sandstones 92
4.6 Diagenesis 95
4.6.1 Quartz overgrowth 97
4.6.2 Carbonate cementation 98
4.6.3 Feldspar dissolution and overgrowths 100
4.6.4 Clay mineral authigenesis 101
4.6.4.4 Chlorite 104
4.6.5 Pyrite 104
4.7 Porosity in the Hawaz sandstones 104

5. Sequence Stratigraphy 109
5.1 Introduction 109
5.2 Methodology 111
5.3 Sequence stratigraphic techniques 112
5.4 Sequence stratigraphy procedure 114
5.5 Sequence stratigraphy signatures 115
5.5.1 Tectonism 116
5.5.2 Eustasy 117
5.5.2.1 Continental flooding cycles 118
5.5.2.2 Sequence Cycles 118
5.5.3 Sedimentation 119
5.6 Accommodation space 119
5.7 Sediment supply 120
5.8 Sequence stratigraphy of the Hawaz Formation in the type well A1-NC186 and H27-NC115 121
5.8.1 Introduction 121
5.8.2 Objectives 123
5.9 Sedimentology and sequence stratigraphy analysis of the Hawaz Formation in the type well A1-NC186 and H27-NC115 123
5.10 Sequences and relative sea-level control in the Hawaz Formation 129

6. Wireline logging 132
6.1 Objectives 132
6.2 Log suit used in sequence stratigraphy 132
6.2.1 Gamma-ray logs (GR) 132
6.2.2 Spontaneous potential logs 133
6.2.3 Sonic velocity logs (DT) 135
6.2.4 Formation density logs (RHOB) 135
6.2.5 Neutron porosity logs (NPHI) 135
6.3 Analysis of wireline log trends 137
6.3.1 Geological interpretation of the Hawaz Formation from gamma-ray log 137
6.4 Generalized stratigraphic sequence analysis of the Hawaz Formation from wireline log trends 144
6.4.1 Introduction 144
6.4.2 Sequence stratigraphic interpretation of the Hawaz Formation from wireliine log trends 145
6.5 Electrosequence analysis of the Hawaz Formation 148
6.5.1 Transgressive systems tract 150
6.5.2 Highstand systems tract 150
6.6 Sequence stratigraphy and relative sea-level curves 150
6.6.1 Introduction 150
6.6.2 Relative sea-level curves of the Hawaz Formation 151

7. Depositional Model 152
7.1 Depositional model of the Hawaz Formation in A1-NC186 and H27-NC115 152

8. Conclusions 162

References 164

List of Figures

CHAPTER 1

Fig. 1.1. General location map of Libya showing the study area in SW Libya. 2
Fig. 1.2. NC115 and NC186 concessions including the studied wells. 4
Fig. 1.3. Stratigraphic column in NC115 (Aziz, 2000). 5
Fig. 1.4. Map showing general tectonic framework of Libya and the location of the Murzuq Basin. 6
Fig. 1.5. Precambrian and Palaeozoic Outcrops in Libya (Hallett, 2002). 8
Fig. 1.6. Precambrian and Lower Palaeozoic lithostratigraphic nomenclature (Hallett, 2002). 10
Fig. 1.7. Upper Palaeozoic lithostratigraphic nomenclature (Hallet, 2002). 19
Fig. 1.8. lithostratigraphic Nomenclature for the Triassic, Jurassic and Lower Cretaceous rocks of Libya and adjacent areas (Hallett, 2002). 25

CHAPTER 2

Fig. 2.1. Grain-size cumulative frequency curve for depth 4415ft in well A1-NC186 based in thin section grain-size analysis plotted on lognormal probability paper, showing different percentile Phi values used in the grain-size parameter equations. 33
Fig. 2.2. Grain-size cumulative frequency curves for the Hawas Formation based on thin section grain-size analysis plotted on lognormal probability paper, A1-NC186. 36
Fig. 2.3. Plot of mean versus standard deviation (Friedman, 1967). 41
Fig. 2.4. Plot of third moment (skewness) versus standard deviation (Friedman, 1967). 41
Fig. 2.5. Plot of mean-size versus standard deviation in A1-NC186. 42
Fig. 2.6. Plot of standard deviation versus skewness in A1-NC186. 42
Fig. 2.7. Histogram of roundness of the Hawaz Formation, A1-NC186. 46
Fig. 2.8. Histogram of roundness of the Hawaz Formation, H27-NC115. 46

CHAPTER 3

Fig. 3.1. Slabbed core samples from type well A1-NC186 (A at 4705 ftand B at 4715 ft) showing burrowed and bioturbated fine-grained sandstone subfacies.....51

Fig. 3.2. Slabbed core samples from type well A1-NC186 (A at 4413 ft and B at 4445 ft) and H27-NC115 (C at 4723 ft and D 4759 ft) showing burrowed and bioturbated fine to medium-grained sandstone subfacies.....53

Fig. 3.3. Shoreface model for ichnofacies, based on facies observation in the Cretaceous interior seaway, western interior of North America (Frey et al. 1990).....54

Fig. 3.4. Slabbed core samples from well A1-NC186 at 4630ft, showing ripple cross-lamination.....55

Fig. 3.5. Slabbed core samples from well A1-NC186 (A at 4563 ft, and B at 4566 ft) and H27-NC115 (C at 4858 ft and D at 4965 ft) showing cross-bedded sandstone of facies C.....57

Fig. 3.6. Controls of flow regime by mean flow depth and mean flowvelocity for a constant grain size of bed material, (After Fritz and Moore, 1988).....58

Fig. 3.7. Slabbed core sample from well A1-NC186 (A at 4564 ft), showing low angle cross-bedded sandstone (small arrow) and possible small-scale hummocky cross-stratification (large arrow), andwell H27-NC115 (B at 4740 ft), showing low angle cross-bedded sandstone (large arrow) and the stylolites erosional base (small arrow).....59

Fig. 3.8. Slabbed core sample from well A1-NC186 (A at 4653 ft), showingparallel to wavy cross-lamination (small arrow) and wavy or rippledrift cross-lamination (large arrow) and (B at 4771 ft), showing parallelto wavy cross-lamination sandstone in mudstone (arrow).....61

Fig. 3.9. Slabbed core sample from well A1-NC186 at 4731 ft showingburrowed heterolithic sandstone.....63

Fig. 3.10. Slabbed core samples from well A1-NC186 (A at 4442 ft andB at 4526 ft) showing burrowed mudstone and sandstone facies.....65

Fig. 3.11. Slabbed core sample from well A1-NC186 (A at 4648ft) andH27-NC115 (B at 4903ft), 4647ft showing massive sandstone facies in picture. A faint lamination can be seen in A. 66
Fig. 3.12. Slabbed core sample from well A1-NC186 4763 ft showingcross-laminated siltstone facies. 67
Fig. 3.13. Marine ichnofacies diagram representing the trace fossils, including the Skolithos and Cruziana ichnofacies found inthe Hawas Formation (After Pemberton, 1992). 69
Fig. 3.14. Lithology, sedimentary environments and sea-level change inthe cored section of type well A1-NC186. 70
Fig. 3.15. Lithology, sedimentary environments and sea-level change in the cored section of type well H27-NC115. 71

CHAPTER 4

Fig. 4.1. Composition of the Hawaz Sandstone in A1-NC186. 75
Fig. 4.2. Composition of the Hawaz Sandstone in H27-NC115. 76
Fig. 4.3. Photomicrograph of a quartz aranite in the Hawaz sandstonesat depth 4612ft in A1-NC186, which is dominated by monocrystalline quartz. XPL (X4). 77
Fig. 4.4. SEM picture of quartz grain showing the grain surface. The small pits on the surface are probably due to transport by floating ice to the depositional site. 78
Fig. 4.5. Photomicrograph showing a metamorphic polycrystalline quartz grain (E4-F6), (4569ft) XPL (X20). 79
Fig. 4.6. Photomicrograph showing quartz overgrowths (E7-H7) atdepth 4908ft, PPL (X20). 80
Fig. 4.7. SEM picture showing quartz overgrowth with good crystal faceat 4629ft. ..80
Fig. 4.8. Photomicrograph shows the dissolution of an unstable feldspar grain (A7-H7) in the Hawaz sandstone at depth 4899.5ft, (H27-NC115) PPL (X20). 82
Fig. 4.9. SEM picture shows the dissolution in the feldspars at depth 4629ft. 82
Fig. 4.10. SEM picture shows an elongate mica in the Hawaz sandstone. 84
Fig. 4.11. Photomicrograph showing the mica concentrated in a clay mineral or stylolite layer at depth 4554ft, XPL (X4). 85

Fig. 4.12. SEM picture showing sheets of mica within the Hawaz sandstone at 5198ft. 85

Fig. 4.13. Photomicrograph showing kaolinite replaced grains (E7-F8) and kaolinite fill pore (A1-B2) in the Hawaz sandstone (4629ft), PPL (X20). 86

Fig. 4.14. SEM picture shows irregular wavy plates of kaolinites in A1-NC186. 87

Fig. 4.15. SEM picture showing the smectite within the Hawaz sandstone. 88

Fig. 4.16. Photomicrograph showing tourmaline (C5-D5) and zircon (G8) in the Hawaz sandstone (4584) PPL (X10) 89

Fig. 4.17. Flow diagram for the determination of the textural maturity of a terrigenous clastic sediment or sedimentary rock (Nichols, 1999). 91

Fig. 4.18. Detrital composition of the Hawaz sandstones (A1-NC186 and H27-NC115) plotted on a Pettijohn et al., (1987) classification diagram. 93

Fig. 4.19. Ternary QFRF plot showing the average composition of sandstones and source rocks for A1-NC186 and H27-NC115, which fall within the metamorphic humid climate field, (Suttner et al., 1981). 94

Fig. 4.20. QFL triangle showing the tectonic provenance fields for the Hawaz sandstones in A1-NC186 and H27-NC115 (Dickinson, 1985) 96

Fig. 4.21. Paragenetic sequence of diagenetic events in the Hawaz sandstone, A1-NC186 and H27-NC115. 97

Fig. 4.22. Photomicrograph of quartz overgrowth (F6-H9), in which the quartz grew into the pore on one side which is not filled by clay minerals at the time (H7), at depth 4908 ft (H27-NC115), PPL, (X20). 98

Fig. 4.23. Photomicrograph showing calcite grains within the Hawaz sandstone at depth (4764ft), XPL (X10). 99

Fig. 4.24. SEM picture shows late quartz overgrowth in Hawaz sandstone. 103

Fig. 4.25. Photomicrograph showing the complete dissolution of unstable grain (E5-F6), which enhances the porosity locally in the Hawaz sandstone. PPL (X20) (4584ft A1-NC186). 106

CHAPTER 5

Fig. 5.1. The hierarchy of stratigraphical cycles (After Coe et al., 2002). 110

Fig. 5.2. Diagrammatic sketch of sequences and systems tracts in depth and geologic time in relation to tectonic subsidence, sea level, and relative changes of sea level (After Vail et al., 1991). 114
Fig. 5.3. Sequence stratigraphy interpretation procedure (After Vail et al., 1991). .. 115
Fig. 5.4. Cartoon showing the relationship between relative sea-level, water depth, eustatic sea-level, tectonics (uplift and subsidence), and accumulated sediment (After Coe et al., 2002). 117
Fig. 5.5. Accommodation space through time (After Jervey, 1988) 120
Fig. 5.6. Comparison between sequence stratigraphic interpretation and lithological units (Ghnia and Chang, 2003). 122
Fig. 5.7. Lithological log and sequence stratigraphy systems tract of the Hawaz Formation in type well A1-NC186. 126
Fig. 5.8. Lithological log and sequence stratigraphy systems tract of the Hawaz Formation in type well H27-NC115. 127
Fig. 5.9. A predicted model for the cross section in NC115 and NC186, showing the predicted location of the studied wells 130
Fig. 5.10. Gamma-ray logs correlation between A1, A2-NC186 and H27-NC115, showing the major trend in GR log, which reflect the similarity of the systems tracts over long distance. 131

CHAPTER 6

Fig. 6.1. Wireline logs from type well A1-NC186, with interpreted lithologies showing the most distinctive sand and shale sections. 134
Fig. 6.2. Wireline logs from type well H27-NC115, with interpreted lithology showing the most distinctive sand and shale sections. 136
Fig. 6.3. Idealized log trends, assuming saltwater-filled porosity (After Emery and Myers, 1996). 138
Fig. 6.4. Determination of lithology using information provided by a gamma-ray logging tool (After Rider, 1991). 139
Fig. 6.5. Changes in sandstone grain-size are reflected by changes in the gamma ray value (After Rider, 1996). 140
Fig. 6.6. Gamma-ray log (GR), lithology, trends in systems tract and relative sea-level change in type well A1-NC186 141

Fig. 6.7. Gamma-ray log (GR), lithology, trends in systems tract and relative sea-level change in type well H27-NC115 142
Fig. 6.8. Facies indication from gamma-ray (or SP) log shape. These are idealized examples of both log shape and sedimentary facies (After Rider, 1996). 143
Fig. 6.9. Model log patterns for sequence tracts, with possible sequence stratigraphic interpretation (After Rider, 1996). 146

CHAPTER 7

Fig. 7.1. Depositional model for the Hawaz Formation in the western-central Gargaf Arch (After Vos, 1981). 153
Fig. 7.2. Block diagram of a braided delta system and an example of a modern braid delta from Alaska. 153
Fig. 7.3. Cross section showing the two facies association recognized in the Hawaz Formation (shoreface and shelf). 154
Fig. 7.4. Block diagram of a typical sandy, bedload-dominated braided stream system illustrating bed forms common to these systems. 155
Fig. 7.5. Schematic depositional model of the Hawaz Formation in A1-NC186 and H27-NC115. Note the absence of the fan delta system described by Vos (1981) in the west-central Gargaf Arch, to the W/NW of the study area. 155
Fig. 7.6 Luning et al. (2000) interpretation for early Silurian hot shale deposition in North Africa and Arabia. 157
Fig. 7.7. Conceptual model for the upper Ordovician organic-rich "hot" shale in Jordan. (a) Initiation of the anoxic puddle. (b) Expansion of the puddle during the HST (After Armstrong et al., 2005). 157
Fig. 7.8. Cartoon showing major evolution stages in NC115 (After Ghnia and Chang, 2002). 159
Fig. 7.9. A. In basic surface form, Yosemite Valley resembles a fault-block basin, or graben, more than it does a glacial valley. B. Beneath the thick lake sediments is the rest of a U-shaped glacial valley, note a block of rock that has dropped down between faults (After Bill, 1932). 159
Fig. 7.10. Seismic line showing the U shaped vally in the Hawaz Formation, but without evidence of a fault control suggested by Ghnia and Chang (2002), and Echikh and Sola, (2000). The U shape probably formed by glaciation. 160

Fig. 7.11. General depositional model for late Ordovician to early Devonian sediments in North Africa with emphasis on the lowermost Silurian hot shales. Systems tracts belong to a second-order sequence (Luning et al., 2000). 161

List of Tables

Table. 2.1. Definition of moment measures (Friedman, 1960), where f=frequency of the different grain-size grades present, mϕ= mid point of each grain-size grade in phi values. 34

Table 2.2 Grain-size parameters in A1-NC165 using Folk and Ward (1957) equations. 37

Table 2.3 Grain-size parameters in A1-NC186 using Friedman's (1962) equations. 38

Table 2.4 Grain-size parameters in H27-NC115 using the Folk and Ward (1957) equations. 39

Table 2.5 Grain-size parameter in H27-NC186 using Friedman's (1962) equations. 39

Table 2. 6. Degree of roundness for the descriptive characterisation of roundness (after Russell, et al. 1978). 44

Table 2.7 Degree of roundness, based on the descriptive characterization of roundness (After Russel-Taylor-Pettijohn, 1978) for the Hawaz Formation, A1-NC186. 44

Table 2. 8 Degree of roundness, based on the descriptive characterization of roundness (After Russel-Taylor-Pettijohn, 1978) for the Hawaz Formation, H27-NC115. 47

Table 3.1 Core samples used in this study from type wells A1-NC186 and H27-NC115 showing the cored intervals and core sample depths. 50

Table 4.1 Model composition of sandstone samples from the Hawaz Formation, A1-NC186 and H27-NC115. 106

1. Introduction

The Murzuq Basin is one of several intracratonic basins located on the North African platform that have a predominantly marine Palaeozoic clastic infill.

This study investigates the petrography, sedimentology and sequence stratigraphy of the Cambro-Ordovician Hawaz Formation intervals drilled by Repsol Oil Operations in A1-NC186 and H27-NC115, on the northwestern flank of the Murzuq basin, southwest Libya (**Fig. 1.1**), with the intention of assessing its reservoir characteristic and petroleum potential. The primary reservoir target in the Murzuq basin is the Mamuniyat Formation, not the Hawaz. However, the Hawaz Formation becomes the main reservoir target where the Mamuniyat Formation is absent.

1.1 Aims of the study

The main aims of the study are as follows:

1) To examine the petrographic characteristics of the sandstones in the Hawaz Formation, in order to identify texture, mineral composition, diagenetic features and porosity with a view to assessing the reservoir potential of the sandstone.
2) To intergrate the petrographic data with conventional core analysis data in order to gain an understanding of the controls on reservoir quality, in addition to comparing results from different facies component of the formation.
3) To attempt to produced a revised stratigraphic subdivision of the Cambro-Ordovician reservoir interval.
4) To provide a detailed sedimentological description of the core from wells A1-NC186 and H27-NC115.
5) To integrate the sedimentological and wireline log data in order to derive depositional models which adequately account for the Hawaz Formation in the study wells.
6) Apply sequence stratigraphic methods of analysis to the Hawaz Formation, using the variation in facies tracts and stacking patterns in relation to changes in base level.

1.2 Location map

The Murzuq Basin covers a huge area (about 350,000km^2 in the SW Libya. The concessions NC115 and NC186 are located in the northwestern part of the basin, which covers an area of about 8,660 km^2 (**Fig. 1.1**).

Activity in NC-115 concession area has passed through three stages: (1) in the fist exploration phase from 1956 to 1980, 17 wells were drilled, with an oil discovery in B2-1 (Atshan) and hydrocarbon shows in several other wells; (2) the second 'Rompetrol' phase from 1980 to 1992 resulted in wells drilled on twelve structures, with commercial discoveries in six of these (Rompetrol, 1987); and (3) the 'Repsol' phase which was restricted to the central part of the block, within an area about 5,000km^2, for the development stage, which started in 1993, and has been characterized by the development of the three main fields discovered to date (A, B and H) (Aziz, 2000). The exploration activity in the NC-186 (Repsol YPF) and recently (Repsol Oil Operations) started in may 1998, once the Libyan authorities approved the exploration and production sharing agreement signed with the National Oil Corporation.

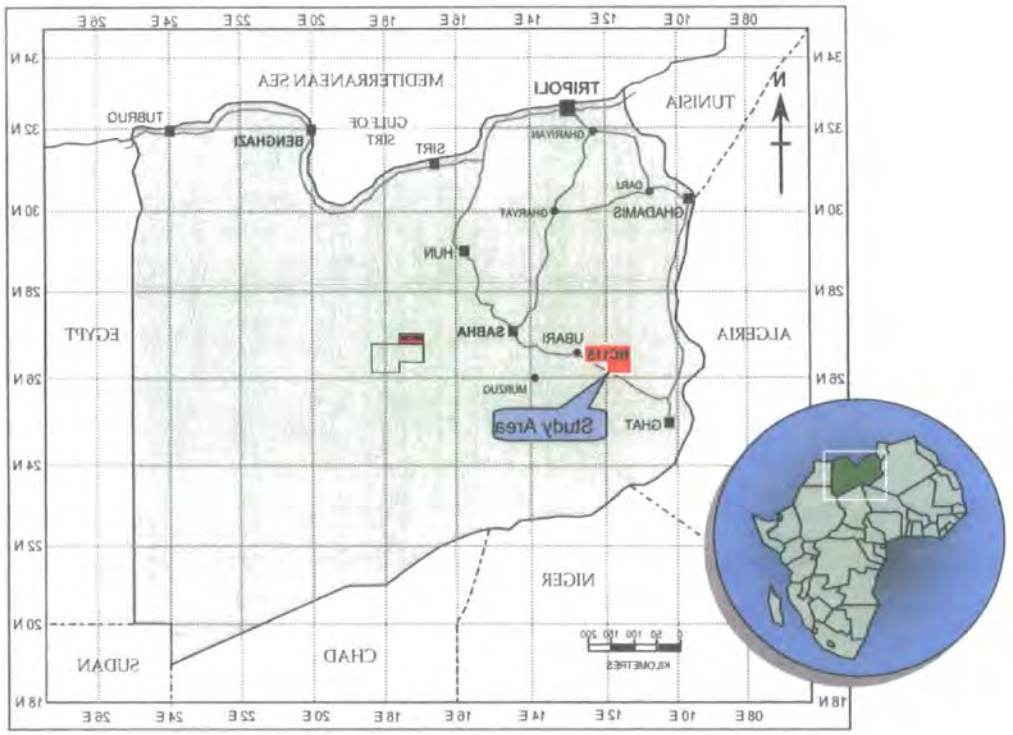

Fig. 1.1. General location map of Libya showing the study area in SW Libya.

1.3 Methodology and available material

The material used for this study includes slabbed core photographs, core samples, which were cut into thin-sections for petrographic analysis, wireline data and conventional core analysis data from the two studied wells.

A total of 125 thin sections were examined from the two studied wells (A1-NC186 and H27-NC115), each sample being vacuum impregnated with blue resin to facilitate recognition of porosity. Each thin section was point counted (300 grains) with the summary petrographic data presented in Chapter four.

1.4 Wireline log data

Electrical wireline logs from A1 and A2 in NC186 concession, and H9, H20, H22, H24 and H27 from concession NC115 have also been used in this study. The data provided by Repsol Oil Operations "Exploration Department" is in excel format. The only wells that penetrated the whole Hawaz Formation are A1 and A2-NC186 and H27-NC115 (**Fig. 1.2**).

The electric wireline log data include Gamma-ray (GR), Spontaneous potential (SP) and Neutron porosity (NPHI). These were used for facies correlation, determining the position of marker beds, and the thickness of facies units and systems tracts sequence boundaries. However, the gamma ray log was the most useful for delineating facies geometries and depositional relationships. Depth of the core, wireline logs and thickness of internal structures is given in imperial and metric units.

1.5 Stratigraphic succession in the Murzuq Basin

The first geologists working in western Libya established the broad stratigraphic framework of the Murzuq Basin (Desio, 1936; Lelubre, 1946; Freulon, 1954; Wells, 1955; Brady, 1957; Howard, 1957; Thompson, 1960; Collomb, 1962; Klitzsch, 1963, 1981; Hoen, 1968; Bellini and Massa, 1980). The work of Castro et al. (1985) and Pierobon (1991) represent important steps in the advancement of our

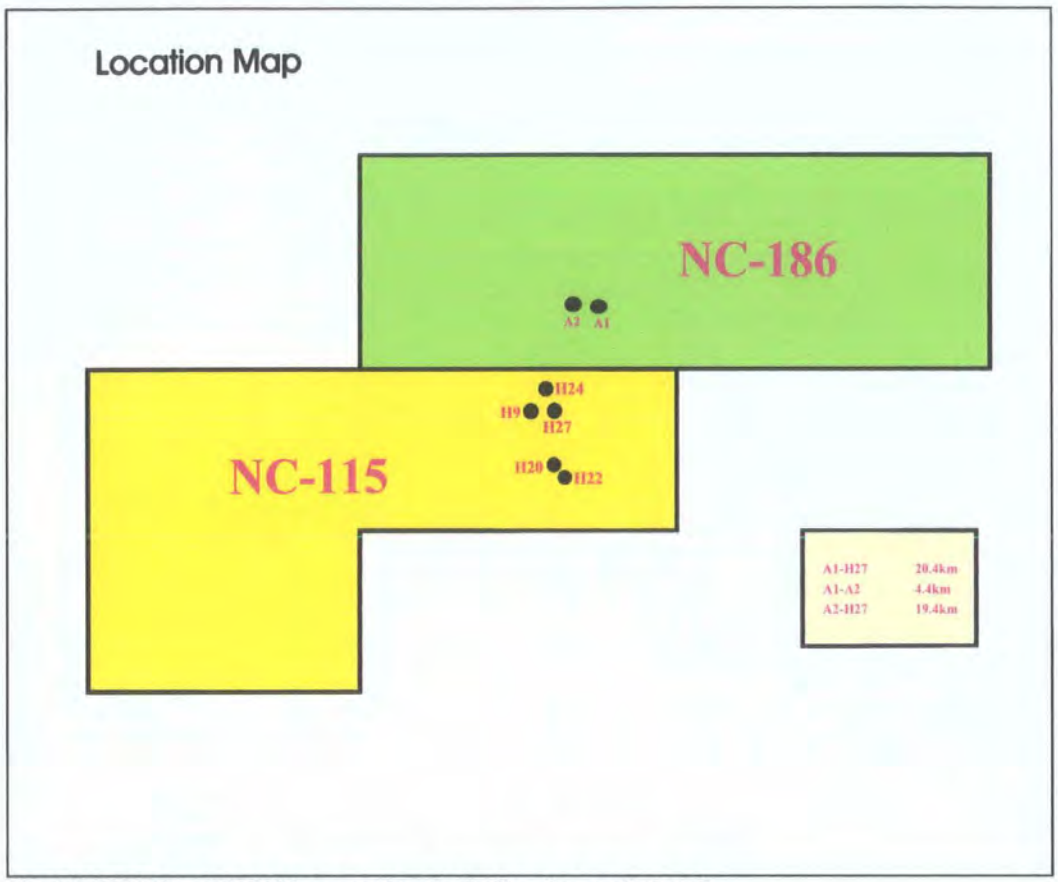

Fig. 1.2. NC115 and NC186 concessions including the studied wells.

knowledge of this basin (Echikh and Sola, 2000). The stratigraphic column ranges from the Precambrian to the Quaternary (**Fig. 1.3**). Most sedimentary units forming the stratigraphic column of the basin are widespread and have good correlation between subsurface and outcrops (Pierobon, 1991). The Palaeozoic succession consists predominantly of clastic sediments which have good lateral correlation. Marine deposits dominate but with recurrent continental influences (Aziz, 2000). The sedimentary fill of the Murzuq basin is typical of Palaeozoic basins in other parts of the world. The depositional history is relatively simple, with some prominent characteristic facies patterns (Pierobon, 1991).

The present structural framework of the Murzuq Basin, (**Fig. 1.4**) reflects the successive effects of tectonic movements related to Ordovician, Silurian/Devonian, late Palaeozoic, Mesozoic and Tertiary tectonism, but the Hercynian compressional

Era	PERIOD/ SUBPERIOD		EPOCH	AGE My	Former RP Terminology	new Terminology	Present Formations	Ispo m
C	Quaternary or		Holocene	0.01		Quaternary		40
E	Pleistocene		Plastocene	1.64	Q	AlMahruqa		
N		Neogene	Pliocene	5.2	U			
O	Terti-	22	Miocene	23.3	A	&basalts	Alpine	
Z	ary		Oligocene	35.4	T	Mazul Ninah Fm	Unconformaty	
		Paleogene	Eocene	56.5	E	Bishima Fm.		
65	63	42	Paleocene	65	R	Surfah Fm.		
M	Cretacous		Upper Cretaceous	97	N A	Zmam Fm		
E			Early		R	Messak Fm.		
S	81		Cretaceous	145.6	Y			
O			Main	157.1		Taouratine Fm		
Z	Jurassic		Dogger	178				150
O	62		Lias	208				
I			Late	235	Post-			
C	Triassic		Mid	241.1		Zarzaitine Fm.		290
180	37		Lower	245				
			Zechstein	256.1				
	Permian		Rot-				Hercynian	
	45		Liegendes	290		Tiguentourine fm.	Unconformaty	
P			Stephanian	303	Tassilian			
	Carbon-	Upper	Westphalian	318	Dembaba Fm	Dembaba Fm.		37
	iferous	43	Namurian	332.9	Assedjefar Fm	Assedjefar Fm.		70
A			Visen	349.5	Collenia Beds			
		Lower			Marar Fm	Marar Fm.		365
	73	30	Tournaisian	362.5	Devonian			
L								
			Late	377.4	(A. Wanin Fm)	A. Wanin Fm.		115
E					Acacus Fm	2BDS II"		
	Devonian		Middle	386		"BDSI"		
						Ouan Kasa/		
O	46		Early	408.5		Tadrart Fms.		
			Ludlow/Prid	424		Akakus Fm.		
	Silurian		Wenlock	430.4				
Z								?
	31		Landovery	439	Tanezzuft Fm	Tanezzuft Fm.		275
						Hot Sh Mbr		15
O			Ashgill	443.1	Mamuniat Fm	Mamunitat Fm.		166
		Upper			Melez	Melaz Shuqran		32
			Cara-					
I	Ordo-		doc	463.9	Shugran Fm.	Fm.		
	vician	Middel	Llanv/Lland.	476.1	Hawaz/	Hawaz Fm.		162
			Arenig	493	Ash Shablat	Ash Shablat		
C	71	Lower	Termadoc	510	Fm.	Fm.		
			Upper	517.0	Hasswnah Fm	Hassawnah Fm.		222
	Cambrian		Middel	536.0				
							Unconformaty	
			Lower					
325	60			570				
	INFRACAMBERIAN				Mourizide Fm.	Mourizide Fm.		297
	PRECAMBERIAN				Basement	Basement		

Fig. 1.3. Stratigraphic column in NC115 (Aziz, 2000).

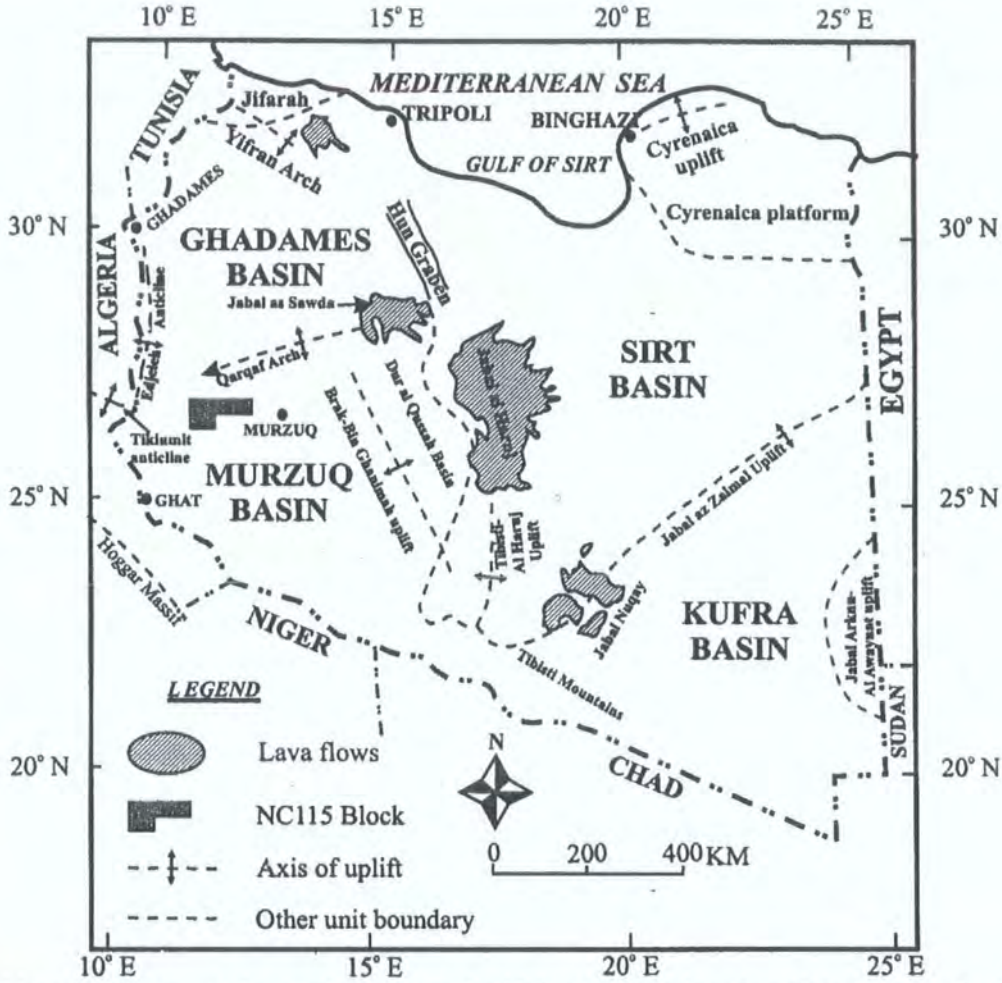

Fig. 1.4. Map showing general tectonic framework of Libya and the location of the Murzuq Basin.

movements had the greatest effects. The multiphase evolution of this basin has produced a great variety of trap types. The main trapping mechanisms are controlled by structural and glacially related palaeogeomorphological factors, but other more subtle traps may also occur, related to stratigraphic truncation and permeability barriers (Echikh and Sola, 2000).

1.5.1 Precambrian

Basement rocks exposed along the basin margins (**Fig. 1.5**) are generally divided in two groups: a high-grade metamorphic suite comprising mica-schist, gneiss and amphibolites, associated with granite and granodiorite, and a low-grade metamorphic suite of quartzite, phyllite, schist and arkose, including locally preserved unmetamorphosed deposits of the so-called Mourizidie Formation (Burollet, 1963). The lithostratigraphic nomenclature of the Precambrian to Silurian is based on Hallett (2002) (**Fig. 1.6**).

1.5.2 Infracambrian

1.5.2.1 Mourizidie Formation: infracamberian (Algonkian)

The Mourizidie is disconformably overlain by the basal conglomerate of the near horizontal strata of the Cambrian Hasawnah Formation. In the Murzuq basin few wells have so far penetrated this sequence, but in well A1-NC115, some 75 m of extrusive acidic to intermediate rocks (rhyolite to rhyodacite) were penetrated in a section equivalent to the Mourizidie (Pierobon, 1991).

The Mourizidie Formation, as defined by Jacqué (1962), overlies the Precambrian with a distinct angular unconformity and is itself discordantly overlain by basal conglomerates of the Cambrian Hasawnah Formation (Aziz, 2000).

1.5.3 Cambro-Ordovician

The Cabro-Ordovician system of Libya was first defined in the area of the Al-Qarqaf arch. It is widespread over large portions of the North African craton (Pierobon, 1991). North Africa was located on the northern margin of Gondwana, and formed a passive margin during most of the Palaeozoic, from which the Avalonian and Cadomian terranes broke away during the Ordovician and migrated northwards towards Laurentia and Baltic (Hallett, 2002).

Sedimentation during the Cambrian period was controlled by the mature relief and tectonically stable Precambrian platform, which was inundated by very shallow seas. Similar conditions prevailed through out the early Ordovician period, but the close of the Ordovician period was marked by widespread glacial influence throughout the whole of the central Sahara, resulting in the deposition of periglacial sediments with a cold water fauna (Mamgian, 1980).

The roughly peneplaned surface of the Precambrian platform was transgressed during the late Cambrian, creating a predominantly tidal and subtidal sedimentary environment with occasional fluviodeltaic incursions (Aziz, 2000).

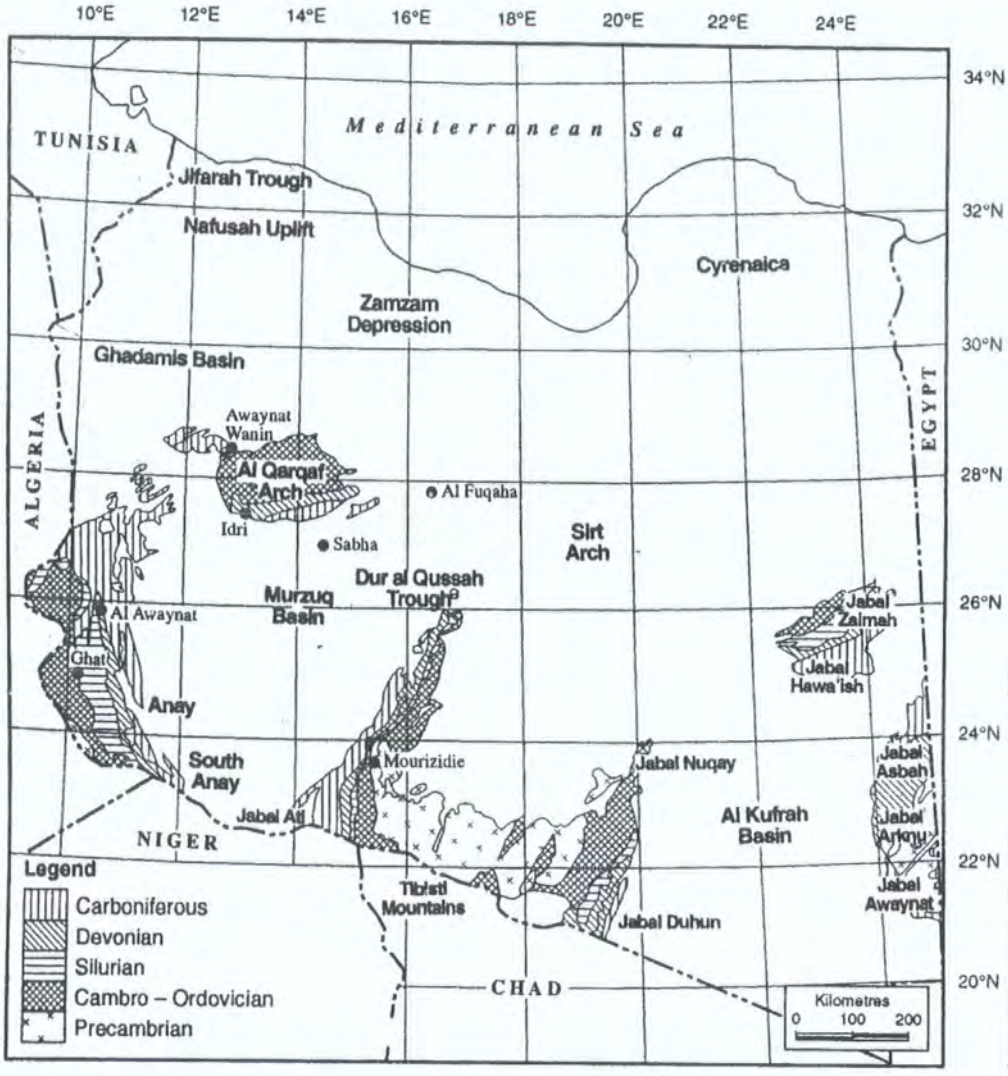

Fig. 1.5. Precambrian and Palaeozoic Outcrops in Libya (Hallett, 2002).

1.5.3.1 **Hasawnah Formation:** Upper Cambrian

The earliest clastic sequences overlying the Precambrian basement in western Libya were The Hasawnah Formation, defined by Massa and Collomb (1960) based on extensive outcrops covering 16 000 km^2 of the Jabal Hasawnah on the Al Qarqaf Arch (Hallett, 2002) (**Fig. 1.5**). It is typically developed as a medium to coarse-grained, cross-bedded sandstone with conglomeratic interbeds. A similar development is seen in outcrops on the western margin of the basin in the Ghat area (Aziz, 2000).

The Hasawnah Formation is unconformably overlain by the fine-grained Ordovician clastics of the Ash Shabiyat Formaton (Collomb, 1962); in the subsurface

they are difficult to distinguigh from each other (Pierobon, 1991). The Hasawnah Formation unconformably overlies the grey friable medium to coarse-grained biotite Precamberian granite, with a basal conglomerate of variable thickness. The conglomerate consists of quartz pebbles within a matrix of quartz sandstone with rare feldspar. Cross-bedding is also present in the conglomeratic horizons. The conglomerate is overlain by light grey to brown, medium to coarse-grained, mostly cross-bedded sandstones (Mamgian, 1980).

The depositional setting of the Hasawnah Formation is normally interpreted as a braided-stream deposit due to the high sandstone/shale ratio (Pierobon, 1991). The Hasawnah Formation has moderate to poor reservoir quality, in that the diagenetic growth of clay minerals has had a negative effect on pore space, as has quartz overgrowths, both of which have reduced reservoir quality, However, the abundant fractures in the core indicate an enhanced reservoir potential (Aziz, 2000).

1.5.3.2 Ash Shabiyat Formation: Lower Ordovician (Tremadocian)

The Ashabiyat Formation introduced by Havlicek and Massa (1973), for the basal Ordovician succession is well developed in Jabal Achebyat after which it has been named (V. D. Mamgian, 1980). According to Bellini and Massa (1980), the formation is represented by 65 m of medium to coarse-grained, *Tigillites*-bioturbated sandstone, and common trace fossils like *Cruziana* and *Harlania*. This formation name has not been accepted by some authors, who prefer to include the corresponding interval in the lower part of the Hawaz Formation (Pierobon, 1991).

In the area of Al Qarqaf Arch the contact with the underlying Hasawnah Formation is conformable. It can be divided into a lower and an upper unit. The lower unit comprises thin-bedded, flaggy sandstones, often ferruginous, containing *Tigillites* and *Harlania*. The thickness is about 25 m. Cross-bedding is rare, which is taken to indicate a deeper depositional environment. The upper unit, which reaches 40 m in thickness, is more thickly bedded and more extensively cross-bedded, and bears some similarity to the Hasawnah Formation (Hallett, 2002).

PERIOD	EPOCH/STAGE	S.W. LIBYA	GHADAMIS BASIN	ALGERIA TRIASSIC BASIN	JABAL KUHUN	JABAL HAWA'ISH
SILURIAN	PRIDOLI	AKAKUS		AKAKUS	AKAKUS	AKAKUS
	LUDLOW					
	WENLOCK	TANZUFT		ARGILES DE FEGAGUIRA	BEDO	TANZUFT
	LLANDOVERY					
		IYADHAR	BI'R TLAKSHIN			
ORDOVICIAN	ASHGILLIAN	ARGILES MICRO	JIFARAH	ARG MICRO CONGLOMETATIQUES	MUNCHAR	HAWA'ISH
		MAMUNIYAT		GRIS DE OUED SARET		
	CARADOCIAN	TASGHART				
	LLANDEILIAN	MELAZ SHUQRAN	BI'R BEN TARTAR	ARGILES D'AZZEL		
	LLANVIRNIAN					
	ARENIGIAN	HAWAZ	KASBAH LEGUINE	GRES DE OUARGLA QUARTZITES DE HAMRA		
	TREMADOCIAN	ASH SHABIYAT	SANRHAR	GRES D'EL ATCHANE ARGILES D'EL GASSI		
CAMBRIAN		HASAWNAH	SIDI TOUI	GRES D'EL GASSI(Ri, RalT) GRES DEH. MESSAOUD (R3, R2, RA)	TEDA ZOUMA	UNDIFFERENTIATED
INFRA-CAMBRIAN		MOURIZIDIE				
PRECAMBRIAN		TIBISTIAN				

QARQAF GROUP

Fig. 1.6 Precambrian and Lower Palaeozoic lithostratigraphic nomenclature (Hallett, 2002).

According to Belini and Massa (1980) the Aah Shabiyat Formation represents the transitional Cambro-Ordovician succession.

Lithologicaley the Ash Shabiyat and the Hasawnah Formations are very similar (Pierobon, 1991). The Ash Shabiyat Formation represents a marine transgressive unit in southern Libya. The age is assumed to be Tremadocian, on the basis of stratigraphic position and supposed correlation with Tremadocian dated rocks in the subsurface (Hallett, 2002).

1.5.3.3 Hawaz Formation: Middle Ordovician (Llandeilian/ Llanvirnian)

The Hawaz Formation was formally introduced by Massa and Collomb (1960) after Jabal Hawaz (West of Jabal al Qarqaf). It typically consists of cross-bedded, quartzitic sandstones, in part kaolinitic, with thin shaley intercalations (Pierobon, 1991). Collomb later divided the formation into three subdivisions, an upper 'Tigillites superieurs', middle 'Gres intermediaries' and a lower '*Tigillites inferieurs*' (Mamgian, 1980). The uppermost Ordovician Mamuniyat Formation is normally considered to be the primary reservoir interval in NC115. However, this formation is not preserved in the eastern part of the H-field where the Hawaz Formation directly underlies the lowermost Silurian Tanezzuft shale source rocks and constitutes the main reservoir target (Aziz, 2000).

The Hawaz Formation represents the onset of the first major Palaeozoic marine transgression in the area (Echikh and Sola, 2000). It consists of fine to medium-grained, coarsening-upward, well-cemented, hard sandstone, with siltstone, mudstone and fine sandy interbeds. The Hawaz Formation is very similar to the upper parts of the Hasawnah Formation, and the contact between the two units can be difficult to establish. In several wells the two units are therefore combined, with a total thickness varying between 699m (A1-NC115) and 246m (A1-1) (Aziz, 2000).

The formation ranges from 50m (Dŭr al qussah) to 280m (Al Qarqaf) in thickness at outcrop. Castro et al. (1985) described the Hawaz from outcrops in the western Al Qarqaf as a typical prograding alternation of thin, non-resistant layers, made up of very fine sandstones and siltstones with ripple-drift and micrograded laminae, and thick beds of fine to medium-grained, tabular to sigmoidal cross-bedded sandstone (Della Favera, 1984). The same authors suggested a probable transitional to

a shallow marine (foreshore to shoreface) depositional setting, comparable with the present "offshore tidal sands" (shoal massifs) of the continental shelves of northern Brazil, the North Sea and the Yellow Sea (Pierobon, 1991).

1.5.3.4 **Melaz Shuqran Formation:** Upper Ordovician (Caradocian)

Named after Melez Shuqran Mountains in the western part of Jabal Al Hasawnah, by Massa and Collomb (1960), the formation is characterized by shales and siltstones along with fine-grained sandstones deposited in a quiet marine, preiglacial environment. It transgregressively overlies the Hawaz Formation in the type area but directly rests on the Hasawnah Formation in the Dŭr el Gussa area (Mamgian, 1980). It is a pelitic to fine clastic sequence consisting of varicoloured, chloritic, thin-bedded shales and siltstones intercalated with fine-grained sandstone exhibiting micro-hummocks, wave ripples and bioturbations which attest to a shallow marine facies (Pierobon, 1991).

The Melaz Shuqran Formation is well develoed in the Idri area on the Al Qarqaf Arch, and has also been mapped along the western flank of the Murzuq Basin. In the Tikiumit area the Melaz Shuqran Formation exhibits good examples of ice rafted blocks of granite, schists and conglomerate up to 0.5m in diameter randomly distributed within a fine-grained sandstone matrix. The sandstones show extensive subaqueous slump features. The thickness of the formation in this area is about 45m. In the subsurface of the Murzuq Basin the Melaz Shuqran Formation contains radioactive shales with high thorium content which are interbedded with minor siltstones and sandstones. The thickness of this unit is 25m in well C1-NC58 but in other wells ranges from 15m to 75m. Its absence in well H1-NC115 and reduced thickness in well D1-NC115 may be indicative of the effect of Caradocian tectonism in this area (Hallett, 2002).

Within NC115 the formation consists predominantly of dark gray to blackish shales, with thin interbeds of siltstones and fine-grained, gray, micaceous sandstones. Palynological analyses indicate that the Melaz Shuqran Formation is late Ordovician (Caradoc) in age (Aziz, 2000).

1.5.3.5 Tashgart Formation: Upper Ordovician (Caradocian/ Ashgillian)

In mapping the wadi Tanezzuft area on the western flank of the Murzuq Basin Radulovic (1985) found a distinctive unit between the Melaz Shuqran Formation and the Mamuniyat Formation which he called the Tashgart Formation (Hallett, 2002). The deposition of the Tashgart Formation develops gradually from the Melaz Shuqran Formation. The lithologic change is well marked in that the greenish grey shales and siltstones of the Melaz Shuqran Formation are overlain by brownish and purplish grey medium to coarse-grained sandstones of the Tashgart Formation (Grubic et al., 1991).

The formation is extremely conglomeratic at Ghat but shows more distal features northwards in the Tikiumit area. It has not been found outside this small area. The formation is barren of fossils but is assumed to be Caradocian in age. Abugares and Ramaekers (1993) disputed the turbidite origin, and regarded the Tashgart Formation as simply the lower part of the Mamuniyat Formation. It is probably more appropriate to regard the Tashgart as a member of the Mamuniyat Formation rather than as a separate formation (Hallett, 2002).

1.5.3.6 Mamuniyat Formation: Upper Ordovician (Ashgillian)

The Mamunitat Formation represents the primary reservoir target in the Murzuq Basin and most particularly in the fields in the NC115 licence area. It consists of regressive coarse clastics, provenanced from emergent areas. It generally comprises massive, cross-bedded, and fine to coarse-grained to conglomeratic sandstones, with siliceous and sometimes mixed cements. The thickness of the Mamuniyat Formation is highly variable (Aziz, 2000). It was first described by Massa and Collomb (1960) from the western part of Jabal Al Hasawnah in the vicinity of Mamuniyat, after which it has been named. Subsequently Collomb (1962) presented a detailed description of the type area in which he recognised a variety of facies types in the 100 to 140m thick succession (Mamgian, 1980).

The Mamuniyat Formation can be subdivided into Upper, Middle and Lower members, based on textural properties, sedimentological characteristics and sequence stratigraphic analysis (Fello, 2001). The subsurface occurrence of the Mamuniyat

Formation is widespread, with thicknesses in the range 20-170m, but with a regional thickening towards the Al Qarqaf high (Pierobon, 1991).

The formation develops conformably from the Melaz Shugran (Ghat and Wadi Tanezzuft area) and Tashgart Formation (Wadi Tanezzuft and Tikiumit area). The composition of the Mamuniyat Formation is relatively simple and monotonous. It consists of thick-bedded to massive, less frequently thin-bedded quartz sandstones, mainly whitish-grey, yellowish or pink in colour (Grubic et al., 1991).

The Mamuniyat Formation represents the second glacial-marine cycle of the Palaeozoic in Murzuq. A periglacial depositional setting is interpreted based on ecological grounds (Pierobon, 1991).

1.5.4 Silurian

The first major marine transgression covering the greater part of the North African craton started in the early Silurian period as a result of melting of ice sheets that covered the Hoggar, Tibesti, Jabal Al Awaynat and probably Jabal Al Hasawnah massifs (Mamgian, 1980). The transgression produced thin, locally developed, basal silty sandstones in some areas, after which thick, "hot" black, radioactive, graptolitic shales were deposited. These shales, rich in organic debris, form one of the principal petroleum source rocks in Libya and Algeria (Hallett, 2002). The early Silurian sea is thought to have invaded the Murzuq Basin from the NNW (Aziz, 2000).

1.5.4.1 **Tanezzuft Formation:** Lower Silurian (Llandoverian)

The Tanezzuft Formation is an important stratigraphic unit from the standpoint of petroleum exploration. It has proven to be one of the major source rocks of North Africa and its distribution and extent are therefore of prime importance (Hallett, 2002). The formation was formally introduced by Desio (1936b) after Wadi Tanezzuft about 65km NE of Gat. Its type section was measured by Klitzsch (1963) at Takharkhouri pass 35km south of Ghat. The Tanezzuft Formation is a sequence of dark grey to black, graptolitic shales with intercalations of siltstone and fine-grained sandstones, often forming rhythmical alternations (Pierobon, 1991). It is easily recognized in the

field because of its typical relief with rounded and heavily dissected predominantly greyish to pink coloured hills (Grubic et al., 1991).

Tanezzuft Formation shales have been penetrated in all wells in NC115, and a total of 146m of core has been taken from 22 wells. The thick basal Tanezzuft shale overlies and seals the main reservoir interval and therefore the main hydrocarbon source rock, both regionally and locally (Aziz, 2000).

The Tanezzuft Formation and overlying Akakus Formation demonstrate that these formations are diachronous. Bellini and Massa (1980), produced evidence to show that in the Murzuq Basin the Tanezzuft Formation was deposited during the early and mid-Llandoverian. In the southern Ghadamis Basin it is mid-Llandoverian to Wenlockian in age, and in the northern Ghadamis Basin it is largely Wenlockian and Ludlovian in age. This interpretation has subsequently been questioned. Abugares and Ramaekers (1993) suggested on the basis of well-log correlations, that multiple unconformities are present within the Tanezzuft Formation, and that recent palynological data does not support the simple south to north diachroneity suggested by Bellini and Massa (Hallett, 2002).

1.5.4.2 **Akakus Formation:** Upper Silurian (Wenlockian / Pridolian)

The term "Akakus sandstone" was introduced by Desio (1936a) after Jabal Akakus in the Ghat area. Klitzsch (1969) described a type section formed by 340m of fine-grained sandstone containing frequent trace fossils (*Harlania harlani* Conread; *Cruziana* sp.; *Tigillites* sp.), interbedded with dark-grey, graptolitic shales in the lower and middle parts (Pierobon, 1991). The type section of the Akakus Formation has a similar history to that of the Tanezzuft Formation. The original description by Desio from a location in the Jabal Akakus, north of Ghat was incomplete, and a replacement type section was established by Klitzsch from an area to the south of Ghat where a complete section is present. Subsequently Klitzsch, having studied the eastern margin of the Murzuq Basin, indicated that the type section may represent only the lower part of the formation. At the type locality the Akakus Formation comprises 240m of fine to medium-grained silty sandstone, thinly bedded, frequently cross-bedded, with ripple and flute marks (Hallett, 2002).

The Akakus Formation conformably overlies the Tanezzuft Formation and is unconformably overlain by the Tadrart Formation (Mamgian, 1980). In the Ghat, Wadi Tanezzuft and Al Awaynat areas, the Akakus Formation terminates with a conspicuous ferricrete 0.1-4m thick, characterized by ample ferruginous concretions and convolute structures (Grubic et al., 1991).

The Akakus sandstones represent the regressive phase of the Early Silurian transgression. Castro et al. (1985) pointed out the continental to transitional (nearshore marine) character of the sedimentation in outcrops from Takharkhouri to Al Awaynat. They conclude that deposition of regressive clastics began after the transgressive acme was reached in the Middle Silurian (Pierobon, 1991). The traces of Harlania are ubiquitous and highly characteristic being up to 40cm long and other trace fossils are also numerous, including *Tigillites dufrenoyi*, *Arthrophycus alleghaniesis*, *Corophioides sp.*, *Cruziana sp.*

1.5.5 Devonian

The Devonian period in Liby is marked by major palaeogeographical changes brought about by the culmination of epeirogenic movements during the late Caledonian orogeny. It witnessed the development of discrete basins of deposition which gradually evolved from the shallow epicontinental sea covering the stable platform until the Lower Silurian period (Mamgian, 1980). The lower Devonian rocks are widespread in western and southwest Libya. In the Murzuq basin they are mainly represented by sandstones of the Tadrart Formation. The Ouan Kasa Formation has limited regional expression (Pierobon, 1991).

The stratigraphic nomenclature for the Upper Palaeozoic is shown in **Fig. 1.7**. It has long been believed that the Silurian-Devonian boundary in Libya is almost everywhere unconformable, as reflected by the 'horizon d'Iknouen', and that the Lochkovian stage is absent in all areas (Hallett, 2002).

1.5.5.1 **Tadrat Formation:** Early Devonian (Sigenian)

The Tadrart Formation was introduced by Burollet (1960). Its type section was described by Klitzsch (1965, 1969) at Takharkhouri pass along the eastern margin of Wadi Wan Kasa. In Klitzsch's type section the Tadrart displays 310m of continental to subcontinental sandstones (Pierobon, 1991). The formation has the shape of a thick lens deposited south of Al Qarqaf arch. The lower boundary of this formation towards the Akakus Formation is disconformable. It is marked by a conspicuous ferricrust and a sharp change in the type of stratification. The formation is thickest and best developed in the Al Awaynat area where it is 350m thick (Grubic et al., 1991).

The Tadrart Formation has been mapped along the western flank of the Muzuq Basin from Tikiumit to the border with Niger. In this area the Tadrart Formation is made up of lenticular sandstone bodies representing filled channels within a braided-river sequence. This facies association led Clark-Lowes and Ward (1991) to suggest strong similarities between the Tadrart and Nubian Formations. Grain-size ranges from fine-grained to conglomeratic. The distribution of the Tadrart Formation within the Murzuq Basin has been greatly affected by Devonian tectonism. Sparse fossil evidence and characteristic trace fossils suggest an early Devonian age (Hallett, 2002).

1.5.5.2 **Ouan Kasa Formation:** Early Devonian (Emsian)

The Ouan Kasa Formation was first described by Borbhi and Chiesa (1940) in Wadi Wan Kasa. In Klitzsch's type section at Takharkhouri it reaches a thickness of 43m. Castro et al. (1985) reported thin, coarsening-upward sequences with wavy-lenticular and flaser-bedded, occasionally bioturbated siltstones and fine-grained sandstones, grading into tabular cross-bedded sandstone at the top (Pierobon, 1991). The formation accumulated in a low-energy setting ranging from brackish lagoon to shallow sublittoral and offshore bar environments. It is unconformably overlain by sandstones of the Awaynat Wanin Formation, and has been mapped along the western margin of the Murzuq Basin from Tikiumit to South Anay (Hallett, 2002). The separation of the Ouan Kasa from the Tadrat in the subsurface is not evident. Electric logs from wells A1-76 and H1-NC58 suggest a rapid transitional passage from the

estuarine upper Tadrart to the shallow marine-neritic Ouan Kasa sandstone and siltstones (tidal bar facies) (Pierobon, 1991).

1.5.5.3 **Awaynat Wanin Formation:** Middle-Late Devonian (Couvinian / Strunian)

Borghi (1939) recognized rocks of the middle Devonian age in the Awaynat Wanin area, but the name Awaynat Wanin Formation was first introduced by Lelube (1946). Massa and Collomb (1960) gave the first systematic description of the formation (Hallett, 2002). Massa and Collomb (1960) and Collomb (1962) thought that the name originated from 1851 when Overweg (1851) had, for the first time, reported Devonian fossils from this area (Mamgian, 1980). Bellini and Massa (1980) described a type section of 225m in the western Al Qarqaf area, appointing four units of chronostratigraphic significance (Pierobon, 1991).

Pierobon (1991) suggested the geological setting of the Qwaynat Wanin Formatoin was predominantly marine with fluvial deltaic deposits occuring in its middle and upper parts. Castro et al. (1985) reported two types of deltaic facies at outcrop: fine-grained suspension deposits (delta front) and coarse-grained traction sediments (fluvial-distributary channels), all of them intensely reworked by tide and storm waves (Pierobon, 1991). In the subsurface the formation has been cored in four wells in NC115. These show a mud-dominant development; sandstones were present but had a generally very poor reservoir quality. Previous studies of the Awaynat Wanin Formation have suggested middle to late Devonian age (Eifelian to Famennian) in its type area (Aziz, 2000).

1.5.5.4 **Tahara Formation:** Late Devonian (Famennian / Strunian)

The Tahara Formation was established by Burollet and Manderscheid in 1967, and was refined by Massa, Termier and Termier in 1974. The formation was defined as a 60-70m shale-sandstone cycle from a type section in B1-49 well in the southern Ghadamis Basin. It outcrops in a small area to the northwest of Awaynat Wanin where two coarsening-upwards cycles are exposed separated by a hard ground (Hallett, 2002).

PERIOD	EPOCH/STAGE	EUROPEAN EQUIVALENTS	WEST LIBYA		IDRI-SABHA AREA	ALGERIA ILLIZI BASIN	JABAL DUHUN	JABAL HAWA'ISH
PERMIAN	LATE	BUNTER	BI'R AL JAJA	CONTINENTAL EQUIVALENTS			'CONTINENTAL POST-TASSILIEN'	
	MID	ZECHSTEIN						
	EARLY	ROTLIEGENDES	AL WATYAH					
CARBONIFEROUS	GZELIAN	STEPHANIAN	TIGUENTOURINE					
	KASIMOVIAN							
	MOSCOVIAN	WESTPHALIAN	DIMBABAH			'A' RESERVOIR		
	BASHKIRIAN	NAMURIAN				'B' RESERVOIRS		
	SERPUKHOVIAN		ASSEDJEFAR					
	VISEAN		COLLENIABEDS MARAR			'D' RESERVOIRS	OUNGA	ZALMAH
	TOURNAISIAN							
DEVONIAN	FAMENNIAN	STRUNIAN	AWAYNAT WANIN	TAHARA AO I	ASHKIDAH	'F2' RESERVOIR	BINEM	BLITA
					TARUT			
	FRASNIAN			AO III	DABDAB			
					QUTTAH			
	GIVETIAN			AO II	IDRI	'F3' RESERVOIR		
	EIFELIAN	COUVINIAN		AO I EMGHAYET	BI'R AL QASR	'F4' RESERVOIR		
	EMSIAN		WAN KASA			'F5' RESERVOIR		
	PRAGIAN	SIEGENIAN	TADRART			'F6' RESERVOIR	TADRART	TADRART
	LOCHKOVIAN	GEDINNIAN						

Fig.1.7. Upper Palaeozoic lithostratigraphic nomenclature (Hallet, 2002).

The lower Tahara displays thin bedsets with lenticular wavy-bedded shale and very fine sandstone at the base grading upwards, in a cyclic fashion, into hummocky to cross-bedded sandstones. Each cycle is more than a few meters thick and is marked by intense bioturbation (Skolithos) and oxidized levels (commonly bearing ferruginous oolites) in the top part. The upper Tahara is quite similar. Topping the cycles are massive and sigmodal to tabular cross-bedded sandstones (Pierobon, 1991). The sequence of sixteen shallowing-upwards cycles have been recognized within the Tahara Formation, representing a shelf-shoreface succession in a storm-dominated environment. It is characterised by a palynological assemblage which marks the transition from the Devonian to the Carboniferous (Late Famennian-Strunian age) (Hallett, 2002).

1.5.6 Carboniferous

Deposition of Carboniferous rocks in Libya was controlled by tectonic events associated with the collision of western Gondwana with Laurasia to Pangaea. These orogenic events resulted in compression, uplift, and the gradual emergence of a series of southwest-northeast intercratonic sags and arches which increasingly affected sedimentation during the Carboniferous (Hallett, 2002). In the Murzuq basin the Carboniferous outcrops are more widespread, and nearly girdle the basin, except for the northern part (**Fig. 1.5**). The northernmost outcrops in the Murzuq basin are exposed at the intersection of Lat. 28°N and Long 11° E, and can be traced southwards, extending into the territory of Chad (Mamgian, 1980).

1.5.6.1 **Marar Formation:** Lower Carboniferous (Tournaisian / Visean)

The Marar Formation was first defined by Lelubre in 1948 by reference to a type section at Qararat Marar northwest of the Al Qarqaf Arch. At the type location the Marar Formation comprises about fifty stacked cycles of silty claystones, micaceous siltstones and feldspathic quartz-sandstones. The claystones are greenish-grey, silty and gypsiferous, and the sandstones and siltstones ferruginous, flaggy and often ripple-marked. The sandstones are sometimes conglomeratic at the base, frequently cross-bedded and contain brachiopods and pelecypods (Hallett, 2002). In NC115 the formation is penetrated by all wells drilled in the block. The formation

unconformably overlies Devonian deposits and is represented by rhythmic alternations of marine shales and sandstones. The shales are frequently silty, micacous and pyritic, compact, dark gray to blackish in colour, while the sandstone is light gray, fine to very fine-grained and poorly consolidated by siliceous, clay or sometimes carbonate cement. Occasionally, thin shaly limestone beds also occur. The formation becomes increasingly sandy upwards (Aziz, 2000).

1.5.6.2 **Assedjefar Formation:** Upper Carboniferous (Namurian)

The Assedjefar Formation was defined in 1952 by Lelubre for a sequence of deltaic and shallow marine rocks conformably overlying the Marar Formation in the HAMADAT Tanghirt area of west Libya (Hallett, 2002). Collomb (1962) has described a 190m thick succession with variable facies from east to west in the type area. In the east the Assedjefar Formation consists of about 100m of fine to coarse-grained, cross-bedded sandstones containing fossil wood with two thin beds of sandy and silty claystone, followed by a sequence of marly carbonates. In the west, within 15km, the facies changes to more or less equal proportions of sandstones and claystones, followed by marls and a few interbeds of carbonates. Near the base some oolitic dolomite banks, and fossilferous sandstones with fossil wood are also present (Mamgian, 1980).

The subsurface thickness within the NC115 concession ranges between 25 and 136m (Aziz, 2000). According to fossil assemblages and palynological analysis this formation is assigned a Namurian age. The upper boundary of the Assedjefar Formation is gradational and conformable with the Dembab Formation, and is marked by stromatolitic structures (Pierobon, 1991).

1.5.6.3 **Dembaba Formation:** Upper Carboniferous (Westphalian)

The Kimbaba Formation represents the last of the Carboniferous marine formations preserved in Libya. It was originally defined by Lelubre (1952) for a series of mainly carbonate rocks overlying the Assedjefar Formation in the Hamadat Tanghirt area (Hallett, 2002).

Collomb (1962) has provided the general description from the type area, without designating a type section. In the type area the Cembaba Formation consists of about 40m of gypiferseous claystone in the lower part, with a grayish blue limestone within the lower 10m above the base, containing stromatolitic structures generally ascribed to Collenia type forms. It is interesting to note that the Collenia type structures have developed at two different levels within the Carboniferous sequence. The first Collenia type structures appear at the top of the Marar Formation, but are confined to the southern part of Hammadah and western part of Murzuq basin. The second level of stromatolitic limestones appearing near the base of Dembaba Formation has been observed in both areas of Carboniferous outcrop, along the southern flank of Hammadah basin and along the western and eastern flank of the Murzuq basin. It has also been recorded from the Djado region in the territory of Chad. The upper part of the Dembaba Formation in the type area consists of about 60m of light "grau dolomits" and highly fossiliferous dolomitic limestone with thin interbeds of claystone, capped by slumped limestone (Mamgian, 1980).

Within NC115 the Dembaba Formation shows an alternation of shales and limestone with fine-grained sandstone and siltstone. The formation ranges in thickness between 10 and 65m (Aziz, 2000).

1.5.6.4 Tiguentourine Formation: Upper Carboniferous – Early Permian (Stephanian / Rotliegendes)

The term Tiguentourine Formation was probably first introduced by de Lapparent and Lelubre (1948) for the lower part of their continental post Tassilien Group. It was followed by later workers and defined by Burollet (1960) as consisting of 'reddish brown to mauve clays and shales often slightly dolomitic, with characteristic gypsum beds near the base' named after the spring of Tiguentourine in Algerian territory (Mamgian, 1980). The thickness of this formation ranges between 130 and 520m in the subsurface (Pierobon, 1991).

According to the surveyors of the Geological map of Libya the Tiguentourine Formation is not present at outcrop along the western margin of the Murzuq Basin

where the Dembaba Formation is overlain directly by the Triassic Zarzaitine Formation (Hallett, 2002).

1.5.7 Hercynian Unconformity

The advent of the Permian period in Libya is marked by the large-scale withdrawal of Palaeozoic seas from the major centres of sedimentation, and the emergence of all of the Caledonian and Hercynian structural elements, with the possible development of lagoonal to limnic environments along their flanks. The complete absence of marine Permian rocks at outcrop suggests the possibility of their absence due to erosion (Mamgian, 1980).

Hercynian tectonic movements affected the Murzuq Basin from the late Carboniferous to the Permian, and sediments of this age are generally missing. The general thickness of preserved Carboniferous strata increases northwestwads in the Murzuq Basin and into the southern Ghadames Basin (Aziz, 2000). The Permian is generally thought to be missing in the Murzuq Basin and this period is presumed to represent the main phase of Hercynian uplift and fault rejuvenation in the area (Echikh and Sola, 2000).

1.5.8 Triassic

Triassic rocks in Libya occur in four main domains: the predominantly marine rocks of the Nafusah escarpment and in the offshore, the eastern extension of the Algerian Triassic Basin into the Ghadamis area, the grabens in the subsurface of eastern Libya, and the continental rocks of the interior (Hallett, 2002).

Subsidence in the Murzuq basin began again during the Triassic and was accompanied by uplift of the Al Qarqaf arch. This is shown both by changes in the thickness and by the SW and SE directions of palaeotransported material (Grubic et al., 1991). In the Murzuq Basin the 'Continental post-Tassilien' has been subdivided into three formations: the Tiguentourine Formation of Late Carboniferous-early Permian age, the Zarzatine Formation of Jurassic age, and the Taouratine Formation of Jurassic age (Hallett, 2002) (**Fig. 1.8**).

1.5.8.1 Zarzaitine Formation (Post-Tassilian)

This formation was introduced by Burollet (1960). It outcrops over many parts of the Murzuq Basin (**Fig. 1.8**), particularly in the west of the NC-115 area, and it unconformably overlies the Dembaba Formation across the Hercynian unconformity (Aziz, 2000). The formation was first described from the Zarzaitine field area of eastern Algeria. In this area the formation was divided into three informal members: a lower unit of multi-coloured claystones and fine-grained sandstones, a middle unit of mottled claystones, argillaceous limestones and dolomites, with thin bands of gypsum and anhydrite, and an upper unit of friable, argillaceous sandstones, claystones, dolomites and gravels. The total thickness is about 400m. In Algeria the age is considered to extend from the Triassic to mid Jurassic (Hallett, 2002) (**Fig. 1.8**).

1.5.9 Jurassic

After a break in deposition after the Triassic Zarzaitine Formation, essentially continental conditions governed the area during the deposition of the Taouratine Formation. The domain was covered by a system of braided rivers with alluvial plains and periodic lakes (Grubic et al., 1991). The 'Continental Post-Tassilien' Group of Kilian is divided into three formations of which the Taouratine is the youngest. It overlies the Triassic Zarzaitine Formation and is overlain by the 'Continental intercalaire' of Kilian which is usually taken to equate with the Nubian Sandstone (Hallett, 2002).

1.5.9.1 Taouratine Formation

The Taouratine Formation was first described by de Lapparent and Lelubre (1948) from the Taouratine area in the eastern Illizi Basin of Algeria. In this area it can be subdivided into three units, a lower member of alternating mottled sandy claystones and ferruginous sandstones which contain plants and vertebrate remains indicative of late Jurassic age, a middle member of sandy dolomitic limestone and marls of mid-Jurassic to early Cretaceous age, and an upper unit of claystones, friable sandstones and occasional limestones which have been dated as Vraconian (late Albian-early Cenomanian). The thickness is about 350m (Hallett, 2002).

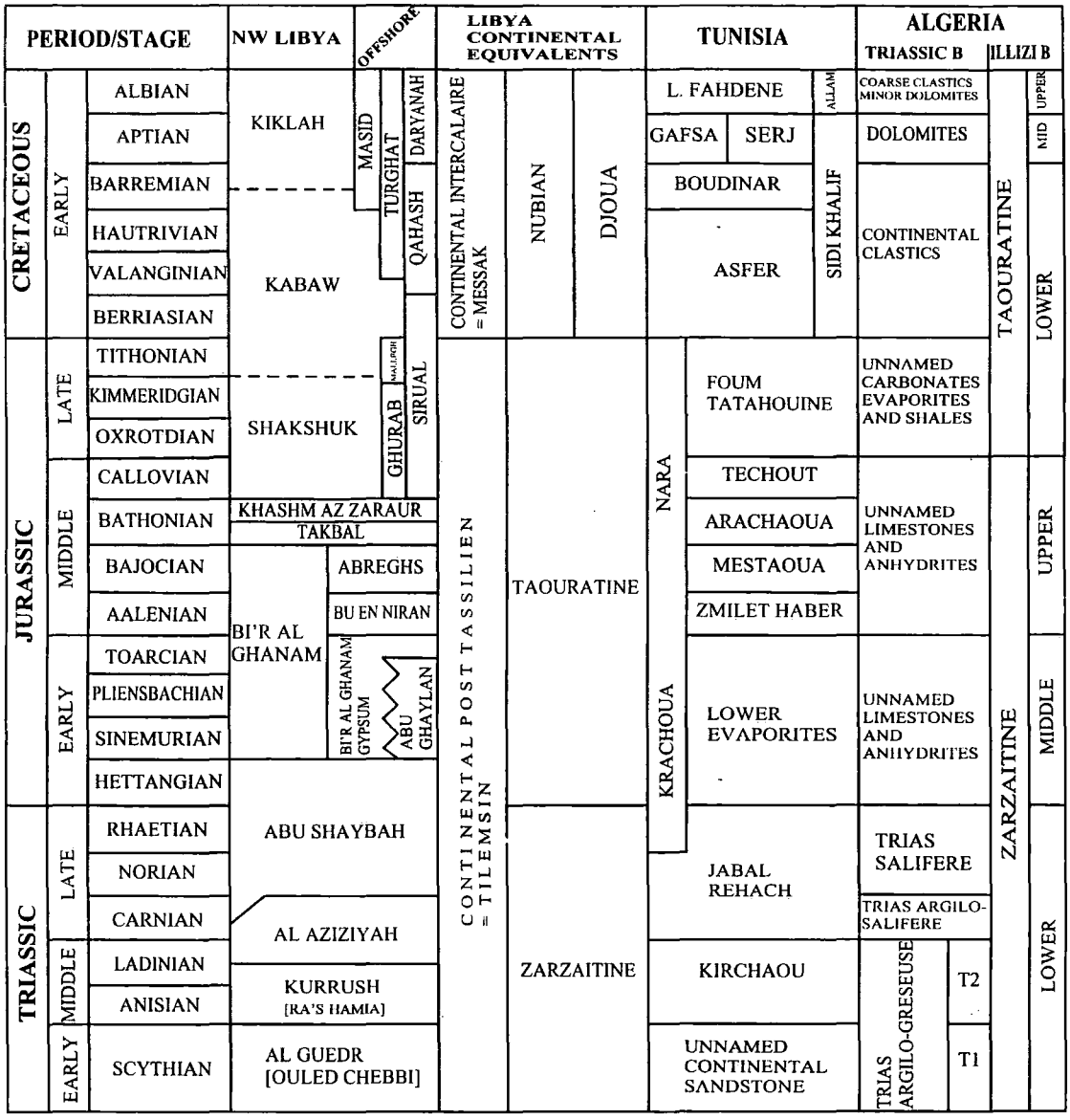

Fig. 1.8. lithostratigraphic Nomenclature for the Triassic, Jurassic and Lower Cretaceous rocks of Libya and adjacent areas (Hallett, 2002).

This formation outcrops in the center of NC115 and unconformably overlies the Zarzaitine Formation. It consists of pale red quartzitic conglomerates, with alternating interbeds of sandstone, siltstone and claystone, deposited in a braided river system. The formation has been penetrated by most wells in NC115, with a thickness of around 400m (Aziz, 2000).

1.5.10 Cretaceous

In the late Jurassic to early Cretacous local movements, caused by the differential opening of the Atlantic Ocean, and extension in the nearby Sirte Basin, produced NW-SE trending faults, such as those cutting the northwestern parts of the Murzuq Basin. Uplift and erosion of the flanking Tihemboka and Tibesti highs during the Mesozoic resulted in the deposition of thick continental sandstone sequences in the present central parts of the basin (Echikh and Sola, 2000).

1.5.10.1 Messak Formation

The Messak Formation was introduced by Klitzsch (1971) who named it after Jabal Msak Mallat. It is unconformable over the Taouratine Formation and also partly over the Zarzaitine Formation (Anay area). The boundary is almost everywhere marked by a lateritic horizon 0.6-6m thick (Grubic et al., 1991), and it comprises 330m of continental sandstones and shales, frequently conglomeratic, often cross-bedded, and occasionally ferruginous (Hallett, 2002).

The formation is late Jurassic to early Crtaceous in age, and is usually divided into a lower Jarmag Member and an upper Awbari Member, both consisting of continental clastics deposited in a predominantly braided stream environment, but with interbedded lake and swamp deposits (Aziz, 2000).

1.5.11 Quaternary

A great part of Murzuq basin is covered by recent aeolian sands forming dune systems separated by deflation valleys. The highest dunes reach over 300m above the valley floors, and are concentrated in the basin's central portions. The sand grains show polished surfaces, are well sorted and lack bounding cement; the presence of conglomeratic pavements indicates ephemeral fluvial systems (flash-flood "playas") (Pierobon, 1991).

2. Texture

2.1 Introduction

Geologists have long been fascinated by the problem of extracting geologic information from grain-size analyses of sand and sandstone. Although it is one of the most widely used terms in sedimentology, the "size" of a particle is not uniquely defined except perhaps for only the most simple of geometric objects such as a sphere (diameter) or a cube (length of an angle) (Pettijohn et al.,1987). The statistical parameters derived from the study of grain-size distributions are useful in facies mapping and the genetic interpretation of sandstone (Friedman, 1957). The most important textural feature of conglomerates and sandstones is grain-size, both the average size and the distribution of sizes in the rock (Donald R. and Fred Schwab, 1996). Grain-size analysis can be used to distinguish between sediments of different depositional environments and facies, and provide information on the deposition processes and flow conditions, (Tucker, 1991). Friedman (1958) derived empirical methods for converting grain-size data from thin section to sieve analysis to overcome the problem of random sectioning. Furthermore, the efficiency of thin section analysis decreases from the coarse to the fine grades (Pelto, 1952). However, Friedman's methods are not always applicable to coarse-grained, poorly sorted sandstone in that the sieve size distribution agrees most closely with the uncorrected thin section distribution (Turner, 1969). With this conversion, each percentile read from the cumulative curve of the thin section analysis can be converted to the percentile of the weight distribution curve of the calculated sieve analysis (Muller, 1967).

2.2 Different methods of measuring grain-size

2.2.1 Sieving

Sieve size analysis measures grain diameter by allowing sand to settle through a nest of sieves. Each sieve is a cylinder floored with a wire-mesh screen with square apertures of fixed dimensions (2mm, 1mm, 0.5mm, 0.25mm, 0.125mm, and 0.0625mm). In sieve analysis, therefore, clast diameter is the width of the smallest

aperture through which grains pass (Donald and Schwab, 1996). Determination of grain-size and sorting measures in loosely consolidated and unconsolidated rocks by sieving is standard procedure, but it cannot be readily applied to cemented and indurated rocks, such as quartzite. Attempts to disaggregate the grains in tightly cemented rocks results in grain breakage and erroneous results. In subsurface work the geologist has to rely to a great extent on cores of indurated rocks and on cuttings, neither of which easily lends itself to sieve analysis (Friedman, 1962).

2.2.2 Petrographic microscope

This method is preferred for ancient, well-indurated sandstones that cannot be disaggregated easily. (Features other than texture are also best examined in thin section). A petrographic microscope is fitted with an ocular micrometer, an eyepiece bearing a scale subdividing the field of view into discrete metric units (Donald and Schwab, 1996). By conducting mechanical analyses by means of a microscope, it is important that the sample used be representative of the material being studied. No fixed rules can be given for the size of the final sample, inasmuch as individual practice varies from counting a few hundred grains to counting several thousand. One "rule of thumb" that may be used is to count a minimum of 300 grains for statistical accuracy, and convert the numbers to percentages by classes. This is followed by counting an additional hundred or so grain, and the percentages are recalculated on the entire number of grains counted (Krumbein and Pettijohn, 1938). More sophisticated methods of measuring grain-size use expensive equipment such as laser beam technology, which may require considerable expertise (Donald and Schwab, 1996). For silica-cemented sandstone such as the Hawas sandstone, the most suitable method for determining grain-size is in thin section under the microscope using a micrometer eyepiece graticule and point counter.

2.3 Discussion of grain-size parameters

One of the basic parameters which the geologist employs in studying the aerial distribution of sands is the grain-size distribution. Grain-size and the various measures derived from the statistical analysis of the grain-size distribution, such as sorting measures, lend themselves to quantitative analysis and can be plotted on maps and

contoured. They reflect the energy gradients responsible for transportation and deposition of sand bodies and are, therefore, important in reconstructing the geological environment (Friedman, 1962). Once the grain-size distribution has been obtained the sediment can be characterized by several statistical parameters, including mean grain-size, mode, median grain-size, sorting and skewness. A further parameter, kurtosis, has little geological significance (Tucker, 1991). Many authors, instead of giving the absolute grain-size in mm, use the phi symbol, (ϕ), introduced by Krumbein (1934), which is the negative logarithm to the base 2, ϕ=-log2 x, where x is the grain diameter in mm (Mueller, 1967). The phi symbol (ϕ), as originally adopted by Kumbein (1934, 1936), is used to denote a grade scale in which all divisions are equal in grade (Page, 1955). Page has proposed a conversion table from mm to phi.

2.3.1 Mean grain-size (average grain size)

Inman (1952) suggested ((ϕ6+ϕ84)/2) as a measure of mean size. This serves quit well for nearly normal curves, but fails to reflect accurately the mean size of bimodal and strongly skewed curves (Folk and Ward, 1957). Folk and Ward used another measure of the mean Mz determined by the formula:

$$Mz = \frac{(\phi 16 + \phi 50 + \phi 84)}{3}$$

Here, ϕ16 may be considered roughly as the average size of the coarsest third of the sample, and ϕ84 as the average size of the finest third; the addition of the ϕ50 (the average of the middle third) thus completes the picture and gives a better overall representation of the true phi mean (Folk and Ward, 1957). Friedman (1958) proposed another equation for grain-size parameters, as shown in **Table 2.1**. Both methods have been used in this study, and the results presented in **Table 2.2**.

3.3.2 Mode

No good mathematical formula exists for accurate determination of mode. The best approximation is probably that given by Croxton and Cowden (1939), but this works well only when the distribution is symmetrical in the region neighboring the

mode; it fails in skewed curves. The maximum percentage occurring within a half-phi diameter range in any sample has been termed the "modal concentration" and may have some value as an auxiliary measure of the degree of sorting in the region about the mode (Folk and Ward, 1957). Strictly defined, the mode is the phi (or millimeter) value of the mid-point of the most abundant class interval. Most sediments are unimodal, that is one class dominates, but bimodal and even polymodal sediments are not uncommon, where the mode is of little value, and further analysis requires more complex statistics (Tucker, 1991).

3.3.3 Median

The median diameter is defined as the middle member of the distribution. It is that diameter which is larger than 50 percent of the diameters in the distribution, and smaller than the other 50 percent. For its graphic determination, therefore, it is only necessary to draw a cumulative curve of the grain-size distribution and read the diameter value which corresponds to the point where the 50 percent line crosses the cumulative curve (Krumbein and Pettijohn, 1938). The mean and the median are equal in a symmetrical distribution, but differ from each other in a asymmetrical distribution (Inman, 1952). The median is a very misleading value and should be abandoned as a measure of average size inasmuch as it is based on only one point of the cumulative curve. For example, a sediment consisting of 40 percent pebbles and 60 percent fine sand may have the same median as one with 60 percent fine sands and 40 percent clay (Folk and Ward, 1957).

3.3.2 Standard deviation (sorting)

The standard deviation of a distribution is a measure of the average spread of the curve about its arithmetic mean, and it is the most widely used measure of dispersion in conventional statistics (Krumbein and Pettijohn, 1938). Geologists are often interested in the standard deviation of the grain-size in clastic sedimentary rocks. This statistic is commonly referred to as the degree of size-sorting (or, for the seek of brevity, sorting) (Harrell, 1984). In the phi notation the standard deviation of a frequency distribution can be approximated by obtaining one-half distance between

the 16th and 84th percentile diameters on a cumulative frequency curve (**Fig. 2.1**). The recommended relation

$$\sigma\phi = \frac{(\phi 84 - \phi 16)}{2}$$

was suggested by Krumbein et.al (1938) and Otta (1939), and referred to as the phi deviation measure (Inman, 1952). For many normal curves this measure is adequate. However, it is based only on the central part of the distribution and ignores fully one-third of the sample especially the "tails", which offer some of the most valuable information. Although theoretically, it would be best to include everything from the first to the 99th percentiles, Inman (1952) has shown that data are seldom reliable beyond the 5th and 95th percentiles. Hence, these percentiles provide a practical end point, and if they are used, only one-tenth of the sediment is excluded from the sorting measure. Inasmuch as the spread between the 5th and 95th percentiles includes 3.3 standard deviations, a standard deviation measure based only on the extremes is

$$\sigma\phi = \frac{\phi 95 - \phi 5}{3.3}$$

However, neither the $\phi 84$-$\phi 16$ measure nor the $\phi 95$-$\phi 5$ measure is adequate by itself for complex bimodal sediments, although, it could be obtained by combining the two and taking their average. This measure, called the Inclusive Graphic Standard Deviation, is found by formula

$$\sigma I = \frac{\phi 84 - \phi 16}{4} + \frac{\phi 95 - \phi 5}{6.6}$$

In discussing sorting, it is also useful to have a verbal scale, so that information may be communicated to non-specialists (Folk and Ward, 1957). Terms used to describe the sorting values obtained from the Folk and Ward formula are:

Phi < 0.35	very well-sorted
0.35-0.5	well-sorted
0.5-0.71	moderately well-sorted
0.71-1.0	moderately-sorted
1.0-2.0	poorly- sorted
> 2.0	very poorly-sorted

Sorting of the sediment is determined by several factors. First, there is the question of the sediment source. For example, if granite sources the sediment, the grain-size will be quite different from sediment sourced by reworking sandstone. The second factor is grain-size itself. Sorting is dependent on the grain-size in that coarse gravel and conglomerates, and fine silts and clays, are generally more poorly-sorted than sand-size sediments which are more easily transported, and therefore more prone to sorting by wind and water. The third factor, which is based on sorting, is interpretation of the deposition mechanism. Sediments, which were deposited quickly, such as storm beds, or those deposited from viscous flows, such as mud flows, are generally poorly sorted. Sediments which have been worked and reworked by wind or water, such as the sandy deposits of deserts, beach and shallow shelf seas for example, are much better sorted (Tucker, 1991).

2.3.5 Skewness

To measure the non-normality of a distribution, it is necessary to compute either skewness (or symmetry) are kurtosis (or peakness) (Folk, 1966). Inman (1952) suggested two measures of skewness. The first one

$$\alpha\phi = \frac{(\phi 84 + \phi 16 - 2(\phi 50))}{(\phi 84 - \phi 16)}$$

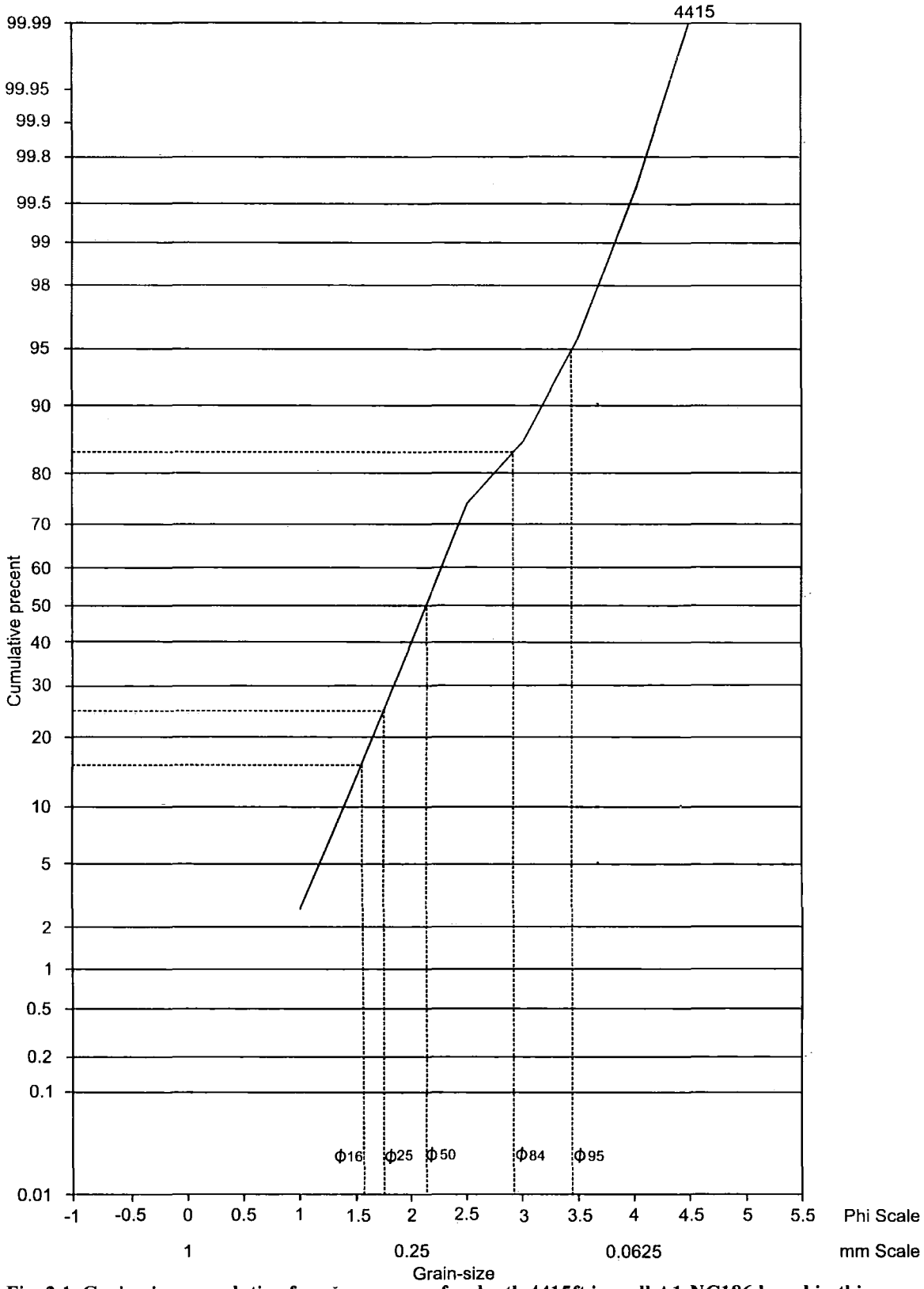

Fig. 2.1. Grain-size cumulative frequency curve for depth 4415ft in well A1-NC186 based in thin section grain-size analysis plotted on lognormal probability paper, showing different percentile Phi values used in the grain-size parameter equations.

determines the asymmetry of the central part of the distribution whereas the second one

$$\alpha 2\phi = \frac{(\phi 95 + \phi 5 - 2(\phi 50))}{(\phi 84 - \phi 16)}$$

measures the asymmetry of the tails of the distribution. A better measure of overall skewness may be obtained by averaging these two values according to the formula, Inclusive Graphic Skewness (Folk and Ward, 1957)

$$SkI = \frac{(\phi 16 + \phi 84 - 2(\phi 50))}{2(\phi 84 - \phi 16)} + \frac{(\phi 5 + \phi 95 - 2(\phi 50))}{2(\phi 95 - \phi 5)}$$

Terms for skewness derived from the Folk and Ward (1957) formula are

< + 0.30	strong fine-skewed
+0.30 to +0.10	fine-skewed
+0.10 to -0.10	near-symmetrical
-0.10 to -0.30	coarse-skewed
> -0.30	strongly coarse-skewed

Mean	$\chi\phi=1/100\Sigma fm\phi$
Mean deviation	$MD\phi=(1/100)\ \Sigma f\ \lvert m\phi-\chi\phi\rvert$
Standard deviation	$\sigma\phi=(\Sigma f(m\phi-\chi\phi)^2/100)^{0.5}$
Skewness	$\alpha 3\phi=(1/100)\ \sigma\phi^{-3}\Sigma f(m\phi-\chi\phi)^3$
Kurtosis	$\alpha 4\phi=(1/100)\ \sigma\phi^{-4}\Sigma f(m\phi-\chi\phi)^4$

Table. 2.1. Definition of moment measures (Friedman, 1960), where f=frequency of the different grain-size grades present, mϕ= mid point of each grain-size grade in phi values.

2.4 Thin section grain-size analysis of sandstone from wells A1-NC186 and H27-NC115

The grain-size of the Hawas Formation based on 110 thin sections from wells A1-NC186 and H27-NC115 has been determined by measuring the apparent long diameter of at least 300 quartz grains per thin section with the aid of a micrometer eye-piece and mechanical stage, according to the methods in Krubein and Pettijohn (1938). The measured values were then grouped into 0.25 phi classes and the number frequency in each class converted into percentages of the total number of grains counted. Cumulative curves were drawn by plotting grain-size fractions against cumulative number-percent frequency on log probability paper (**Fig. 2.2**). Statistical grain-size parameters (mean-size, standard deviation, skewness, and kurtosis) were calculated from these cumulative curves, using the formulas of Folk and Ward (1957) and Friedman (1962). The results are shown in **Table 2.2** and **Table 2.3** for A1-NC186, and **Table 2.4** and **Table 2.5** for H27-NC115. Moreover, visual inspection of the cumulative curve may show whether two or more populations are present, and reveal any possible errors in the analytical methods employed (Pettijhon et al., 1987). The mean-size of the sands ranges from 1.3ϕ to 3.5ϕ in A1-NC186 and from 1.29ϕ to 2.39ϕ in H27-NC115. According to Folk and Ward (1957), and Friedman (1962), the sands fall within the medium to very fine sand grade on the Udden and Wentworth grain-size scale. The sorting of the sandstones, as measured by the ϕ standard deviation (σI), gives values ranging from 0.32ϕ to 0.69ϕ (well-sorted to moderately well-sorted) in A1-NC186 and from 0.34ϕ to 0.69ϕ (well-sorted to moderately well-sorted) in H27-NC115 respectively. The average skewness (Sk) of sandstone from A1-NC186 is near symmetrical (0.026), with a range between -0.36 to +0.53. The average skewness of sandstone from H27-NC115 is near symmetrical (-0.06), with a range between -0.94 to +0.15.

2.5 Interpretation of grain-size parameters

Grain-size analysis can be used to distinguish between sediments of different environments and facies, and provides information on the depositional processes and flow conditions (Tucker, 1991). For many years sedimentary petrographers have attempted to use grain-size to determine sedimentary environments. One of the major

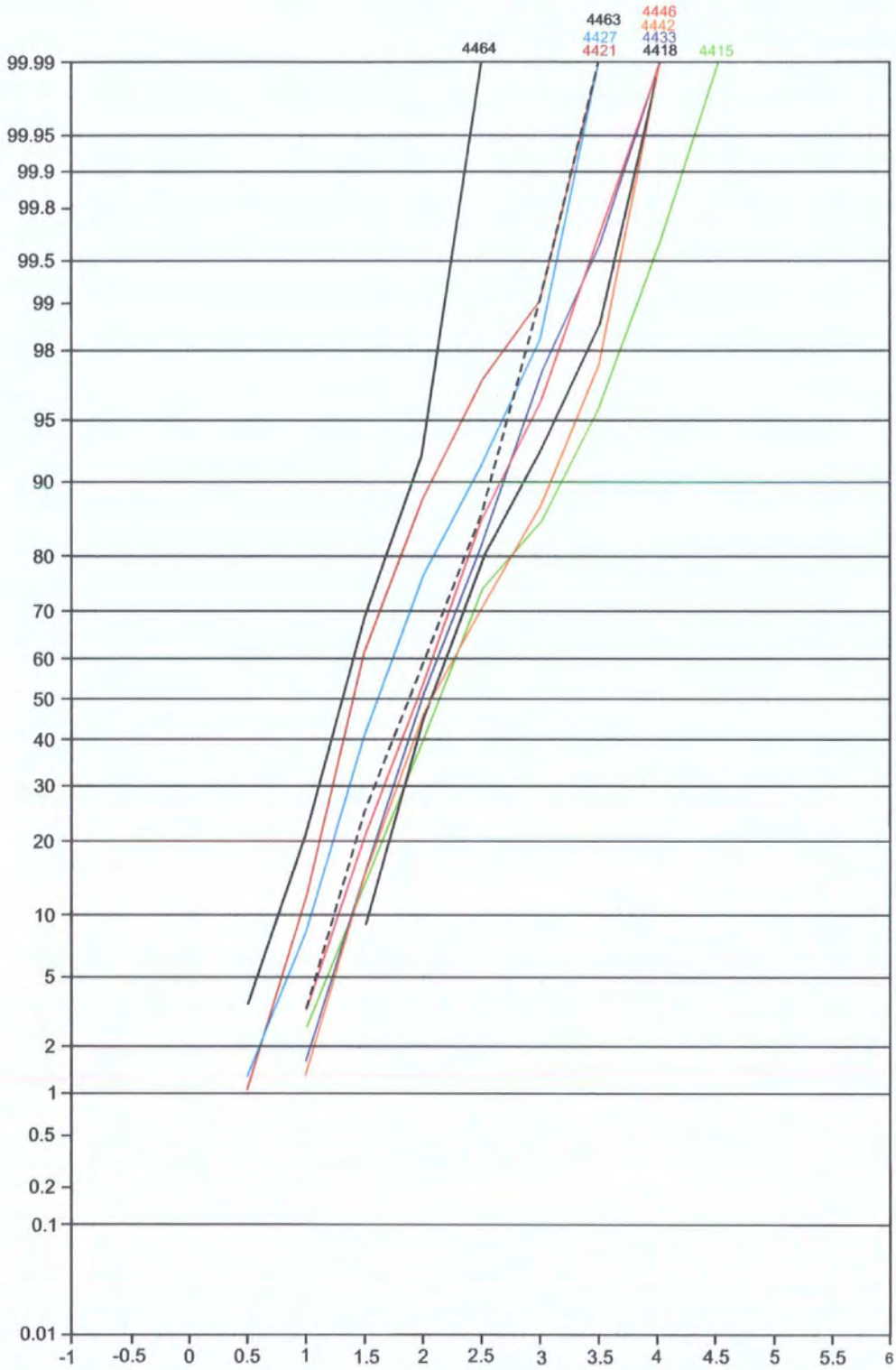

Fig. 2.2. Grain-size cumulative frequency curves for the Hawas Formation based on thin section grain-size analysis plotted on lognormal probability paper, A1-NC186.

Depth (ft)	0.05	0.16	0.25	0.50	0.75	0.84	0.95	Mean size	sorting	Skewness	Kg
4412	1.17	1.64	1.87	2.30	2.71	2.87	3.25	2.270	0.623	-0.227	0.718
4415	1.06	1.53	1.69	2.11	2.49	2.88	3.42	2.173	0.694	0.427	0.773
4418	1.22	1.58	1.71	2.06	2.42	2.60	2.98	2.082	0.520	0.100	0.507
4421	0.63	1.03	1.12	1.38	1.75	1.91	2.33	1.440	0.478	0.248	0.436
4427	0.69	1.10	1.24	1.61	1.97	2.22	2.68	1.642	0.580	0.202	0.593
4433	1.09	1.51	1.63	1.82	2.38	2.54	2.89	1.956	0.531	0.538	0.549
4442	1.10	1.51	1.65	2.07	2.60	2.87	3.32	2.149	0.676	0.492	0.860
4446	1.02	1.32	1.54	1.95	2.33	2.47	2.91	1.911	0.574	-0.026	0.615
4463	1.01	1.26	1.46	1.86	2.28	2.44	2.80	1.853	0.564	0.066	0.596
4464	0.51	0.83	1.03	1.29	1.59	1.79	2.09	1.302	0.480	0.040	0.365
4476	1.01	1.22	1.40	1.80	2.22	2.40	2.83	1.806	0.569	0.233	0.611
4479	1.04	1.24	1.41	1.74	2.07	2.29	2.64	1.755	0.505	0.190	0.437
4482	1.02	1.21	1.37	1.73	2.09	2.28	2.56	1.740	0.502	0.114	0.459
4494	0.93	1.15	1.28	1.66	2.06	2.26	2.49	1.690	0.513	0.129	0.500
4497	0.67	1.06	1.20	1.56	1.91	2.07	2.41	1.567	0.516	-0.043	0.507
4503	0.96	1.16	1.29	1.64	1.95	2.13	2.43	1.641	0.465	0.089	0.394
4509	1.01	1.21	1.38	1.76	2.17	2.35	2.70	1.776	0.540	0.179	0.546
4515	1.06	1.32	1.52	1.85	2.22	2.36	2.70	1.842	0.509	0.034	0.470
4518	0.88	1.20	1.38	1.75	2.14	2.35	2.72	1.766	0.566	0.104	0.570
4526	1.07	1.48	1.71	2.23	2.69	2.88	3.31	2.196	0.690	-0.160	0.903
4527	0.80	1.10	1.21	1.53	1.87	1.99	2.34	1.541	0.456	0.087	0.414
4530	0.60	1.02	1.12	1.41	1.76	1.90	2.27	1.443	0.472	0.099	0.435
4533	0.65	1.05	1.17	1.49	1.91	2.11	2.46	1.553	0.540	0.211	0.550
4539	1.04	1.21	1.35	1.67	1.97	2.15	2.43	1.679	0.447	0.092	0.353
4542	1.01	1.19	1.34	1.67	1.93	2.08	2.41	1.647	0.433	0.035	0.337
4545	1.32	1.67	1.84	2.22	2.56	2.74	2.96	2.209	0.515	-0.131	0.482
4548	1.09	1.34	1.52	1.79	2.11	2.29	2.53	1.807	0.455	0.050	0.348
4549	1.05	1.22	1.36	1.66	1.92	2.02	2.37	1.635	0.400	0.033	0.300
4554	1.14	1.51	1.61	1.89	2.22	2.35	2.55	1.917	0.423	-0.025	0.350
4557	1.12	1.48	1.59	1.88	2.24	2.38	2.72	1.914	0.469	0.115	0.421
4562	1.06	1.32	1.51	1.78	2.08	2.27	2.53	1.789	0.462	0.044	0.345
4563	1.01	1.15	1.27	1.58	1.87	1.97	2.33	1.567	0.405	0.101	0.324
4566	1.03	1.21	1.36	1.70	2.01	2.21	2.45	1.708	0.464	0.067	0.381
4569	1.05	1.27	1.45	1.72	1.98	2.16	2.42	1.717	0.431	0.001	0.298
4571	2.07	2.54	2.71	3.14	3.54	3.77	4.12	3.150	0.617	-0.076	0.702
4576	0.90	1.12	1.23	1.53	1.86	1.97	2.35	1.543	0.432	0.139	0.372
4579	0.87	1.11	1.20	1.47	1.82	1.94	2.33	1.508	0.431	0.221	0.368
4582	1.06	1.27	1.45	1.71	1.95	2.10	2.38	1.695	0.406	-0.018	0.272
4584	1.07	1.29	1.47	1.73	1.98	2.17	2.42	1.731	0.425	0.016	0.286
4590.5	1.06	1.32	1.51	1.75	1.98	2.17	2.46	1.746	0.424	0.021	0.266
4591	1.02	1.20	1.35	1.68	1.96	2.14	2.45	1.673	0.452	0.085	0.356
4597.7	1.06	1.25	1.41	1.68	1.91	1.99	2.37	1.642	0.383	-0.004	0.266
4601.6	1.06	1.40	1.55	1.79	2.05	2.22	2.43	1.803	0.413	-0.043	0.279
4603.5	1.08	1.35	1.53	1.79	2.10	2.29	2.57	1.812	0.460	0.081	0.350
4607	1.04	1.34	1.54	1.84	2.20	2.35	2.65	1.844	0.499	0.008	0.441
4609	0.96	1.14	1.25	1.56	1.85	1.95	2.32	1.552	0.410	0.084	0.334
4612	0.86	1.10	1.20	1.47	1.79	1.91	2.21	1.493	0.407	0.122	0.328
4613.5	1.17	1.56	1.70	2.08	2.42	2.58	2.92	2.073	0.521	-0.077	0.513
4614	1.08	1.38	1.57	1.97	2.34	2.48	2.85	1.939	0.543	-0.052	0.560
4618	1.04	1.43	1.59	1.92	2.26	2.39	2.67	1.913	0.488	-0.121	0.451
4629	1.23	1.58	1.69	2.01	2.30	2.40	2.66	1.997	0.422	-0.103	0.354
4632	1.06	1.28	1.47	1.72	1.95	2.10	2.38	1.701	0.405	-0.018	0.264
4637	0.76	1.10	1.21	1.54	1.88	2.02	2.41	1.553	0.481	0.100	0.452
4641	1.05	1.21	1.35	1.65	1.89	1.98	2.34	1.613	0.390	0.024	0.292
4642.3	0.88	1.12	1.23	1.53	1.86	1.98	2.36	1.544	0.440	0.133	0.385
4650	2.07	2.34	2.53	2.80	3.11	3.26	3.46	2.799	0.443	-0.041	0.332
4664	1.20	1.60	1.75	2.13	2.46	2.64	2.90	2.125	0.519	-0.146	0.496
4665	1.02	1.22	1.39	1.70	1.97	2.14	2.39	1.686	0.435	-0.011	0.325
4671	1.11	1.43	1.56	1.80	2.07	2.24	2.44	1.823	0.404	-0.002	0.277
4676	1.16	1.57	1.71	2.08	2.42	2.58	2.86	2.077	0.509	-0.125	0.495
4683	1.25	1.62	1.77	2.13	2.40	2.51	2.85	2.085	0.465	-0.179	0.415
4685	1.17	1.54	1.66	1.98	2.31	2.43	2.74	1.982	0.458	-0.035	0.416
4689	1.10	1.43	1.57	1.82	2.14	2.31	2.57	1.855	0.444	0.061	0.347
4691	1.22	1.58	1.69	2.00	2.35	2.47	2.86	2.018	0.471	0.084	0.439
4695	1.11	1.50	1.61	1.90	2.23	2.36	2.63	1.922	0.445	-0.013	0.390
4698	1.51	1.70	1.86	2.19	2.47	2.65	2.91	2.179	0.448	0.017	0.351

Table 2.2 Grain-size parameters in A1-NC165 using Folk and Ward (1957) equations.

Depth (ft)	5%	16%	25%	50%	75%	84%	95%	Mean size	sorting	Skewness	Kg
4701	1.50	1.68	1.83	2.17	2.46	2.64	2.92	2.163	0.455	0.050	0.369
4707.1	1.51	1.69	1.84	2.15	2.40	2.49	2.83	2.112	0.402	-0.031	0.306
4710	1.56	1.78	1.95	2.22	2.46	2.61	2.87	2.202	0.408	-0.023	0.272
4716	1.55	1.74	1.90	2.19	2.43	2.54	2.85	2.157	0.396	-0.024	0.278
4722	1.50	1.67	1.82	2.14	2.41	2.51	2.86	2.109	0.416	0.012	0.330
4725	1.53	1.80	2.01	2.23	2.45	2.59	2.87	2.209	0.399	-0.068	0.243
4728	1.52	1.79	2.00	2.24	2.47	2.64	2.88	2.224	0.419	-0.065	0.261
4731.1	1.68	2.08	2.21	2.58	2.91	3.08	3.40	2.577	0.512	-0.062	0.498
4731.8	1.63	2.00	2.10	2.38	2.65	2.80	2.94	2.390	0.398	-0.104	0.296
4737	1.38	1.66	1.82	2.14	2.37	2.46	2.76	2.087	0.409	-0.152	0.316
4740	1.53	1.82	2.02	2.24	2.46	2.60	2.88	2.219	0.398	-0.064	0.241
4749	1.59	1.91	2.05	2.28	2.51	2.68	2.90	2.291	0.392	-0.029	0.244
4755	1.63	2.01	2.10	2.35	2.65	2.78	2.95	2.378	0.392	-0.041	0.295
4758	1.68	2.06	2.15	2.39	2.69	2.82	2.96	2.422	0.384	-0.061	0.288
4764	2.06	2.26	2.43	2.66	2.86	2.93	3.09	2.617	0.322	-0.135	0.181
4769.2	2.60	3.01	3.17	3.57	3.84	3.93	4.22	3.504	0.477	-0.363	0.443
4776	1.78	2.09	2.19	2.48	2.77	2.87	3.00	2.481	0.380	-0.116	0.287
4777.5	2.61	3.03	3.13	3.39	3.70	3.82	3.97	3.415	0.406	-0.112	0.323

Continued Table 2.2.

Depth (ft)	Mean size	Sorting	Skewness	Kg		Depth (ft)	Mean size	Sorting	Skewness	Kg
4412	2.300	0.603	0.081	3.489		4601.6	1.805	0.389	-0.023	3.550
4415	2.185	0.682	0.425	2.986		4603.5	1.832	0.425	0.300	2.739
4418	2.115	0.517	0.575	3.384		4607	1.863	0.484	-0.090	3.303
4421	1.462	0.488	0.755	4.348		4609	1.585	0.407	0.298	3.427
4427	1.663	0.563	0.386	3.257		4612	1.513	0.390	0.206	3.420
4433	2.025	0.523	0.156	2.913		4613.5	2.093	0.500	0.179	2.874
4442	2.165	0.655	0.352	2.525		4614	1.978	0.517	0.107	2.490
4446	1.960	0.568	0.178	2.879		4618	1.920	0.474	-0.300	3.182
4463	1.887	0.537	0.071	2.418		4629	2.010	0.390	0.018	2.800
4464	1.314	0.466	-0.214	3.935		4632	1.728	0.366	0.118	2.862
4476	1.847	0.556	0.356	2.786		4637	1.587	0.471	0.404	3.224
4479	1.785	0.481	0.467	3.022		4641	1.658	0.368	0.404	3.067
4482	1.767	0.498	0.338	3.151		4642.3	1.580	0.428	0.424	3.006
4494	1.708	0.499	0.288	2.515		4650	2.813	0.409	0.018	2.706
4497	1.587	0.502	0.232	3.162		4664	2.132	0.481	-0.118	2.662
4503	1.665	0.460	0.342	3.382		4665	1.705	0.399	-0.035	2.592
4509	1.798	0.520	0.091	2.697		4671	1.825	0.370	0.149	2.867
4515	1.882	0.498	0.383	3.244		4676	2.080	0.479	-0.278	3.005
4518	1.788	0.524	0.160	2.564		4683	2.113	0.432	-0.096	2.688
4526	2.228	0.666	-0.031	2.649		4685	1.995	0.421	0.015	2.406
4527	1.570	0.431	0.265	2.681		4689	1.863	0.415	0.222	2.805
4530	1.452	0.481	-0.142	4.663		4691	2.047	0.455	0.253	3.114
4533	1.577	0.545	0.518	3.441		4695	1.932	0.449	0.330	3.607
4539	1.707	0.424	0.461	3.000		4698	2.198	0.420	0.062	2.661
4542	1.682	0.424	0.329	3.347		4701	2.178	0.450	-0.154	3.702
4545	2.223	0.486	-0.024	2.835		4707.1	2.148	0.384	-0.035	2.855
4548	1.833	0.428	0.472	2.984		4710	2.225	0.363	0.024	2.602
4549	1.680	0.377	0.424	2.926		4716	2.192	0.362	0.074	2.730
4554	1.918	0.399	0.109	2.540		4722	2.147	0.405	0.131	2.933
4557	1.927	0.446	0.319	2.893		4725	2.228	0.366	-0.240	3.197
4562	1.812	0.436	0.301	2.981		4728	2.233	0.385	-0.382	3.439
4563	1.603	0.396	0.370	3.044		4731.1	2.592	0.486	0.056	2.755
4566	1.728	0.436	0.234	2.521		4731.8	2.378	0.364	-0.282	2.465
4569	1.742	0.403	0.259	3.264		4737	2.113	0.374	-0.275	2.858
4571	3.153	0.595	-0.015	2.771		4740	2.235	0.373	-0.338	3.810
4576	1.578	0.420	0.411	2.984		4749	2.292	0.352	-0.118	2.989
4579	1.543	0.429	0.617	3.856		4755	2.367	0.362	-0.072	2.718
4582	1.722	0.365	0.088	2.720		4758	2.417	0.359	-0.214	3.372
4584	1.755	0.384	0.292	2.714		4764	2.643	0.286	-0.180	3.098
4590.5	1.772	0.403	0.381	3.543		4769.2	3.513	0.450	-0.464	2.771
4591	1.703	0.439	0.418	3.169		4776	2.488	0.359	-0.134	3.014
4597.7	1.693	0.363	0.437	3.365		4777.5	3.405	0.390	-0.305	3.263

Table 2.3 Grain-size parameters in A1-NC186 using Friedman's (1962) equations.

Depth (ft)	5%	16%	25%	50%	75%	84%	95%	Mean size	Sorting	Skewness	Kg
4743	0.76	1.12	1.25	1.60	1.92	2.08	2.44	1.599	0.495	0.002	0.459
4834	1.11	1.52	1.63	1.92	2.25	2.38	2.65	1.939	0.446	-0.024	0.391
4875	0.86	1.21	1.40	1.78	2.14	2.29	2.46	1.758	0.513	-0.228	0.489
4895	1.04	1.19	1.31	1.62	1.87	1.97	2.29	1.590	0.384	0.026	0.288
4899.5	1.03	1.20	1.34	1.66	1.94	2.09	2.39	1.650	0.430	0.048	0.335
4908	1.03	1.25	1.43	1.73	2.01	2.20	2.44	1.730	0.451	0.000	0.331
4910	1.06	1.29	1.47	1.74	1.98	2.17	2.42	1.731	0.427	0.004	0.285
4920	0.85	1.11	1.23	1.53	1.80	1.90	2.10	1.513	0.383	-0.086	0.292
4926	1.05	1.25	1.41	1.76	2.12	2.29	2.50	1.766	0.480	0.034	0.417
4937	0.69	1.06	1.17	1.50	1.81	1.93	2.25	1.494	0.454	-0.057	0.409
4940	0.74	1.08	1.18	1.45	1.78	1.90	2.21	1.478	0.429	0.069	0.363
4947	0.60	0.99	1.10	1.40	1.79	1.95	2.32	1.447	0.499	0.158	0.483
4951	1.01	1.19	1.33	1.67	1.96	2.13	2.40	1.661	0.447	0.047	0.358
4954	1.01	1.12	1.20	1.45	1.75	1.87	2.06	1.476	0.346	0.126	0.234
4965	1.03	1.17	1.29	1.60	1.90	2.01	2.35	1.594	0.411	0.116	0.331
4975	1.00	1.13	1.23	1.51	1.80	1.91	2.20	1.517	0.377	0.114	0.282
4982	0.64	1.03	1.12	1.38	1.71	1.84	2.00	1.417	0.408	-0.046	0.325
4991.5	0.59	0.85	1.03	1.28	1.56	1.75	1.98	1.291	0.435	0.028	0.302
4995	2.04	1.27	2.46	2.73	2.99	3.19	3.46	2.397	0.694	-0.941	0.307
5008	1.16	1.53	1.65	1.96	2.27	2.38	2.57	1.956	0.424	-0.132	0.358
5183	1.35	1.63	1.76	2.08	2.34	2.43	2.69	2.048	0.401	-0.127	0.314
5198	1.56	1.79	2.99	2.21	2.42	2.49	2.82	2.163	0.366	-0.065	-0.295
5204	1.52	1.76	1.96	2.23	2.49	2.66	2.89	2.220	0.431	-0.061	0.293
5411	1.16	1.55	1.67	1.99	2.28	2.39	2.60	1.976	0.428	-0.186	0.364
5425	1.13	1.53	1.66	2.01	2.29	2.39	2.55	1.977	0.430	-0.301	0.368
5436	1.43	1.68	1.83	2.14	2.38	2.47	2.79	2.096	0.404	-0.104	0.308

Table 2.4 Grain-size parameters in H27-NC115 using the Folk and Ward (1957) equations.

Depth (ft)	Mean size	Mean D	Sorting	Skewness	Kg
4743	1.627	0.000	2.331	0.002	0.006
4834	1.938	0.000	1.870	-0.002	0.010
4875	1.770	0.000	2.346	-0.003	0.005
4895	1.625	0.000	1.252	0.005	0.017
4899.5	1.680	0.000	1.684	0.005	0.011
4908	1.750	0.000	1.767	0.001	0.009
4910	1.753	0.000	1.517	0.003	0.012
4920	1.528	0.000	1.300	0.001	0.018
4926	1.792	0.000	2.091	0.003	0.006
4937	1.512	0.000	1.807	0.002	0.009
4940	1.492	0.000	1.608	0.002	0.012
4947	1.460	0.000	2.309	0.002	0.005
4951	1.682	0.000	1.778	0.002	0.008
4954	1.498	0.000	1.175	0.015	0.025
4965	1.632	0.000	1.535	0.007	0.011
4975	1.542	0.000	1.391	0.006	0.018
4982	1.418	0.000	1.608	0.003	0.013
4991.5	1.310	0.000	1.614	0.005	0.011
4995	2.753	0.000	1.783	0.002	0.010
5008	1.962	0.000	1.577	-0.001	0.010
5183	2.067	0.000	1.347	-0.003	0.015
5198	2.202	0.000	1.118	-0.002	0.025
5204	2.233	0.000	1.531	-0.004	0.012
5411	1.980	0.000	1.654	-0.002	0.011
5425	1.975	0.000	1.702	-0.006	0.010
5436	2.127	0.000	1.415	-0.003	0.015

Table 2.5 Grain-size parameter in H27-NC186 using Friedman's (1962) equations.

problems in the analysis of grain-size distributions is that the same sedimentary processes occur within a number of different environments and consequently textural

response is similar. Comparison of grain-size curves and the interpretation of separate populations are aided by the use of log-probability plots (Visher, 1969). It has been established that many size distributions show marked discontinuities, particularly when plotted as cumulative size distributions on log arithmetic probability paper. Sindowski (1957) and Visher (1969) have suggested that, in many cases, it seems possible to dissect the curve into a limited number of straight-line segments, suggesting that the whole population is actually composed of a number of different truncated Normal distributions. Visher (1969) and other authors have interpreted these segments of the cumulative curve as identifying subpopulations of grains moved by different mechanisms of sediment transport (Middleton, 1976). Comparisons with Visher's interpretations clearly show that marine sand is the dominant sand in A1-NC186 and H27-NC115. Also the steeper the probability curve the more well-sorted the sediment, as shown in **Fig. 2.2** (Robert Cadigan, 1961). Although the grain-size textural parameters are algebraically defined, so that they are geometrically independent, a significant trend may exist in a given set of samples between any two textural parameters plotted as a scatter diagram. These trends can reveal pertinent and interesting geological information not evident in individual frequency distributions of the size parameters (Hubert, 1963). In recent years various sedimentologists have published conflicting opinions on the environmental sensitivity of textural parameters (mean diameter, standard deviation, skewness and kurtosis) calculated from the grain-size analysis of modern beach, river, and aeolian sands.

Friedman (1967) also demonstrated that a plot of standard deviation vs. mean size and standard deviation vs. skewness were particularly effective in differentiating between beach and river sand. **Figures 2.3 and 2.4** show Friedman's plots. To better understand the geological significance of the different grain parameters used in this study, a standard deviation verses mean-size plot, and standard deviation verses skewness plot are shown in **Figs. 2.5 and 2.6**. Comparison with Friedman's plots, show that the Hawaz grain-size data plots from wells A1-NC186 and H27-NC115 fall clearly in the shallow marine sandstone (beach sandstone) field, which supports the interpretation, based on their lithofacies characteristics presented in Chapter 3. The last discriminator in this study is the plot of mean size versus standard deviation. The skewness versus standard deviation is less sensitive with some 15% of the data points falling in the river sand land.

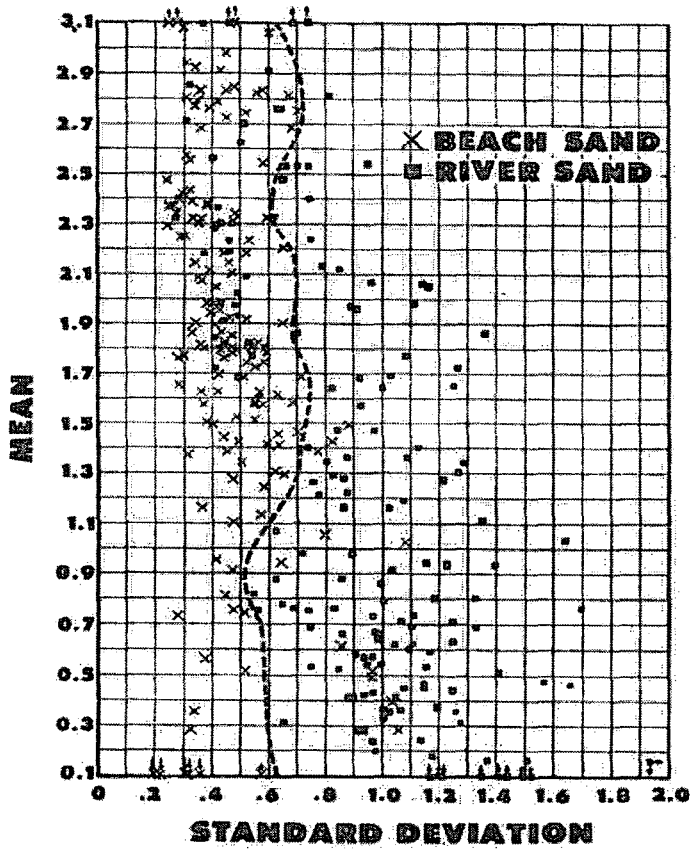

Fig. 2.3. Plot of mean versus standard deviation (Friedman, 1967).

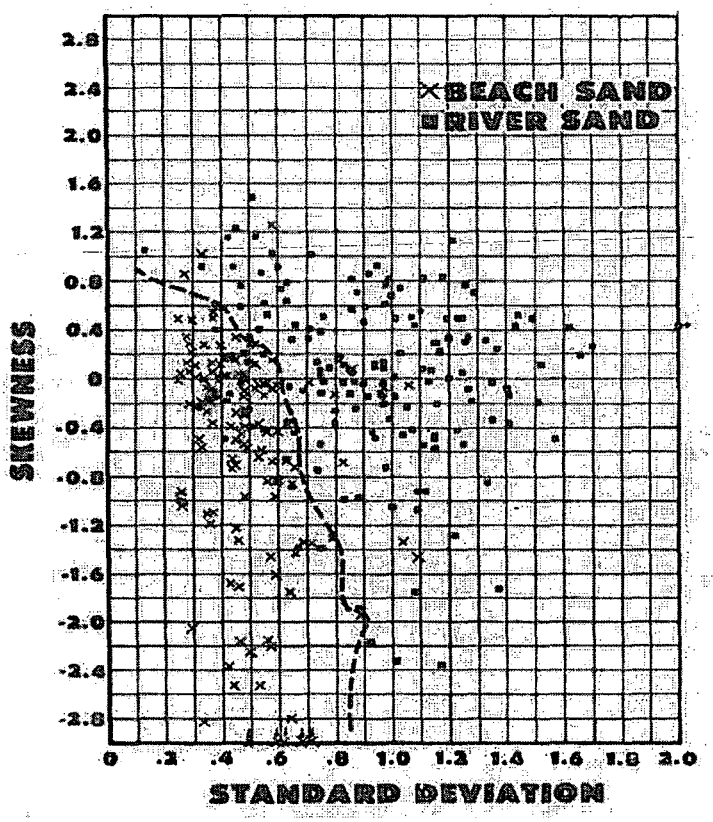

Fig. 2.4. Plot of third moment (skewness) versus standard deviation (Friedman, 1967).

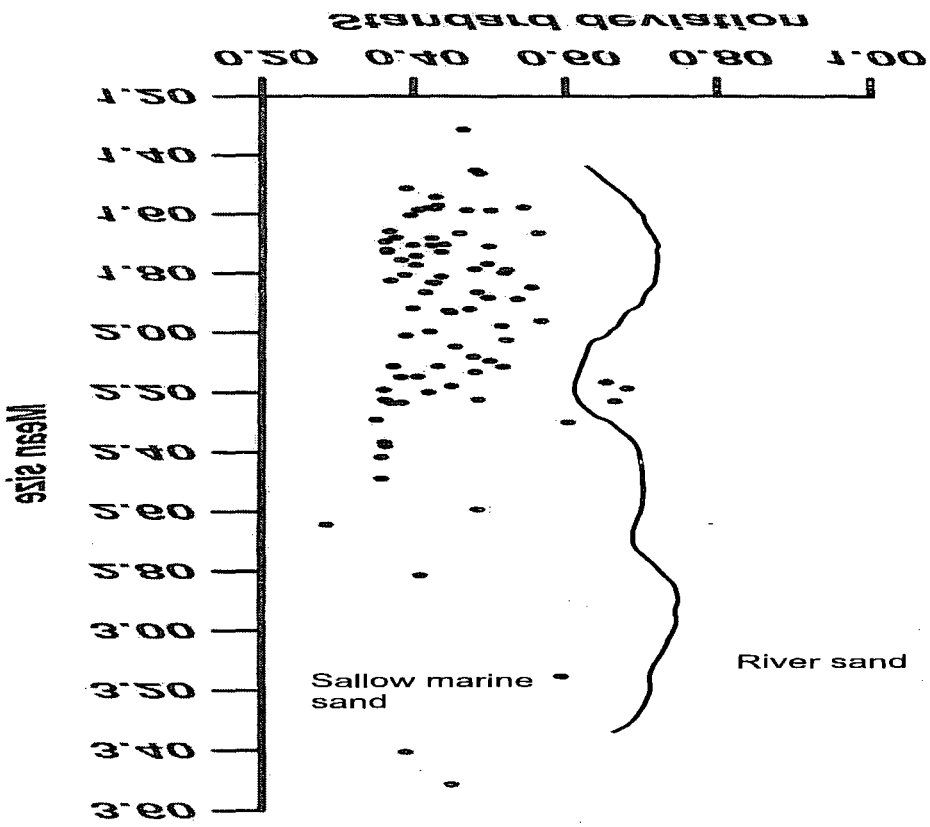

Fig. 2.5. Plot of mean-size versus standard deviation in A1-NC186.

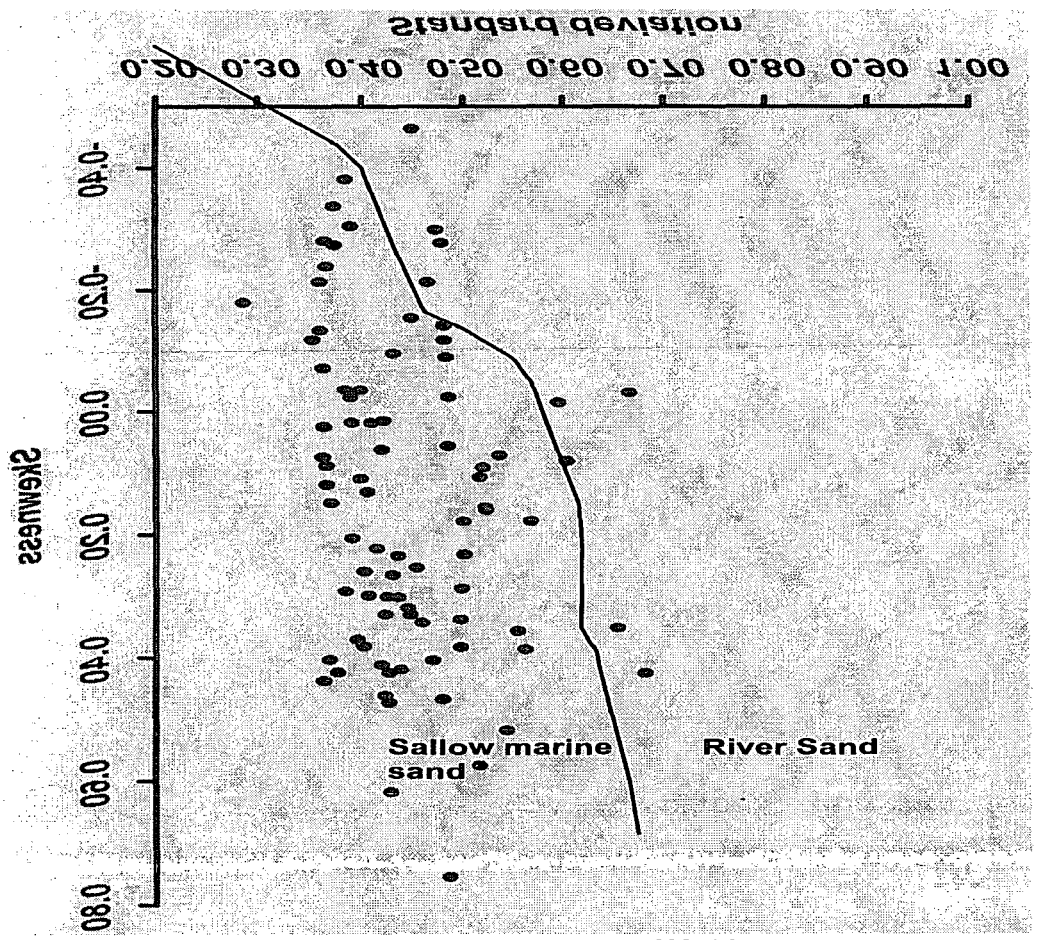

Fig. 2.6. Plot of standard deviation versus skewness in A1-NC186.

2.6 Roundness

Roundness is an estimate of the smoothness of the surface of a grain. Roundness may be quantified as the ratio of the mean radius of curvature of the grain corners to the radius of the largest inscribed circle (Leeder, 1982). Shape and roundness are the properties of sand grains that have significance for the study of the effect of the transport process on the debris furnished by the source area. These properties reveal the modification of angular grains of many shapes by abrasion, solution, and current sorting (Pettijohn et al., 1987). Roundness was first defined by Wentworth (1919) as "the average radius of the sharpest corner to the radius of the largest inscribed circle". This definition was modified by Wadell (1932) who proposed that it should be the ratio of the average radius of all the corners and edges to the radius of the largest inscribed circle (Selley, 1988). Russell and Taylor (1937) draw up comparative tables with 5 different degrees of the classes of roundness for the comparative determination of roundness (**Table 2.6,** Muller, 1967). Powers (1953) defined six roundness grades instead of five in such a way that the class limits closely approximate a geometric scale (very angular, angular, sub angular, sub rounded, rounded and well rounded). All such studies have shown that roundness increases with distance of travel most rapidly at first and then more slowly (Pettijohn, 1975). The roundness of a particle depends upon the sharpness of the edges and corners. It is independent of the shape. Roundness is a physical property of all sediments, and needs to be described. Where fossils are absent from a sedimentary layer it may prove useful in determining the environment of deposition (Powers, 1953). Although, round overgrowths are decisive evidence of multicycle grains, they are usually so small in number as to be impractical for graphic mapping. Multicycle grains are easiest to recognize with cathode-luminescence (Sippel, 1968). The term roundness, however, has been used or misused in the literature and in many cases has been used interchangeably with shape (Russell and Taylor, 1937).

When a particle of sand-size is transported from one site to another, some reduction in size occurs. The roundness and sphericity of the particles also change. These changes are due partly to abrasion, but apparently are caused by selective transport, which tends to segregare grains on the basis of density, size, and roundness (Plumley, 1948).

Degree of roundness Russel-Taylor-Pettifohn	Degree of roundness Wadell	Geometrical mid-point approximateed
Angular	0-0.15	0.125
Sub angular	0.15-0.25	0.200
Sub rounded	0.25-0.40	0.315
Rounded	0.40-0.60	0.500
Well-rounded	0.60-1.00	0.800

Table 2. 6. Degree of roundness for the descriptive characterisation of roundness (after Russell, et al. 1978).

Small particles show less tendency to become rounded, and grains of the same mineralogy are likely to show the same shape and roundness after a certain distance of transport (Dapples et al., 1953). According to Pettijohn (1957) "the roundness of sand is probably correlated with its mineralogical maturity, in that the high purity sands are generally the best rounded, and the immature sands less rounded or angular.

Roundness values throughout the Hawaz sandstone for A1-NC186 and H27-NC115 were estimated from thin section by comparison with the visual roundness chart of Pettijohn (1987) by determining the roundness of 300 grains per thin section (**Tables 2.7 and 2.8**). According to the descriptive characterization of roundness (Pettijohn et al., 1987) the Hawaz Formation contains mostly subrounded to subangular grains with individual grains showing the affects of abrasion (**Figs. 2.7, 2.8 and Tables 2.7, 2.8**). The abrasion and roundness of sand in the Hawaz sandstone is related to maturity, according to Nichols (1999) rounded to angular values are regarded as evidence of texturally mature sandstone.

Depth (ft)	Well rounded	Rounded	Subrounded	Subangular	Angular	Interpretation
4412	0	7.3	55.3	33.6	3.6	SR-SA
4415	0	6.3	46	37.3	10.3	SR-SA
4418	0	0.6	38.6	37.3	23.3	SR-SA
4421	0	4.3	52.3	34.6	8.6	SR-SA
4427	0	0.3	35	43	21.6	SA-SR
4433	0	13.3	50.3	23.6	12.6	SR-SA
4442	0	4	55.6	23.6	16.6	SR-SA
4446	0	0.3	35	40.3	24.3	SA-SR
4463	0	0.3	26	41	32.6	SA-A
4464	0	1.3	28	48.6	22	SA-SR
4476	0	5	35	46	14	SA-SR
4479	0	0.3	35	48	16.6	SA-SR

Table 2.7 Degree of roundness, based on the descriptive characterization of roundness (After Russel et al., 1978) for the Hawaz Formation, A1-NC186.

Depth (ft)	Well rounded	Rounded	Subrounded	Subangular	Angular	Interpretation
4482	0	5.3	43	38.3	13.3	SR-SA
4494	0	3	33	45.3	18.6	SA-SR
4497	0	5.3	44.3	40	10.3	SR-SA
4503	0	2.3	48	40.6	9	SR-SA
4509	0	12.3	40.3	34.6	12.6	SR-SA
4515	0	4.6	59	27.6	8.6	SR-SA
4518	0	3	64	25	8	SR-SA
4526	0	0.3	46.3	25.3	28	SR-SA
4527	0	1	60	30.6	8.3	SR-SA
4530	2.3	25	55	17.3	0.3	SR-SA
4533	0	26	52.3	18.6	3	SR-SA
4539	0	31.3	50.3	18.3	0	SR-SA
4542	0	10.3	59.6	27	3	SR-SA
4545	0	0.6	49.6	27.6	22	SR-SA
4548	0	0.3	47.6	32.3	19.6	SR-SA
4549	0	1.3	48	28.6	22	SR-SA
4554	0	0	28.6	39.6	31.6	SA-A
4557	0	0	27.3	31	41.6	A-SA
4562	0	0.3	37.6	34.6	27.3	SR-SA
4563	0	7	41.3	29.3	22.3	SR-SA
4566	0	11.3	39.3	38.6	10.6	SR-SA
4569	0	19	45	30	6	SR-SA
4571	0	1	22.6	28	48.3	A-SA
4576	0	5.6	37.3	36	21	SR-SA
4579	0	3.3	49.3	38.3	9	SR-SA
4582	0	12.3	52.3	28.6	6.6	SR-SA
4584	0	2.3	55.3	27.3	15	SR-SA
4590.5	0	2	42.3	33.3	22.3	SR-SA
4591	0	40.3	34.6	16.6	8.3	R-SR
4597.7	0	30	35.3	23	11.6	SR-R
4601.6	0	12.6	42.3	34.3	10.6	SR-SA
4603.5	0	15.3	35.3	29.6	19.6	SR-SA
4607	0	24.6	35.6	24	15.6	SR-SA
4609	0	23.6	39	25.6	11.6	SR-SA
4612	0	24.3	44.6	20.6	10.3	SR-R
4614	0	8.3	34.6	37.6	19.3	SA-SR
4618	0	4	42	34	20	SR-SA
4629	0	5	31	35.6	28.3	SA-SR
4632	0	0	51	35.3	13.6	SR-SA
4637	0	0	46	35	19	SR-SA
4641	0	0	48.6	36.6	14.6	SR-SA
4642.3	0	7.6	39.3	36.6	16.3	SR-SA
4650	0	3	24.6	38.6	33.6	SA-A
4664	0	0	20.6	49.6	29.6	SA-A
4665	0	7.6	46	33.3	13	SR-SA
4671	0	6.3	46.3	38.3	9	SR-SA
4676	0	0	15	49	36	SA-A
4683	0	3	46	41.3	9.6	SR-SA
4685	0	7	43.3	36.6	13	SR-SA
4689	0	1	35	40.3	23.6	SA-SR
4691	0	0.3	28.6	40.3	30.6	SA-A
4695	0	1	32.6	36	30.3	SA-SR
4698	0	0	34	37.6	28.3	SA-SR
4701	0	0.3	24	46.3	29.3	SA-A
4707.1	0	0.3	28.3	37.6	33.6	SA-A
4710	0	0	18.6	36.6	44.6	A-SA
4716	0	0	19.3	36	44.6	A-SA
4722	0	0	12.6	39.6	47.6	A-SA
4725	0	0	25.3	40.6	34	SA-A
4728	0	0	23.6	42.6	33.6	SA-A
4731.1	0	0.6	26.6	35	37.6	A-SA
4731.8	0	0	13	45.6	41.3	SA-A
4737	0	0	34.6	38.3	27	SA-SR
4740	0	0.3	21.6	44.3	33.6	SA-A
4749	0	0	23.6	41.6	34.6	SA-A

Continued Table 2.7.

Depth (ft)	Well rounded	Rounded	Subrounded	Subangular	Angular	Interpretation
4755	0	0	26.6	34.6	38.6	A-SA
4758	0	0.3	18.3	39.6	41.6	A-SA
4764	0	0	15.6	35.6	48.6	A-SA
4776	0	0	15.6	32.6	51.6	A-SA
Average	**0.03**	**5.88**	**37.58**	**34.79**	**21.59**	**SR-SA**

Continued Table 2.7.

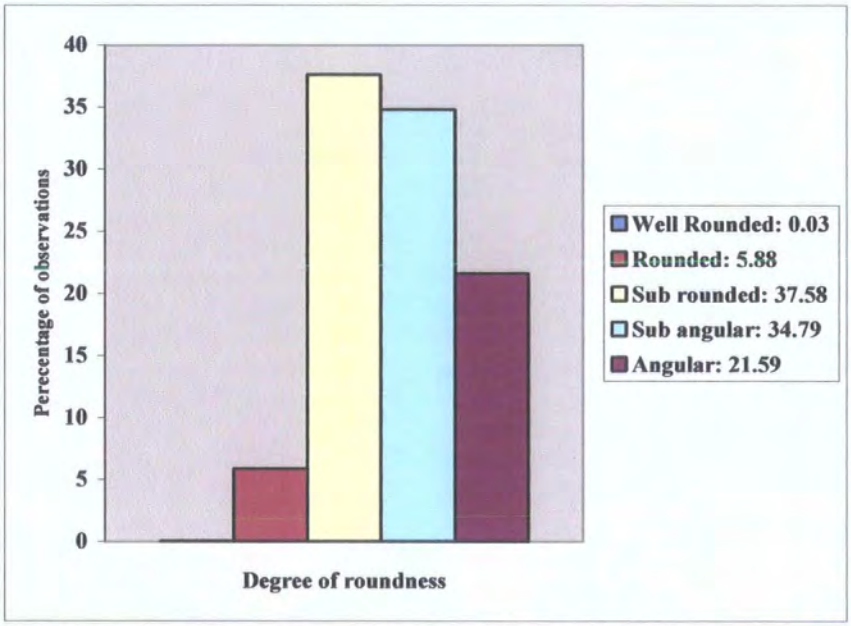

Fig. 2.7. Histogram of roundness of the Hawaz Formation, A1-NC186.

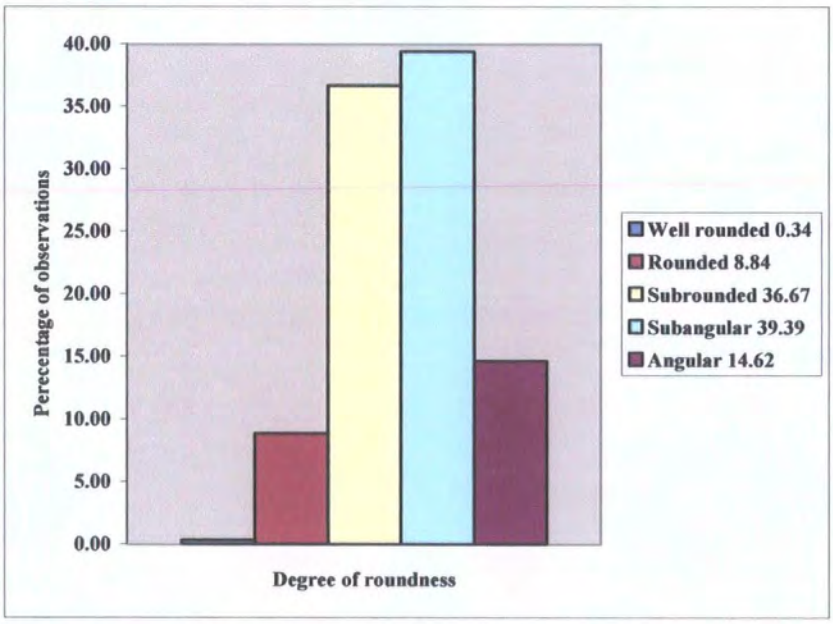

Fig. 2.8. Histogram of roundness of the Hawaz Formation, H27-NC115.

Depth (ft)	Well rounded	Rounded	Subrounded	Subangular	Angular	Interpretation
4743	0.3	10	35.3	35.3	19	SR-SA
4834	0	1.6	21.6	49.6	27	SA-A
4875	0	4.6	25	45.6	24.6	SA-SR
4895	0	9.6	44.3	35.6	10.3	SR-SA
4899.5	0	15.3	44.3	33.3	7	SR-SA
4908	0	7.6	38.6	38.3	15.3	SR-SA
4910	0	1.3	30.6	46.6	21.3	SA-SR
4920	0	0	32	58.6	9.3	SA-SR
4926	0	0.3	18	49.6	32	SA-A
4937	1	19	44	31.6	4.3	SR-SA
4940	2.3	21.6	44	30.6	1.3	SA-SR
4947	0	14.6	45	37	3.3	SR-SA
4951	0	13	45.3	36.3	5.3	SR-SA
4954	3	24.6	47.3	23.6	1.3	SR-R
4965	0	13	46.6	37.6	2.6	SR-SA
4975	2	28.3	47.3	20.3	2	SR-R
4982	0	22	44.3	29.6	4	SR-SA
4991.5	0	2	38.3	43	16.6	SA-SR
4995	0	0.3	15	47.3	37.3	SA-A
5008	0	0.3	35	39	25.6	SA-SR
5183	0	1	27	49.6	22.3	SA-SR
5198	0	0.6	34.3	41.3	23.6	SA-SR
5204	0	0	26.6	42.6	30.6	SA-A
5411	0.3	9	44	37	9.6	SR-SA
5425	0	6.6	44.3	38.6	10.3	SR-SA
5436	0	3.6	35.3	46.6	14.3	SA-A
Average	**0.34**	**8.84**	**36.67**	**39.39**	**14.62**	**SA-SR**

Table 2. 8 Degree of roundness, based on the descriptive characterization of roundness (After Russel et al., 1978) for the Hawaz Formation, H27-NC115.

3. Sedimentology

3.1 Introduction

Sedimentation, through the construction of its root and suffix, is a noun of action or act of doing. Geologically it means the act or process of depositing sediment, and without needlessly changing the prior accepted definitions of the two parts of the word it can mean nothing else. The word sedimentology encompasses not only the material itself and its deposition, but also its genesis, transportation, diagenesis, geochemistry, physics, and statistics applicable to its existence (Alan Lohse, 1951).

3.2 Facies Analysis

Facies is a Latin word meaning face, figure, appearance, aspect, look, condition. It signifies not so much a concrete thing, as an abstract idea. The word was introduced into the geological literature by Nicolaus Steno (1669) for the entire aspect of a part of the Earth's surface during a certain interval of geologic time (Curt Teichert, 1958). The word facies is now used in both a descriptive and an interpretive sense. Descriptive facies include lithofacies and biofacies, both of which are terms used to refer to certain observable attributes of sedimentary rock bodies that can be interpreted in terms of depositional or biological processes (Miall, 1984). The setting in which sediment accumulates is familiar as geomorphological entities such as rivers, lakes, coasts, shallow seas, and so on. One of the goals of sedimentary geology is to determine the environment in which any given succession of sedimentary rocks accumulated (Walker et. al, 1992; Reading and Levell, 1996). The facies concept is not just a convenient means of describing rocks and grouping sedimentary rocks seen in the field, it also forms the basis for the interpretation of strata. The lithofacies characteristics result from the physical and chemical processes which were active at the time of deposition of the sediments, and the biofacies and ichnofacies provide information about the palaeoecology during and after deposition (Gary Nichols, 1999).

3.3 Facies models

The primary goal of facies analysis is to produce a facies model which is in effect a hypothesis about the environments signified by the rocks and fossils under study (Hallam, 1981). Johannes Walther in 1893 was the first to thoroughly describe the relationship between time equivalency and lithologic equivalency. He determined that a vertical succession of strata would be formed by the lateral migration of adjacent environments containing the original sediments that eventually became rocks (Fritz and Moor, 1988).

3.4 Sedimentary Facies in the Hawaz Formation

The analysis of sedimentary facies of the Hawaz Formation is based on lithology, grain-size, sedimentary structures and biogenic feature seen in core section and wireline logs. Many of the facies described are very similar to one another and are differentiated in some cases on subtle differences in texture and biogenic features. This chapter describes and interprets the facies in two type wells, A1-NC186 and H27-NC115. Most of the samples used for this study are from well A1-NC186 (84 samples) which have been cut into thin sections, with H27-NC115 providing 26 samples which have also been thin-sectioned. In addition 7 thin-sections were provided by Repsol for H27-NC115 (**Table 3.1**).

The following facies have been recognized and are described below, based on detailed description and analysis of both the colour photographs of the slabbed core and e-logs.

3.4.1 Facies (A): Burrowed sandstone facies

Description. This facies forms the bulk of the cored section and consists largely of burrowed sandstone interbedded with thin, burrowed muddy sandstone. This facies is represented by the cored interval from 4412 ft to 4540 ft and from 4689 ft and 4725 ft in type well A1-NC186, and from 4720 ft to 4729.5 ft, 4743 ft to 4832 ft, 4870 ft to 4892 ft, 4926 ft to 4953 ft and 4511 ft to 4536 ft in type well H27-NC115.

Well name	Core No.	Top ft	Bottom ft	Recovery ft	Recovery %	Samples depth
A1-NC186	1	4412	4440			4412, 4415, 4418, 4421, 4427.
	2	4440	4494			4433, 4442, 4446, 4463, 4464, 4476, 4479, 4482.
	3	4494	4550			4494, 4497, 4503, 4509, 4515, 4518, 4526, 4527, 4530, 4533, 4539, 4542, 4545, 4548, 4549.
	4	4554	4614			4554, 4557, 4562, 4563, 4566, 4569, 4571, 4576, 4579, 4582, 4584, 4590.5, 4591, 4597.7, 4601.6, 4603.5, 4607.5, 4609, 4612, 4613.5.
	5	4614	4674			4554, 4557, 4562, 4563, 4566, 4569, 4571, 4576, 4579, 4582, 4584, 4590.5, 4591, 4597.7, 4601.6, 4603.5, 4607.5, 4609, 4612, 4613.5.
	6	4674	4732.5			4676, 4683, 4685, 4689, 4691, 4695, 4698, 4701, 4707.1, 4710, 4716, 4722, 4725, 4728, 4731.1, 4731.8.
	7	4734	4777.5			4737, 4740, 4749, 4755, 4758, 4764, 4769.2, 4776, 4777.5.
H27-NC115	3	4707	4709.3			
	4	4713	4768.3			
	5	4771	4832.75			
	6	4833	4892.3			
	7	4893	4953			4908, 4920, 4926, 4937, 4947, 4951.
	8	4953	4967			4954, 4965.
	9	4972	5020			4982, 4991.5, 5008, 5020.
	10	5177	5206.25			5183, 5198, 5204.

Table 3.1 Core samples used in this study from type wells A1-NC186 and H27-NC115 showing the cored intervals and core sample depths.

This facies is dominated by vertical burrowing which passes through beds and destroys most internal sedimentary structures (Vos, 1981). Turner (2002) describes the upper part of the Hawaz succession as consisting predominantly of intensely rippled and vertically burrowed fine-grained, thinly bedded, well-sorted white sandstone. This facies can be divided in to two subfacies.

3.4.1.1 Subfacies (A1): Burrowed and bioturbated fine-grained sandstone subfacies

This subfacies occurs in the lower part of type well A1-NC186, between 4665-4730 ft, 4732-4950 ft, and between 4511 ft to 4536 ft in type well H27-NC115 (**Fig. 3.1**). It comprises fine-grained, pale grey to brownish sandstone, depending on clay content. Where it contains more clay the colour is light grey whereas in other intervals the colour is brownish. The sandstone is well-sorted, containing angular-subrounded grains, and is characterized by burrows and local bioturbation (10-40%), most notably *Skolithos*, *Cruziana* and *Diplocraterion*. The burrows are from 2-5 mm in diameter, and up to 4cm long, including horizontal burrows such as *Paleophycus*, *Planolites* and rare *Thalassinoides*. Bedding is poorly defined or where defined it as thinly bedded, with stylolitic mudstone partings defining bed boundaries. The content of mud in this subfacies is more than in the upper burrowed sandstone subfacies.

This subfacies is overlain by the heterolithic facies and underlain gradually by the burrowed heterolithic facies.

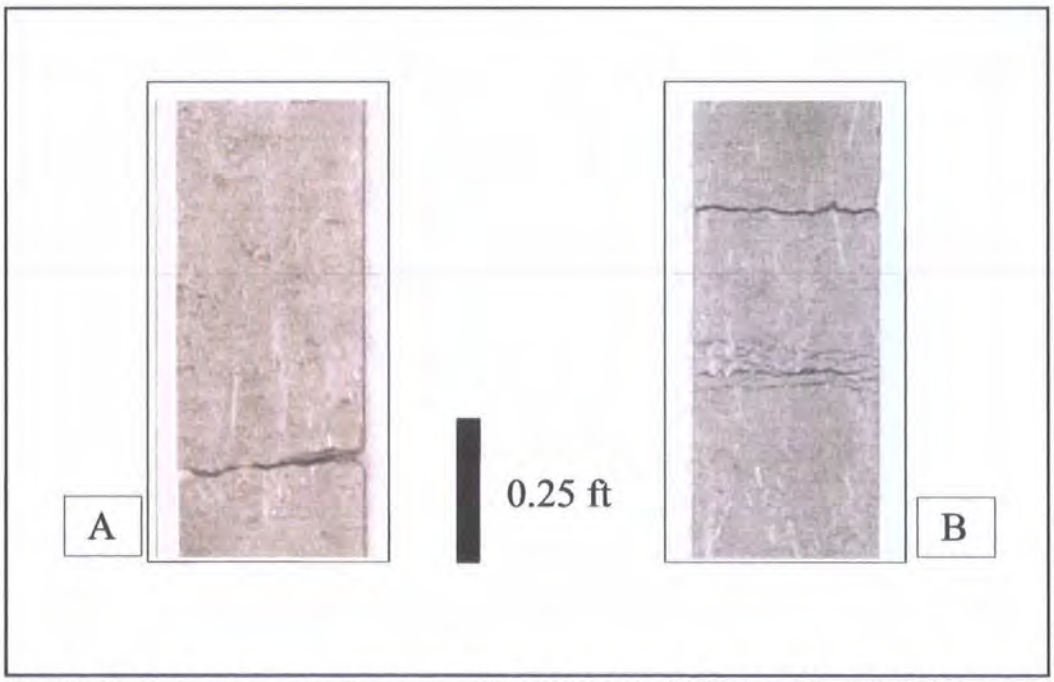

Fig. 3.1. Slabbed core samples from type well A1-NC186 (A at 4705 ft and B at 4715 ft) showing burrowed and bioturbated fine-grained sandstone subfacies.

3.4.1.2 Subfacies (A2): Burrowed and bioturbated fine to medium-grained sandstone subfacies

This subfacies is the most abundant in the cored section of the Hawaz Formation in A1-NC186 and H27-NC115. It occurs in the upper part of the cored section between 4412 ft to 4540 ft and 4605 ft to 4626 ft in type well A1-NC186, and from 4720 ft to 4729.5 ft, 4743 ft to 4832 ft, 4870 ft to 4892 ft and 4926 ft to 4953 ft in type well H27-NC115 (**Fig. 3.2**). It is represented by burrowed, clean to argillaceous, medium dark-grey to olive grey micaceous sandstone. The dark colour indicates a significant amount of organic matter. The clean sandstone is medium to fine-grained, moderately well-sorted to well-sorted, with a predominance of subrounded to subangular grains. Bedding in this subfacies is absent or poorly defined by stylolitic, micaceous ripple cross-lamination and parallel lamination of the more clay-rich sandstone, depending on the intensity of burrowing and bioturbation. The sandstone is characterised by a high density of burrows (40-60%) using the diagram of Doser and Bottjer (1989), with the intensity of the burrowing decreasing with depth. The burrows range from 3-11mm in diameter, and in the bottom of this subfacies they are about 31cm long.

The argillaceous sandstone is intensely burrowed, dominated by *Siphonichnus*, *Diplocraterion* and long slender non-branched *Skolithos* burrows usually filled with fine-grained sediment. Horizontal burrows such as *Paleophycus Planolites* and rare *Thalassiniodes* also occur. Some local fining-upward and coarsening-upward trends can be recognised from the gamma well log response and grain-size trends. This facies has a poor reservoir quality due to its mud content.

Interpretation. The intense burrowing, presence of marine burrowing organisms, and ripple cross-lamination and parallel lamination, are consistent with deposition in a shallow water marine environment. Bottom conditions were ideal for colonisation by a variety of burrowing organisms, suggesting a well oxygenated environment supplied with nutrients, possibly from a nearby terrestrial input. The association of clean and dirty sandstones may reflect differing energy levels within the near shore environment, which is interpreted as a lower shoreface/nearshore shelf. The argillaceous sandstones are considered to represent normal background sedimentation interrupted periodically

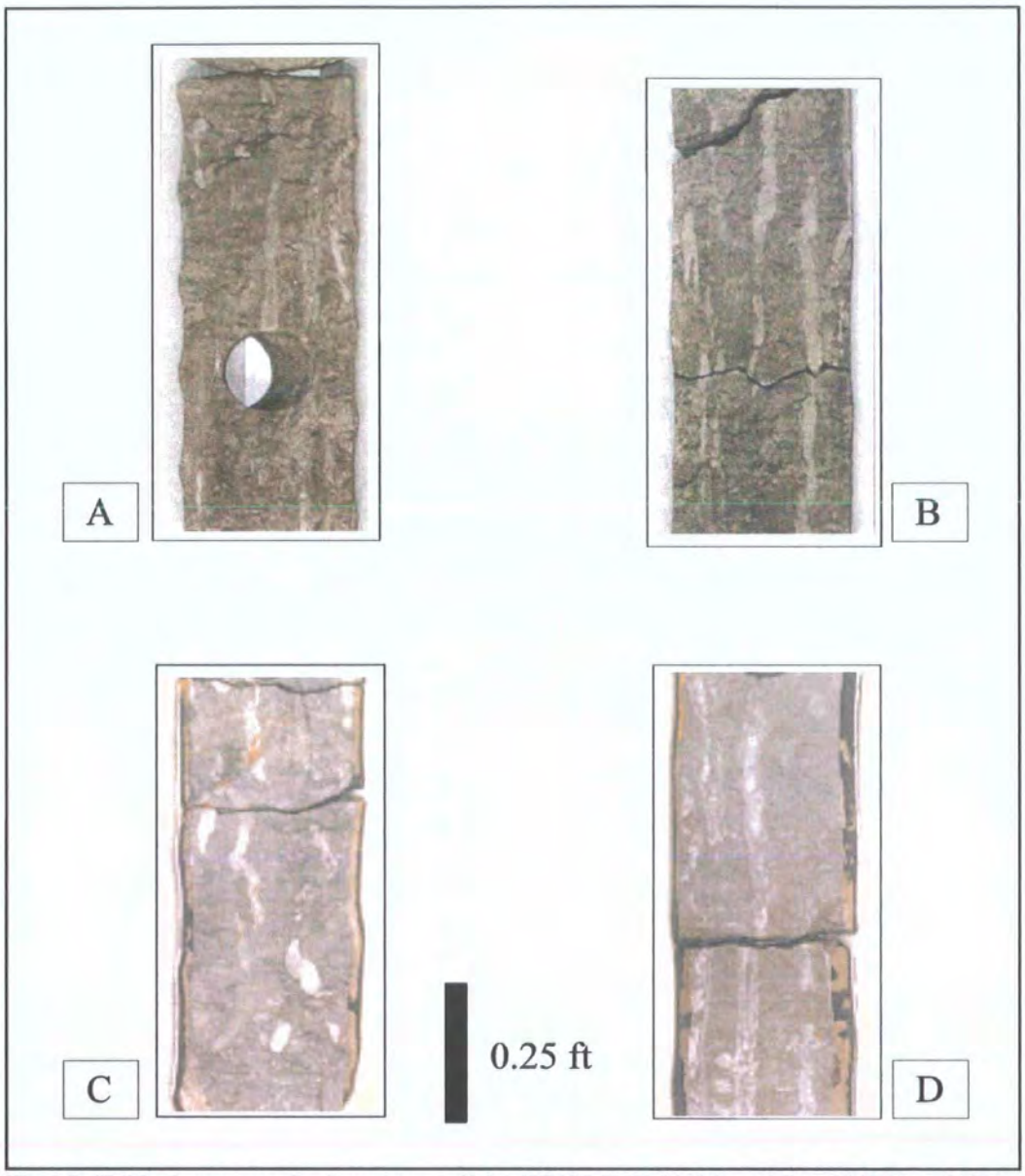

Fig. 3.2. Slabbed core samples from type well A1-NC186 (A at 4413 ft and B at 4445 ft) and H27-NC115 (C at 4723 ft and D 4759 ft) showing burrowed and bioturbated fine to medium-grained sandstone subfacies.

by higher energy events, possibly related to shelf storms or flooding from the land resulting in deposition of the more reworked, better-sorted cleaner sandstone.

The high density ichnofacies suggest deposition took place in a low energy fully marine environment. Skolithos is indicative of relatively high levels of wave or current energy, and typically is developed in slightly muddy to clean, well-sorted,

loose or shifting particulate substrates. The *Skolithos* ichofacies ordinarily grades landward into supratidal or terrestrial zones and seaward into the *Cruziana* ichnofacies. The *Cruziana* ichnofacies is most characteristic of subtidal, poorly sorted and unconsolidated substrates. Conditions typically range from moderate energy levels, in shallow waters below fair-weather wave base to low energy levels above storm wave base (**Fig. 3.3**) (Pemberton et al., 1992). The change from a *Cruziana* ichnofacies to a mixed *Skolithos-Cruziana* assemblage may be related to increasing energy and more proximal and unstable substrates, possibly resulting from relative sea-level falls (Oloriz Fredrico, 2000).

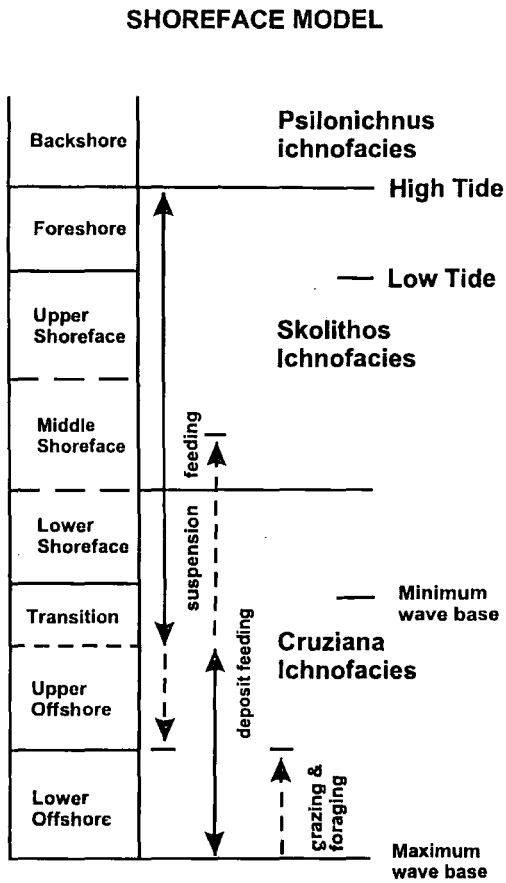

Fig. 3.3. Shoreface model for ichnofacies, based on facies observation in the Cretaceous interior seaway, western interior of North America (Frey et al. 1990).

3.4.2 Facies (B): Ripple cross-laminated sandstone

Description. This facies overlies the burrowed mudstone and sandstone facies at 4570 ft and the heterolithic facies at 4643 ft in A1-NC186. The middle part of this facies is intercalated with the cross-stratified facies C and D. This facies occurs at depths 4566-4568 ft and between 4620-4643 ft in well A1-NC186 (**Fig. 3.4**). It consists of

fine to medium-grained, light brownish grey sandstone. The sandstone is well-sorted to moderately well-sorted, clean to slightly argillaceous and micaceous. The sandstones which are quartz rich, with individual grains mostly subrounded to subangular, are locally interbedded with thin, micaceous mudstone. The sandstone is characterized internally by small-scale sets of ripple cross-lamination <3 cm thick, and rare sets of low angle cross-stratifaction. The core samples of this facies are not adequate to determine the geometry of the cross- stratification. At 4628 ft the cross-laminations is disrupted by burrows, most notably *Skolithos* and *Palaeophycus*.

Fig. 3.4. Slabbed core samples from well A1-NC186 at 4630ft, showing ripple cross-lamination.

Interpretation. For many years, two basic types of ripple mark were widely recognized, based on their planform geometry: symmetrical and asymmetrical. These have been interpreted generally as the products of wave action and current flow respectively (Tanner, 1967). Where waves alone are responsible for ripple generation, the stronger positive (normally shoreward) component of oscillation controls the ripple internal structure. Although this conclusion is based on samples from relatively shallow water, the water depths include the border between rippled and unrippled sand where the waves are just beginning to feel bottom (Newton, 1968). The argillaceous, micaceous nature of the sandstone, and ripple cross-lamination suggests

an environment swept by low energy currents promoting the formation of ripple-scale bedforms. Bedform formation was probably controlled mainly by bottom current velocities, down to normal wave base, which together with the high incidence of mud in these sediments and local burrowing suggest the possibility of a nearshore shelf environment, possibly distal to the low-angle, cross-bedded and high angle cross-bedded facies C and D. Some of the foreset irregularities are similar to intraset deformation features attributed to shear stress exerted on the top of the sandy bedforms, accompanied by pre-deformation sediment liquefaction. Campbell (1971) described similar low angle cross-laminations between parallel bedding surfaces as deposited in the surf zone bordering beaches.

3.4.3 Facies (C): Cross-bedded sandstone facies

Description. This facies occurs at 4559 ft for at least 22cm, 4563.5 ft for at least 17cm, 4566 ft for at least 19cm, 4593 ft, 4601 ft and 4605 ft in well A1-NC186, and at 4858-4861 ft, 4862.5-4865.8 ft, 4868.5- 4870 ft, 4909 ft, around 4964-4967 ft, 4974 ft and 4978-4982 ft, in well H27-NC115 (**Fig. 3.5**). It comprises light olive grey, fine to medium-grained, well-sorted, clean sandstone, dominated by subrounded to subangular grains, with occasional rounded grains. It is internally structured by small to medium-scale, high-angle planar, tabular cross-bedding (15°-25°), with individual foresets from 16cm to 40cm thick displaying thin <1mm thick stylolitic mud drapes. Some small sets (<5cm thick) of cross-lamination, locally disrupted by burrows, especially *Skolithos* burrows occur in A1-NC186 at 4418 ft and 4623.5 ft. Local borrowing occurs in A1-NC186 but in H27-NC115 burrows are absent or poorly defined. Some cross-bedded sets are underlain by an erosion surface or burrowed sandstone. This facies shows good permeability and porosity, the permeability ranges from 442.0md to 666.3md and the porosity ranges from 15% to 18% in well A1-NC186. In well H27- NC115 the permeability ranges from 324md to 784md and porosity from 13.1% to 20%.

Interpretation. The presence of well-sorted, fine to medium-grained, locally burrowed sandstone with small to medium-scale planar, tabular cross-bed sets is indicative of the development of two-dimensional dune bedforms, within a relatively high energy marine environment. Cross-beds are interpreted to represent lower-flow

regime sedimentation under unidirectional and/or combined-flow currents. The presence of burrowing and mud drapes suggests a possible tidal influence. Maximum current velocities during transport episodes for cross-beds were probably in the range of a few tens of cm/sec to 1m/s (**Fig. 3.6**) (Winn, 1991). The high angle of the forests suggests a high rate of bedload-dominated sediment supply to the dune slip face during migration, with most of the finer suspension load carried downcurrent beyond the slip face.

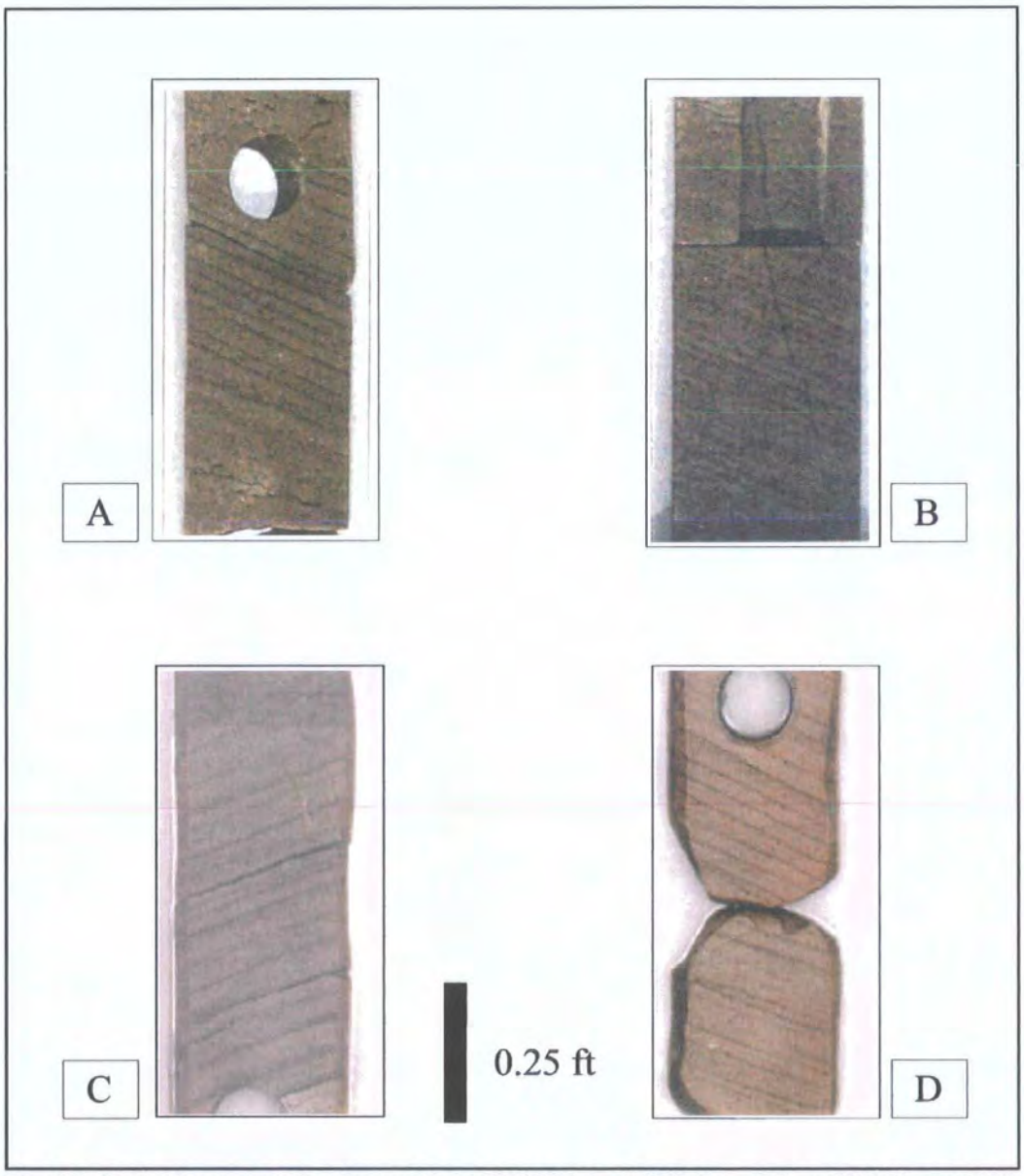

Fig. 3.5. Slabbed core samples from well A1-NC186 (A at 4563 ft, and B at 4566 ft) and H27-NC115 (C at 4858 ft and D at 4965 ft) showing cross-bedded sandstone of facies C.

Based on the relationship between dune bedform height and current strength documented by Allen (1982), current velocities of the order of 3 m^{s-1} may have been responsible for bedform generation and migration. Such high energy conditions are typically found in lower to middle shoreface, wave-dominated environments characterised by wave-generated two and three-dimensional bedforms, which differ in dimensions according to energy levels coming off the shelf. The *Skolithos* ichnofacies is typically found in high energy nearshore shallow water conditions associated with moving sands, and is consistent with a lower-middle shoreface interpretation. This facies has the highest poroperm values in the Hawaz Formation, and has good reservoir potential.

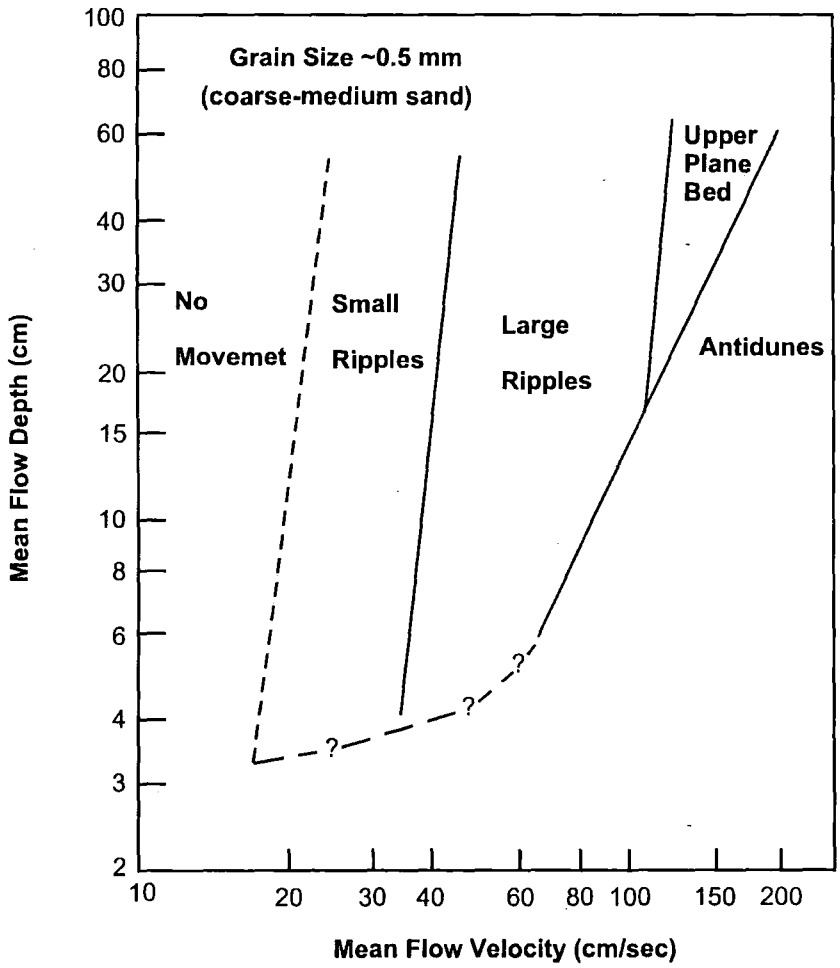

Fig. 3.6. Controls of flow regime by mean flow depth and mean flow velocity for a constant grain size of bed material, (After Fritz and Moore, 1988).

3.4.4 Facies (D): Low angle cross-bedded and planar-laminated sandstone facies

Description. This facies is well developed at 4564 ft and 4603 ft in type well A1-NC186, and between 3729.5-4741 ft in well H27-NC115. It comprises light brownish, fine-grained, moderately-sorted, clean sandstone, characterised by sets of low angle (<15°) cross-bedding, which vary in set thickness from 15 to 45cm, and less commonly low angle (5°) lamination, with stylolitic clay drapes. At 4564.5 ft, in well A1-NC186, the low angle cross-bedding occurs between slightly higher angle cross-bedding, and the angularity of the foresets increases upward. Foreset laminae are well defined and usually <10cm thick. Burrows are abundant in some intervals in well A1-NC186, especially at 4630 ft and 4632 ft. The base of this facies is sharply defined by an erosion surface at 4740.5 ft in well H27-NC115. Some of the low angle intersecting foresets could be part of large-scale hummocky cross-stratification (**Fig. 3.7**).

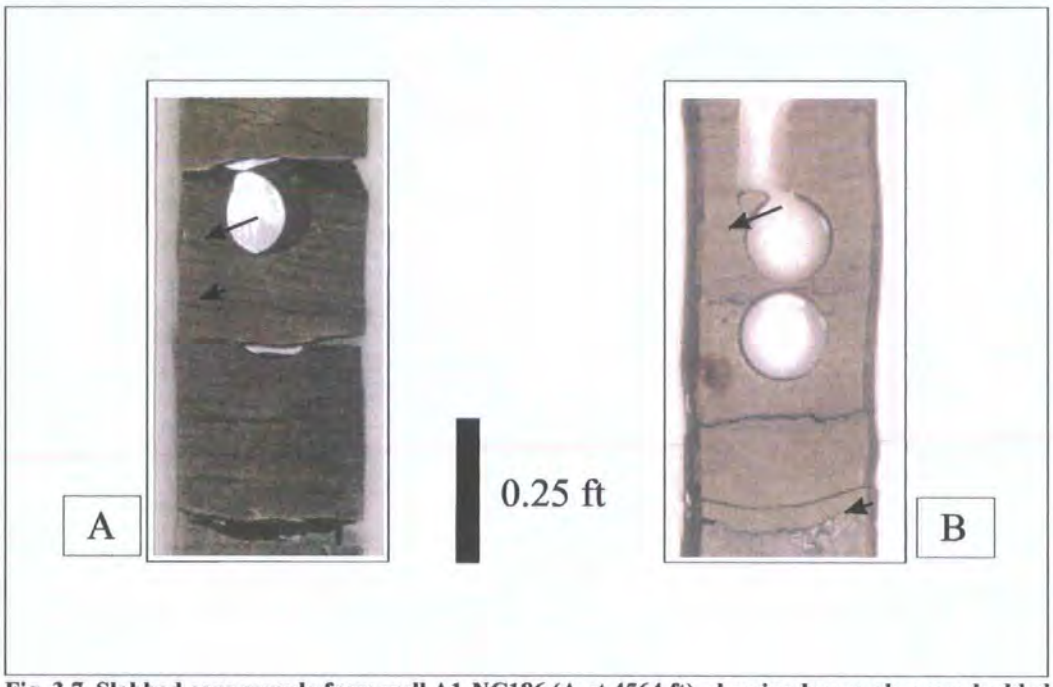

Fig. 3.7. Slabbed core sample from well A1-NC186 (A at 4564 ft), showing low angle cross-bedded sandstone (small arrow) and possible small-scale hummocky cross-stratification (large arrow), and well H27-NC115 (B at 4740 ft), showing low angle cross-bedded sandstone (large arrow) and the stylolites erosional base (small arrow).

Interpretation. The low angle, clay-draped foresets suggest that a significant component of suspension load was periodically supplied to the slip face of the dune bedforms, possibly during lower energy intervals (? slack water), such as reversing tides when clay and silt were released from the separation bubble or eddy system to the downstream slip face. Although there is no direct evidence of a strong tidal influence on deposition, it could account for the clay drapes on foresets. Most fines deposited in this way concentrate on the lower part of the slip face producing downward thinning, tangentially-based foresets. The low foreset angle suggests that the dune bedforms may have formed close to the dune-plane bed hydrodynamic boundary, as the dunes become washed out and foreset angles significantly decline. The low dip angles on many foresets may have been caused by the effect of wave action on a unidirectional current. Many low-dipping cross-beds are interpreted as a form of hummocky cross-stratification (Nøttvedt and Kreisa, 1987).

The localised presence of an erosion surface at the base of the facies could be indicative of channelisation, or a local, high energy event on the shoreface. This facies may be the distal facies equivalent of the high angle cross-bedded facies C, comparable with a landward shift from lower to middle-upper shoreface, along a transgressive coastline, concomitant with increased accommodation space.

3.4.5 Facies (E): Heterolithic facies

Description. This facies occurs between 4643-4646 ft, 4649.5-4664 ft and 4766.5-4777.5 ft in A1-NC186 well, and between 4985′-5020 ft in type well H27-NC115 (**Fig. 3.8**). It is the second most abundant facies in the Hawaz Formation in the study area and attains a thickness of about 9 meters. It typically comprises very thin to thin-bedded sandstone interbedded with thin beds of siltstone or micaceous black mudstone, the boundary between these lithologies showing subtle gradations in colour. The upper portion of this facies is dominated by thin to medium-bedded fine-grained sandstone, siltstone and mudstone. The sandstone is moderately well-sorted and contains mostly subrounded to subangular grains. It occurs either as individual beds, separated by interbeds of mudstone or siltstone, or as amalgamated lenticular beds with little or no finer sediment between them. Individual sandstone beds are 6cm thick, and predominantly fine to medium-grained, parallel laminated sandstone, with very

low angle ripple cross-stratification, bounded sharply by muddy siltstone. Trace fossils are abundant in the sandstone including *Skolithos* and *Planolites*.

The siltstone consists of thin to very thin-bedded, plane-laminated to rippled beds of fine sandstone rich in silt flakes, bounded by wavy to parallel bedding surfaces. The lower portion of this facies consists of carbonaceous grey-black mudstone, which is typically laminated or massive. Bioturbation is rare in these mudstones. Within this facies some sections comprise black silty mudstone with some parallel to rippled cross-laminated sandstone (4771, at A1-NC186), whereas in other places the sandstone section is thicker with cross-laminations (4776, at A1-NC186). The parallel lamination is disturbed by occasional burrows.

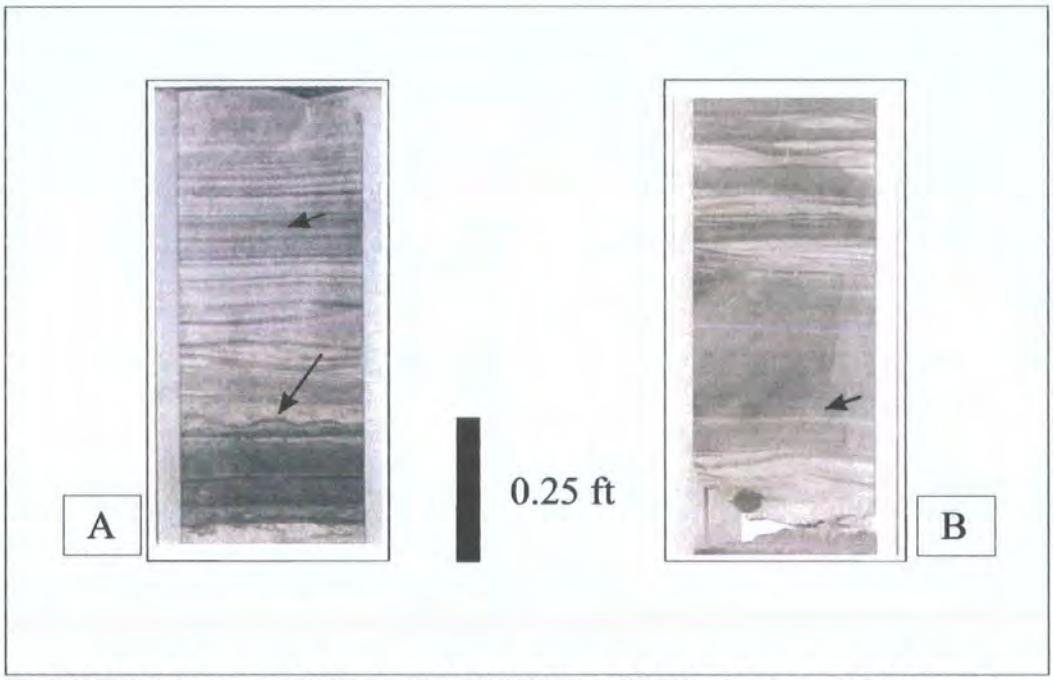

Fig. 3.8. Slabbed core sample from well A1-NC186 (A at 4653 ft), showing parallel to wavy cross-lamination (small arrow) and wavy or ripple drift cross-lamination (large arrow) and (B at 4771 ft), showing parallel to wavy cross-lamination sandstone in mudstone (arrow).

Interpretation. The position of this facies above the lower shoreface burrowed fine grained sandstone, and the marine fauna, indicate an offshore shelf receiving mainly fine-grained sediments. This facies is interpreted to have been deposited from suspension under low energy storm-influenced conditions, below fair weather wave base, in an open-marine inner-shelf environment. The genesis of several occurrences of laminated sand and silt in nature is not clearly understood. Most sand and silt layers

begin with a sharp base and mostly grade upwards into overlying mud layers. The sand layers are either evenly laminated or are developed as laminated rhythmites, in which the lower laminae are thicker and coarser grained and grade upwards into thinner and finer-grained laminae. The presence of escape burrows suggests that storm-sand layers and some of the accompanied mud layers were deposited rapidly. Storm and hurricanes are considered to be the main factors in the genesis of these laminated sands. (H. E. Reineck and Singh, 1972) (**Fig. 3.8**).

The dominance of shale and subordinate thinner siltstone and sandstone indicates a shelf receiving mainly fine-grained detritus (Turner, 1980). The laminations are composed of clay and silt, with smaller amounts of very fine-grained sand in the heterolithic siltstone, all deposited from suspension (Pedersen, 1985). Settling from suspension after storms appears to be the main process responsible for the sandy intercalations (De Raaf, et. al 1977). The upward decrease in thickness of finer grained interbeds through the facies as well as the upward increase in abundance of thicker sandstone beds indicates a progradational shallowing environment (Vos 1977) and decrease in accommodation space. In the shallower part of the shelf any sediment will be extensively reworked by wave processes. Sand deposited in these settings is texturally and (usually) compositionally mature with wave ripple cross-lamination and horizontal-stratification. Streaks of mud in flaser beds may have been deposited during intervals of lower wave energy in deeper water further offshore (Gary Nichols, 1999). Johnson (1977) interpreted this type of facies as a very low energy facies, in which two hydraulic regimes were present. Low energy periods are represented by deposition of silt layers from suspension, whilst high energy conditions were marked by the introduction of sand layers, also from suspension since there is an absence of current-formed structures. During these higher energy periods oscillatory wave motions were the dominant process (Johnson, 1977).

Formation of sandstone and shell beds is attributed mainly to storm wave surge currents. Individual beds probably record a single event of storm turbulence with resuspension of sand from the shelf floor, followed by sand deposition from suspension, with wave surge currents causing ripple-drift and ripple cross-lamination, as well as hummocky cross-bedding (Vos, 1977).

3.4.6 Facies (F): Burrowed heterolithic sandstone facies

Description. This facies comprises centimetre to decimetre-thick alternations of sandstone and siltstone-claystone, which mostly occur in the lower part of type well A1-NC186, where it is represented by the cored interval 4417 ft, and 4472 ft, between 4730.5-4731 ft and between 4750-4760.5 ft. It is lithologically variable, from sandy heterolithic to muddy heterolithic and argillaceous sandstone; the mud content varies throughout the facies. Some small sets of cross-lamination could also be distinguished in the sandstone. The effect of biogenic reworking can be seen in the light grey coloured mottling of shale and sand, with some coarse-grained siltstone, (e.g. 4731 ft) **(Fig. 3.9)**. The entire facies shows a general coarsening-upward trend, and is intercalated with burrowed sandstone. The burrows are sand-filled vertical and horizontal burrows, dominated by *Cruziana*, *Skolithos* and *Planolites*. They are up to 30cm long and 4mm-8mm in diameter. The sandstones are fine to medium-grained, and well-sorted with angular to subangular-grains. Primary lamination is disrupted by burrows and bioturbation, and is defined by dark clay/organic rich, irregular laminae and pale sandy laminae, again disrupted by burrows and bioturbation. The intensity of burrows (40-60%) has obscured the original sedimentary structures.

Fig. 3.9. Slabbed core sample from well A1-NC186 at 4731 ft showing burrowed heterolithic sandstone.

Interpretation. Burrowed heterolithic sandstone has been widely described as distal shoreface to innermost shelf (offshore shelf), receiving fine-grained sediments (Vos, 1977), deposited under storm influenced conditions. The offshore shallow marine environment is sedimentologically complex because of the number of different processes which operate within it (Banks, 1973), and probably it is the least well understood of all sedimentary environments (Anderton, 1976). To produce the alternation of mudrock and rippled sandstone, processes operated at two different intensities. Sands and silts were emplaced and deposited under the oscillatory and current conditions related to storms and their late-stage phases. Some muds were deposited by post-storm fall-out of material placed into turbulent suspension during storms, whereas other muds accumulated more slowly during inter-storm periods. Parts of the heterolithic succession that are richer in rippled sandstone formed during periods when sand was more available and storms were more frequent, more intense, and/or closer. Mudrock-rich parts of the heterolithic succession formed at times of sand starvation, possibly when storms were less frequent, weaker, and/or more distant. Alternation of sandstone-dominated and mudrock-dominated parts of the succession might reflect either changing patters of storm incidence or changes in shelf bathymetry (Cotter, 1985).

3.4.7 Facies (G): Burrowed mudstone and sandstone facies

Description This facies occurs in different parts of well A1-NC186, for example, at 4442 ft, 4452 ft, between 4462-4463.5 ft, 4525.5-4526.5 ft, 4544.5-45447.5 ft and 4570-4575.5 ft (**Fig. 3.10**). In type well H27-NC115 it occurs at 4767 ft and between 4925-4926 ft. It comprises mudstone irregularly interbedded with very thin to medium-bedded, very fine to locally fine-grained sandstone, containing small-scale wave and current ripple cross-lamination. The amount of sandstone to mudstone varies from 90% to 55-60%. The facies is locally disrupted by vertical and horizontal burrows, most notably *Planolites*, *Palaeophycus*, *Teichichnus*, and *Skolithos*. This facies is gradationally intercalated with burrowed fine to medium-grained sandstone.

Interpretation. The interbedded silty mudstone and wave and current ripple cross-laminated sandstone indicate differing energy levels during deposition. The silty mudstone may represent normal background sedimentation and the sandstone higher energy, possibly storm-influenced sedimentation. The mix of high energy (Skolithos)

and low energy (Planolites) trace fossils supports the interpretation of variable energy levels during deposition. Skolithos is characteristically developed in high energy shallow water conditions, whereas Planolites is typically developed below normal fair weather wave base in well sorted sands and silts in relatively quiet water conditions. The variety and abundance of burrows is again consistent with a marine environment, particularly a nearshore shelf.

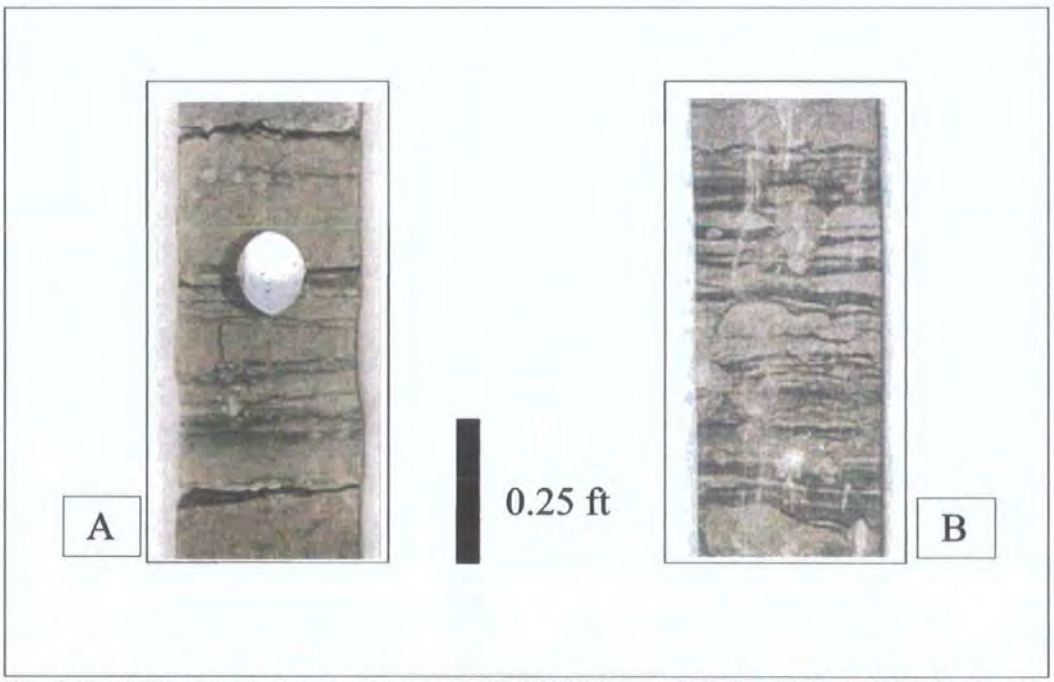

Fig. 3.10. Slabbed core samples from well A1-NC186 (A at 4442 ft and B at 4526 ft) showing burrowed mudstone and sandstone facies.

3.4.8 Facies (H): Massive sandstone facies

Description. This facies is more prominent in well H27-NC115 than in well A1-NC186. It occurs between 4896-4907 ft, in type well H27-NC115, and between 4646 ft and 4649.5 ft in type well A1-NC186 (**Fig. 3.11**). This facies consists predominantly of fine to medium-grained, clean to slightly argillaceous, light olive grey sandstone. The sandstones comprise well-sorted, subrounded to subangular-grains, and are characteristically massive or contain faint horizontal laminations. The massive sandstone grades upwards into horizontal parallel laminated sandstone, with some black drapes or irregular wisps of organic matter.

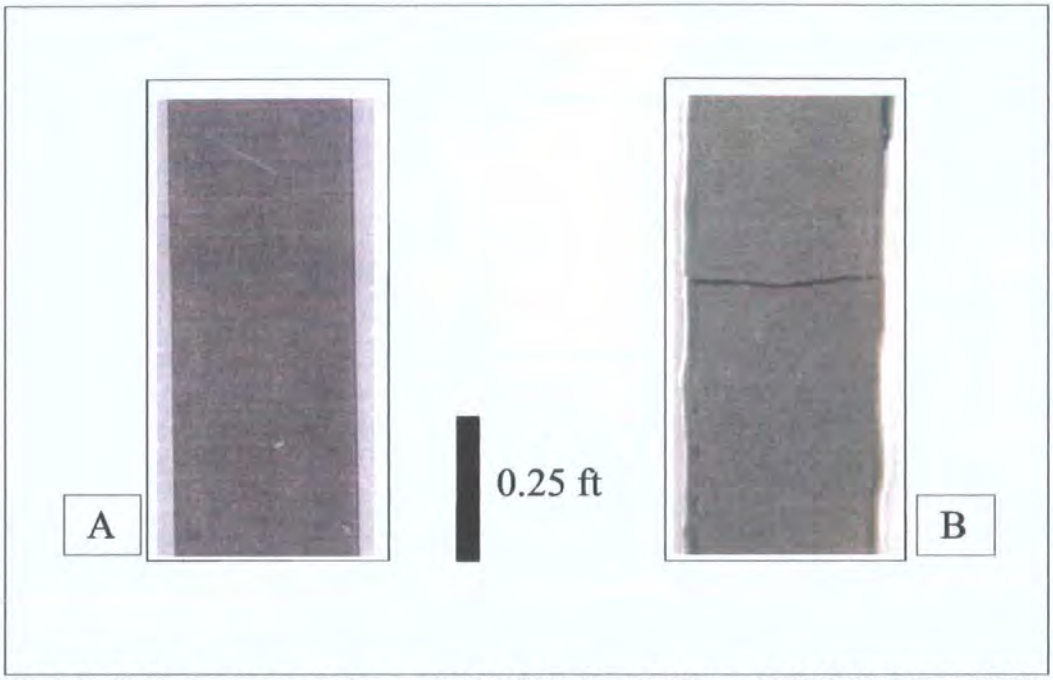

Fig. 3.11. Slabbed core sample from well A1-NC186 (A at 4648ft) and H27-NC115 (B at 4903ft), 4647ft showing massive sandstone facies in picture. A faint lamination can be seen in A.

Interpretation. Lamination in sandy sediments is the interleaving of particles in thin layers which differ slightly among themselves in average grain size. It can arise, in the context of a turbidity current, only if an individual grain is free to transfer a sufficient number of times between the sub-population and the static bed so that it can become associated with others similar to it in a patch on the bed moving beneath the current (Allen, 1991). In some cases the lack of internal stratification may be a result of post-depositional liquefaction or intense bioturbation, but in many, if not most examples, the massive sand divisions appear to be the products of discrete depositional events from one or more gravity currents. The massive sand may grade laterally or vertically into sand that exhibits some diffuse internal stratification (Kneller and Branney, 1995).

3.4.9 Facies (I): Ripple cross-laminated siltstone facies

Description. This facies occurs in the lower part of the cored section in type well A1-NC186 between 4761.5-4764 ft (**Fig. 3.12**), and between 5130-5160 ft in well H27-NC115. It comprises very fine-grained, micaceous and burrowed, very well-sorted to well-sorted siltstone with patches of pyrite. The siltstone is characterised by small-sets of ripple cross-laminated foresets which are separated by streaks of paler colour sand,

with some soft sediment deformation. Burrows are from 1.5 mm to 7 mm in diameter, the most notable burrows are *Skolithos*. The siltstone facies is bounded above by the burrowed heterolithic facies, which has a higher mud content and greater intensity of burrowing. Below it is bounded by the heterolithic facies which also has a higher mud content.

Fig. 3.12. Slabbed core sample from well A1-NC186 4763 ft showing cross-laminated siltstone facies.

Interpretation. Siltstone can be interpreted as being deposited from suspension in outer shelf areas. Neither the wave component, dominant during deposition of the thin-bedded facies, nor the current component can be thought of as 'fair-weather' processes in that silt deposition from suspension presumably occurred at yet lower water velocities. However, even during silt deposition waves were capable of rippling the bottom, producing the silty drapes on foresets. It is impossible to say whether this represents fair weather activity or silt deposition after storm stirring (Levell, 1980). This facies may have been deposited in a shallow marine shelf environment during periods of little detrital influx from the fluvial system. The silt and sand streaks were rather rapidly deposited from suspension which started to fall out suddenly and terminated gradually. During the settling wave oscillation apparently could reach the bed thus moulding the lamination into a weak cross-lamination. This suggests that the

silt and sand intercalations represent thin storm sandlayers which to variable degrees are affected by wave agitation related to the same storm (De Raaf et al., 1977).

3.5 Facies interpretation

The grain-size analysis and the biological and primary sedimentary structures in the Hawas formation, suggest that it was deposited in a shallow nearshore and marine shelf environment. The repetition of similar facies suggests a recurring pattern of similar depositional processes and environments. This is attributed to a dynamic interaction between the lower shoreface and the upper shoreface and inner and outer shelf. The lower shoreface facies in the upper part of the sucession is overlain by the upper shoreface which in turn is overlain erosionally by distal shelf. The lower part of the cored section of the Hawaz Formation comprises lower shoreface overlain by distal shelf overlain in turn by the inner shelf, recording rising and falling sea level.

Most of the bathymetric curves for Caradoc and Ashgill sequences have two aspects in common. The Caradoc part of the curve shows a long term rise in sea level from the early Caradoc, the so-called gracilis transgression, and the Ashgill curve shows a short term fall and rise in sea level close to the end of the series (Brenchley et al., 1994). The fining upward burrowed lower shoreface sediments may represent the same scenario of a transgressive long term sea level rise, overlying the regressive sequences from distal shelf to upper shore face (**Fig. 3.14**) and (**Fig. 3.15**). This reflects either non-deposition of lower shoreface sediments or possibly glacial erosion or erosion during the post glacial marine regression in this area, leading to deposition of the Tannezuft shale source rocks. The cross-lamination and cross-stratification, which were destroyed by abundant burrowing, especially by suspension feeders, implies turbid oxygen-rich waters. Also the downward decrease in intensity of burrowing suggests a change from high to low energy. Pemberton et. al, (1992) recognized nine recurring ichnofacies, by a particular ichnogenera, but it is not an exclusive suite of environmental gradients (**Fig. 3.13**). An individual fining or coarsening-upwards sequence may be interpreted in terms of migrating tidal channels or progradation of the shoreface. Regardless to GR response the parasequence between 4555-4645 ft reflects upward shoaling (upper shoreface) and comprises interbedded cross-bedded, low angle cross-bedded and cross-laminated sandstones,

which represents good reservoir quality in the Hawaz Formation. In the Hawaz Formation it has been observed by Vos (1981) and Turner (2002) that palaeoflow was to the north. Fello (2002) in his study stated an offshore direction of the flow towards to northeast.

The low angle cross-bedding can be formed by (a) the slow accretion of sediment on an inclined surface or (b) the accretion of sediment on the lee-slope of a rise or bank under upper phase plane bed conditions (Anderton, 1976).

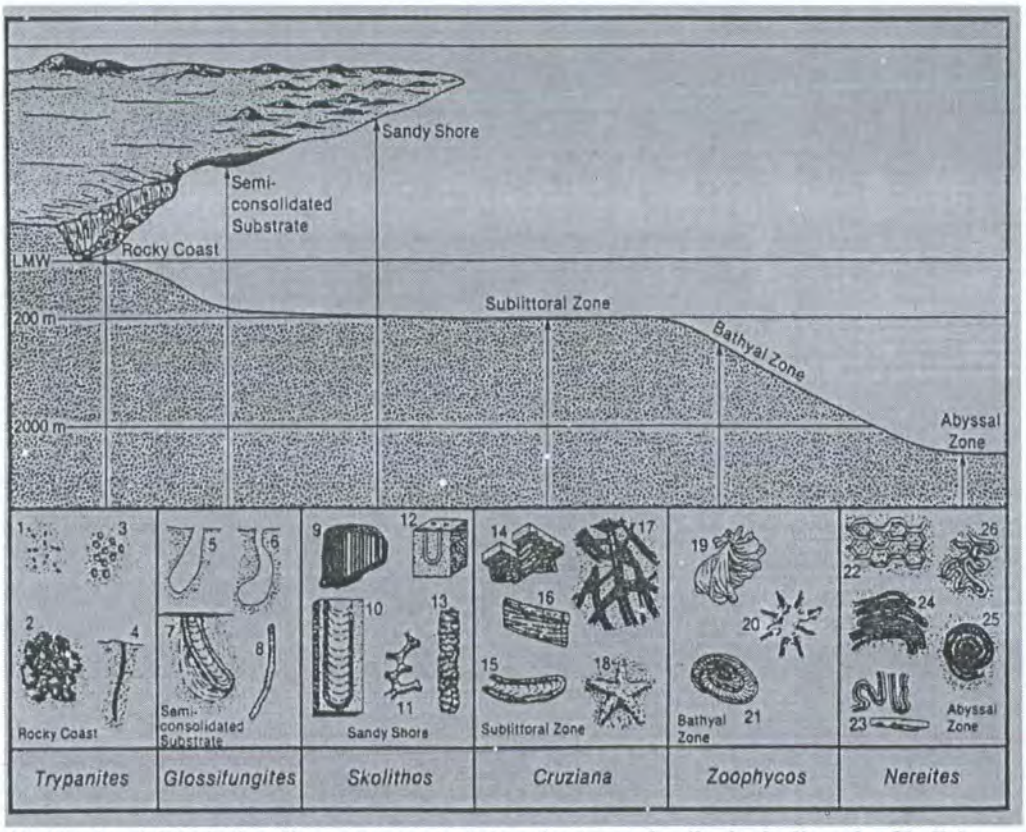

Fig. 3.13. Marine ichnofacies diagram representing the trace fossils, including the Skolithos and Cruziana ichnofacies found in the Hawas Formation (After Pemberton, 1992).

Two possible mechanisms, both involving wave transport and further dispersal of sand, are suggested. Inman and Bagnold (1963) noted that long, low waves transport sands onshore. Such waves have orbital diameters many times greater than the wavelengths of the ripples on the bottom and could move sand across crests of several small-scale ripples (Campbell, 1966). Therefore, this facies combination could have deposited as channel sand bodies, and the presence of burrowing and mud drapes suggests a tidal influence.

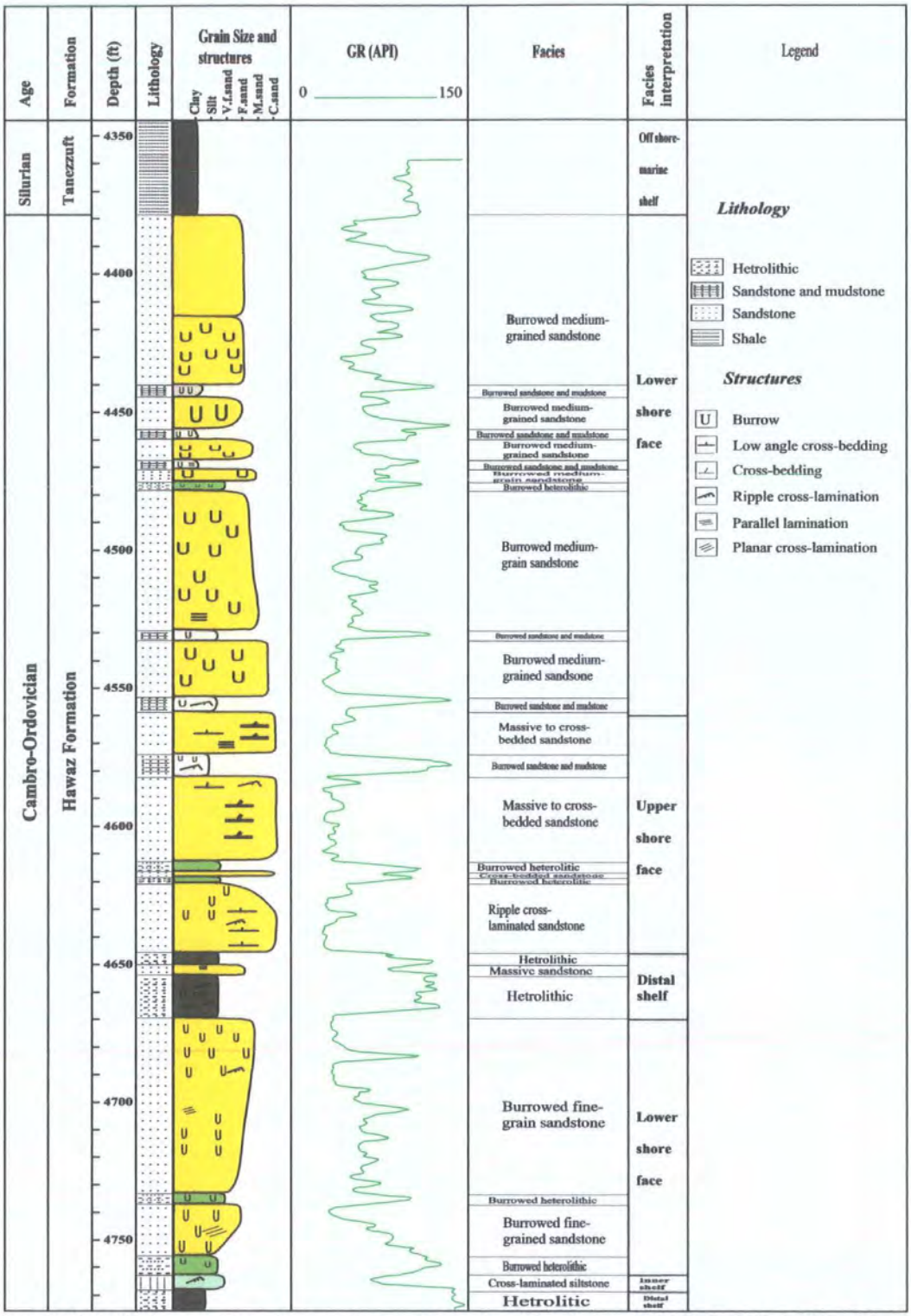

Fig. 3.14. Lithology, sedimentary environments and sea-level change in the cored section of type well A1-NC186.

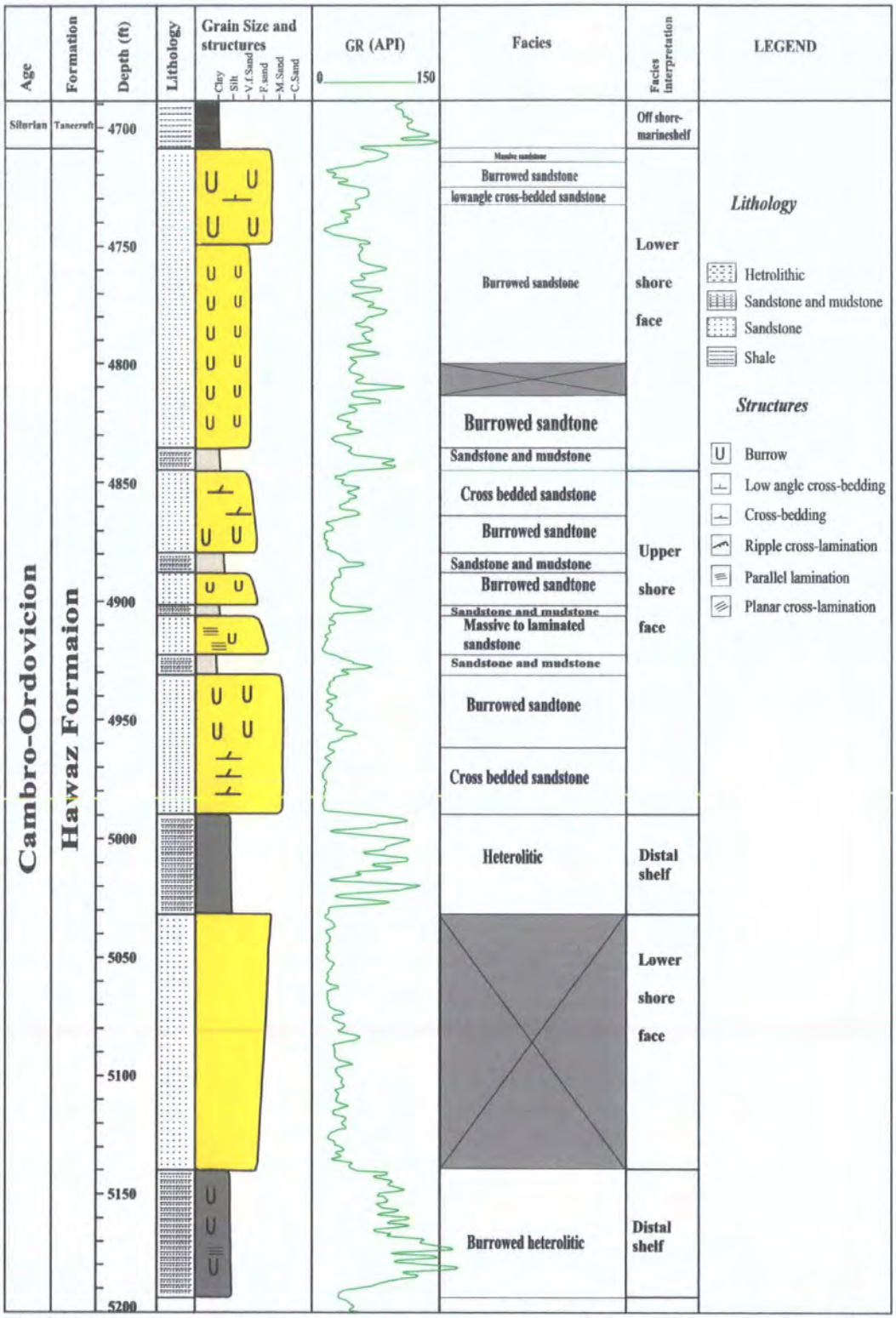

Fig. 3.15. Lithology, sedimentary environments and sea-level change in the cored section of type well H27-NC115.

The distal shelf, which occurs below the upper shoreface, with an erosive contact, comprises the heterolithic facies, in which the individual sandstone beds probably record a single storm event, and the development of storm wave surge currents causing turbulence and resuspension of shelf floor sand. The thin rippled sandstone beds suggest that the sand was deposited as thin sheets. The low energy period between storm sandstone deposits records a period when suspension mud and silt were deposited giving the mudstone and siltstone laminae. The upward decrease in silt and mud, and increase in sand size, represents a response to higher shoaling energy (Turner, 1980). To conclude, the Hawaz formation was deposited in a shallow marine environment dominated by tidal currents on a shelf subjected to periodic storm- generated wave activity.

4. Petrology and Diagenesis

4.1 Introduction

Petrograpic analysis provides a means of assessing the composition of the sandstone and relating this to their provenance, tectonic setting, diagenatic evaluation and economic potential (Pettijohn et al., 1987).

4.1.1 Objectives

The main objectives of the petrographic study are to:

- Assess the mineral composition
- Classify the sandstones
- Reconstruct their diagenetic history
- Determine the source rock provenance and composition
- Provide additional evidence of the sedimentary facies and depositional environment
- Define reservoir quality.

4.1.2 Samples and methods

This study is based on a total of 110 thin sections, cut from 84 hand specimens from A1-NC186, and 18 hand specimens from H27-NC115. In addition 7 thin sections were provided by Repsol from H27-NC115. However, only 79 thin sections from A1-NC186 and 25 thin sections from H27-NC115 have been used, because the rest are siltstone or shale. The thin sections have been impregnated with blue resin in order to facilitate the microscopic examination of texture and quantitative analysis of composition and porosity.

Because the mineralogy of a sandstone is primarily inherited from the source area, modified by sedimentary processes and diagenesis, a mineralogical examination provides one of the most useful approaches to obtain information about the

provenance, including tectonics and climate, the effects of transportation, including distance and direction, and the addition of minerals during sedimentation and diagenesis (Pettijohn et al, 1987).

The thin sections were analysed using a point counter in order to determine the percentage of quartz, feldspar, rock fragments, heavy minerals, mica, kaolinite, calcite, pyrite, matrix and porosity. The analysis was carried out using a Swift automatic point counter and mechanical stage. Three hundred grains were counted per slide for statistically reproducible results and then the results recalculated to 100%. The porosity measurements were estimated by standard modal analysis techniques and the porosity in the Hawaz Formation classified into three types for counting purposes: primary porosity, secondary porosity and microporosity. The coloured photographs of the slabbed core have been used to support the interpretation of the depositional environments based on facies analysis. Additional information has been derived from the following wireline logs: GR (Gamma Ray), NPHI (Neutron log), RHOZ (Density Log), SP (Spontaneous Potential Log) and DT (Sonic Log).

4.2 Compositional analysis

The modal composition of the Hawaz sandstone provides evidence of the composition of the source and the diagenetic events that affected the post depositional burial history of the sandstone.

The detrital particles in siliciclastic rocks in the Hawaz sandstone in A1-NC186 and 27-NC115, have been divided into six categories: (a) rock fragments, (b) quartz, (c) feldspar, (d) micas, (e) heavy minerals and authigenic (f) clay minerals and other constituents (**Figs. 4.1 and 4.2**).

4.2.1 Quartz

Quartz is the most common mineral in sandstone and the most physically and chemically stable under sedimentary conditions at the Earth's surface. Most quartz grains are derived from plutonic granitoid rocks, acid gneisses and schists.

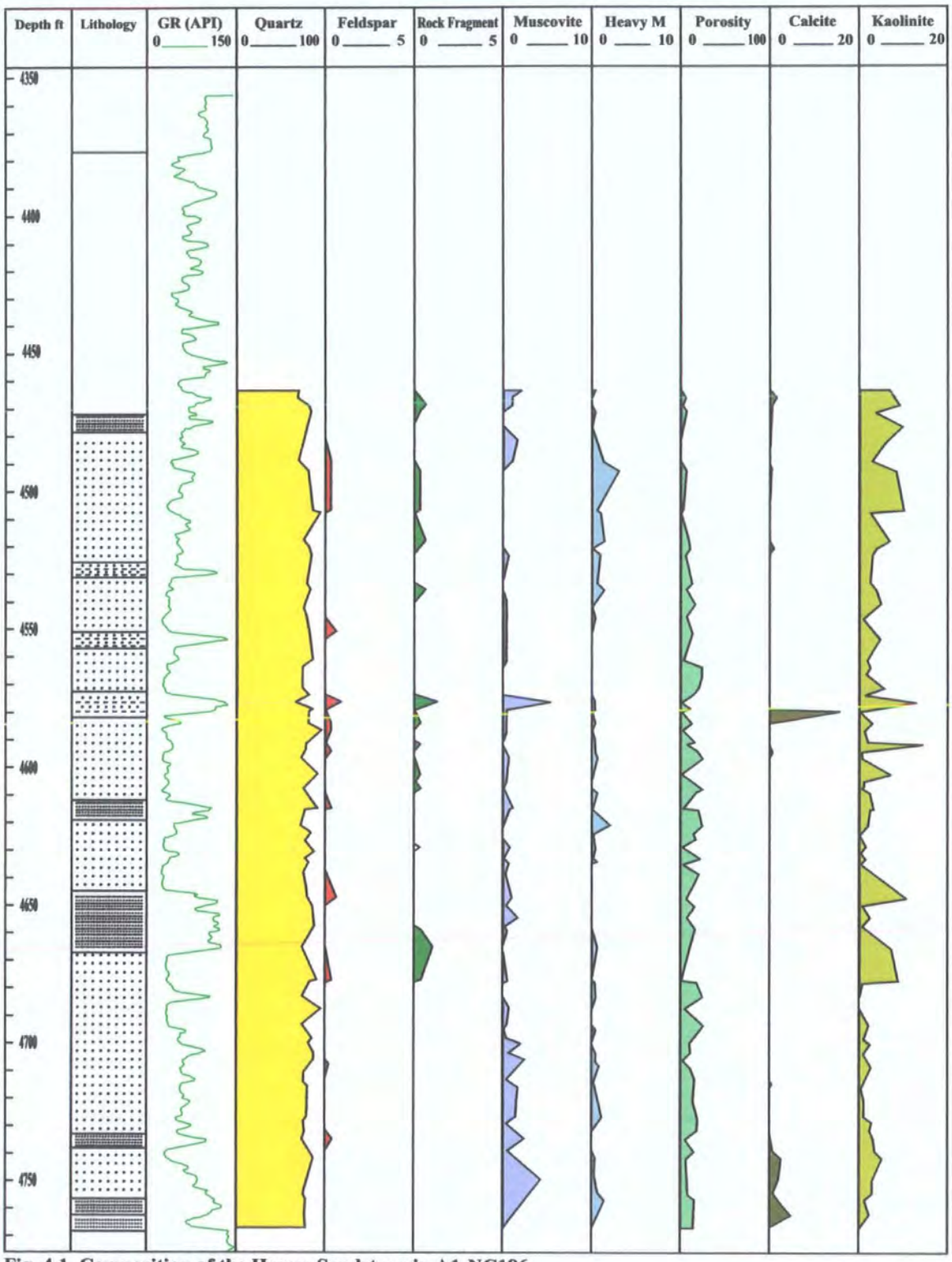

Fig. 4.1. Composition of the Hawaz Sandstone in A1-NC186.

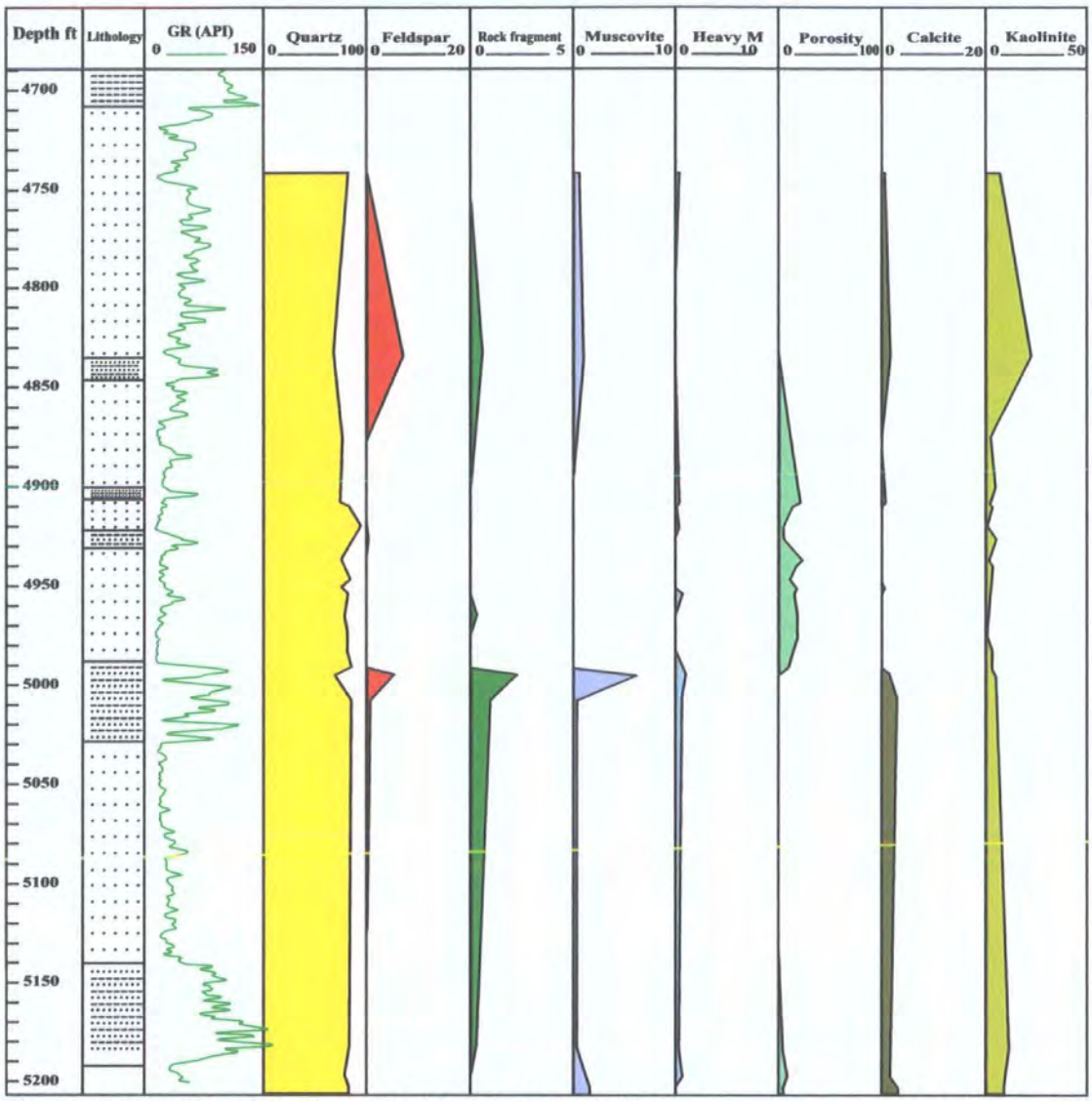

Fig. 4.2. Composition of the Hawaz Sandstone in H27-NC115.

Two main types of quartz can be distinguished: monocrystalline quartz grains composed of a single crystal, and polycrystalline grains composed of two or more crystals (Tucker, 1991). Quartz is the chief detrital constituent of most sandstones, from as little as 40% in some arkoses and graywackes to nearly 100% in pure orthoquartzites (Bokman, 1952). Quartz grains may be broken or abraded during transport, but with a hardness of 7 on Mohs' scale quartz grains remain intact over long distances and long periods of transport. In hand specimen quartz grains show

little variation, coloured varieties such as smoky or milky quartz and amethyst occur but mostly quartz is seen as clear grains (Nichols, 1999). The quartz from a variety of

source rocks may be distinguished on the bases of undulosity and the distinction remains valid even when based solely on flat-stage measurements. The undulosity of monocrystalline quartz, together with the amount of polycrystalline quartz and the number of crystals of which they are composed, leads to discrimination in both recent and ancient sands into plutonic, low-rank, and high-rank metamorphic parentage. The use of undulosity in detrital monocrystaline quartz for provenance interpretation has declined significantly since Blatt and Christie (1963) suggested that the broad overlap in undulosity between plutonic and metamorphic quartz makes determination of undulosity in quartz of little value in source rock identification (Basu et al., 1975). Nevertheless, it has been shown that quartz can be used as a tool in reconstructing the sources of clastic sediments by taking into account only those characteristics which are considered to be definitive, and evaluating them in a manner that minimizes subjective tendencies (Bokmen, 1952).

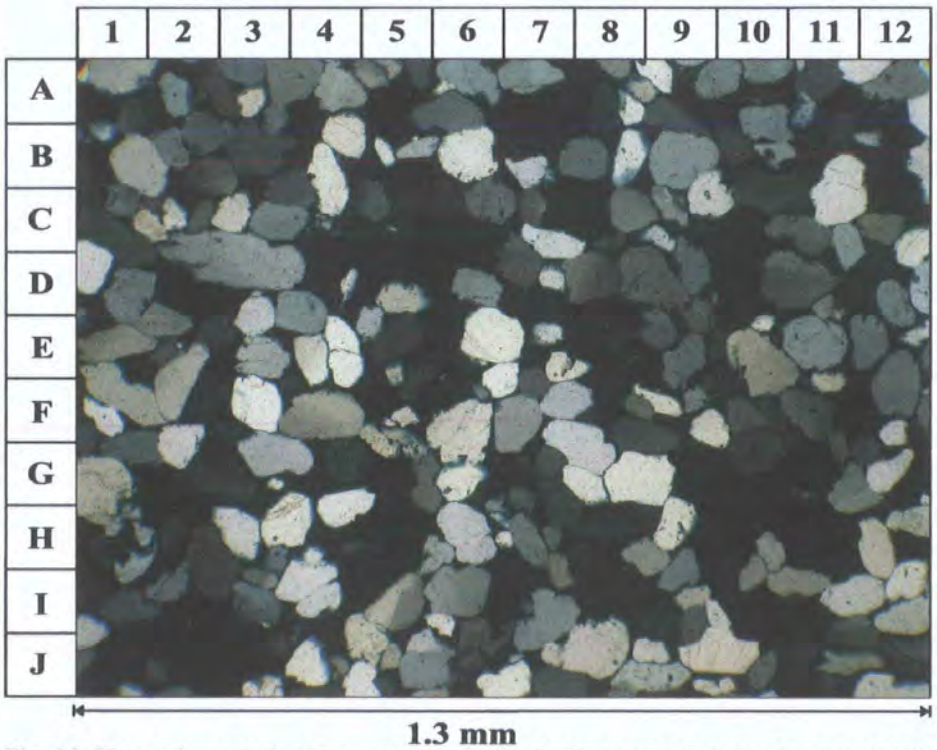

Fig. 4.3. Photomicrograph of a quartz aranite in the Hawaz sandstones at depth 4612ft in A1-NC186, which is dominated by monocrystalline quartz. XPL (X4).

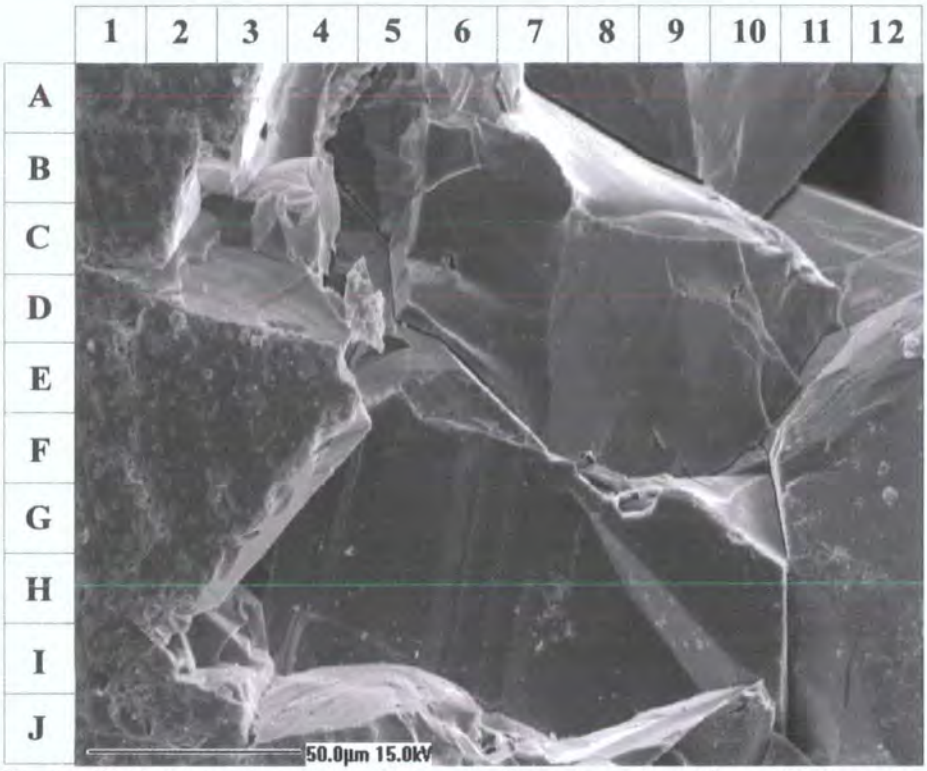

Fig. 4.4. SEM picture of quartz grain showing the grain surface. The small pits on the surface are probably due to transport by floating ice to the depositional site.

The crystalline rocks that are the source of nearly all silicate mineral grains in sandstones reach the surface by means of tectonic uplift, and during this process most quartz crystals are plastically deformed. This deformation is seen in thin sections as undulatory extinction, that is, the crystal does not extinguish as a single unit on slight rotation of the microscope stage, but extinguishes in sectors through a rotation of several degrees (Blatt, 1992).

In wells A1-NC186 and H27-NC115, the Hawaz sandstones are composed mainly of quartz grain (**Fig. 4.3**), dominated by monocrystalline grains (96 to 99%), relative to feldspar and rock fragments with some 2% of polycrystalline grains. The grains are medium to very fine-grained, subrounded to subangular, well-sorted to moderately well-sorted, and near symmetrically skewed. In the SEM picture (**Fig. 4.4**) the quartz grain surface shows small features (wisps) which may be an indication that the grains were carried out by floating ice to the place where it was deposited (**Fig. 4.4**).

Most of the quartz grains in the Hawaz sandstones in these two wells show strong undulose extinction, which are more abundant in strained source rocks, especially metamorphic rocks. Also the polycrystalline quartz grains are characterized by relatively straight boundaries between equant grains, and straight to slightly undulose extinction (**Fig. 4.5**).

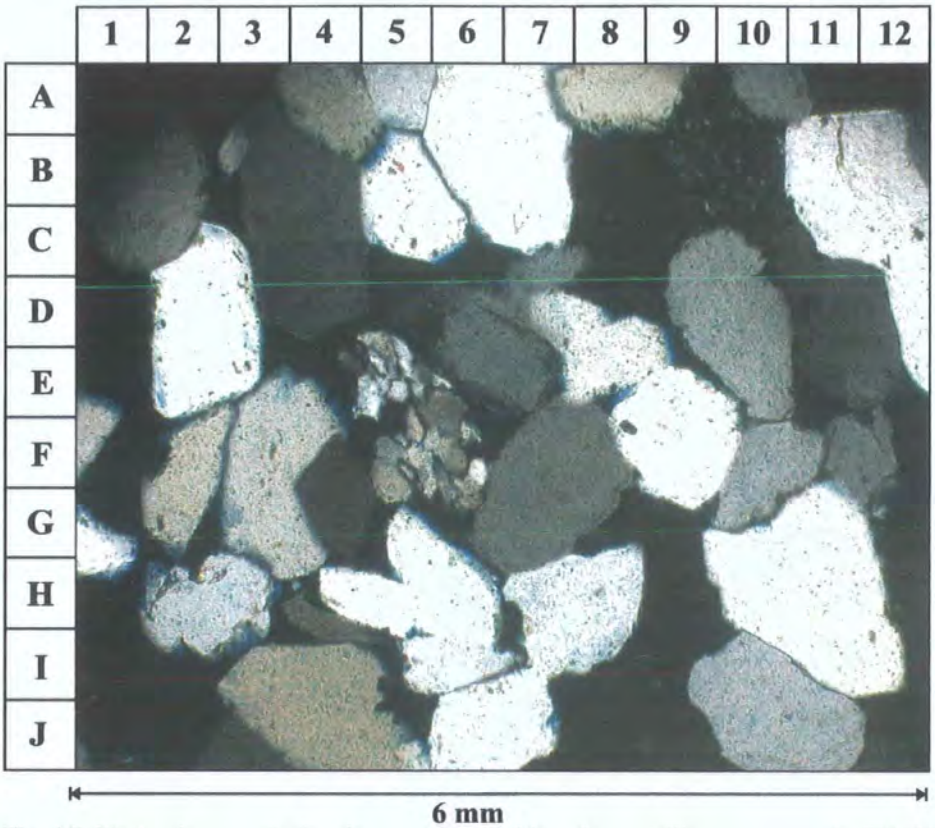

Fig. 4.5. Photomicrograph showing a metamorphic polycrystalline quartz grain (E4-F6), (4569ft) XPL (X20).

The grain contact types in the Hawaz sandstones are related to the particle shape and packing, and the packing depends on the spatial density of particles in a sediment accumulation. Most monocrystalline quartz grains have concavo-convex contacts, suggesting that these grains have undergone considerable compaction during burial. Sutured contacts are also recognized. These varieties of grain contact types can be used as a rough measure of the degree of compaction and packing, and thus the depth of burial of the sandstone.

Quartz overgrowths can be recognised in thin-section either by dust rims between detrital grains and the overgrowth, or by the development of excellent

rhombohedral crystal terminations growing into pore space (**Fig. 4.6**). Quartz overgrowth can also be recognized under SEM (**Fig. 4.7**).

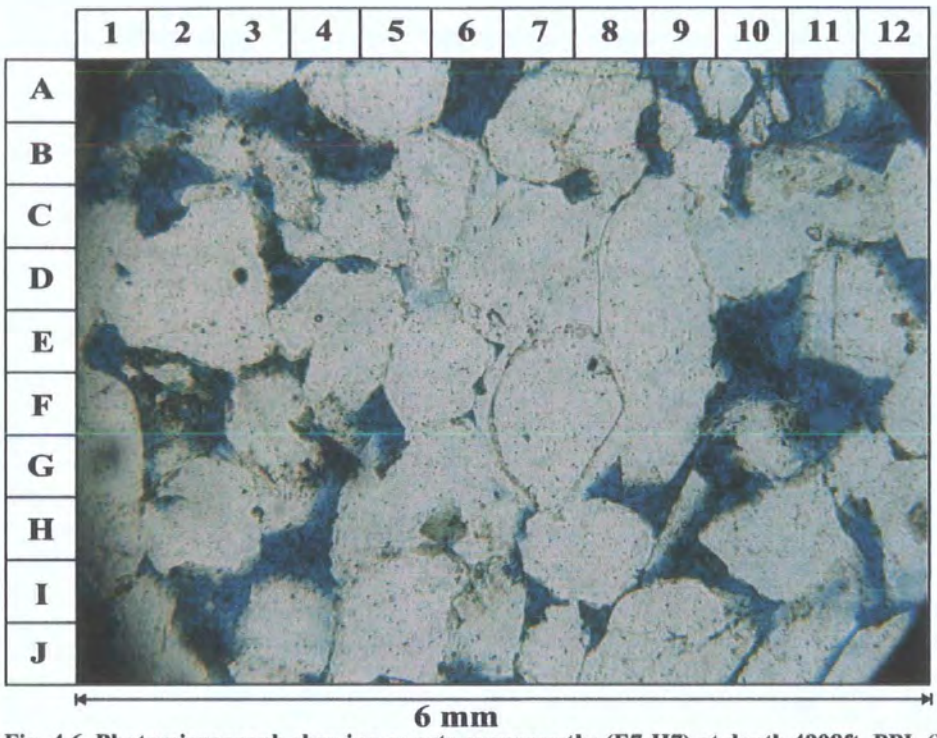

Fig. 4.6. Photomicrograph showing quartz overgrowths (E7-H7) at depth 4908ft, PPL (X20).

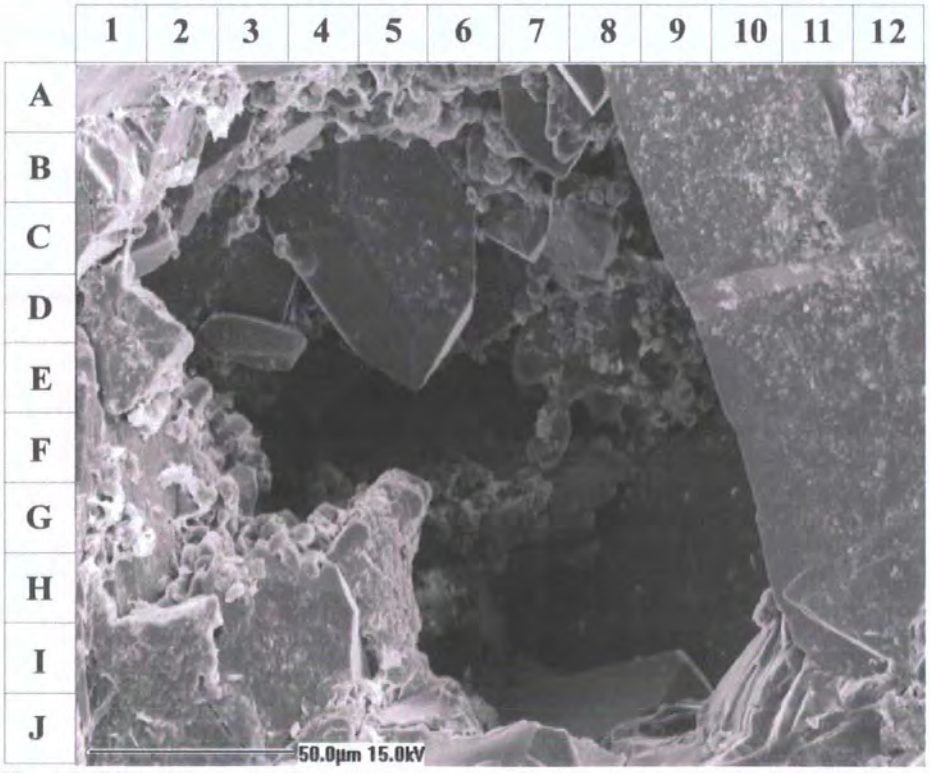

Fig. 4.7. SEM picture showing quartz overgrowth with good crystal face at 4629ft.

4.2.2 Feldspar

The feldspar content in most sandstones averages between 10 and 15%, but in arkoses it may reach 50%. The mechanical stability of feldspar is lower than that of quartz, since feldspars are softer and have a stronger cleavage. This leads to disintegration of feldspar crystals during transportation, particularly in high energy depositional environments, so that on a broad scale, for example, fluviatile sediments contain more feldspar than beach or shallow marine sediments (Tucker, 1991). The alteration of feldspar has been considered to reflect climatic conditions prevailing at the time at the depositional site. Feldspar occur nearly in all types of crystalline rocks, so that feldspar grains of sand-size can be derived from granitoid igneous rocks, gneisses and schists in large amounts. The percentage and type of feldspar in sandstone depends on the rate and type of tectonic activity, and climate.

Feldspars are the second most abundant mineral in most sandstones (Boggs, 1995). The complex nature of the feldspar minerals has resulted in their being subdivided into many categories on the basis of their chemical, physical and structural characteristics. The categories of feldspar normally used by sedimentary petrologists are: (i) potassium (orthoclase, microcline and sanidine); (ii) plagioclase (albite through anorthite); and (iii) perthite (an intergrowth of sodium feldspar and potassium feldspar) (Blatt, 1992). The relative proportions of K-feldspar and albitic and anorthic plagioclases may be controlled either by the relative abundance of those feldspars in the igneous and metamorphic source rocks or by differential stability at the Earth's surface (Pettijohn et al., 1987).

The Feldspars are the second most abundant detrital grain type in the Hawaz sandstones ranging from traces to 9%. The bulk of the feldspar grains are either K-feldspar or microcline, with lesser amounts of plagioclase. The untwinned orthoclase is characterized by low relief and cleavage. The potassium feldspars show petrographic evidence of alteration (**Fig. 4.8**) which can also be recognized under the SEM (**Fig. 4.9**). Most K-feldspar grains appear quite fresh or slightly broken, whereas the microcline and plagioclase encountered have been affected by dissolution. The microcline feldspar can be recognized by its grid twining.

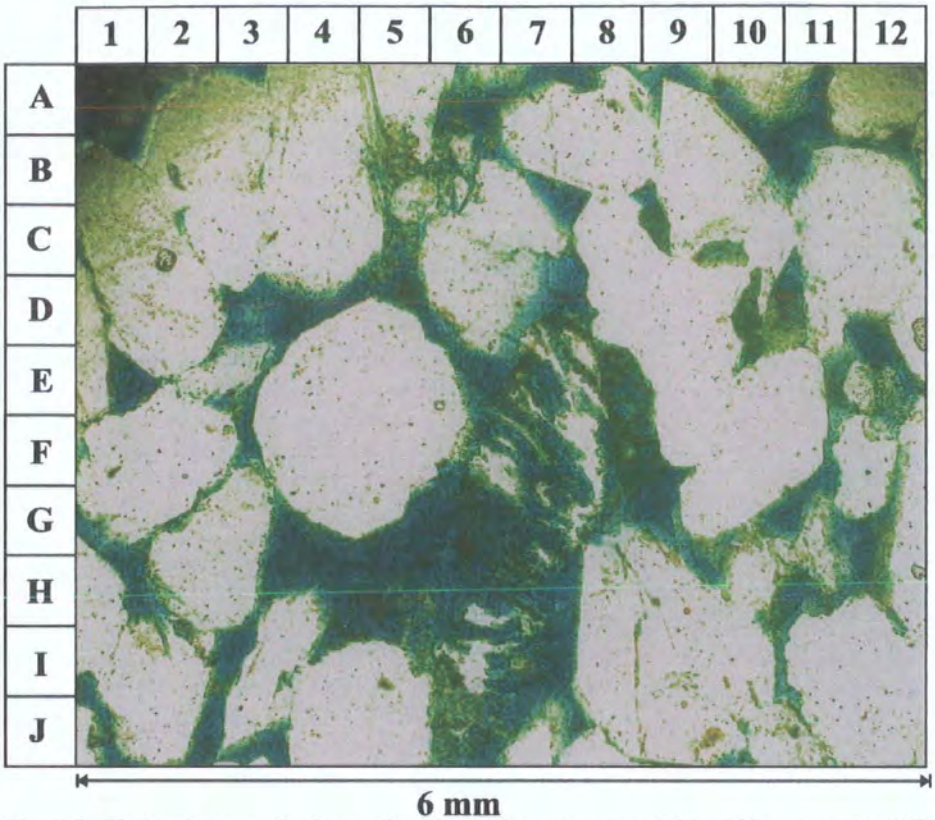

Fig. 4.8. Photomicrograph shows the dissolution of an unstable feldspar grain (A7-H7) in the Hawaz sandstone at depth 4899.5ft, (H27-NC115) PPL (X20).

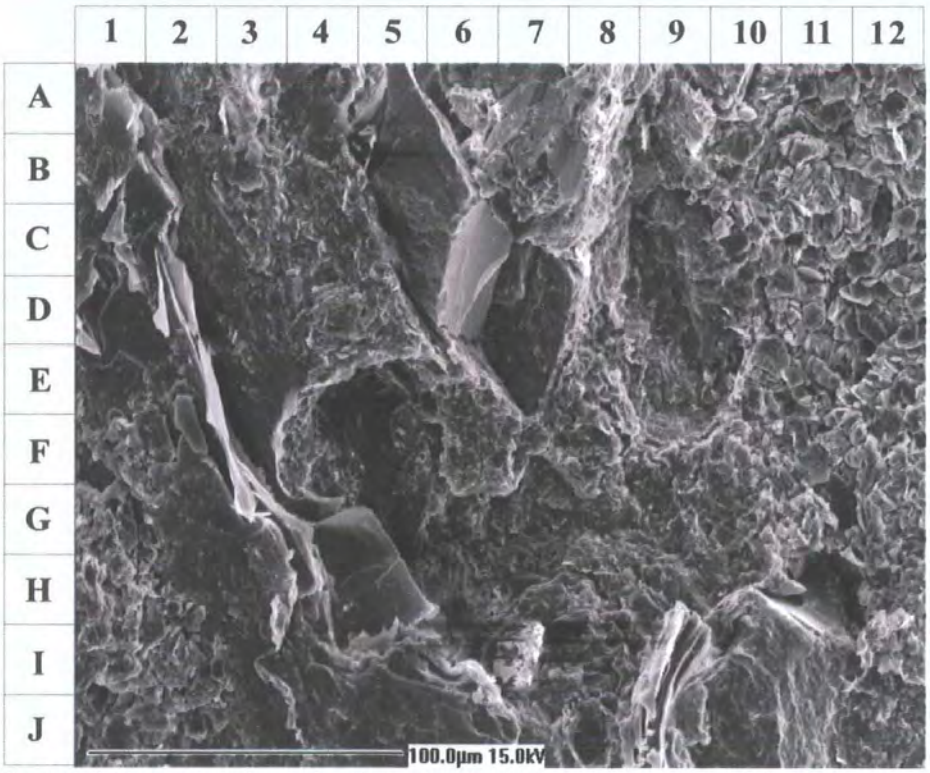

Fig. 4.9. SEM picture shows the dissolution in the feldspars at depth 4629ft.

4.2.3 Rock fragments

Pieces of polymineralic source rock form 15-20% of the average sandstone but can supply much more than 15% of the provenance information about the rock (Blatt, 1992). The composition of the rock fragment depends basically on source-rock geology and durability of particles during transportation. In sandstone the lithic fragments are commonly fine-grained sedimentary and metasedimentary rocks such as mudstones, siliceous sedimentary rocks such as chert, and igneous, in particular volcanic rocks (Tucker, 2001). The coarser-grained source rocks will contribute mostly mineral grains but, depending upon the ratio of the grain-size of the source rock to the grain-size of the sandstone, they may also provide rock fragments. Thus, the larger the grain-size of the sandstone, the more likely is the occurrence of rock fragments, and the better the assessment of source terrane lithologies (Pettijohn et al, 1987).

Rock fragment in the Hawaz sandstone are present, but not common, ranging from traces up to 3% in both wells A1-NC186 and H27-NC115. They consist of metamorphic polycrystalline quartz rock fragments or chert, with a few clay mineral fragments. Most of the polycrystalline quartz grains in thin section are subrounded to rounded.

4.2.4 Mica

Sand-size detrital mica, because of its platy mature, would be expected to be the hydraulic equivalent of smaller particles of other minerals. As a result of the transportation and depositional characteristics of mica, its areal distribution in sediments reflects short-term response to environmental energy conditions. The absence of mica in recent sediments should indicate that either no mica is being contributed, or that energy conditions are such that winnowing, and/or by-passing of fines are important processes. The presence of mica flakes, on the other hand, indicates possible deposition, or that winnowing and/or by-passing are not being carried out efficiently (Doyle et al., 1967).

The mica in the Hawaz sandstone ranges from traces up to 3%, locally 6%, and it occurs as elongate grains under the SEM (**Fig. 4.10**). It consists predominantly of muscovite, which occurs as elongate flakes associated most commonly with thin stylolitic clay layers, and burrows (**Figs. 4.11** and **4.12**). Biotite is rarely present. Muscovite is easily identified by its platy nature and parallel extinction. It is colourless in plane-polarized light and shows bright second-order colours under crossed polars. Muscovite is distinguished by its tabular appearance bent through compaction between quartz grains.

Fig. 4.10. SEM picture shows an elongate mica in the Hawaz sandstone.

4.2.5 Clay minerals

Clay minerals are the most common mineral group in sedimentary rocks, totalling about 45% by weight or volume. They are very small particles, commonly less than 1µm in size. The major clay minerals are kaolinite, montmorillonite, and illite. Nearly all clay-bearing sedimentary rocks contain more than one type of clay mineral (Blatt, 1982).

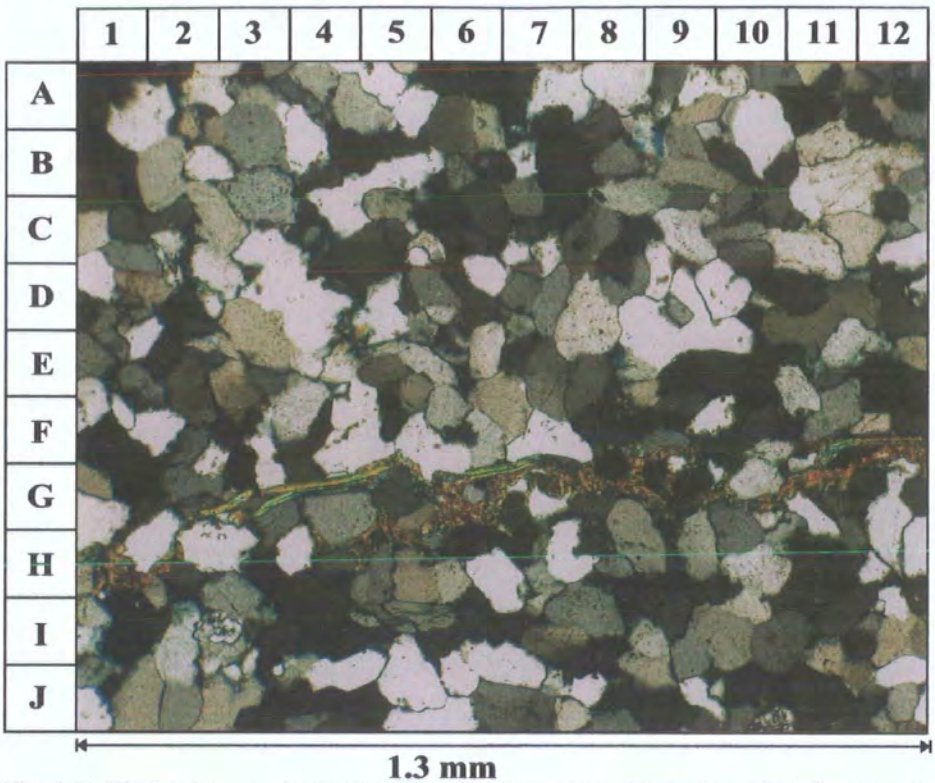

Fig. 4.11. Photomicrograph showing the mica concentrated in a clay mineral or stylolite layer at depth 4554ft, XPL (X4).

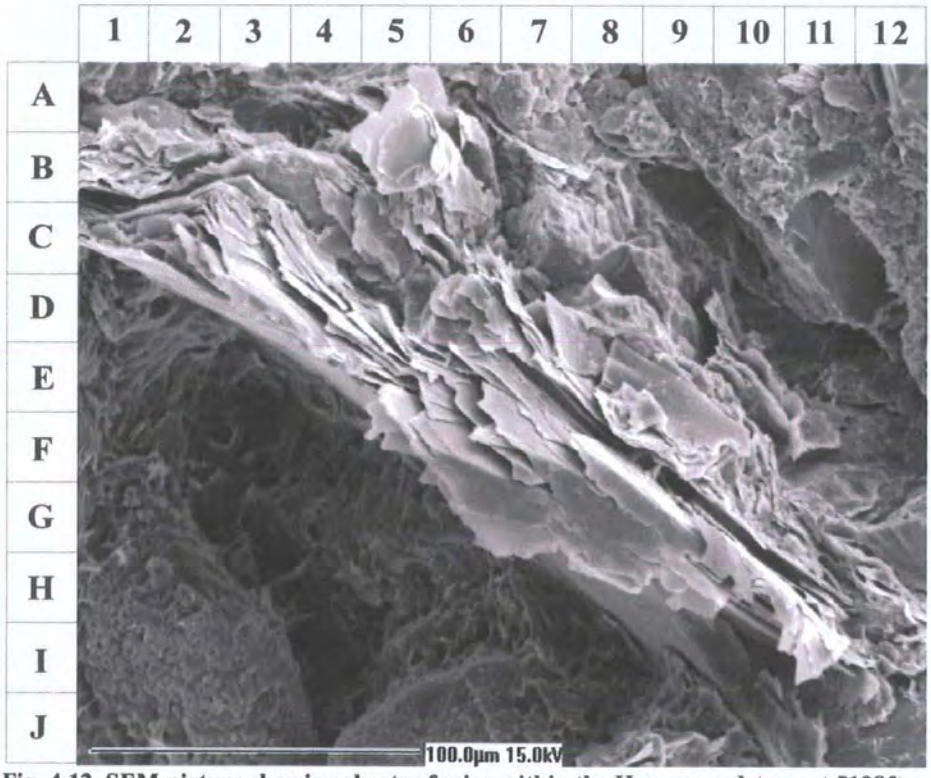

Fig. 4.12. SEM picture showing sheets of mica within the Hawaz sandstone at 5198ft.

Clay minerals in sandstones may be both detrital and authigenic. Detrital clay-mineral types cannot be identified with the petrological microscope, but some authigenic clays can. All the chief clay-mineral groups are represented in sandstones: kaolinite, illie, chlorite, smectite and mixed-layer clay. Detrital clays reflect the source-area geology, climate and weathering processes (Tucker, 2001).

The major origin of clay minerals is as subaerial weathering products of silicate minerals. All of the major clay groups are found in weathered residues and soils. Which clays will be found depends on the interaction of climate, geomorphology and parent rock. Humid climates and well-drained topographies lead to extensive weathering of feldspars and their silicates to kaolinite. Lower rainfall and poorer drainage may result in the formation of smectite from the same parent materials. Mafic silicates in many climates will go to smectite. Illite products may form in intermediate to humid climates (Pettijohn et al., 1987).

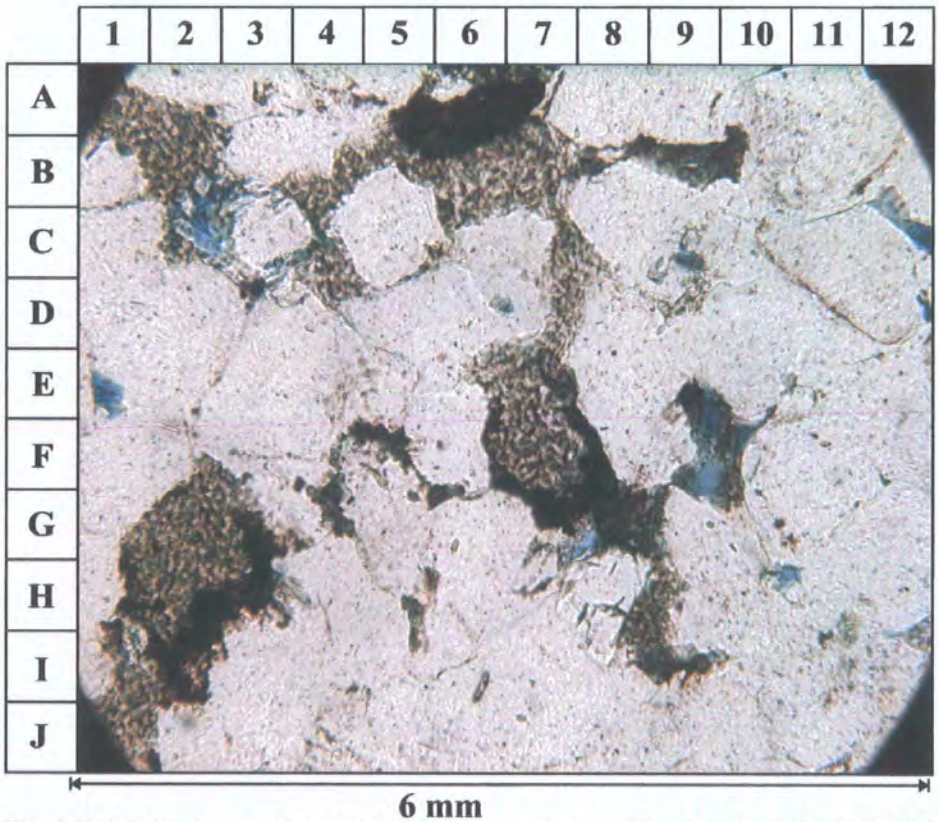

Fig. 4.13. Photomicrograph showing kaolinite replaced grains (E7-F8) and kaolinite fill pore (A1-B2) in the Hawaz sandstone (4629ft), PPL (X20).

The clay minerals in the Hawaz sandstones are dominated by kaolinite (**Fig. 4.13**), which is colourless in plane-polarized light and grey-dark grey in cross-polarized light, with weak birefringence. It partly fills both primary and secondary porosity. Secondary porosity probably formed from feldspar crystals which were subsequently dissolved, leaving a residue of kaolinite clay (Scholle, 1979), showing well developed pseudo-hexagonal basal plates in curved vermicular stacks, (**Fig. 4.14**). Other clay minerals present in the Hawaz Formation are smectite, illite and chlorite, which are present in amounts ranging from traces to up to 1%. The smectite under the SEM (**Fig. 4.15**) shows irregular, wavy plates or sheets which the characteristic of most smectites. Illite forms needle-shaped crystals with strong birefringence, but it hasn't been recognised in the selected SEM samples. Chlorite is precipitated from pore fluids in rare patches on detrital grains, and from rock weathering and alteration of ferromagnesian minerals, such as biotite.

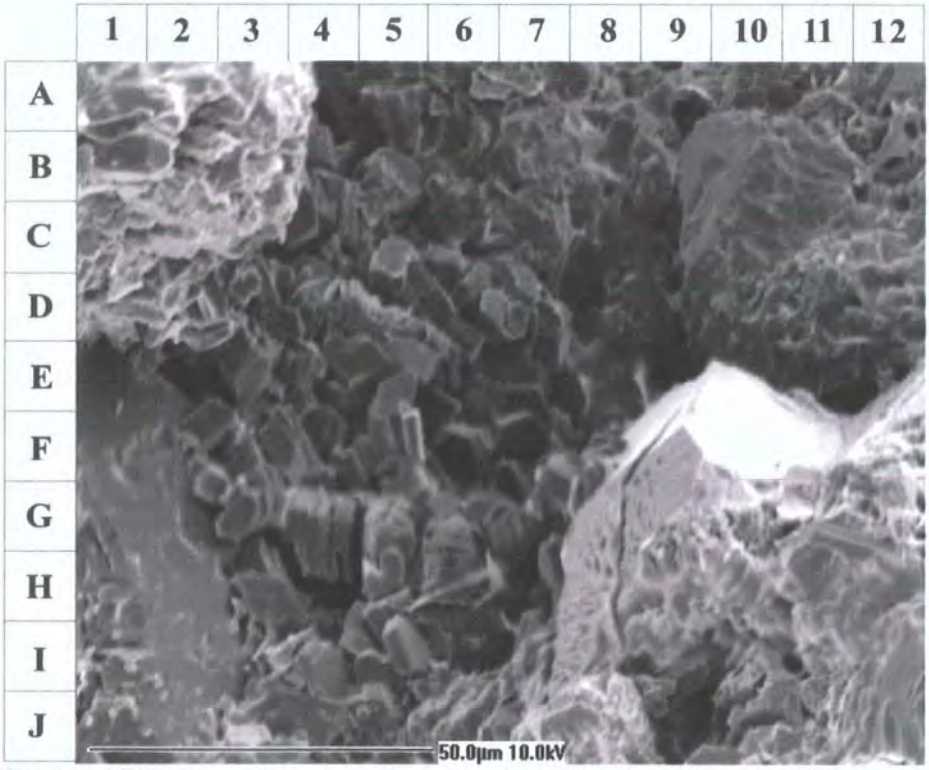

Fig. 4.14. SEM picture shows irregular wavy plates of kaolinites in A1-NC186.

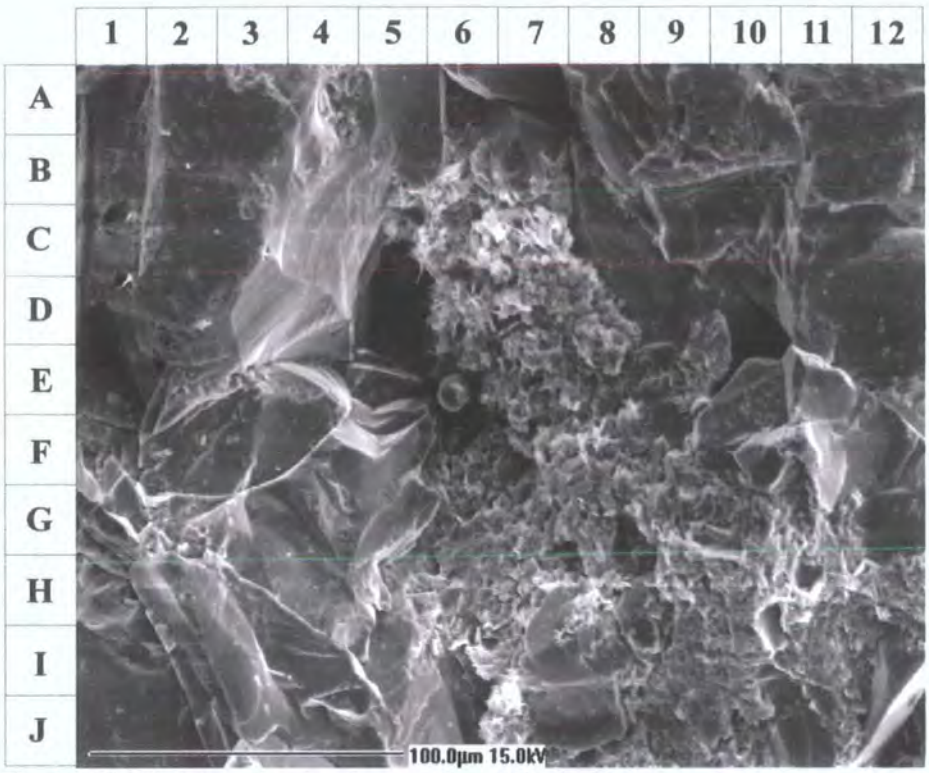

Fig. 4.15. SEM picture showing the smectite within the Hawaz sandstone.

4.2.6 Heavy minerals

The heavy minerals are chiefly silicates and oxides, many of which are very resistant to chemical weathering and mechanical abrasion. The common non-opaque heavy-mineral grains are apatite, epidote, garnet, rutile, staurolite, tourmaline and zircon (Tucker, 2001). The heavy minerals typically form less than 1% of sandstone. The percentage is commonly related to the proportion of lithic fragments in the light-mineral fraction of the rock, particularly the proportion of metamorphic lithic fragments (Blatt, 1992).

The study of heavy minerals can give useful information on provenance and events in the source area. Certain heavy minerals, such as garnet, epidote and staurolite, are derived from metamorphic terrains, whereas others, rutile, apatite and tourmaline for instance, indicate igneous source rocks (Tucker, 2001). Special attention has been given to two of the commonest stable heavy minerals, tourmaline and zircon, in much the same way that the quartz varieties have been studied in the

[illegible]

In the Hawaz Formation two main types of non opaque heavy minerals have been observed, zircon and tourmaline (Fig. 4.16). The zircon occurs as rounded detrital grains, surrounded by a black halo, commonly showing an abraded bipyramidal prismatic form, and sub-rounded in shape indicating long distance of transport. It is colourless, and shows a strong birefringence. Tourmaline in the Hawaz Formation is characterized by colourless to pale green-olive green prismatic crystals showing undulatory extinction and strong pleochroism.

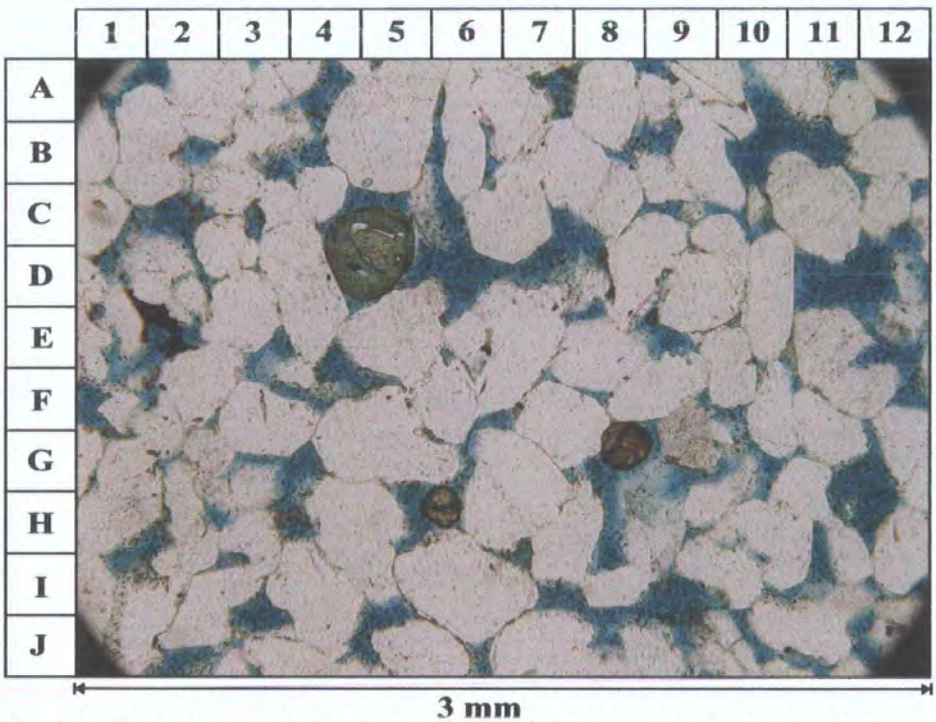

Fig. 4.16. Photomicrograph showing tourmaline (C5-D5) and zircon (G8) in the Hawaz sandstone (4584) PPL (X10).

4.2.7 Other constituents

Pyrite

The mineral pyrite FeS_2 is a common and widespread authigenic constituent of sediments and sedimentary rocks where it is almost always found associated with organic matter. This association is not fortuitous. FeS_2 forms from aqueous solution only in the presence of elemental sulphur or substances that produce elemental

sulphur during decompaction (Berner, 1970). Several types of pyrite are present, with some having provenance significance whereas others are post-depositional in origin (Gavinil et al., 2002). Pyrite is most common in marine sandstones because of the availability of the sulphate in seawater, but it is only an accessory diagenetic mineral. Pyrite is commonly altered to goethite/limonite on surface weathering (Tucker, 2001).

Pyrite crystal in the Hawaz Formation range from traces up to 1%. Although the cubic pyrite grains are authigenic rather than detrital, they show the typical yellow-gold metallic colour of pyrite in reflected light.

4.2.8 Sandstone maturity in the Hawaz Formation

A distinction may be drawn between mineralogical maturity, which is strongly influenced by the composition of the source rock area, and textural maturity, which is more related to the history of transport and deposition (Nichols, 1999). Typically, compositionally immature sediments are located close to their source area or they have been rapidly transported and deposited with little reworking from a source area of limited physical and chemical weathering (Tucker, 2001). It is widely believed that sorting is best when sand is repeatedly exposed to reworking by currents of moderate intensity. Probably the worst sorting occurs in sands subject to one brief episode of mass transport, such as a submarine slide, which is deposited below wave base in deep water (Pettijohn et al., 1987).

Folk in 1951 described four stages of textural maturity. (1) Immature stage in which the sediment contains considerable clay and fine mica, the non-clay portion is itself poorly sorted, and the grains are angular. (2) Sub-mature stage in which the sediment contains very little or no clay, but the non-clay portion is still itself poorly sorted and the grains are angular. (3) Mature stage in which the sediment contains no clay and is well-sorted, but the grains are still subangular. (4) Super-mature stage (Folk, 1951).

The framework grains in the Hawaz sandstones are subrounded to subangular well sorted to moderately well sorted and texturally mature (**Fig. 4.17**) (Nichols, 1999).

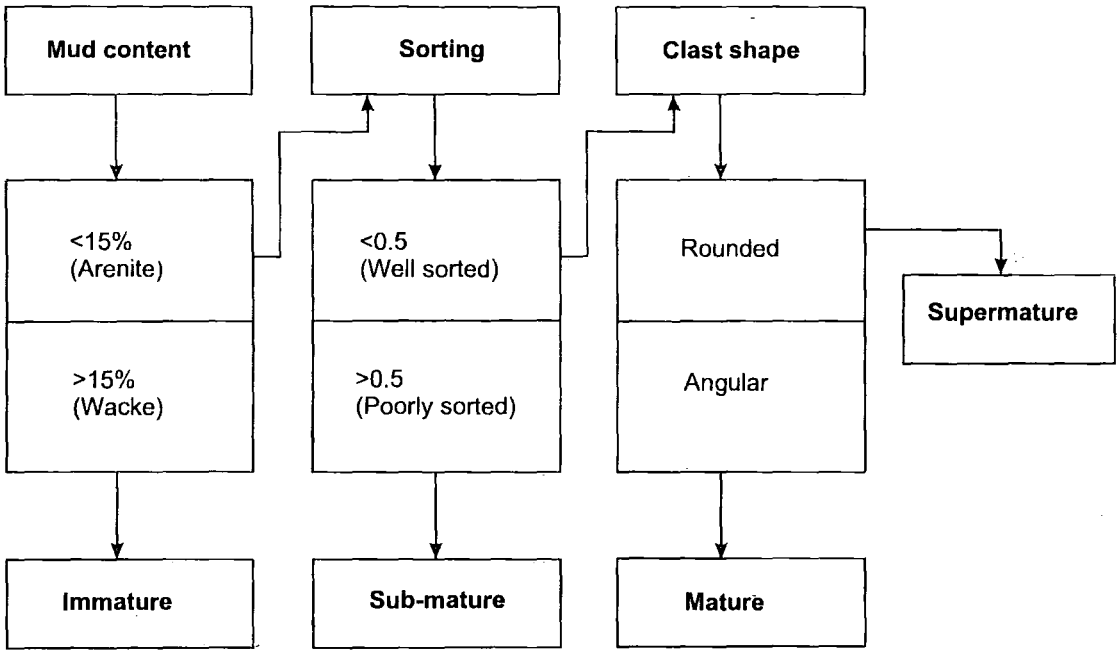

Fig. 4.17. Flow diagram for the determination of the textural maturity of a terrigenous clastic sediment or sedimentary rock (Nichols, 1999).

4.3 Classification

A full description of sandstones usually includes some information concerning the types of grain present. Informal names such as 'micaceous sandstone' are used when the rock clearly contains a significant amount of a distinctive mineral, in this case mica (Nichols, 1999). There are several classification schemes available and most use a triangular diagram with end members of quartz (Q), feldspar (F) and rock fragments (L). The triangle is divided into various fields, and rocks with an appropriate modal analysis are given a particular name (Tucker, 1991). A widely used simple classification of sandstones is presented by Pettijhn et al. (1987) based on the origin of the sandstone. The classification distinguishes between the "clean" sands or arenite-sands with less than 15 percent matrix and the "dirty" sands or wackes with more than 15 percent matrix (Pettijohn et al., 1987).

The sandstones of the Hawaz Formation are classified according to Pettijohn et al. (1987) as mainly arenites, quartz-rich but feldspar and rock fragment poor (**Fig. 4.18**). The percentage of quartz in the Hawaz sandstones ranges between 96 to 99%, relative to feldspar and rock fragments, and the quartz is dominated by monocrystalline grains with abundant polyctystalline grains.

Many quartz arenites originate as shallow marine (but above storm wave base) sands that accumulated along or near the shoreline as beach, shoreline dune, tidal flat, spit, barrier island, or longshore bar deposits (Prothero et al., 1996).

4.4 Provenance

The term provenance, derived from the French "provenir", meaning to originate or to come forth, has been used to encompass all the factors relating to the production or "birth" of the sediment (Pettijohn et al., 1987). Sand composition, which is initially a function of the breakdown of a particular parent rock type under a given set of climate-induced weathering conditions, is subject to later modification during transportation, deposition, and diagenesis (Suttner et al., 1981). In many cases quartz arenites are the products of extended periods of sediment reworking, so that almost all grains other than quartz have been broken down by mechanical abrasion. Climate in the source area can also play a major role in producing quartz arenites. A warm humid climate will lead to the removal of many unstable grains, and if this is coupled with low relief and slow sedimentation rates, quartz will dominate the detritus. Many quartz grains in these arenites could be second cycle, derived from pre-existing sediments (Tucker, 2001).

Ternary diagrams have been used to plot the Hawaz sandstone composition data for A1-NC186 and H27-NC115 (**Fig. 4.19**). These indicate that they were derived from similar parent rocks, under humid climatic conditions from plutonic and metamorphic rocks. According to Suttner, et al. (1981) humid weathering raises the proportion of quartz relative to feldspar (Dickinson, 1985).

4.5 Tectonic setting of the Hawaz sandstones

Detrital modes of sandstone suites primarily reflect the different tectonic settings of provenance terranes, although various other sedimentological factors also influence sandstone compositions. Comparisons of sandstone compositions are aided by grouping diverse grain types into a few operational categories having broad genetic

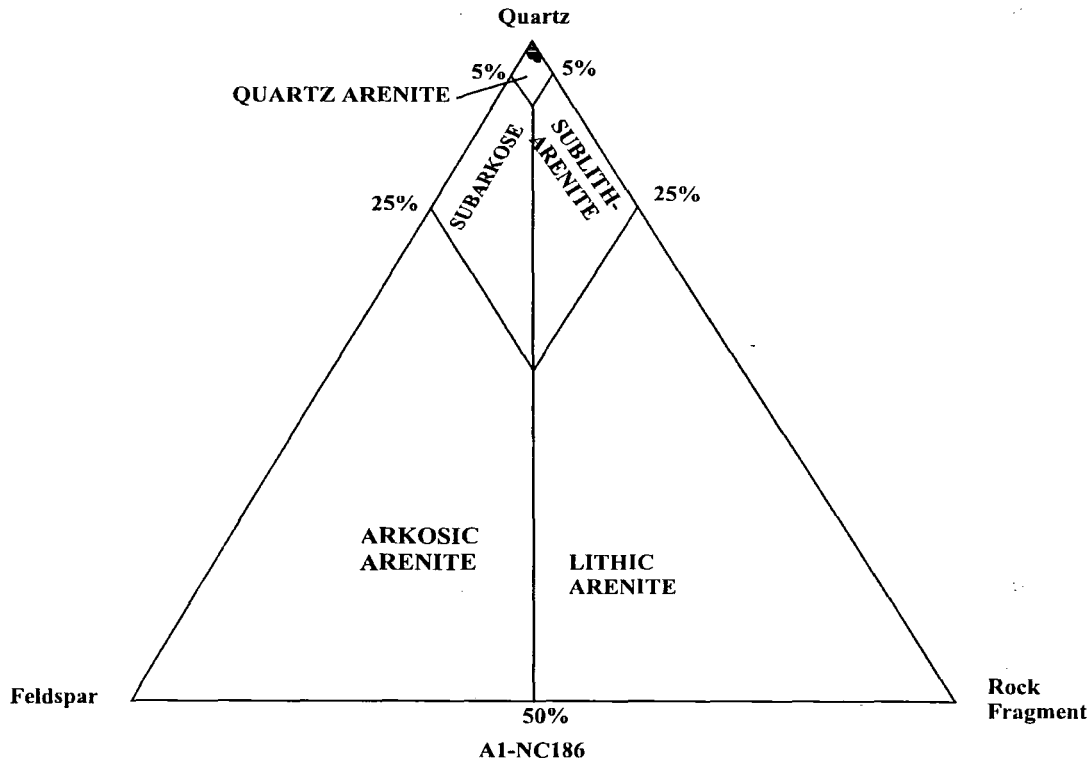

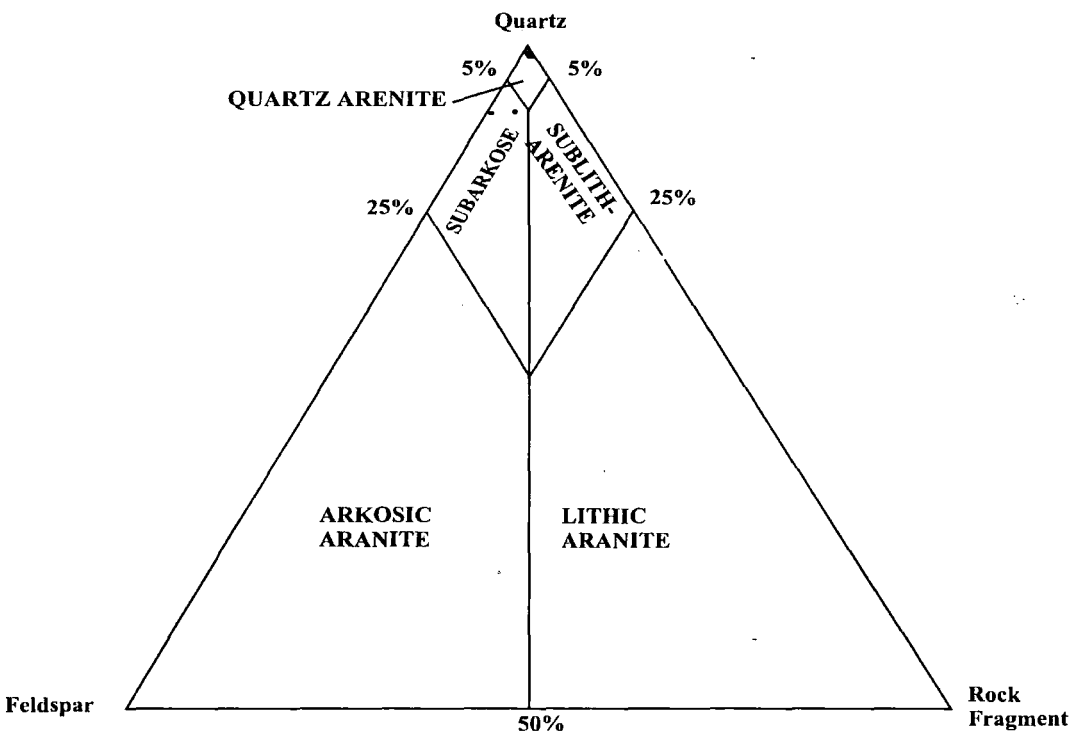

Fig. 4.18. Detrital composition of the Hawaz sandstones (A1-NC186 and H27-NC115) plotted on a Pettijohn et al., (1987) classification diagram.

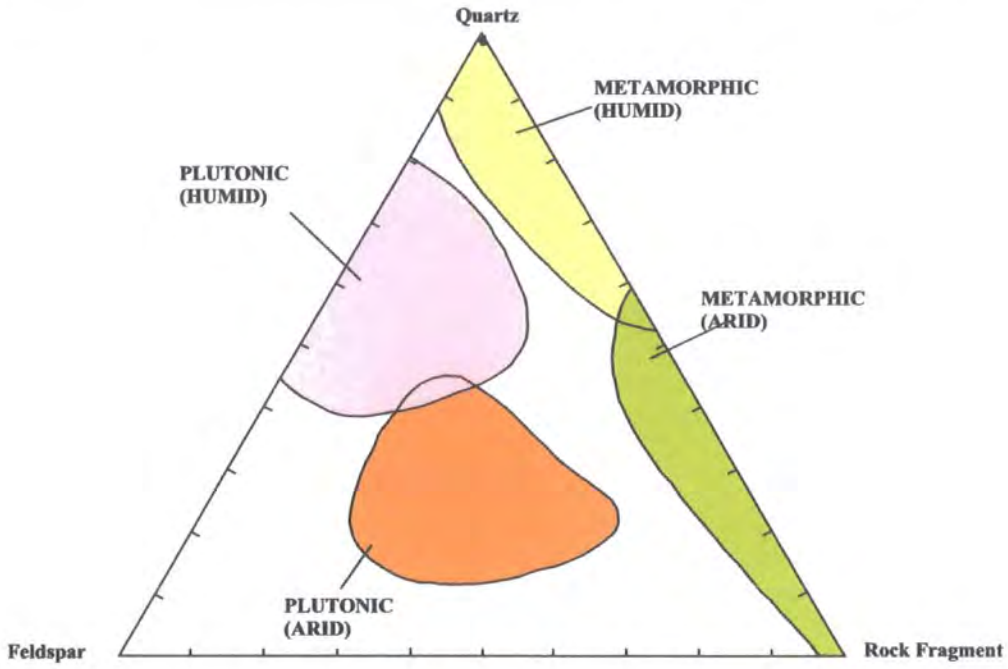

A1-NC186

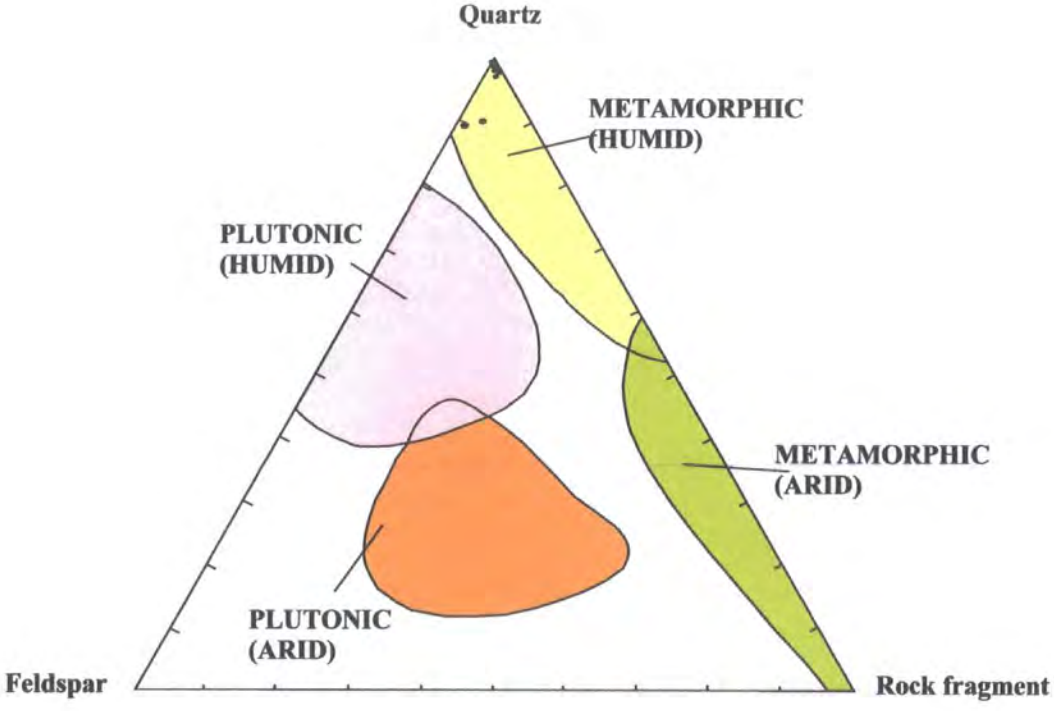

H27-NC115

Fig. 4.19. Ternary QFRF plot showing the average composition of sandstones and source rocks for A1-NC186 and H27-NC115, which fall within the metamorphic humid climate field, (Suttner et al., 1981).

significance. Compositional fields associated with different provenances can then be displayed on standard triangular diagrams (**Fig. 4.20**) (Dickinson, 1985). The major drawback of such techniques is that they show where the sands come from, rather than where they are deposited. While there are certainly broad associations between source and basin, it is by no means fixed (Macdonald, 1993).

Ternary diagrams have been used to plot the Hawaz sandstone compositional data for A1-NC186 and H27-NC115. These indicate that the Hawaz sandstones fall within the cratonic interior field, (**Fig. 4.19**) which generally can be interpreted as being derived from high topographic areas located a long distance from the depositional area producing the quartz-rich sandstones. Multicycle reworking on cratons might be required to develop mature quartz sandstone (Dickinson, 1985).

4.6 Diagenesis

Diagenesis is defined as all the physical, chemical, and biological changes that a sediment is subjected to (excluding folding and fracturing) after the grains are deposited but before they are metamorphosed (Blatt, 1992).

Diagenesis takes place at temperatures and pressures higher than those of the weathering environment but below those that produce metamorphism. There is no clear boundary between the realm of diagenesis and metamorphism (Boggs, 1995).

Diagenesis has been divided into two broad stages: early diagenesis, for processes taking place from deposition and into the shallow-burial realm, and late diagenesis for those processes affecting the sediments at deeper levels, and on uplift. The terms eogenesis, mesogenesis and telogenesis have been used for early and burial diagenesis and diagenesis-on-uplift, respectively (Tucker, 2001).

From the microscope observations various diagenetic features can be recognized in the Hawaz Formation including quartz overgrowth, calcite cement, chemical compaction, including pressure dissolution of minerals, and kaolinite and pyrite cement (**Fig. 4.21**).

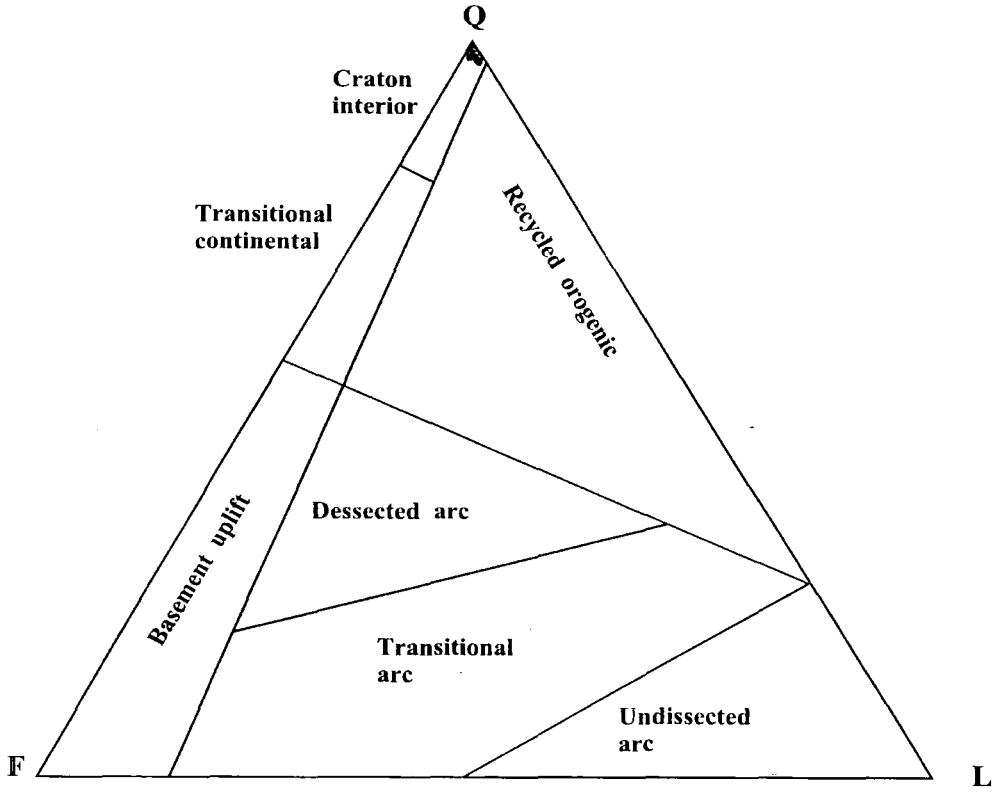

A1-NC186

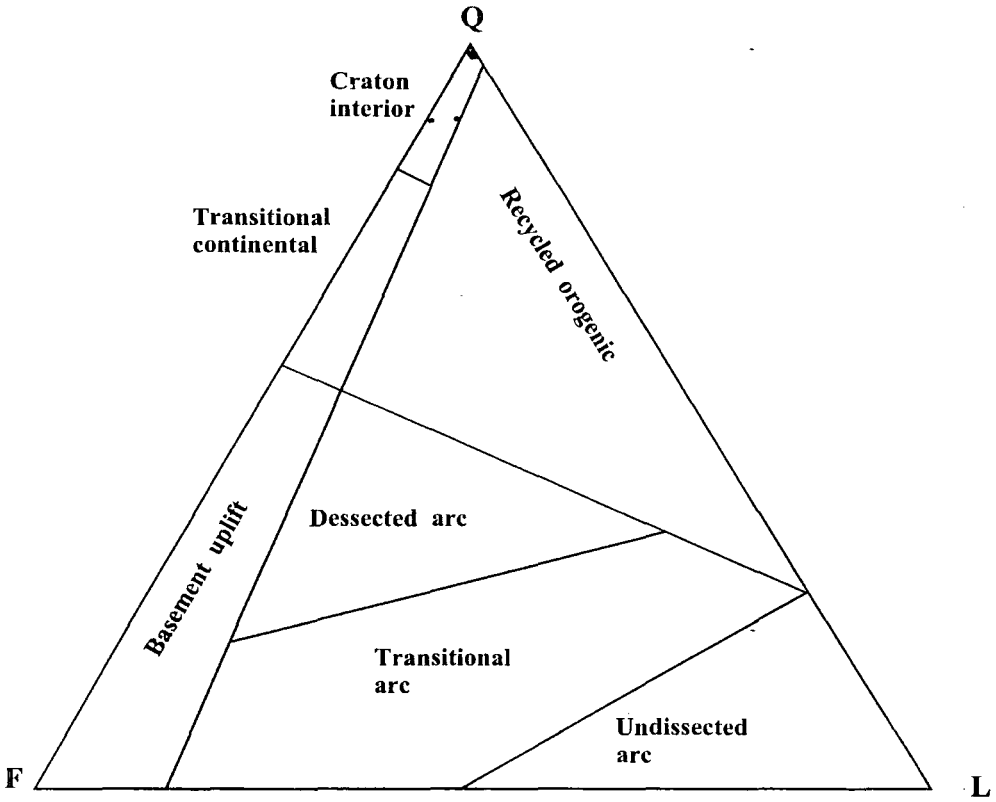

H27-NC115

Fig. 4.20. QFL triangle showing the tectonic provenance fields for the Hawaz sandstones in A1-NC186 and H27-NC115 (Dickinson, 1985).

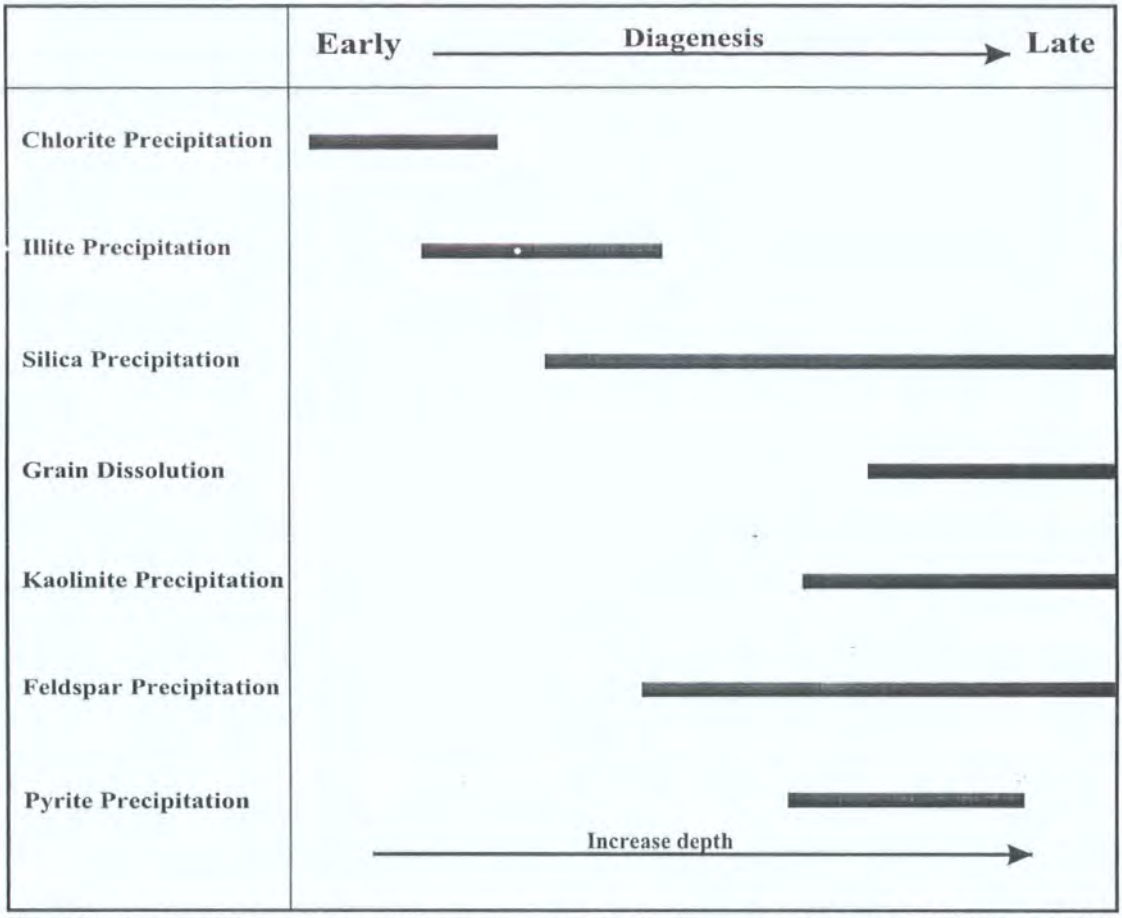

Fig. 4.21. Paragenetic sequence of diagenetic events in the Hawaz sandstone, A1-NC186 and H27-NC115.

4.6.1 Quartz overgrowth

Quartz is the most common silicate mineral that acts as a cement. In most sandstones, the quartz cement is chemically attached to the crystal lattice of existing quartz grains, forming rims of cement called overgrowths. Overgrowths can be recognized by a line of impurities or bubbles that mark the surface of the original grain. Quartz overgrowths are particularly common in quartz-rich sandstones (Boggs, 1995). The quartz overgrowth is the first diagenetic precipitate and characterizes early burial (Siever et al., 1962), but it can occur at any time in the diagenetic sequence (Hancock et. al, 1978).

From thin sections analysis and SEM studies, it can be demonstrated that the deposition of quartz overgrowths occurred at an early diagenetic stage and continued to grow periodically throughout burial diagenesis, as evidenced by preservation of

primary intergranular volume. The early quartz overgrowths can be seen under the microscope by a dust rim but good crystal terminations are scarce or absent (**Fig. 4.6**). Late stage quartz overgrowths can be distinguished by the quartz filling the pore space on one side, destroying the porosity, and being surrounded by crystals on the other sides (**Figs. 4.7** and **4.22**).

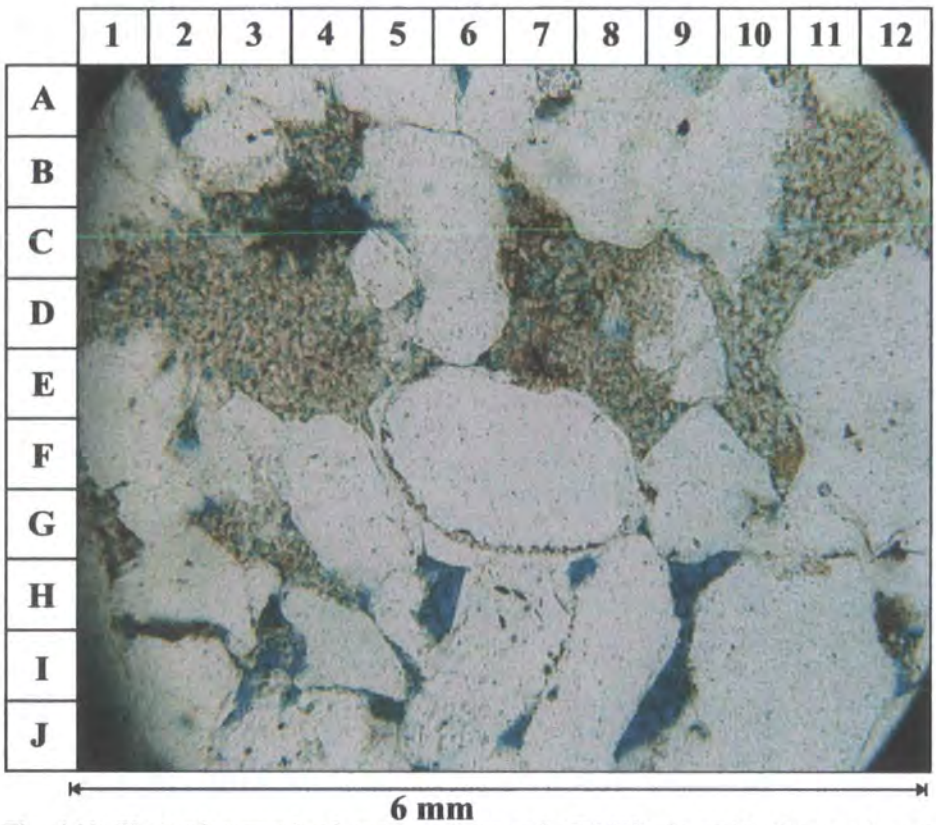

Fig. 4.22. Photomicrograph of quartz overgrowth (F6-H9), in which the quartz grew into the pore on one side which is not filled by clay minerals at the time (H7), at depth 4908 ft (H27-NC115), PPL, (X20).

4.6.2 Carbonate cementation

The most common diagenetic phase in sandstone (up to 30%) is carbonate cements in the form of calcite and dolomite, which rarely coexist in one sample. Dolomite occurs chiefly as a sparry interstitial cement or more rarely as a replacement of detrital plagioclase or as a fracture fill. The bulk of the calcite and dolomite is interpreted to be a relatively early cement, because when abundant within a rock, associated detrital micas are compacted (Boles, 1982).

Calcite is one of the most common cements in sandstones, but other carbonate cements of more local importance are dolomite and siderite. The cement may vary from a uniform to patchy distribution, to local segregations and concretions. The two main types of calcite cement are poikilotopic crystals and drusy calcite spar (Tucker, 1991). Carbonate cementation is favoured by increasing concentration of calcium carbonate in pore waters and increasing burial temperature (Boggs, 1995). They take several forms. In most cases each individual pore is filled by a single crystal of calcite, whilst in others, the calcite crystallized in large "poikilitic" patches which enclose many sand grains (Pettijon et al,. 1987).

Carbonate cementation in the Hawaz Formation (A1-NC186 and H27-NC115) is volumetrically minor, and dominated by calcite. The calcite occurs both as isolated patches between grains as a grain-support, and as pore-filling (**Fig. 4.23**). The calcite causes corrosion of the margins of quartz grains. The calcite can be interpreted as an early cement which has been dissolved and the space probably filled by authigenice kaolinite.

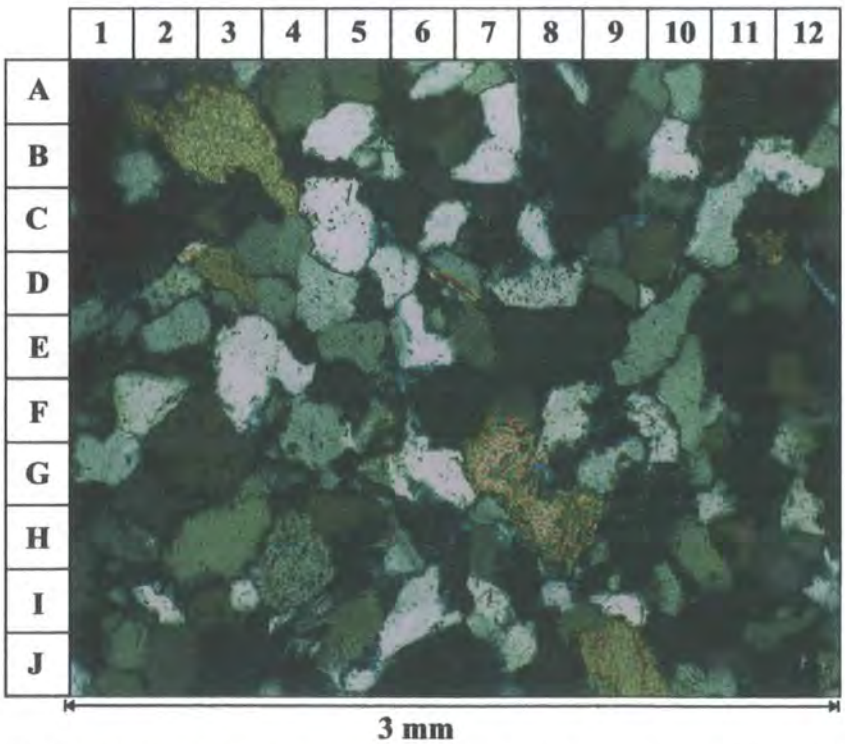

Fig. 4.23. Photomicrograph showing calcite grains within the Hawaz sandstone at depth (4764ft), XPL (X10).

Calcite pore-filling cement forms locally very early in the burial history of the Hawaz sandstone. Early formation of the calcite is indicated by (1) loosely packed sand, which commonly preserves the initial intergranular areas, and (2) the apparent random distribution of calcite-cement over the entire range of burial depths (Galloway, 1974).

4.6.3 Feldspar dissolution and overgrowths

Solution of feldspar in sedimentary rocks is common in some formations and contributes significantly to the porosity. Solution of feldspar leads to significant increase in porosity in some beds. Although there are some feldspar voids which appear to be isolated in thin section, they may have intergranular connections outside the plane of the thin section. The fact that the voids are easily filled by impregnation in the preparation of thin sections indicates that they now constitute part of the effective porosity (Heald et al., 1973).

The solution of feldspar in the Hawaz sandstone represents an increase in porosity in the samples where the solution occurs by leaching the feldspar grains. However, an incomplete leaching of plagioclase feldspar is also seen. Dissolution is related to porewater movements from undersaturated environments dominated by waters of meteoric origin that move downward and laterally in a basin. In these waters the Na^+/H^+ and K^+/H^+ activity ratios are low compared to silica activities. Authigenesis is related either to local isochemical changes or to porewater movements that transport waters high in Na^+/H^+ or K^+/H^+ ratio from lower formations (Pettijohn et al., 1987).

In the Hawaz sandstones, feldspars are incompletely leached (**Fig. 4.8**) and some of the feldspars altered to clay minerals or replaced by calcite or probably kaolinite. Complex secondary porosity has been generated by the dissolution of feldspar. Also feldspar overgrowths locally grow on or around detrital feldspar grains and fill the porosity.

4.6.4 Clay mineral authigenesis

Clay minerals can be modified and altered during early and late diagenesis, and into metamorphism (Tucker, 1991). The major emphasis of studies on clays in sandstones has been on the formation of interstitial kaolinite or dickite, characteristically associated with quartz aranites, the neoformation of clays from pore water, and the transromation of mixtures of detrital smectites and micaceous clays (Pettijohn et al., 1987). The main change is an alteration of smectites to illite via mixed-layer clays of smectite-illite. This alteration involves the incorporation of K^+ ions into the smectite structure and loss of interlayer water (Tucker, 1991). The authigeneic clay minerals reduce the space in pores, increase microporosity as well as the ratio of surface area to volume, and increase the physical resistance to fluid flow as crystals grow outward from pore walls, especially the long, fibrous, illite crystals. The abundance and kinds of authigenic clays, like the primary clays, should always be related to the sub-environments of a sandstone body (Pettijohn et al., 1987).

In addition to the four common clay minerals illite, kaolinite, montmorillonite and chlorite, mixed-layer clays are also common (Tucker, 1991). Immediately after sediment burial begins these minerals will suffer the effects of diagenesis and will transform to stable minerals suitable for the physical and chemical environments encountered during burial (Aoyagi and Kazoma, 1980).

4.6.4.1 Kaolinite

Kaolinite minerals are related to the surficial zones of the earth's crust where they are formed. They are characterized by the hexcoordination of aluminium. During diagenesis they are very sensitive to the geochemical environment, stable in acid conditions, unstable in alkaline conditions. However, the increase in temperature by burial causes their destruction sooner or later (Segonzac, 1970).

Some of the authigenic kaolinite that is so common in sandstones is derived from the diagenetic dissolution of detrital feldspar. Another kind of kaolinite has the appearance of a well-crystallised, pure pore filling that was precipitated from a solution and shows no evidence of alteration from a precursor feldspar or other clay minerals. The presence of either kind of kaolinite may be evidence for an invasion of

relatively fresh ground-waters entering the sandstone from a recharge outcrop belt in which there was a supply of distilled silica from chemical weathering (Pettijohn et al., 1987).

Kaolinite clusters commonly conform to spaces interstitial to sand grains but show little, if any, effect of compaction. Additionally, kaolinite commonly replaces quartz including overgrowth. Thus, kaolinite formation postdates both compaction and quartz overgrowths (Bucke and Mankin, 1971). Some authigenic kaolinite that is so common in sandstones is derived from the diagenetic dissolution of detrital feldspar (Pettijohn et al., 1987).

Throughout the Hawaz sandstone kaolinite is the most common authigenic clay mineral developed within the sandstones. It is a late stage authigenic mineral postdating early quartz overgrowth. Kaolinite precipitation occurs as an alteration product from the dissolution of feldspar grains and from circulating pore fluid. Kaolinite develops as discrete particle clays and forms a characteristic pattern of irregular face to face stacks of pseudo-hexagonal plates or books which can be readily identified under SEM and the microscope. The vermicular kaolinite stacks seen in the Hawaz sandstone are generally curved and intertwining with considerable intercrystalline porosity (**Figs 4.13** and **4.14**).

4.6.4.2 Smectite (montmorillonite)

Smectite is a special kind of clay, a mineral that absorbs water and swells substantially. Each crystal of the mineral is made up of a system of sheets of alternating aluminum-oxygen and silicon-oxygen molecules. Between the sheets the air is charged with an electrostatic force that sucks in water, so that the crystal swells up to 8 times its original size. The smectite structure is similar to those of micas but contain water with cations in interlayer positions (Pettijohn et al., 1987). The smectite in the Hawaz sandstone can be recognized under the SEM (Figs. 4.14 and 4.24), as clay coating on detrital quartz grains. Individual crystals of smectite cannot be resolved under the SEM, instead, the clay appears as a thin, webby crust, and form a relatively dense and smooth coating on the detrital grain surface.

Fig. 4.24. SEM picture shows late quartz overgrowth in Hawaz sandstone.

4.6.4.3 illite

Illite is the major clay-mineral constituent in both sands and shales. Invariably illite dominates the shales and displays wide variation in relative quantity within sands. Mechanical size fractionation of detrital illite is considered the logical mechanism controlling the distribution (Bucke et al,. 1971).

Illites form a very heterogenous group in the sediments which have hardly suffered diagenesis. Particles of diverse origin are found. They become more regular during burial (Segonzac, 1970). Illite clay continues to precipitate as an intergranular cement, possibly during late stage deep burial diagenesis. Illite is commonly cited as having a detrimental effect on pores. This tends to increase the tortuosity of the flow path and hence decrease the permeability (Tucker, 1991).

Illite cement is a minor component of the authigenic mineralogy of the Hawaz sandstones, and it appears to comprise poorly developed plates infilling porosity and also to occur as a grain coating.

4.6.4.4 Chlorite

Chlorites are the least well-known clay minerals in diagenesis. Detrital particles can be aggraded to chlorite during early diagenesis by passing through the mixed layer stage of corrensite. A massive growth of chlorite is observed in late diagenesis and the anchizone (Segonzac, 1970). Although all chlorite is recorded as clay size, it was found to be present in sand-size phyllite rock fragments in addition to the clay matrix (Bucke et al,. 1971).

In the Hawaz Formation it is likely that poorly crystallised chlorite clay was precipitated in rare patches on detrital grains, post-dated by the precipitation of grain-coating illite exhibiting a short fibrous morphology. It is possible that the chlorite clay was altered to illite. Therefore illite clay began to form early in the diagenetic history of the sandstones. In some samples illite continued to accumulate until the pores were completely filled.

4.6.5 Pyrite

Pyrite was probably precipitated by the reaction of H_2S with iron. H_2S derived from thermal decomposition of organic sulphur compounds then provided a catalyst for thermochemical sulphate reduction and additional H_2S was generated. Some of this thermally produced H_2S was subsequently removed by reaction with iron to precipitate late authigenic pyrite (Edman and Surdam, 1984).

In the Hawaz sandstones the authigenic pyrite occurs as incipient cement lining the secondary pore spaces. Then, the pyrite can be interpreted as a late stage phase of diagenesis.

4.7 Porosity in the Hawaz sandstones

Porosity is defined as the ratio of the pore volume to the bulk of the substance. In oil and gas reservoirs the pore volume is the space available for the storage of the hydrocarbons and water. Porosity is normally expressed as a percentage of bulk volume and is symbolised by ϕ.

$$\text{Porosity } \phi = \frac{\text{Pore volume}}{\text{Bulk volume}} \times 100$$

The total porosity is defined as the ratio of the volume of the pores to the bulk volume of a material regardless of whether or not all of the pores are interconnected. The effective porosity is defined as the ratio of the interconnected pore volume to the bulk volume of a material, i.e. it does not include dead-end pore-space (Bown, 2001).

Absolute porosity refers to the total void space, but since some of this will be within grains, effective porosity is more important. It is the latter which determines the reservoir properties of a rock, together with its permeability and the ability of sediment to transmit fluids (Tucker, 1991). No analysis of permeability for the two studied wells has been attempted. Porosity in sandstone can be divided into three types, primary porosity, secondary porosity and microporosity.

Primary porosity is a direct reflection upon the deposition and compactional processes that the sediment has undergone during initial burial. Sandstones prior to burial have porosities ranging from 35% - 40%, but this is decreased through burial and increasing compaction of the sediments and through the deposition of authigenic cements and clay mineral diagenesis. Final values of irreducible primary porosity may be as low as 4.0% (Schmidt and McDonald, 1979).

In the Hawaz Formation all three types of porosity occur. The mean primary porosity in A1-NC186 is 10.3% and in H27-NC115 it is 11.2%, which show that the Hawaz sandstones in these two wells have suffered considerable loss through burial compaction. Locally the oversize pores and attendance of clay rims are indicative of dissolution of unstable grains (**Fig. 4.25**). The majority of the secondary porosity developed in the Hawaz Formation is through the alteration of unstable detrital grains, especially feldspar. Secondary porosity after feldspar can be recognized in the thin section and SEM (**Fig. 4.15**). Microporosity occurs as pores within kaolinite clay minerals, in association with authigenic clays. Microporosity cannot be accurately estimated and the proportion of microporosity present typically accounts for the frequent underestimation of porosity when measured in thin section by point counting methods.

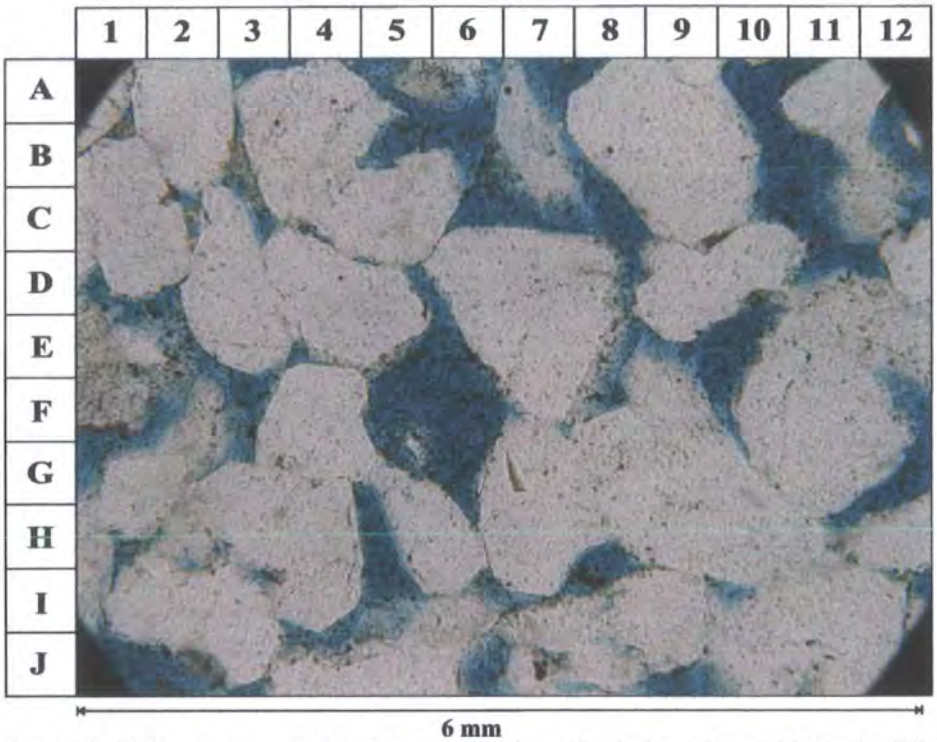

Fig. 4.25. Photomicrograph showing the complete dissolution of unstable grain (E5-F6), which enhances the porosity locally in the Hawaz sandstone. PPL (X20) (4584ft A1-NC186).

Well	Depth (ft)	Geological Formation	Texture				Porosity	Classification (Pettijohn et al., 1987)	Point Counted Data											
									Mineral component (%)						Cement					
			Mean size	Sorting	Skewness	Roundness			Quartz	Feldspar	Rock fragment	Heavy mineral	Muscovite	Chert	Calcite	Kaolinite	Illite	Chlorite	Matrix	Pyrite
A1-NC186	4412	HAWAZ	F S	M W S	N-S	SR-SA	1.3	Quartz arenite	70	0	0	0.3	2	-	0.3	7	-	-	19	0
	4415	HAWAZ	F S	M W S	S F-S	SR-SA	5	Quartz arenite	69	0	0.3	0	1	-	1.3	8.3	-	-	15	0
	4418	HAWAZ	F S	M W S	S F-S	SR-SA	2	Quartz arenite	81.3	0	0.6	0	1	-	0.6	9	-	-	5	0
	4421	HAWAZ	M S	WS	S F-S	SR-SA	6	Quartz arenite	84.6	0	0.3	0.3	0	-	0.3	3.6	-	-	4.6	0
	4427	HAWAZ	M S	M W S	S F-S	SA-SR	4.3	Quartz arenite	80.6	0	0	0	0	-	0.3	9.6	-	-	5	0
	4433	HAWAZ	F S	M W S	F-S	SR-SA	1	Quartz arenite	75.6	0	0	0.6	1.6	-	0.3	6.3	-	-	14.3	0
	4442	HAWAZ	F S	M W S	S F-S	SR-SA	0.6	Quartz arenite	70.6	0.3	0	1.3	1	-	0	3	-	-	23	0
	4446	HAWAZ	M S	M W S	F-S	SA-SR	5.3	Quartz arenite	80.6	0	0.3	3	0	-	0.3	8.3	-	-	2	0
	4463	HAWAZ	M S	M W S	N-S	SA-A	2.3	Quartz arenite	86.3	0.3	0.3	0.6	0	-	0	10	-	-	0	0
	4464	HAWAZ	M S	WS	C-S	SA-SR	1	Quartz arenite	94.6	0	0	1	0	-	0	2.6	-	-	0.6	0
	4476	HAWAZ	M S	M W S	S F-S	SA-SR	9.3	Quartz arenite	76	0	0.6	1.3	0	-	0	7	-	-	5.6	0
	4479	HAWAZ	M S	W S	S F-S	SA-SR	9.3	Quartz arenite	82	0	0.3	0	0	-	0.6	4	-	-	3.6	0
	4482	HAWAZ	M S	W S	S F-S	SR-SA	4.6	Quartz arenite	83.6	0	0	1	0.6	-	0	3	-	-	7	0
	4494	HAWAZ	M S	W S	F-S	SA-SR	12	Quartz arenite	80.6	0	0	0.6	0	-	0	2.6	-	-	4	0
	4497	HAWAZ	M S	M W S	F-S	SR-SA	5	Quartz arenite	82.6	0.6	0.6	1.3	0	-	0	4	-	-	5.6	0
	4503	HAWAZ	M S	W S	S F-S	SR-SA	15	Quartz arenite	77.6	0	0	0	0.3	-	0	5	-	-	2	0
	4509	HAWAZ	M S	M W S	N-S	SR-SA	5.3	Quartz arenite	79.3	0	0	0.3	0.3	-	0	1	-	-	13.6	0
	4515	HAWAZ	M S	W S	S F-S	SR-SA	12.3	Quartz arenite	82.6	0.6	0	0	0.3	-	0	3.3	-	-	0.6	0
	4518	HAWAZ	M S	M W S	F-S	SR-SA	11.6	Quartz arenite	83	0	0	0	0.3	-	0	4.6	-	-	0.3	0
	4526	HAWAZ	F S	M W S	N-S	SR-SA	-	-	-	-	-	-	-	-	-	-	-	-	-	-
	4527	HAWAZ	M S	W S	F-S	SR-SA	3.3	Quartz arenite	85.6	0	0	0	0.3	-	0	2	-	-	8.6	0
	4530	HAWAZ	M S	W S	C-S	SR-SA	22.6	Quartz arenite	75	0	0	0	0	-	0	2.3	-	-	0	0
	4533	HAWAZ	M S	M W S	S F-S	SR-SA	23.6	Quartz arenite	74.3	0	0	0	0	-	0	1.6	-	-	0.3	0
	4539	HAWAZ	M S	M W S	S F-S	SR-SA	19.3	Quartz arenite	75	0	0	0	0	-	0	5.6	-	-	0	0
	4542	HAWAZ	M S	M W S	S F-S	SR-SA	13.6	Quartz arenite	82.3	0	0	0	0	-	0	1.3	-	-	2.6	0

Table 4.1 Model composition of sandstone samples from the Hawaz Formation, A1-NC186 and H27-NC115.

Weiy6ll	Depth (ft)	Geological Formation	Texture				Porosity	Classification (Pettijohn et al., 1987)	Point Counted Data											
									Mineral component (%)						Cement					
			Mean size	Sorting	Skewness	Roundness			Quartz	Feldspar	Rock fragment	Heavy mineral	Muscovite	Chert	Calcite	Kaolinite	Illite	Chlorite	Matrix	Pyrite
A1-NC186	4545	HAWAZ	F S	M W S	N-S	SR-SA	0.3	Quartz arenite	66.3	0.9	1.3	0.3	5.3	-	0	12.6	-	-	12.3	0.3
	4548	HAWAZ	M S	M W S	S F-S	SR-SA	10.6	Quartz arenite	86	0	0	0.3	0.3	-	0	1	-	-	1.6	0
	4549	HAWAZ	M S	W S	S F-S	SR-SA	0	Quartz arenite	82.3	0	0	0	0.3	-	15.6	0	-	-	1.6	0
	4554	HAWAZ	M S	W S	F-S	SA-A	12	Quartz arenite	81.3	0.3	0.3	0.3	0.3	-	0	3	-	-	2.3	0
	4557	HAWAZ	M S	W S	S F-S	A-SA	2.3	Quartz arenite	95.6	0.3	0	0	0.3	-	0	1	-	-	0.3	0
	4562	HAWAZ	M S	W S	S F-S	SR-SA	15	Quartz arenite	82	0	0	0.3	0	-	0	2	-	-	0.6	0
	4563	HAWAZ	M S	W S	S F-S	SR-SA	5.6	Quartz arenite	79	0	0.3	0.3	0	-	0	14.3	-	-	0.3	0
	4566	HAWAZ	M S	W S	F-S	SR-SA	19	Quartz arenite	78	0.3	0	0.3	0.3	-	0.3	0.3	-	-	1.3	0
	4569	HAWAZ	M S	W S	F-S	SR-SA	23.6	Quartz arenite	73.3	0	0	0.6	0.6	-	0	0.6	-	-	1	0
	4571	HAWAZ	V F S	M W S	N-S	A-SA	-	-	-	-	-	-	-	-	-	-	-	-	-	-
	4576	HAWAZ	M S	W S	S F-S	SR-SA	0.3	Quartz arenite	91.6	0	0.3	0.3	0.3	-	0	7	-	-	0	0
	4579	HAWAZ	M S	W S	S F-S	SR-SA	11	Quartz arenite	82.3	0	0	0	0.3	-	0	1	-	-	4	1.3
	4582	HAWAZ	M S	W S	N-S	SR-SA	24.3	Quartz arenite	74.6	0	0.3	0	0	-	0	0.6	-	-	0	0
	4584	HAWAZ	M S	W S	F-S	SR-SA	15.6	Quartz arenite	81	0	0	0.6	0.3	-	0	2.3	-	-	0	0
	4590.5	HAWAZ	M S	W S	S F-S	SR-SA	1.6	Quartz arenite	91.6	0.3	0	0	1	-	0	3	-	-	2.3	0
	4591	HAWAZ	M S	W S	S F-S	R-SR	19.3	Quartz arenite	77.3	0	0	0	0.6	-	0	2.3	-	-	0.3	0
	4597.7	HAWAZ	M S	W S	S F-S	SR-R	24	Quartz arenite	72.3	0	0	2	0	-	0	1.6	-	-	0	0
	4601.6	HAWAZ	M S	W S	N-S	SR-SA	13.6	Quartz arenite	85.3	0	0	0	0	-	0	0	-	-	0.6	0.3
	4603.5	HAWAZ	M S	W S	F-S	SR-SA	16	Quartz arenite	83	0	0	0	0	-	0	0.6	-	-	0.3	0
	4607	HAWAZ	M S	W S	N-S	SR-SA	2.6	Quartz arenite	82	0	0.3	0.3	0.6	-	0	1.3	-	-	12.6	0
	4609	HAWAZ	M S	W S	F-S	SR-SA	10.6	Quartz arenite	87.6	0	0	0.3	0.3	-	0	0.3	-	-	0.6	0
	4612	HAWAZ	M S	W S	F-S	SR-R	21.6	Quartz arenite	77	0	0	0	0	-	0	1.3	-	-	0	0
	4613.5	HAWAZ	F S	W S	F-S	SR-SA	3	Quartz arenite	80	0	0	0.6	0.3	-	0	0.6	-	-	15.3	0
	4614	HAWAZ	M S	M W S	F-S	SA-SR	1.3	Quartz arenite	79.3	0	0	0	0.6	-	0	0.3	-	-	18.3	0
	4618	HAWAZ	M S	W S	C-S	SR-SA	19.3	Quartz arenite	75.6	0	0	0	0.3	-	0	2.6	-	-	2	0
	4629	HAWAZ	F S	W S	N-S	SA-SR	4.3	Quartz arenite	80.6	0.6	0	0	1	-	0	10.6	-	-	2.6	0
	4632	HAWAZ	M S	W S	F-S	SR-SA	14	Quartz arenite	84.6	0	0	0	0.3	-	0	0.6	-	-	0.3	0
	4637	HAWAZ	M S	W S	S F-S	SR-SA	6	Quartz arenite	87.3	0	0	0	1.6	-	0	2.3	-	-	2.6	0
	4641	HAWAZ	M S	W S	S F-S	SR-SA	14.3	Quartz arenite	85	0	0	0	0	-	0	0.6	-	-	0	0
	4642.3	HAWAZ	M S	W S	S F-S	SR-SA	15	Quartz arenite	82.6	0	0.3	0	0.3	-	0	1.6	-	-	0	0
	4650	HAWAZ	F S	W S	N-S	SA-A	10.6	Quartz arenite	74	0	1	0.6	0	-	0	7	-	-	6.6	0
	4664	HAWAZ	F S	W S	C-S	SA-A	0	Quartz arenite	90	0.3	0.3	0	0.3	-	0	8.6	-	-	0.3	0
	4665	HAWAZ	M S	W S	N-S	SR-SA	17	Quartz arenite	82	0	0	0.3	0	-	0	0.6	-	-	0	0
	4671	HAWAZ	M S	W S	F-S	SR-SA	23.3	Quartz arenite	73.6	0	0	0.3	0	-	0	0	-	-	2	0.6
	4676	HAWAZ	F S	W S	C-S	SA-A	3.3	Quartz arenite	95.3	0	0	0	0.6	-	0	0	-	-	0.6	0
	4683	HAWAZ	F S	W S	N-S	SR-SA	24.3	Quartz arenite	73.3	0	0	0	0.3	-	0	2	-	-	0	0
	4685	HAWAZ	M S	W S	N-S	SR-SA	20.6	Quartz arenite	77.3	0	0	0.3	0	-	0	1.6	-	-	0	0
	4689	HAWAZ	M S	W S	F-S	SA-SR	12.6	Quartz arenite	85	0	0	0	0.3	-	0	1	-	-	1	0
	4691	HAWAZ	F S	W S	F-S	SA-A	10	Quartz arenite	79.6	0	0	0	2	-	0	2.3	-	-	6	0
	4695	HAWAZ	M S	W S	S F-S	SA-SR	10.6	Quartz arenite	86.3	0	0	0.3	0.6	-	0	1	-	-	1	0
	4698	HAWAZ	F S	W S	N-S	SA-SR	0.3	Quartz arenite	85.3	0	0	0.3	2.3	-	0	1.6	-	-	10	0
	4728	HAWAZ	F S	W S	S C-S	SA-A	16.3	Quartz arenite	76	0	0	0	1.3	-	0	2.3	-	-	4	0
	4731.1	HAWAZ	F S	W S	N-S	A-SA	-	-	-	-	-	-	-	-	-	-	-	-	-	-
	4731.8	HAWAZ	F S	W S	C-S	SA-A	3.6	Quartz arenite	73	0.3	0	0	2.3	-	0	3	-	-	17.6	0
	4737	HAWAZ	F S	W S	C-S	SA-SR	14.3	Quartz arenite	80.6	0	0	0	0.3	-	0.6	3.3	-	-	0.6	0
	4740	HAWAZ	F S	W S	S C-S	SA-A	5.3	Quartz arenite	86	0	0	0.3	1	-	2.3	5	-	-	0	0
	4749	HAWAZ	F S	W S	C-S	SA-A	5.3	Quartz arenite	80.3	0	0	0.3	4	-	1.6	3	-	-	5.3	0
	4755	HAWAZ	F S	W S	N-S	A-SA	6.3	Quartz arenite	74.6	0	0	0.6	3.3	-	0.3	2.6	-	-	12	0
	4758	HAWAZ	F S	W S	C-S	A-SA	14.3	Quartz arenite	77.3	0	0	1.3	2.6	-	1.3	1	-	-	2	0
	4764	HAWAZ	F S	V W S	C-S	A-SA	13.3	Quartz arenite	76.3	0	0	1	1.3	-	4.6	2	-	-	1.3	0
	4769.2	HAWAZ	V F S	W S	S C-S	-	-	-	-	-	-	-	-	-	-	-	-	-	-	-
	4776	HAWAZ	F S	W S	C-S	A-SA	0.3	Quartz arenite	93	0.3	0	0.3	1	-	1	3.6	-	-	0.3	0
	4777.5	HAWAZ	V F S	W S	S C-S	-	-	-	-	-	-	-	-	-	-	-	-	-	-	-
H27-NC115	4743	HAWAZ	M S	V P S	N S	SR-SA	0	Quartz arenite	81	0	0	0.3	0.6	-	0.6	7	-	-	10.3	0
	4834	HAWAZ	M S	P S	N S	SA-A	0	Subarkose	67.6	7	0.6	0	1	-	1.6	22	-	-	0	0
	4875	HAWAZ	M S	V P S	N S	SA-SR	13.6	Quartz arenite	77	0.3	0.3	0.3	0.3	-	0.3	2.6	-	-	5	0
	4895	HAWAZ	M S	P S	N S	SR-SA	-	-	-	-	-	-	-	-	-	-	-	-	-	-
	4899.5	HAWAZ	M S	P S	N S	SR-SA	19	Quartz arenite	75.3	0	0	0.3	0	-	0.6	4.6	-	-	0	0
	4908	HAWAZ	M S	P S	N S	SR-SA	21	Quartz arenite	75.6	0	0	0.3	0	-	0.6	2.3	-	-	0	0
	4910	HAWAZ	M S	P S	N S	SA-SR	13.3	Quartz arenite	83	0	0	0	0	-	0	3	-	-	0.6	0
	4920	HAWAZ	M S	P S	N S	SA-SR	4.3	Quartz arenite	94.6	0	0	0.3	0	-	0	0.6	-	-	0	0
	4926	HAWAZ	M S	V P S	N S	SA-A	4.3	Quartz arenite	86.6	0.3	0	0	0.3	-	0	5	-	-	3.3	0
	4937	HAWAZ	M S	P S	N S	SR-SA	22.6	Quartz arenite	75.6	0	0	0	0	-	0	1.6	-	-	0	0
	4940	HAWAZ	M S	P S	N S	SA-SR	16.6	Quartz arenite	77.3	0	0	0	0	-	0	3.3	-	-	2.6	0
	4947	HAWAZ	M S	V P S	N S	SR-SA	11.3	Quartz arenite	84.6	0	0	0	0	-	0	2.3	-	-	1.6	0

Continue table 4.1.

Weiy6ll	Depth (ft)	Geological Formation	Texture				Porosity	Classification (Pettijohn et al., 1987)	Point Counted Data											
									Mineral component (%)						Cement					
			Mean size	Sorting	Skewness	Roundness			Quartz	Feldspar	Rock fragment	Heavy mineral	Muscovite	Chert	Calcite	Kaolinite	Illite	Chlorite	Matrix	Pyrite
H27-NC115	4951	HAWAZ	M S	P S	N S	SR-SA	16.6	Quartz arenite	76	0	0	0	0	-	0.3	2.6	-	-	4.3	0
	4954	HAWAZ	M S	P S	N S	SR-R	15	Quartz arenite	82.6	0	0	0.6	0	-	0	1.6	-	-	0	0
	4965	HAWAZ	M S	P S	N S	SR-SA	18	Quartz arenite	79.3	0	0.3	0	0	-	0	1.3	-	-	1	0
	4975	HAWAZ	M S	P S	N S	SR-R	18	Quartz arenite	81.6	0	0	0	0	-	0	0.3	-	-	0	0
	4982	HAWAZ	M S	P S	N S	SR-SA	15	Quartz arenite	81.3	0	0	0	0	-	0.3	3	-	-	0.3	0
	4991.5	HAWAZ	M S	P S	N S	SA-SR	9.3	Quartz arenite	85	0	0	0.6	0	-	0.3	3.3	-	-	1.3	0
	4995	HAWAZ	F S	P S	N S	SA-A	0	Subarkose	69.6	5.3	2.3	1	6.3	-	1.6	4.6	-	-	9	0
	5008	HAWAZ	M S	P S	N S	SA-SR	1.6	Quartz arenite	85.3	0.6	1	0.6	0.3	-	3	5	-	-	2.3	0
	5183	HAWAZ	F S	F S	N S	SA-SR	2.6	Quartz arenite	83	0.3	0.3	0.3	0.3	-	1.6	11	-	-	0.3	0
	5198	HAWAZ	F S	P S	N S	SA-SR	6.3	Quartz arenite	78.3	0	0	0.6	1.3	-	1.3	9.6	-	-	2.3	0
	5204	HAWAZ	F S	P S	N S	SA-A	4	Quartz arenite	82.3	0	0	0	1.6	-	3	8.6	-	-	0.3	0
	5411	HAWAZ	M S	P S	N S	SR-SA	15.3	Quartz arenite	78.6	0	0	0.3	0.3	-	0	5.3	-	-	0	0
	5425	HAWAZ	M S	P S	N S	SR-SA	16	Quartz arenite	79.3	0	0	0.6	0.3	-	0.3	3.3	-	-	0	0
	5436	HAWAZ	F S	P S	N S	SA-A	16.3	Quartz arenite	79.3	0	0	0	0.3	-	0	4	-	-	0	0

Continue table 4.1.

5. Sequence Stratigraphy

5.1 Introduction

The concept of sequence stratigraphy has changed the way in which geologists interpret the development of sedimentary environments in time and space. Rather than correlating rocks using lithology, fossils or other stratigraphical techniques, sequence stratigraphy recognizes packages of strata each of which was deposited during a particular phase in a cycle of relative sea-level change. This genetic approach means that the packages of strata are bounded by chronostratigraphical surfaces. These surfaces include unconformities, formed during relative sea-level fall, and flooding surfaces formed during relative sea-level rise (Coe et al., 2002). Emery and Myers (1996) consider sequence stratigraphy to be a subdiscipline of stratigraphy, the latter being defined broadly as 'the historical geology of stratified rocks'.

There have been many definitions of sequence stratigraphy over the years, but perhaps the simplest is 'the subdivision of sedimentary basin-fills into genetic packages bounded by unconformities and their correlative conformities'. Sequence stratigraphy is used to provide a chronostratigraphic framework for the correlation and mapping of sedimentary faces and for stratigraphic prediction (Emery and Myers, 1996).

Since the initial publication by Wilgus et al. (1988), the concepts of sequence stratigraphy has become widely accepted and applied by the geological community to a broad range of data bases, including conventional and high-resolution seismic data, wireline logs, cores, and palaeontologic and geochemical data (Posamentier and Allen, 1999). Sequence stratigraphy is, therefore, a tool which allows geologists to draw together many different lines of evidence when analysing the fill of a sedimentary basin (Coe et al., 2002).

Coe et al. (2002). stated that there are five orders of cycles commonly recognized in the sedimentary record: first order: *c.* 50 to *c.* 200+ Ma; second order: *c.* 5 to *c.* 50 Ma; third order: *c.* 0.2 to *c.* 5 Ma; fourth order: *c.* 100 to *c.* 200 ka; fifth

order: *c.* 10 to c. 100 ka. Whilst the orders are not rigidly defined because of the wide range of conditions, parasequences are generally high-frequency fourth and fifth order cycles, and depositional sequences are, by definition, one order higher than the parasequences of which they are composed. The majority of sequences are third order cycles. Different processes have been interpreted to control the various orders of cyclicity and it is the interaction of these processes that produces the complex sedimentary record. **Figure 5.1** summarizes the key features of these different orders of cyclicity (Coe et al., 2002).

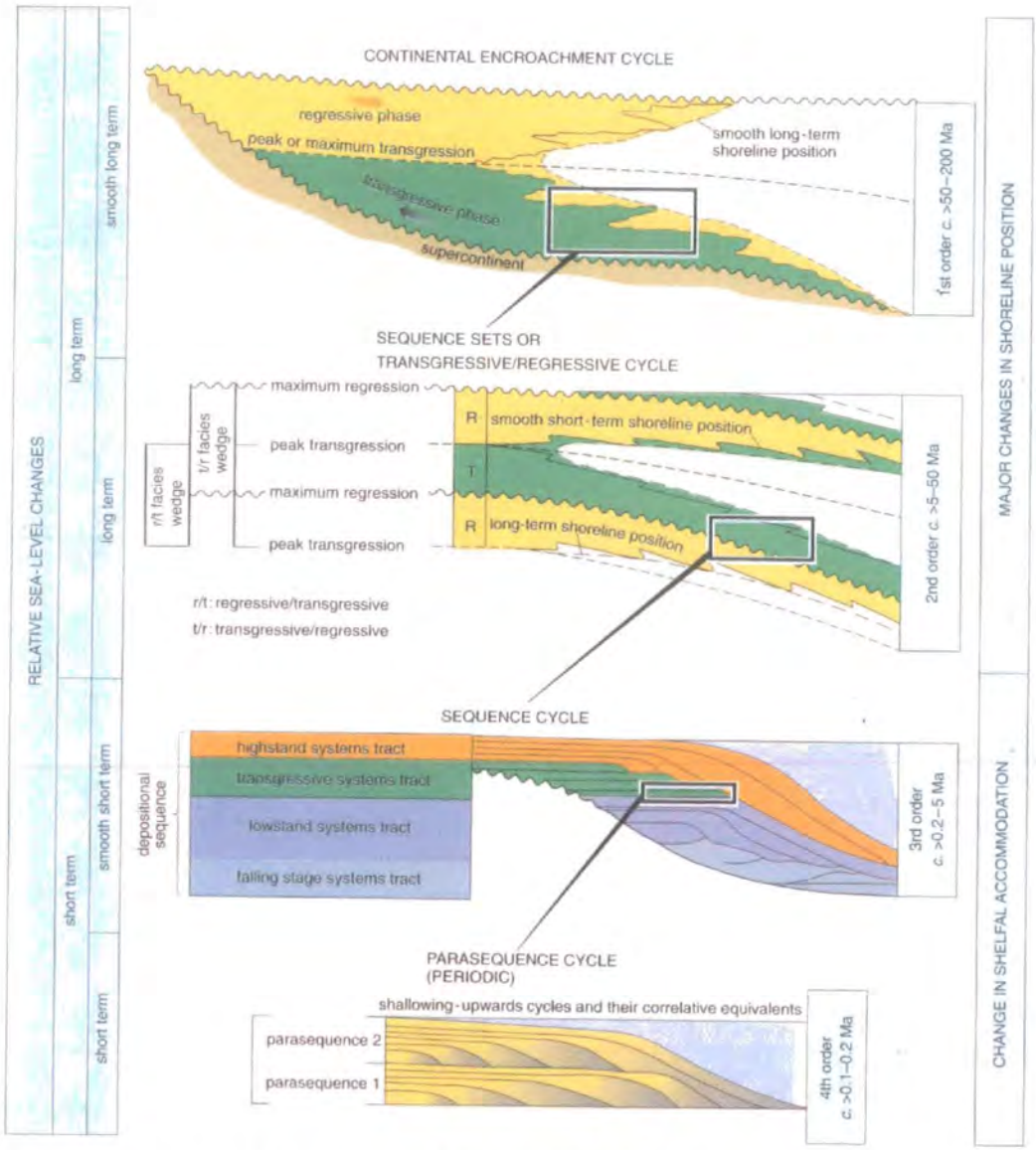

Fig. 5.1. The hierarchy of stratigraphical cycles (After Coe et al., 2002).

5.2 Methodology

Despite some of its shortcomings, the sequence stratigraphic approach represents a powerful geological tool that, if used properly, can have major impact both on exploration and field development (Posamentier et al., 1993).

The sequence-stratigraphic approach, possibly more so then most other kinds of geological analysis, benefits greatly from the use of integrated data sets and application of a systematic, step-by-step approach. Each interpretive step must be carefully and objectively appraised with respect to geologic reasonableness. There are no rigid templates for this approach, rather, as long as proposed geologic explanations violate no basic geologic principle, then they are considered reasonable. This approach is based on four steps,

- **Step-1.** *Establish the palaeogeographic setting.* The first and arguably most important step in sequence-stratigraphic analysis is to *determine the general physiographic setting for the database being analyzed.* Determining the physiographic setting is crucial, in order to narrow the range of possible geologic interpretations for a given set of observations.

- **Step-2.** *Interpret depositional systems and facies using all available data.* This is a critical step that will, to a large extent, determine the validity of the stratigraphic interpretation. Correct identification of the depositional environment will guide which correlation style to use between wells.

- **Step-3.** *Subdivide the stratigraphic succession through the identification of maximum flooding surfaces and sequence boundaries.* Once an environmental interpretation has been made, correlation between wells can be done with greater confidence. Decision points encountered in the process of correlation from one data point to another can be guided by the style of correlation required by specific depositional systems. The correlation process involves the identification of many correlation markers, (e.g., sequence boundaries, unconformities, flooding surfaces, maximum flooding surfaces, transgressive surfaces).

- **Step-4.** *Analyze facies stacking patterns and identify systems tracts.* Once the key surfaces have been located, the next step is to identify the systems tracts that "fill" the space between these surfaces. This phase of sequence-stratigraphic analysis is based on analysis of depositional environments and their vertical stacking patterns. It is crucial that this phase be based on integration of all available data (Posamentier and Allen, 1999).

5.3 Sequence stratigraphic techniques

Stratigraphy is the study of rocks in time and space. It deals with lateral correlation of rock units, and interpreting and understanding geological time from the rock record. The early geologists relied mainly on two techniques to divide the stratigraphical record and correlate it laterally. The first of these is lithostratigraphy: rocks of the same or similar lithology were grouped together into a unit that could be recognized over a wide area (Coe et al., 2002). The basic lithostratigraphical division of the rock record is the *formation,* which can be divided into *members,* that can sometimes be divided further into beds (Coe et al., 2002).

A depositional sequence is a stratigraphic unit composed of a relatively conformable succession of genetically related strata, bounded at its top and base by unconformities or their correlative conformities (Mitchum et al., 1977). The basic units of sequence stratigraphy are depositional sequences, systems tracts, and periodic parasequences or simple sequences. They develop on time scales of 0.5-5 Ma, 0.2-1.0 Ma, and 0.01-0.5 Ma, respectively (Vail et al., 1991). Refinement of the geological time-scale is the key to understanding the rate, duration and order of geological events. Research has shown that close to the Palaeocene/Eocene boundary (55 Ma), there was a marked change in the marine and terrestrial biota. Between 35% and 50% of benthic foraminifers became extinct and there was a large turnover in land mammal assemblages. Associated with these extinctions, there is sedimentological evidence indicating a change to a much warmer, wetter climate (Coe et al., 2002). Bhattachary, (1993) illustrated that recognition of certain key surfaces is critical to the application of sequence-stratigraphic concepts, because they are the surfaces that bound sequences and systems tracts and therefore play a significant role in defining stratal architecture within and between sequences (Bhattacharya, 1993).

A sequence is composed of a succession of systems tracts and is interpreted to be deposited between eustatic-fall inflection points. Two sequence types are recognized: type 1 and type 2. The type 1 sequence is bounded at its base by a type 1 unconformity. This sequence is composed of lowstand, transgressive-, and highstand systems tracts. The type 2 sequence is bounded at its base by a type 2 unconformity and at its top by either a type 1 or type 2 unconformity (Posamentier et al., 1988).

The Lowermost systems tracts (LmST) contain those sediments deposited during falling relative sea-level between the SB and Transgressive surface (TS). The TS represents the first significant flooding of the basin margin during rising relative sea-level. The Transgressive Systems tracts (TST) represent sedimentation between the TS and the maximum rate of relative sea-level rise, which corresponds to the Maximum Flooding Surface (MFS). Sediments deposited during the rising, highest and falling relative sea-level of the half-cycle between the MFS and successive SB are assigned to the Highstand Systems Tracts (HST) (Brown and Fisher, 1977). A marine-flooding surface is a surface separating younger from older strata across which there is evidence of an abrupt increase in water depth (Van Wagoner et al., 1990).

In the terminology of sequence stratigraphy a group of beds showing a shallowing-upward trend is called a parasequence, which is a series of smaller packages of beds. Van Wagoner et al. (1990) stated that "a parasequence is a relatively conformable succession of genetically related beds or bedsets bounded by marine-flooding surfaces or their correlative surfaces. In special positions within the sequence, parasequences may be bounded either above or below by sequence boundaries" (Van Wagoner et al., 1990).

There are four types of systems tracts, but only three will be present in any one sequence. A type 1 sequence has a Type 1 sequence boundary at its base and is composed of a lowstand, transgressive and highstand systems tract. A Type 2 sequence has a Type 2 sequence boundary at its base and is composed of a shelf-margin, transgressive, and highstand systems tract. Depositional sequences and systems tracts are chronostratigraphic intervals because they represent all the rocks deposited within a particular interval of time. Each boundary is age-dated at the minimum hiatus where the strata are conformable. The interval of time between the

lower and upper conformities defines the time period over which the rocks were deposited (Vail et al., 1991) (**Fig. 5.2**).

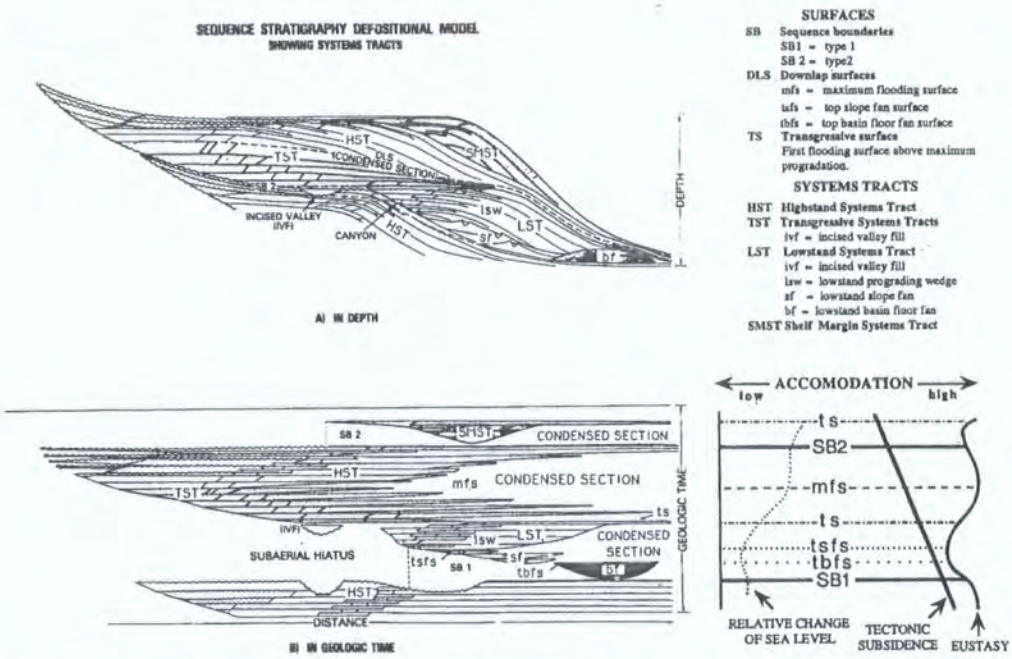

Fig. 5.2. Diagrammatic sketch of sequences and systems tracts in depth and geologic time in relation to tectonic subsidence, sea level, and relative changes of sea level (After Vail et al., 1991).

5.4 Sequence stratigraphy procedure

The following sequence of procedures for interpretation of palaeogeography, geologic history, stratigraphic signatures, and resource evaluation is recommended (Vail 1987) (**Fig. 5.3**).

1) Determine physical chronostratigraphic framework by interpreting sequences, system tracts and parasequences and/or simple sequences on outcrops, well logs and seismic data and age data with high resolution biostratigraphy.

2) Construct geohistory, total subsidence, and tectonic subsidence curves based on sequence boundary ages.

3) Complete a tectono-stratigraphic analysis.

4) Define depositional systems and lithofacies tracts within systems tracts and parasequences or simple sequences.

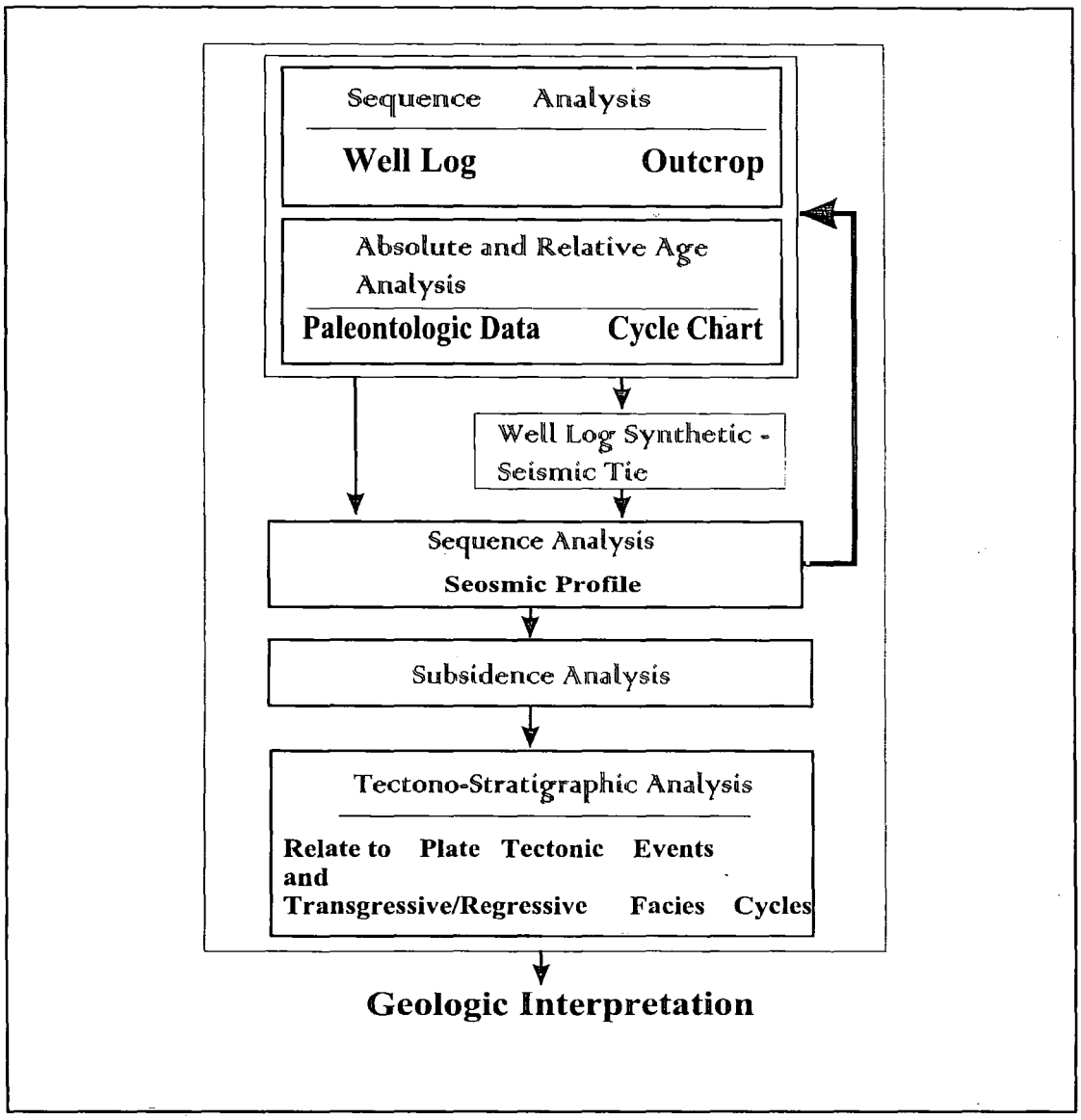

Fig. 5.3. Sequence stratigraphy interpretation procedure (After Vail et al., 1991).

5) Interpret palaeogeography, geologic history and stratigraphic signatures from resulting cross-sections, maps and chronostratigraphic charts.

6) Locate potential reservoirs and source rocks for possible sites of exploration (Vail et al., 1991).

5.5 Sequence stratigraphy signatures

The signature of tectonism, eustasy, and sedimentation can be distinguished by understanding the distribution of each of these variables in terms of their effects on

the stratigraphic record in time and space which tend to vary systematically through time Miall, 2005; Vail et al., 1991.

5.5.1 Tectonism

Tectonism has the greatest influence on increasing or reducing accommodation space. Also, when coupled with climate, it controls the type and amount of sediments filling that space (Vail et al., 1991). Tectonism is characterized by active processes related to plate interactions, and equilibration responses to conditions created by the active processes. Active deformation, or deformation which can be directly linked to fault movement is characterized by high strain rates, offset strata, rotation, and folding.

First-order tectonic events result from thermodynamic processes in the asthenosphere, which drive the plates and deform the earth's crust and upper mantle. Crustal extension and transtension, crustal shortening and transpression, and associated thermal heating and cooling are long-term processes that cause sedimentary basins to form and disappear. Their stratigraphic signatures are uplifts and sedimentary basins.

Second-order tectonic events are characterized by changes in subsidence rates during the evolution of sedimentary basins. They may result from reorganization of the plate-tectonic regime, or from local thermodynamic perturbations. These changes in subsidence rates are apparent on tectonic subsidence curves as they are either concave-upward, or convex-upward. The stratigraphic signatures of both curves are major transgressive-regressive facies cycles.

Third-order tectonic events are folding, faulting, diapirism, and magmatic activity. The stratigraphic signature of these events is tilted and ruptured strata. They are associated with penecontemporaneous events such as slides, slumps, megaturbidites, bentonite beds, datable extrusive flows, and intrusive sills and dikes (Vail et al., 1991).

When tectonic tilting and/or uplift ceases and regional subsidence resumes, the rate of sediment supply delivered down-system diminishes and an upward-shaling succession forms in these down-system environments, with isolated fluvial channels in floodplain shales. In some instances, under the right tectonic circumstances, this diminished sediment supply down-system can lead to the formation of unfilled low areas where lacustrine systems can develop. This could result in a period of lacustrine transgression producing the continental version of a transgressive systems tract. Subsequently, when renewed tectonic tilting occurs, an erosional unconformity again forms, capping the sequence. These sequences are similar to those formed by sea-level variations in shelf settings and form unconformity-bounded sedimentary cycles punctuated by an episode of mud-prone lacustrine transgression (Posamentier and Allen, 1999).

5.5.2 Eustasy

It is useful to define different types of sea-level change. Eustatic sea-level, relative sea-level and water depth all have specific meanings. Eustatic sea-level (or eustasy) is global sea-level and is a measure of the distance between the sea-surface and a fixed datum, usually taken as the centre of the earth (Coe et al., 2002) (**Fig. 5.4**).

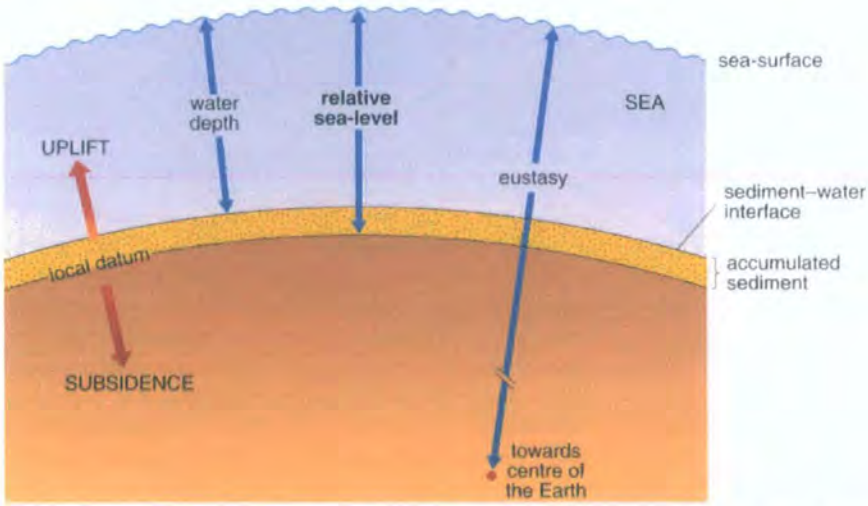

Fig. 5.4. Cartoon showing the relationship between relative sea-level, water depth, eustatic sea-level, tectonics (uplift and subsidence), and accumulated sediment (After Coe et al., 2002).

Five orders of eustatic cycles have been identified in the geological record including continental flooding cycles (first order) and four orders of sequence cycles with periods ranging from 5Ma to 10 ka (second to fifth order) (Vail et al., 1991).

5.5.2.1 Continental flooding cycles

Continental flooding cycles are defined on the basis of major time of encroachment and restriction of sediments on the cratons. They represent first-order eustatic cycles and their stratigraphic signature is the magasequence. There are two Phanerozoic continental flooding cycles (Hallam, 1977; Vail et al., 1977; Fischer 1981). The two continental flooding cycles are recognized on all continents and are believed to be global. The cause of these cycles is believed to be tectono-eustasy (change in ocean basin volume) (Vail et al., 1991).

5.5.2.2 Sequence Cycles

Second- to fifth-order eusatic cycles are recorded by sequence cycles, systems tracts, and periodic parasequences or simple sequences. They are believed to be glacio-eustatic cycles (Mitchum et al., 1977; Bartek et al., 1990) with a smaller magnitude, but higher frequency than tectonically induced transgressive-regressive facies cycles (Vail et al. 1991). Second-order eustatic cycles consist of sets of third-order cycles bounded by major eustatic falls. In general, a set of five to seven third-order cycles form a second-order cycle with a duration averaging 9-10Ma. The boundaries of second-order eustatic cycle are characterized by especially large eustatic falls (>50m). Third-order sequence cycles are the fundamental units of sequence stratigraphy with a cyclicity varying between 0.5-5.0Ma.

Calculations have shown that the total melting of the present-day Antarctic ice cap would result in a sea-level rise of about 60-80 m and that the growth of the Quaternary ice sheets may have forced a glacio-eustatic sea-level fall of *c.* 120 m. Concomitant rates of sea-level change of *c.* 1 cm yr^{-1} have been proposed. This is up to a thousand times more rapid than the average rate for tectono-eustatic mechanisms, so glacio-eustasy can therefore much more readily control the (short-term) third- and probably fourth- and fifth-order cycles (Coe et al., 2002).

5.5.3 Sedimentation

Sediments fill the space created by a relative rise of sea-level. Sediments are deposited episodically and are local in distribution. The stratigraphic signature of the sedimentologic effect is the depositional system. Depositional systems are composed of laminae, laminae sets, beds and bed sets, and episodic parasequences (Campbell, 1967). The objective of sequence stratigraphy is to identify and correlate the genetic chronostratigraphic sequences, systems tracts, and parasequences, and then relate them to the depositional systems and lithofacies tracts. Application of this procedure to many different types of basins has shown a close relationship between the type of systems tract and the dominant depositional systems (Vail et al., 1991).

The facies associations that characterize the different phases of cyclic sedimentation within a sequence can be grouped together as systems tracts. Systems tracts comprise linked depositional systems bounded by key stratigraphic surfaces (Posamentier et al., 1988).

5.6 Accommodation space

Sequence stratigraphy emphasizes the importance of the space that is made available within a basin for sediment to be deposited and the amount of sediment supplied. In order for either marine or non-marine sediment to be deposited, there has to be space available to put it in; this is termed accommodation space (Coe et al., 2002). In marine or lacustrine environments it is determined by the combined movements of the sea (eustasy) or lake surface and the sea/lake floor. The notion of sediment accommodation arguably represents one of the more innovative contributions of sequence stratigraphy (Posamentier and Allen, 1999).

Figure 5.5 illustrates accommodation developed at three points in a basin under differing conditions of subsidence. In this example subsidence is represented as a straight line, the slope of which is equal to the rate of subsidence at each point. Sea-level fluctuation is represented as the same smooth curve in all three cases. The curve describing the development of accommodation with time in each of these three cases

is found simply by addition of the subsidence and sea-level curves. Changes in accommodation are equivalent to changes in relative sea level (Jervey, 1988).

In the shallow marine realm accommodation space can be considered to be created by a rise in sea level relative to the sediment-water interface (the sea bed) at that point. A relative sea level rise can be achieved either by the sea level itself rising or by the sea bed subsiding. The causes of sea level rise, such as melting of ice caps to raise the level of the seas world-wide, may be fundamentally different from causes of subsidence (stretching, flexure or cooling of the lithosphere), but from the frame of reference of a crab sitting on the sea bed the effect is identical (Nichols, 1999).

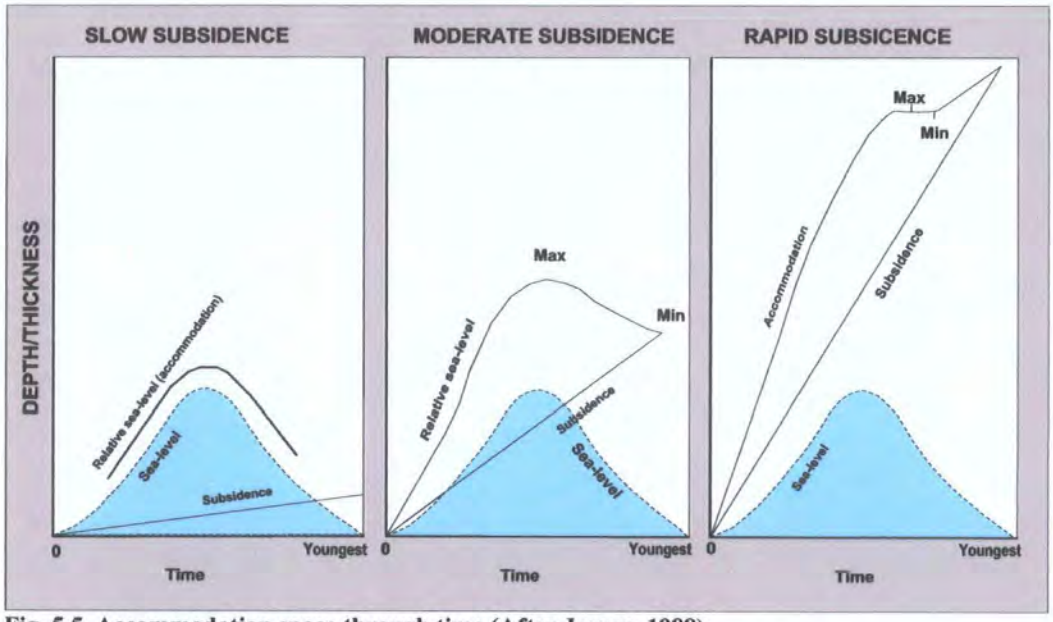

Fig. 5.5. Accommodation space through time (After Jervey, 1988).

5.7 Sediment supply

The rate of sediment supply controls both how much and where accommodation is filled. The balance between sediment supply and relative sea-level rise controls whether facies belts prograde basinward or retrograde landward, and the calibre of sediment supplied to the basin has a strong influence on sedimentary facies (Emery et al., 1996). The amount of sediment supplied to a basin location is a function of the general rate of sediment influx into the basin and proximity to zones of active transport (Jervey, 1988). Variation in sediment supply can control stratal patterns in two ways (Schlager, 1993): 1) for a given rate of change of

accommodation (e.g., as a result of relative sea-level variations or tectonism), the stratigraphic architecture is largely a function of the calibre and volume of local sediment influx, and 2) the volumes and rates of sediment supply can directly modify accommodation through the effect of isostatic and flexural effects of sediment loading (Posamentier and Allen, 1999).

5.8 Sequence stratigraphy of the Hawaz Formation in the type well A1-NC186 and H27-NC115

5.8.1 Introduction

Based on brachiopods, Havlicek and Massa (1973) indicated an Early to Middle Ordovician (Llandeilian to Llanvirnian) age for the Hawaz (Pierobon, 1991). During late Ordovician and early Silurian times North Africa was located on a shallow marine shelf sloping gently northwards for 100's of kilometres towards the North Gondwana shelf margin. The shelf has been interpreted as a platform rather than a ramp style basin because of its almost imperceptable slope, as evidenced by the regionally extensive and very rapid late Ordovician and early Silurian transgression. Upwelling along this shelf has also been suggested as a possible explanation for the organic-rich nature of the 'hot' shales but the sequence stratigraphic implications of this have not been fully explored (Turner, 2002).

The Hawaz Formation consists mainly of clastic rocks, which show shallow marine influences, dominated by shoreline deposites (See Chapter Three). Coastal and shallow shelf environments are the most sensitive to relative sea level change because the facies belts are largely controlled by depth. Water depth increases of a few metres can be readily identified in some coastal deposits by, for example, bioturbated shoreface sands overlying backshore deposits containing rootlets. Sea level falls which cause a forced regression result in a superposition of shallow on deeper facies, such as upper shoreface sands directly on mid-shelf mudstones. Evidence of small changes in sea level is most easily recognized in wave-dominated shorelines which have a microtidal regime (Nichols, 1999).

The Hawaz unit has been lithologically subdivided into 9 layers named from top to bottom H1 to H9 respectively. We recognize that H9 is a different stratigraphic

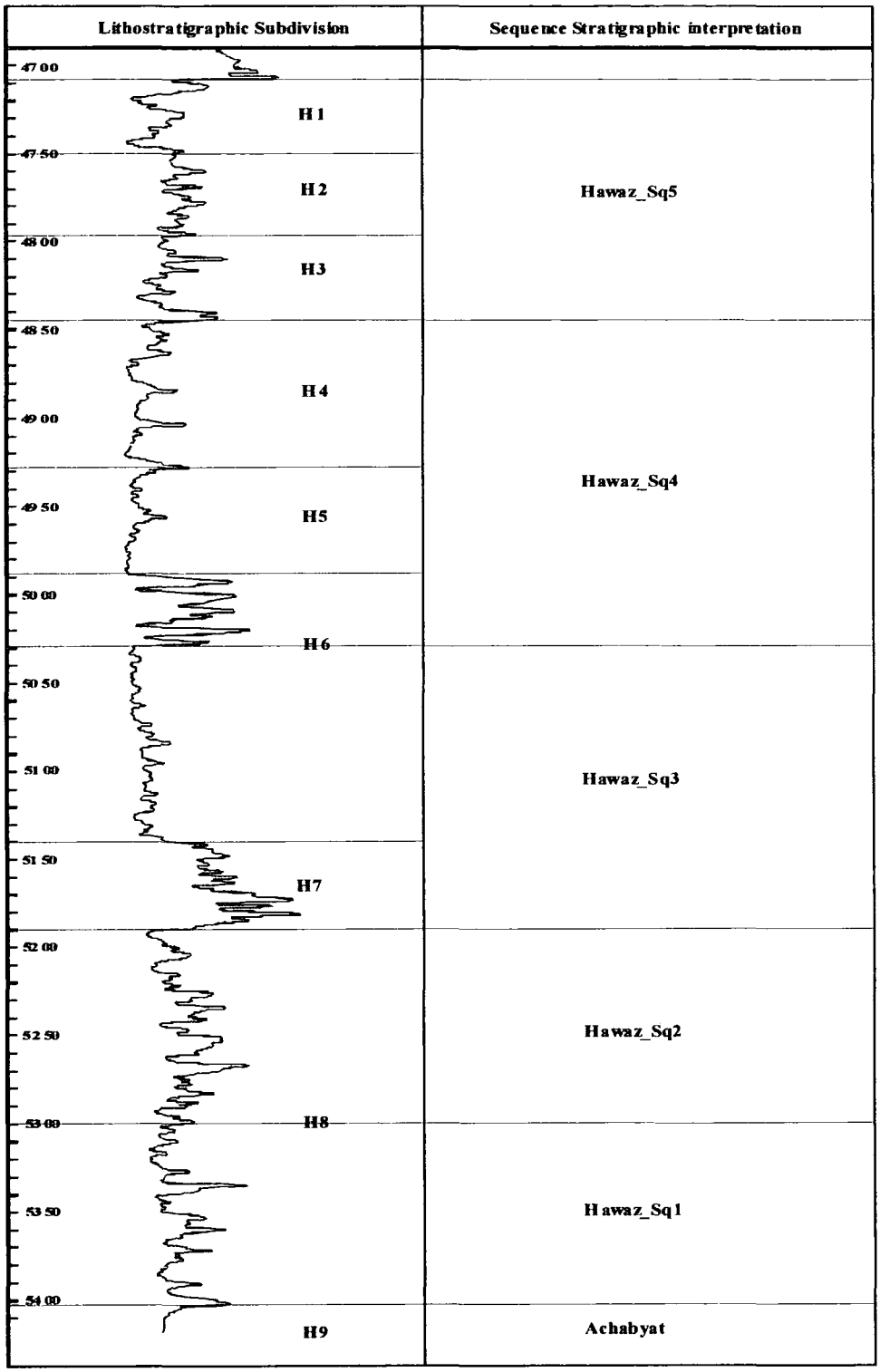

Fig. 5.6. Comparison between sequence stratigraphic interpretation and lithological units (Ghnia and Chang, 2003).

unit and equivalent to the Achebyat Formation. **Figure 5.6** shows the comparison between sequence stratigraphic-subdivision from this study and previous lithological units (Ghnia and Chang, 2003).

High resolution sequence stratigraphy of the Hawaz Formation, based on colour photographs of the slabbed cores and wireline log data, is used for correlating and predicting stratigraphy in the subsurface of A1-NC186 and H27-NC115. The wireline logs used in the correlation are mostly sonic (DT) and Gamma Ray (GR), supplemented by spontaneous Potential (SP).

5.8.2 Objectives

The main objectives of this sequence stratigraphic study are to

1) Assess the vertical variations in the sedimentary succession which are controlled by relative sea-level change, and to provide a chronostratigraphic framework for sedimentary facies and facies associations.
2) To present a sequence stratigraphical model for the Hawaz Formation in A1-NC186 and H27-NC115.
3) To present relative sea-level curves for the interval studied.
4) To obtain a higher degree of stratigraphic resolution by studying the different scales of the depositional sequence.
5) To define the geometrical aspects of the Hawaz sandstone system within this refined stratigraphic framework.

5.9 Sedimentology and sequence stratigraphy analysis of the Hawaz Formation in the type well A1-NC186 and H27-NC115

The lithologies recognized, and their interpretation, has been described in Chapter 3. In this section stacking patterns of lithofacies into parasequences, and parasequence sets in A1-NC186 and H27-NC115, are illustrated and evidence for a major sequence is presented (**Figs. 5.7 and 5.8**). Parasequences are generally

coarsening-upward and fining-upward vertical lithofacies successions, indicating decreasing and increasing water depth due to progradational and retrogradational parasequences. Trangressive and Highstand system tracts can be identified on the basis of geometric and sedimentologic criteria within the shallow marine strata in the Hawaz Formation. There are two TST and Two HST in the cored section of the Hawaz Formation. Both Highstand systems tracts are truncated between maximum flooding surfaces (MFS) at the base and flooding surfaces (FS) at the top, and the contact between the upper Highstand systems tract and the overlying major Transgressive system tract (TST) is defined by an erosion surface, which may be caused by the effects of glaciation in the region at that time. The top of the Transgressive system tract is defined by a transgressive surface (FS) (**Figs. 5.7 and 5.8**). These system tracts has been identified in the two studied wells (A1-NC186 and H27-NC115), and can be correlated with the adjacent wells using the GR log trends (**Fig. 5.10**).

5.9.1 Transgressive systems tract

During transgression, shorelines move landward. Depending mainly on the rate of rise of relative sea level, transgression can vary significantly, and this in turn can profoundly affect the characteristics of the preserved stratigraphic record (Arnott, 1995). The Transgressive systems tract is composed of a succession of backstepping or retrogradational parasequences. It is initiated by the first significant flooding event after the time of maximum regression of the lowstand wedge systems tract (Posamentier et al., 1998).

Two transgressive systems tracts (TST) have been found in wells A1-NC186 and H27-NC115: between 4380 ft and 4645 ft, and between 4658 ft and 4668 ft in A1- NC186, and between 4710 ft and 4990 ft, and 5019 ft and 5032 ft in H27-NC115. It consists of the following facies fine to medium-grained sandstones with alternating mottled and bioturbated beds, ripple to cross-bedded sandstone, burrowed hetrolithic, burrowed sandstone and mudstone and massive to cross-bedded sandstone facies. The facies characteristics of this sandstone are interpreted as upper to lower shoreface shallow marine, as discussed in Chapter 3.

The base of the major TST is distinguished by an erosion surface (**Figs. 5.7 and 5.8**) which may be attributed to a relative lowstand of sea-level. The Lowstand system tract LST may have been present but it has been subsequently eroded, or it may occur in a more landward position.

On the self the lowstand systems tract will have a varied expression. In the case of incised valley formation, stacked fluvial channels (fining upward motifs) will sharply overlie argillaceous, offshore/lower shoreface mudstones and sandstones. In the absence of an incised valley, an interfluvial sequence boundary may be represented by coal formation and soil over offshore sediment. The surface may otherwise be difficult to pick. On the shelf, the down dip portion of the LST is often termed the "lowstand prograding complex". This may be identified by intervals of coarsening upward deltaic or blocky shorefacee deposits sharply overlying offshore facies (Howell and Fitzsimmons, 1999).

The TST is terminated at the base of the Lower Silurian (Tanezzuft shale Formation) (**Figs. 5.7 and 5.8**). The Tanezzuft shale, above this system tract records a major postglactial melting transgressive event. This has been interpreted in two ways

1) Luning et al., (2002) stated that "After the peak of the late Ordovician glaciation during the Hirnantian, ice melting led to a rapid eustatic sea-level rise (see Chapter 7). Later they assumed that "the earliest stages of the transgression, during the latest Ordovician persculptus Zone and the earliest Silurian Rhuddanian Stage, only low-lying areas of the shelf were flooded and shales deposited (see chapter 7). There is usually a sharp contact between Ordovician strata and the latest Ordovician–early Silurian shales" (Luning et al., 2002).

2) Armstrong et al., (2005) disagreed with Luning from their field evidence and stacking patterns seen in the equivalent Jordanian succession, where the black shale lies on the MFS. Armstrong et al. (2005) stated that "the initial organic-rich black shale was deposited in glacially incised shelf sub-basins. As the deglacial transgression progressed, sub-basin margins and interfluves were eventually breached producing a rapid increase in accommodation space. Low sedimentation rates meant that this space could not be filled and the basin became starved. The spread of black shale away from the depocenters within gracially incised shelf depressions or sub-

basins was diachronous" (Armstrong et al., 2005). Postglacial melting of the ice and the flooding surfaces can easily be distinguished by the spiky pattern through the gamma-ray log values.

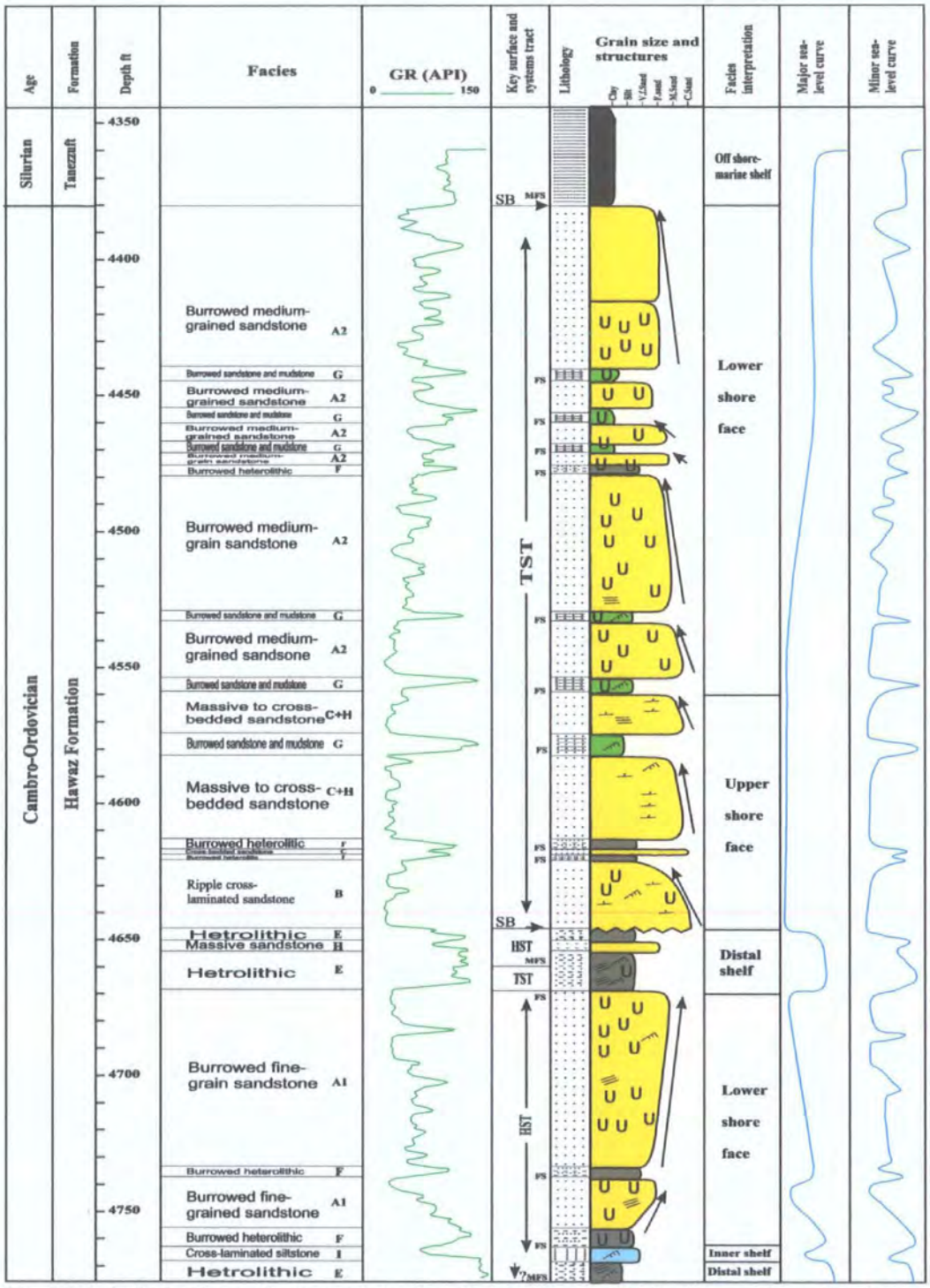

Fig. 5.7. Lithological log and sequence stratigraphy systems tract of the Hawaz Formation in type well A1-NC186.

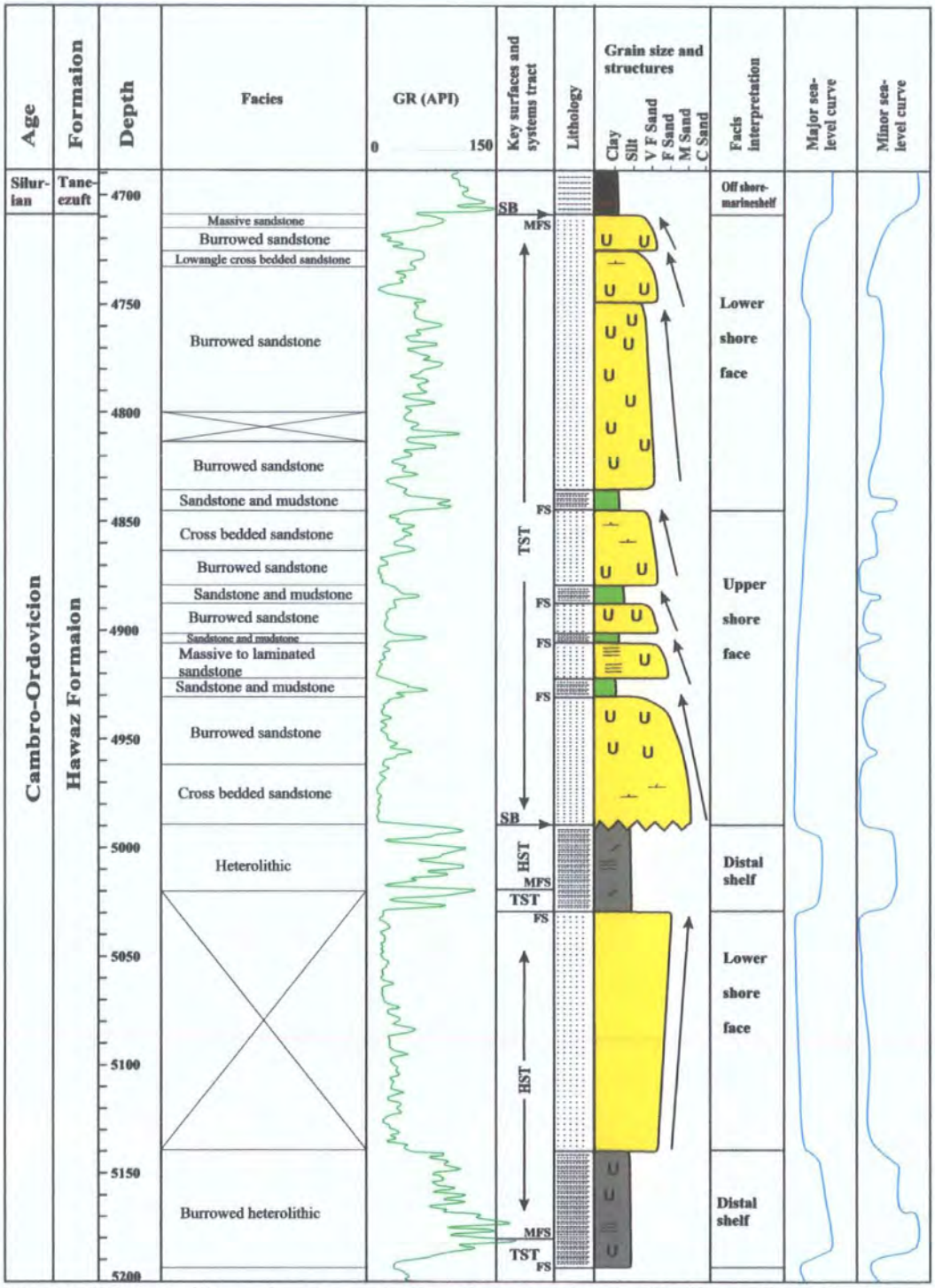

Fig. 5.8. Lithological log and sequence stratigraphy systems tract of the Hawaz Formation in type well H27-NC115.

Figures 5.7 and 5.8 show the sequence stratigraphy analysis of wells A1-NC186 and H27-NC115 respectively. The TST in these wells consists of lower shoreface facies arranged in at least seven stacked, coarsening and fining-upward parasequences, the parasquences. The fining-upward parasequences varying in thickness and make up the major part of the TST sequence in this succession.

5.9.2 Highstand systems tract

When relative sea-level rise slows to the rate at which available sediment flux is equal to or greater than the rate at which accommodation is produced, then transgression ends and either shoreline stillstand occurs or regression resumes. The regressive deposits that form when sediment accumulation rates exceed the rate of relative sea-level rise and increase in accommodation constitute the highstand systems tract (Posamentier and Allen, 1999). The highstand system tract (HST) is characterized by a decelerating rate of relative sea-level rise through time, resulting in initial aggadational and later progradational architecture. Depositional systems may be similar initially to those in the transgressive systems tract, but the infill of shelf areas by progradation, and the decrease in the rate of relative sea-level rise, may lead to a decrease in tidal influence during a highstand systems tract, and a decrease in the amount of coal, and of overbank, lagoonal and lacustrine shales, and channel sandbodies will become more common and more connected (Emery et al,. 1996).

There are two highstand system tracts in the cored section of the Hawaz Formation in type well A1-NC186 and H27-NC115: between 4645 ft and 4658 ft, and below 4668 ft in A1-NC186, and between 4990 ft and 5019 ft and 5032 ft and 5180 ft in H27-NC115, separated by a TST sequence. The upper HST is characterized by hetrolithic facies, interpreted as a distal shelf (discussed in Chapter 3). This HST is bounded above by an erosion surface which is interpreted as a sequence boundary (SB) and below by a MFS which is not easy to recognize, but is represented by the maximum API value on the gamma-ray log (**Figs. 5.7 and 5.8**).

The lower HST is characterized by hetrolithic, burrowed hetrolithic, cross-bedded siltstone and burrowed fine-grained sandstone, and significantly truncated by the overlying flooding surface at the base of the above Transgressive system tract and

the maximum flooding surface at the base of this sequence(**Figs. 5.7 and 5.8**). The sandstones are fine to medium-grained, and well-sorted with angular to subangular-grains, with abundant diverse fossils, including *Skolithos* and *Teichichnus*.

The lower HST is characterized by coarsening-upward sandstone suggesting a progradational stacking pattern and shallowing interval from distal-shelf to shore face deposits.

5.10 Sequences and relative sea-level control in the Hawaz Formation

The Hawaz is an interval where the first significant sea level change can be seen throughout the well logs. The implies that the basin came to a new evolutionary stage from this time. Stable lateral facies distribution, thickness and minor deformation are three characters of this interval. The seismic reflection for this interval is characterized by high to medium reflection density, stable amplitude and parallel configuration. It differs from the post-Ordovician passive continental margin in the lack of divergent reflection patterns. This indicates the possible existence of a very gentle palaeo-relief during deposition. The global palaeogeography during Middle Ordovician time was characterized by a broad marine shelf with a very gentle slope (Ghnia and Chang, 2002).

In the Hawaz Formation the system tracts are arranged in five sequences separated by sequence boundaries (**Figs. 5.7 and 5.8**), based on the recognition of parasequence stacking patterns. This makes it possible to evaluate the effects of long to medium-term changes in relative sea-level, and any possible connections with tectonism and sediment supply. These parasequences may also provide data to evaluate short-term oscillations of relative sea-level (Strand, 2005).

At the base of the Hawaz succession, and after peak flooding, the rate of relative sea-level rise slowed, and the highstand period (HST) followed with a decrease in accommodation space potential in nearshore regions, producing a general shoreline regression. This HST is separated from the following HST above by a thin TST separated below by a FS and above by a MFS. This TST may represent a short term rise in sea-level.

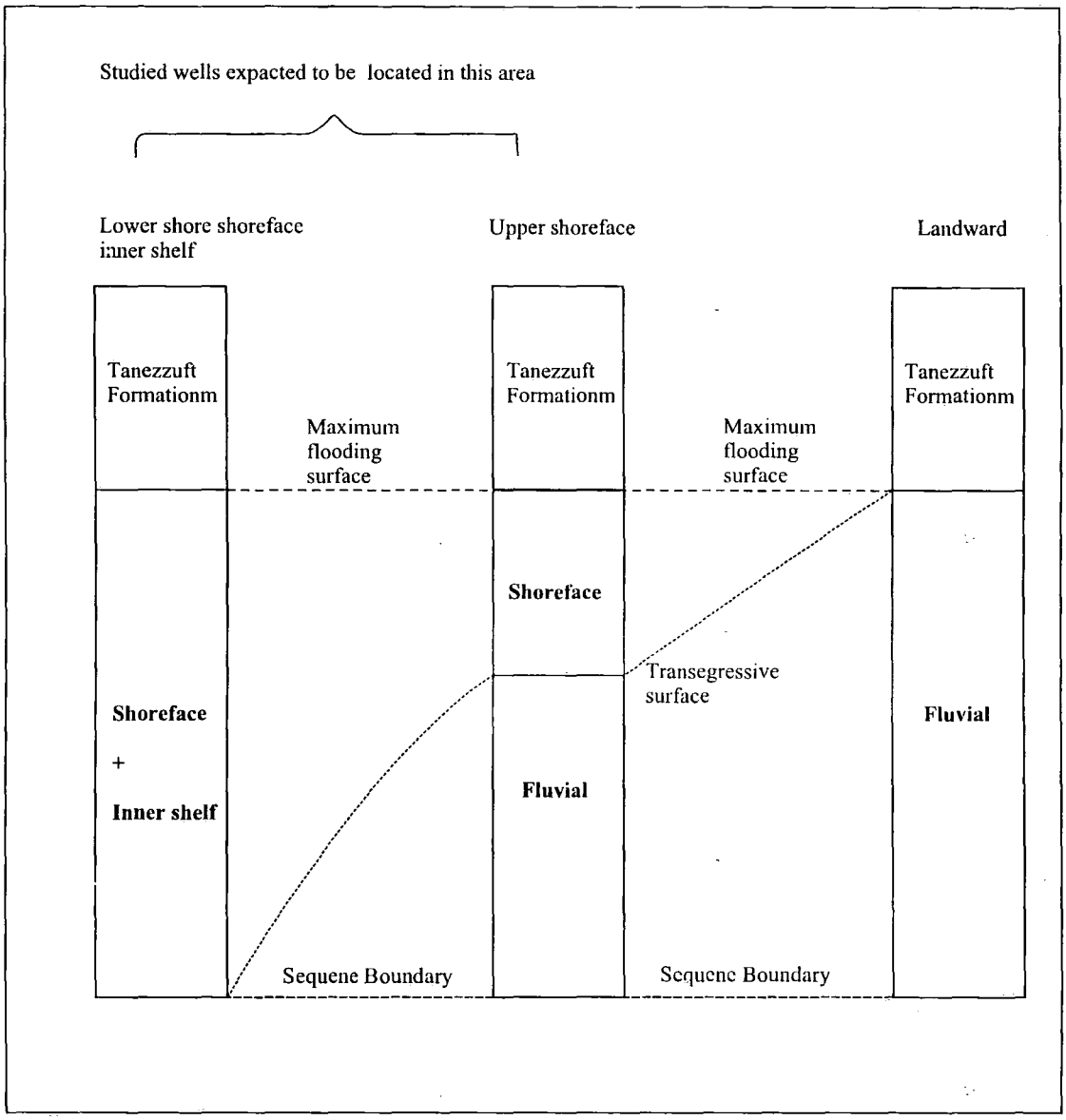

Fig. 5.9. A predicted model for the cross section in NC115 and NC186, showing the predicted location of the studied wells.

In the absence of preserved low stand glacial deposits, the only true low stand is the glacial incision. When the ice melts sediment locked-up in the ice is released to the depositional system and base level begins to rise. Thus, the sediment above the low stand incision is part of an early transgressive systems tract. The equivalent age sediments in southern Jordan comprise glacio-fluvial sediments that pass up into shoreface sandstones as base level continues to rise and accommodation space increases. Thus the shoreface sandstones are late transgressive and the flooding surface at their base is a transgressive surface, and the base of the transgressive black shales above the shoreface sandstones is a maximum flooding surface (**Fig. 5.9**).

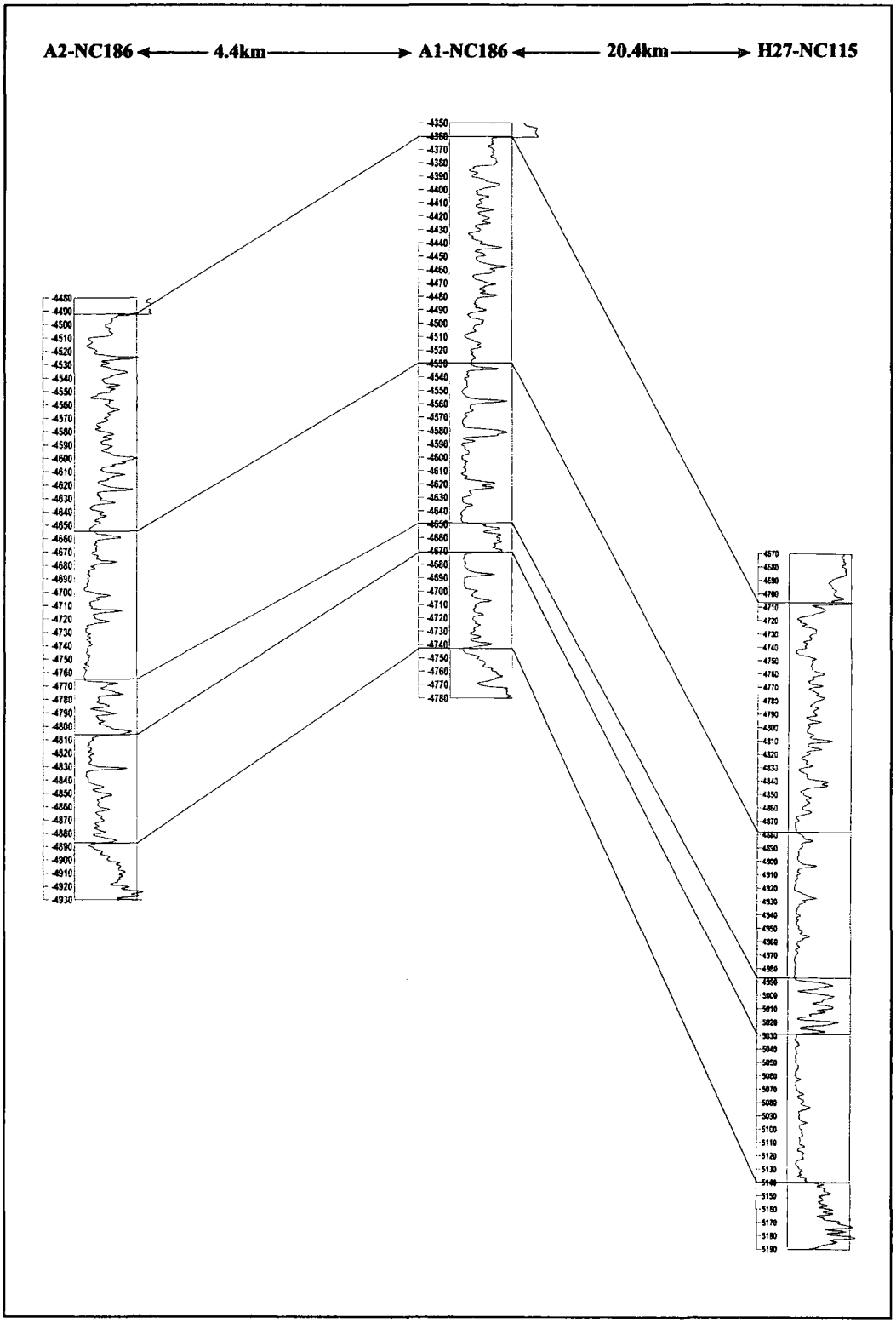

Fig. 5.10. Gamma-ray logs correlation between A1, A2-NC186 and H27-NC115, showing the major trend in GR log, which reflect the similarity of the systems tracts over long distance.

6. Wireline logging

6.1 Objectives

The first goal of well log investigation is to attempt to identify the lithology downhole and its depth of occurrence, define various characteristics and to integrate them with core data, and predict the geometry, continuity and distribution of the reservoir sands both vertically and laterally. The best way of doing this has little to do with downhole logging tools and more to do with surface mud-return logging, or mud-logging.

6.2 Log suit used in sequence stratigraphy

There are now a wide range of instruments, geophysical logging tools, which are lowered down a borehole to record the physical and chemical properties of the rocks. One or more of these instruments will be mounted on a device called a sonde which is lowered down the drill hole (on a wereline) once the drill sting has been removed. Data from these instruments are recorded at the surface as the sonde passes up through the formations. An alternative technique is to fix a sonde mounted with logging instruments behind the drill bit and record data as drilling proceeds. The data recorded by the logging instruments provide information about the lithologies, the porosity and permeability, water and hydrocarbon content of the formations that the borehole has passed through (Nichols, 2000).

The purpose of this section is to illustrate and define the different well log suits that have been used in this study (**Figs. 6.1 and 6.2**).

6.2.1 Gamma-ray logs (GR)

Units: API

The gamma-ray log measures gamma rays emitted by small concentrations of naturally occurring radioactive elements, principally the isotopes of thorium (Th), potassium (K) and uranium (U). Values are measured as a ratio against a standard

sample held by the American Petroleum Institute (API) and are quoted in 'API' units. In general terms, the radioactive isotopes are concentrated in the micas and clay minerals in mudstones, so mudstones record high values of gamma rays, whilst sandstones record low values. The gamma-ray log thus records sandstones and mudstones as 'end-member' low and high values respectively. Intermediate values result from a mixture of lithologies (Coe et al., 2002).

The gamma-ray is also useful in areas where the SP log cannot function well, i.e. cased holes, or oil-base muds, or air-filled holes. In a cased hole, the gamma-ray log is used to help accurately place perforating guns. The gamma tool is occasionally used as a shale indicator and has been used to empirically derive the volume of shale. The gamma ray shale index can be calculated as follows:

$$I_{GR} = \frac{GR - GR_{cl}}{GR_{sh} - GR_{cl}}$$

Where GR = Log response in zone of interest

GR_{cl} = Log response in clean beds

GR_{sh} = Log response in shale beds

This value (I_{GR}) can be inserted into a chart such as Atlas 3-19 and the volume of shale can be determined (Bowen, 2001). Generally the value is not very accurate and tends to give an upper limit to the volume of shale. Moreover, there is no scientific basis for assuming that the relationship between gamma-ray value and shale volume should be linear (Rider, 1996).

6.2.2 Spontaneous potential logs

Units: mV

Spontaneous potential (SP) logs measure the difference in electrical potential between the formation and the surface. They are sensitive to changes in permeability, and are good at distinguishing trends between permeable sands and impermeable shales. The SP log works best where there is a good resistivity contrast between the mud filtrate and the formation water. Opposite impermeable shales the SP curve usually shows a more-or-less straight line on the log, known as the shale base line, and any differentiation within the shale is best done on the gamma or resistivity logs (Emery and Myers, 1996).

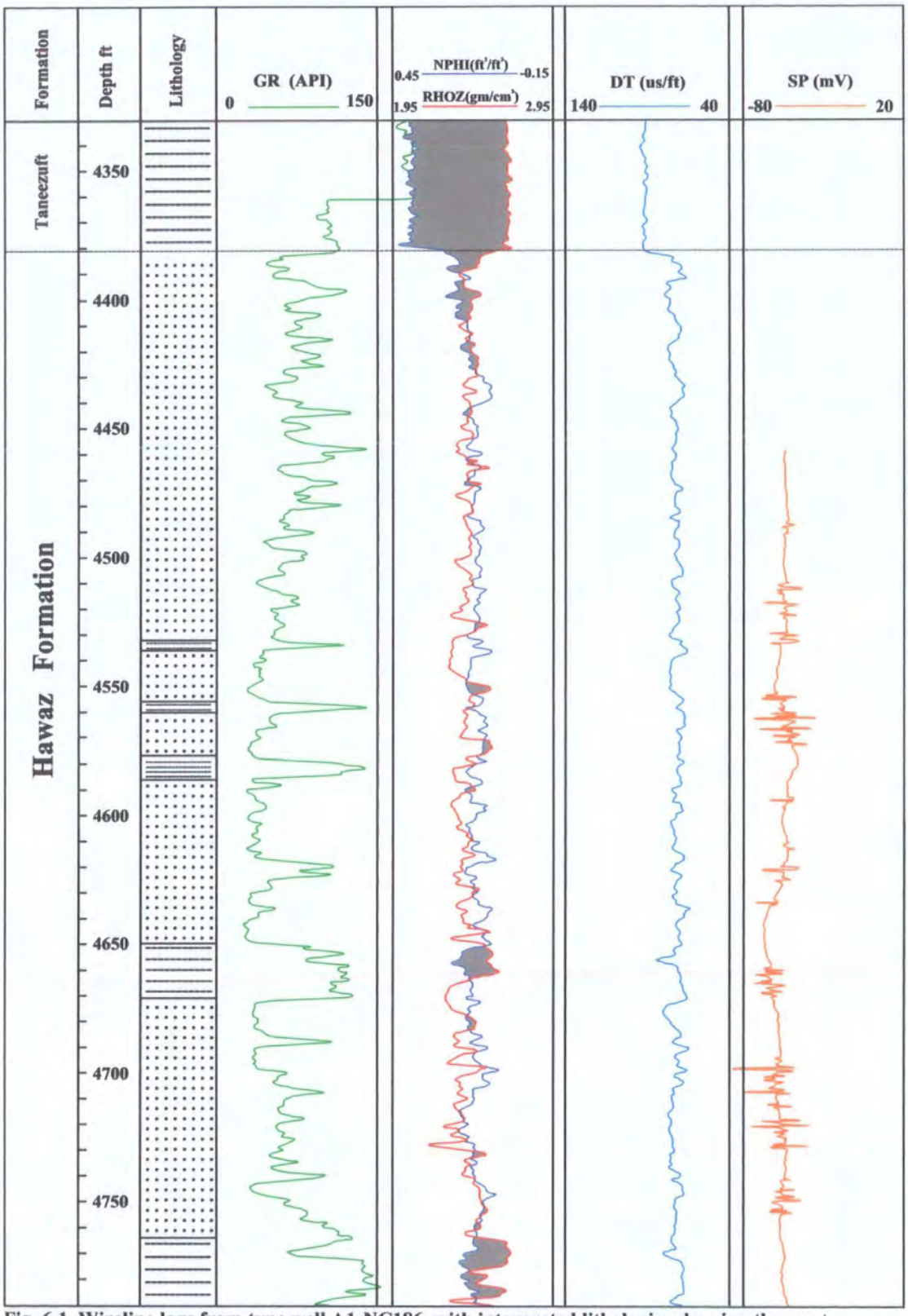

Fig. 6.1. Wireline logs from type well A1-NC186, with interpreted lithologies showing the most distinctive sand and shale sections.

6.2.3 Sonic velocity logs (DT)

Units: μs/ft

Sonic logs measure the sonic transit time through the formation. Transit time is related to porosity and lithology. Shales will have a higher transit time (lower velocity) than sandstones of a similar porosity, which sometimes allows the sonic log to be used as a grain size indicator. High concentrations of organic matter in coals and black shales will result in very long travel times, and these 'troughs' on the sonic log are often indicators of organic-rich condensed section. The log is also affected by post-depositional cementation and compaction, and by the presence of fractures (Emery and Myers, 1996).

6.2.4 Formation density logs (RHOB)

Units: gm/cm^3

These tools work by emitting gamma radiation and detecting the proportion of the radiation which returns to detectors on the tool. The amount of radiation returned is proportional to the electron density of the medium bombarded, and this is in turn proportional to the overall density of the formation. If the lithology is known, the porosity can be calculated as density decreases with increased porosity (Nichols, 2000).

6.2.5 Neutron porosity logs (NPHI)

Units: ft^3/ft^3

Neutrons are continuously emitted from a source mounted on a down hole tool or device, and a detector which measures the energy of returning neutrons. Neutrons lose energy by colliding with a particle of similar mass, a hydrogen nucleus, so this logging tool effectively measures the hydrogen concentration of the formation (Nichols, 2000).

The density-neutron suite (the Schlumberger FDC-CNL suite and other similar curves) is the best indicator of lithology and thus can be used to link lithology and depositional trends. It is one of the best log suits for sequence stratigraphic analysis, but it is not as commonly run as a gamma tool (Emery and Myers, 1996).

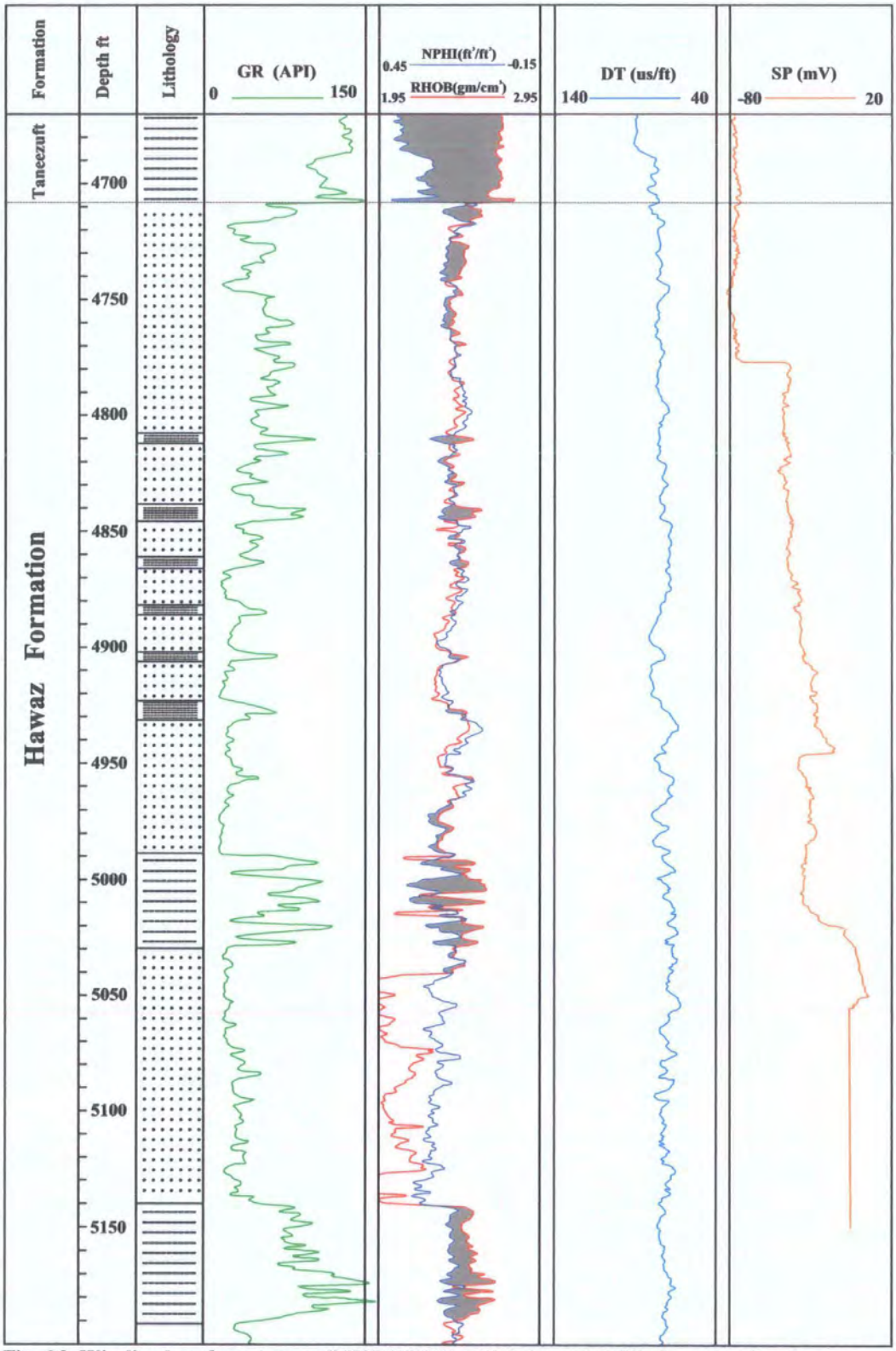

Fig. 6.2. Wireline logs from type well H27-NC115, with interpreted lithology showing the most distinctive sand and shale sections.

6.3 Analysis of wireline log trends

Log patterns may be used at three levels of interpretation:

1) Determination of vertical sequence and bedding architecture,
2) Recognition and mapping of log facies, and
3) Interpretation of depositional environment.

One of the most obvious and earliest uses of wire-line logs, beyond the determination of basic lithology, is the interpretation of vertical sequence. The characteristic erratic, upward-coarsening, and upward-fining textural patterns of aggradational, progradational, and lateral accretion bedding geometries are readily recognized on electric and gamma logs (Galloway and Hobday, 1983).

A number of distinctive trends are recognized frequently on wireline logs, and generally are described from their gamma-log expression. Log trends may be observed as a change in the average log reading, or from shifts in the sand or shale base line (where the sand base line on a gamma log is the line marking the minimum gamma locus of the curve over an interval, and the shale base line is the line marking the maximum gamma locus) (Emery and Myers, 1996). Typical log trends are illustrated in **Fig. 6.3.**

6.3.1 Geological interpretation of the Hawaz Formation from gamma-ray log

The natural gamma-ray logging tool provides the most information by distinguishing between mudrock and either sandstone or limestone. This tool provides a guide to the 'shaleline' of the formation, the gross proportion of clay present. It also picks out organic-rich mudrocks by their anomalously high gamma-ray count. Sandstone beds with high proportions of mica, feldspar, glauconite or heavy minerals have a high natural gamma radiation and can be confused with mudrocks (Nichols, 2000) (**Fig. 6.4**). The gamma ray log does not vary because of changes in grain-size; it varies (often) because of change in clay content (the same is true for the SP).

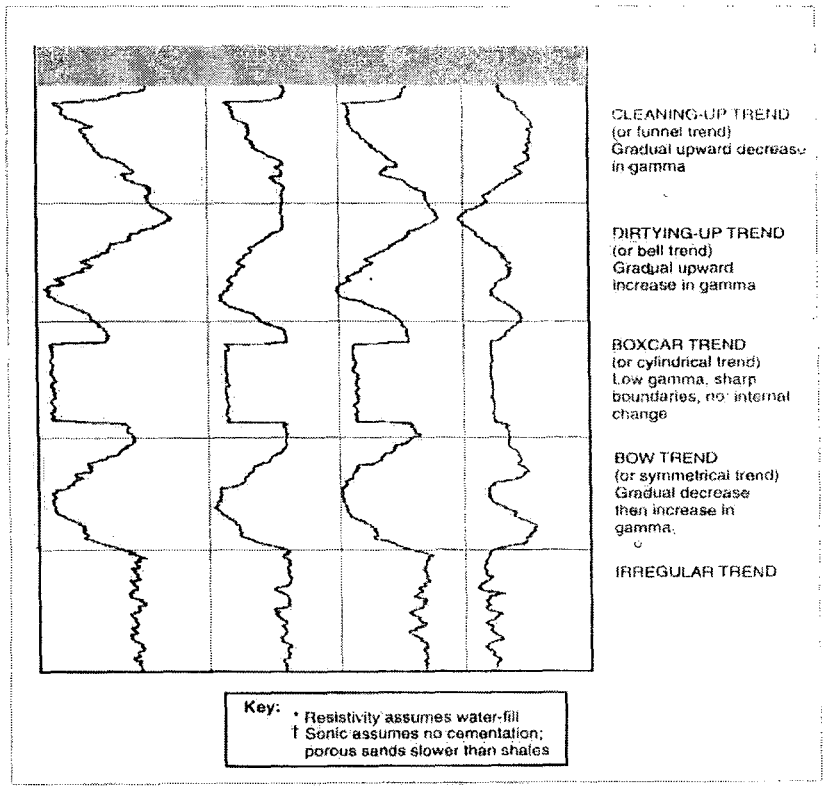

Fig. 6.3. Idealized log trends, assuming saltwater-filled porosity (After Emery and Myers, 1996).

However, sedimentological interpretations based on gamma-ray log shapes require the log to vary with grain size (**Fig. 6.5**). This involves two undeclared assumptions.

1) Gamma-ray variations are related to clay volume change.
2) Clay volume changes are related to grain-size differences.

An interesting and fairly comprehensive scheme for facies identification in detrital sediments (sand-shale) has been developed using gamma-ray log shapes. The basis for the scheme is the relationship between grain-size and shale content. It is shale content that the gamma ray log indicates, but it is interpreted in terms of grain-size. For example, a coarse grained sand will have a very low shale content, a medium-grained sand some shale, and a fine-grained sand may be very shaly. The change in grain-size will be followed by changes in gamma ray value (Rider, 1996) (**Fig. 6.5**). **Figures 6.1** and **6.2** show a suit of wireline logs from the two studied wells A1-NC186 and H27-NC115 that have been used to identify the different lithologies in the Hawaz Formation. For example, the gamma-ray log clearly identifies the mud material or shale sediments deposited on the shelf (between 4650-4677 ft at A1-NC186), from the

sandstone deposited on a more nearshore shallow marine environment. Density log and neutron porosity can be used in determining the lithology as well.

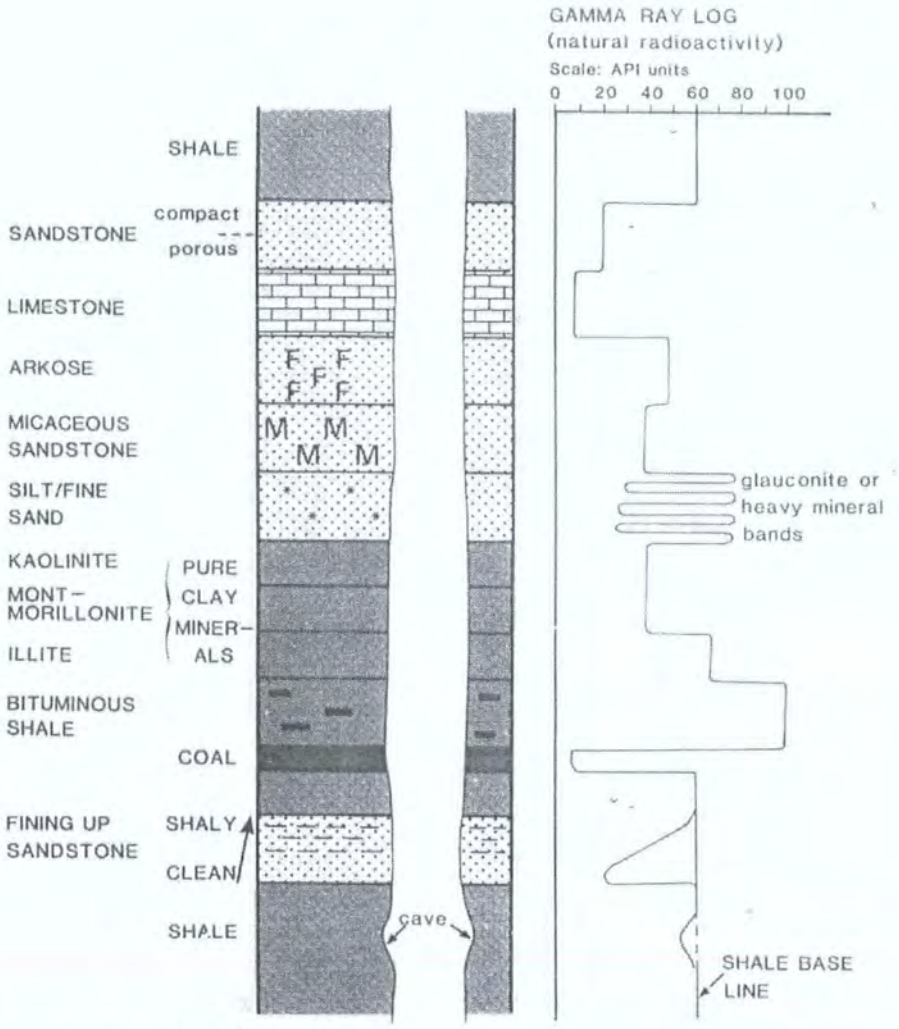

Fig. 6.4. Determination of lithology using information provided by a gamma-ray logging tool (After Rider, 1991).

1) Bell trends:

These show a progressive upward increase in the gamma-ray log reading and gradual upward decrease in grain-size trend (fining upward) indicating increasing clay content or radioactivity of the formation. Between 4990-4840 ft in A1-NC186, there is a major bell trend which can be divided into several bell trends (**Fig. 6.6**). In a shallow marine setting the cleaning-up motif is usually related to an upward transition from

shale-rich to shale free lithologies, owing to an upward increase in depositional energy, upward shallowing and upward coarsening (Emery and Myers, 1996).

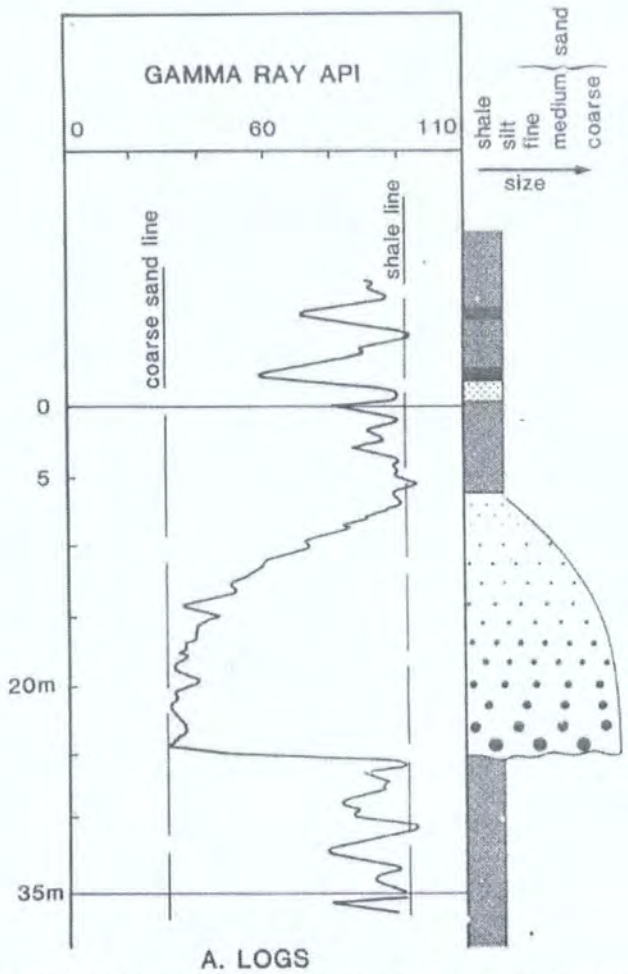

Fig. 6.5. Changes in sandstone grain-size are reflected by changes in the gamma ray value (After Rider, 1996).

2) Funnel trends:

These show a gradual upward decrease in the gamma-ray reading representing a gradual upward change to a coarse-grained lithology, related to a gradual increase in grain-size indicative of a decrease in clay content, for example, from mudstone to sandstone. This trend has been recognized in the Hawaz Formation in A1-NC186, between 4758-4739 ft, and is related to a gradual increase in sandstone grain-size from fine to coarse within the two studied wells.

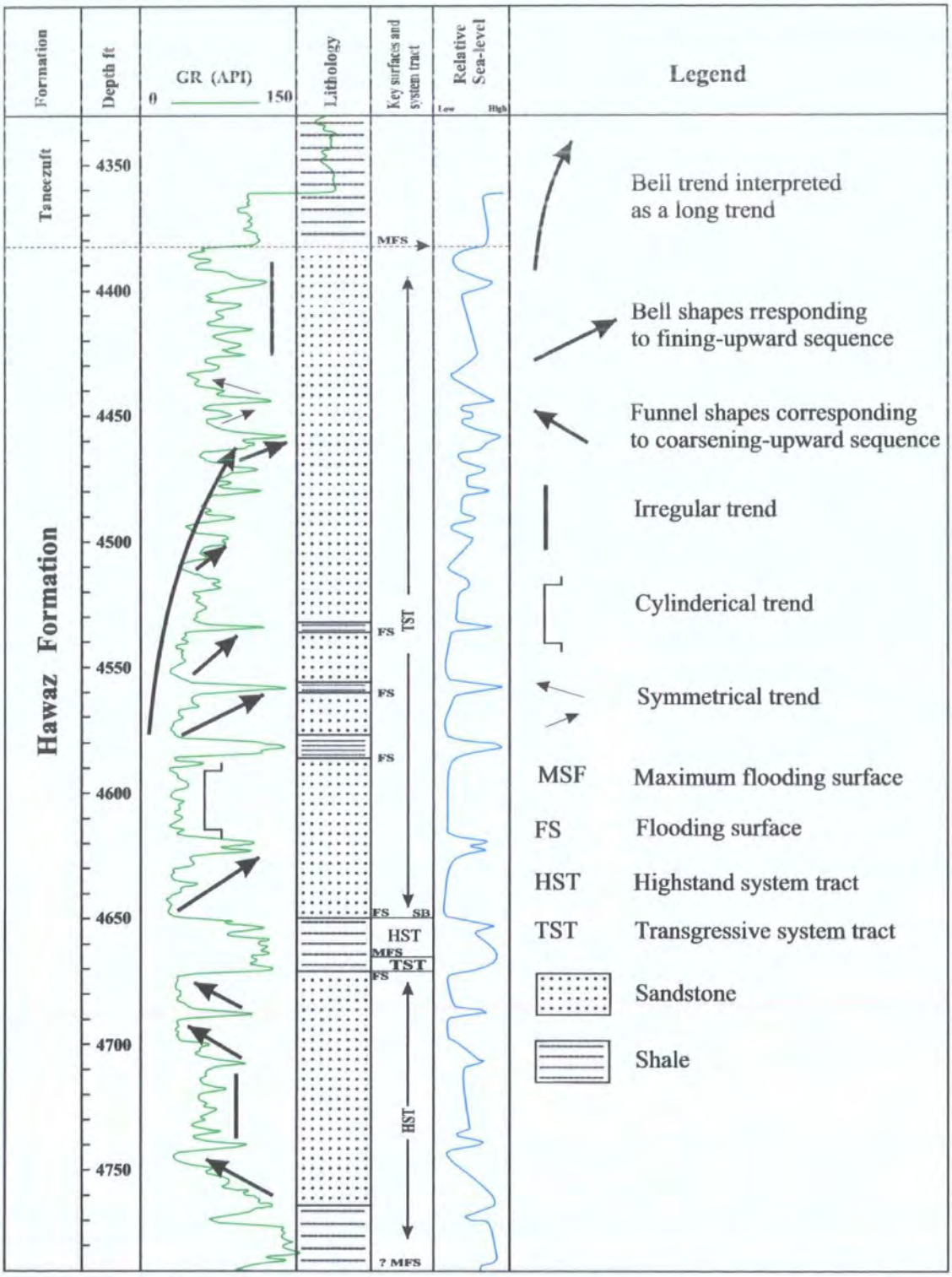

Fig. 6.6. Gamma-ray log (GR), lithology, trends in systems tract and relative sea-level change in type well A1-NC186.

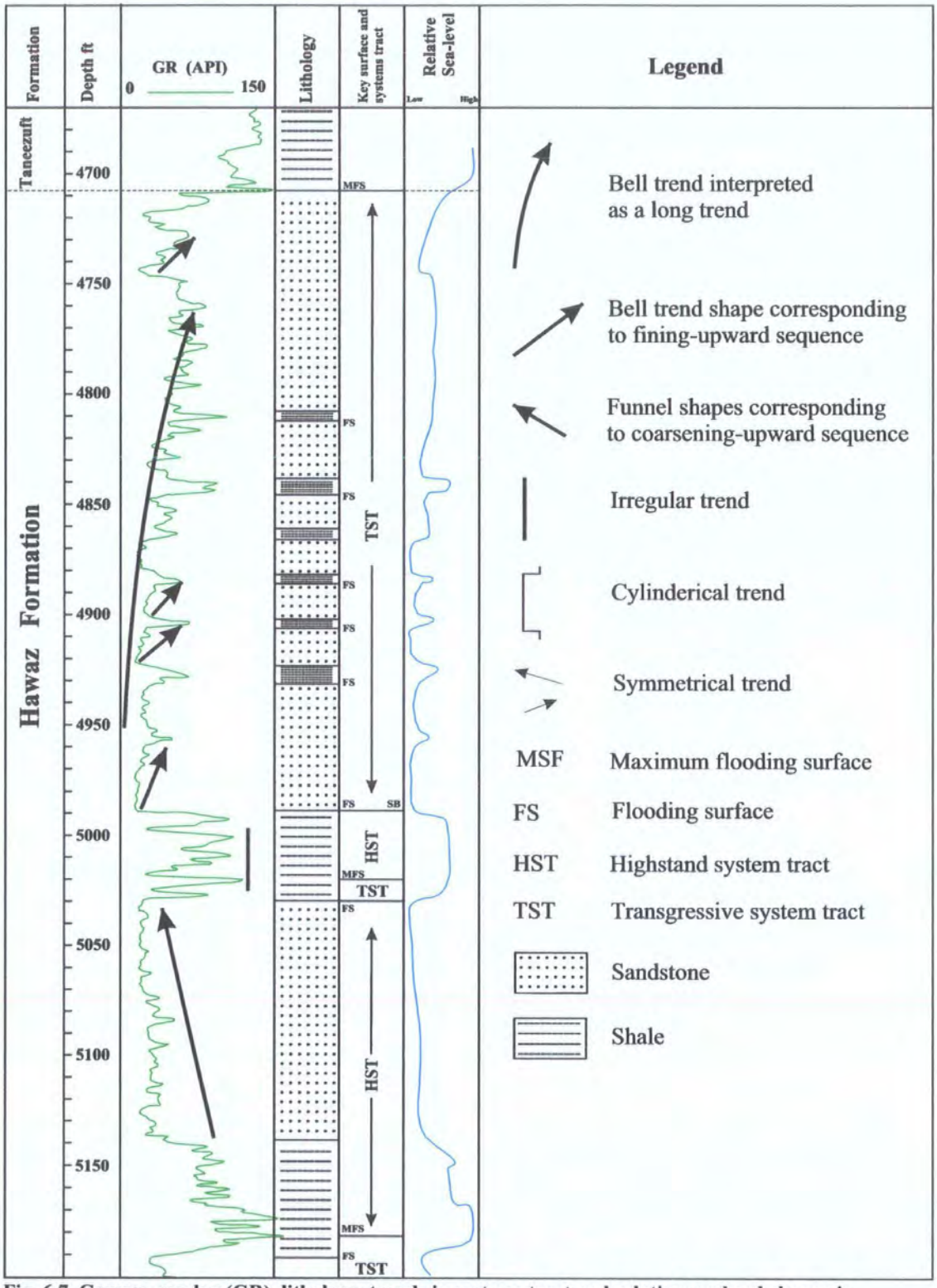

Fig. 6.7. Gamma-ray log (GR), lithology, trends in systems tract and relative sea-level change in type well H27-NC115.

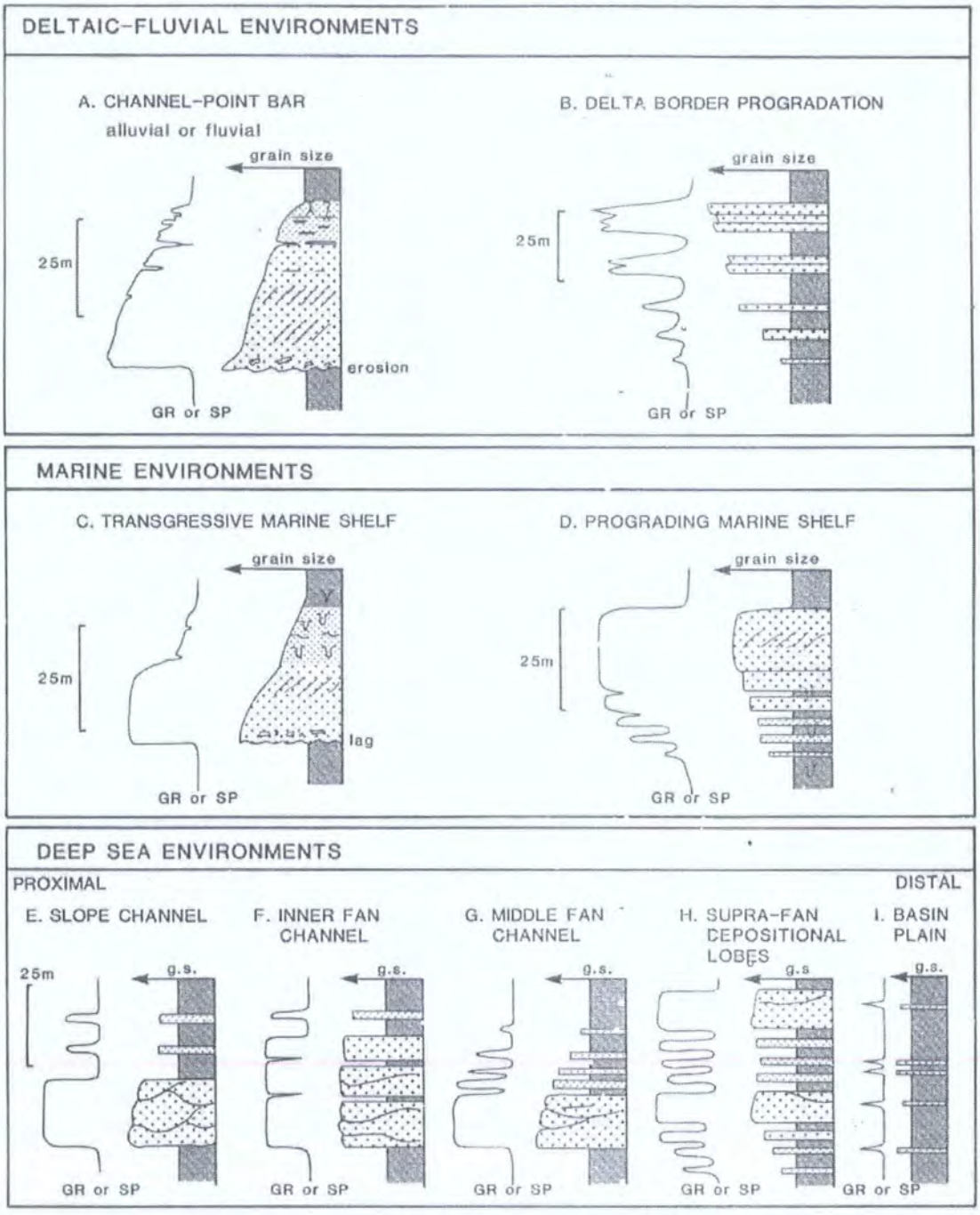

Fig. 6.8. Facies indication from gamma-ray (or SP) log shape. These are idealized examples of both log shape and sedimentary facies (After Rider, 1996).

3) Cylindrical trends (Boxcar log trend):

These consist of low gamma-ray values with a constant reading, set within a higher gamma-ray background value. The boundaries with overlying and underlying shale are abrupt. This type of trend is commonly recognized in shallow marine sediments.

4) Symmetrical trend (Bow trend):

These consist of funnel trends, overlain by a bell trend of similar thickness with no sharp break between the two. It is not common in the study wells, but may be present on some occasions.

The bow trend is seldom developed in a shallow marine setting, where base-level constraints usually lead to thicker progradational and thinner transgressive units (Emery and Myers, 1996).

5) Irregular trend (mixed clean and shaly):

No systematic change is observed, and they lack the clean character of the boxcar shape. This trend may represent aggradation of shale or silt succession (Emery and Myers, 1996).

Besides recognition of simple vertical sequences, comparison of many logs through a genetic stratigraphic unit will likely lead to recognition of recurrent patterns or log motifs. Such motifs or log facies may be characterized by vertical sequence, scale of units, dominant lithologic composition, or the same or different logs and their areal, lateral, and vertical distributions may be examined for systematic patterns (Galloway and Hobday, 1983). A bell-shape indicates a fining-up-ward sequence may be an alluvial/fluvial channel, but also a transgressive sand. A funnel-shape is a coarsening-up sequence which may be due to deltaic progradation or shallow marine progradation (**Fig. 6.8**). The shapes come from the diminution in bed thickness associated with diminution in grain-size, rather than the direct change in grain-size itself (Rider, 1996).

6.4 Generalized stratigraphic sequence analysis of the Hawaz Formation from wireline log trends

6.4.1 Introduction

At the rig site the lithology of the formation being penetrated can be described by the wellsite geologist from the returning cuttings carried out by the drilling fluid to the surface. These cuttings can be removed from the rig system by sieve, or "shale-shaker" as it is known. By determining the length of time it takes from the bottom hole to the surface it is possible to reassign depths to the cuttings acquired over any time interval.

The logging run on the two studied wells was done by the contract company, Schlumberger Wireline Logging Company. This logging run covered the open hole of the two wells including the Hawaz Formation.

The wireline logs used in the correlation in the two studied wells and adjacent wells are mostly Gamma-ray (GR), Spontaneous Potential (SP), Neutron Density (RHOB) and Porosity log (NPHI). The fining-upward sandstone sequences in the upper part of the studied wells, represents transgressive systems tracts, which are the most common wireline log trends for the Hawaz Formation (**Figs. 6.1 and 6.2**). Highstand systems tracts are represented in two intervals of the section by retrogradational trend, particularly in the lowermost part of the cored section.

6.4.2 Sequence stratigraphic interpretation of the Hawaz Formation from wireliine log trends

A genetic stratigraphic sequence is a package of sediment recording a significant depositional episode of basin margin outbuilding and basin filling, bounded by sediments representing periods of widespread basin margin flooding.

To identify a parasequence on the logs, both the facies succession and the bounding marine flooding surfaces must be diagnosed. A facies succession (cycle) is normally seen as in electrosequence analysis as a persistent, upward change in log parameters, both in the fine-grained shale and coarser grained sand intervals, on all the logs (Rider, 1996).

Rider (1996) shows the schematic wireline log characteristic for the sequence stratigraphic interpretation of wireline log patterns (**Fig. 6.9**). This model indicates the key sequence stratigraphic surface (sequence boundary, maximum flooding surface and transgressive surface) that can be used to interpret these key surface in the Hawaz Formation in the study wells as follows:

1) Sequence Boundary (SB):

This results from a fall in relative sea-level and may be difficult to recognize from the well log alone (Emery and Myers, 1996). A sequence boundary is an unconformity

and its correlative conformity; it is a laterally continuous, widespread surface covering at least an entire basin and seems to occur synchronously in many basins around the world (Vail et al., 1977; Vail et al., 1984; Haq et al., 1988). Sequence boundaries are typically easiest to identify in the area around the shoreline of the previous HST (Coe et al., 2002).

The attributes of sequence boundaries are determined by the processes that acted on that surface both during the period of relative sea-level fall and afterwards. The sequence boundary also may be characterized by contrasting facies successions bracketing this surface. Different processes and sedimentary facies characterize different depositional environment; thus, the expression of a sequence boundary is not the same in different parts of a sedimentary basin (Posamentire and Allen, 1999).

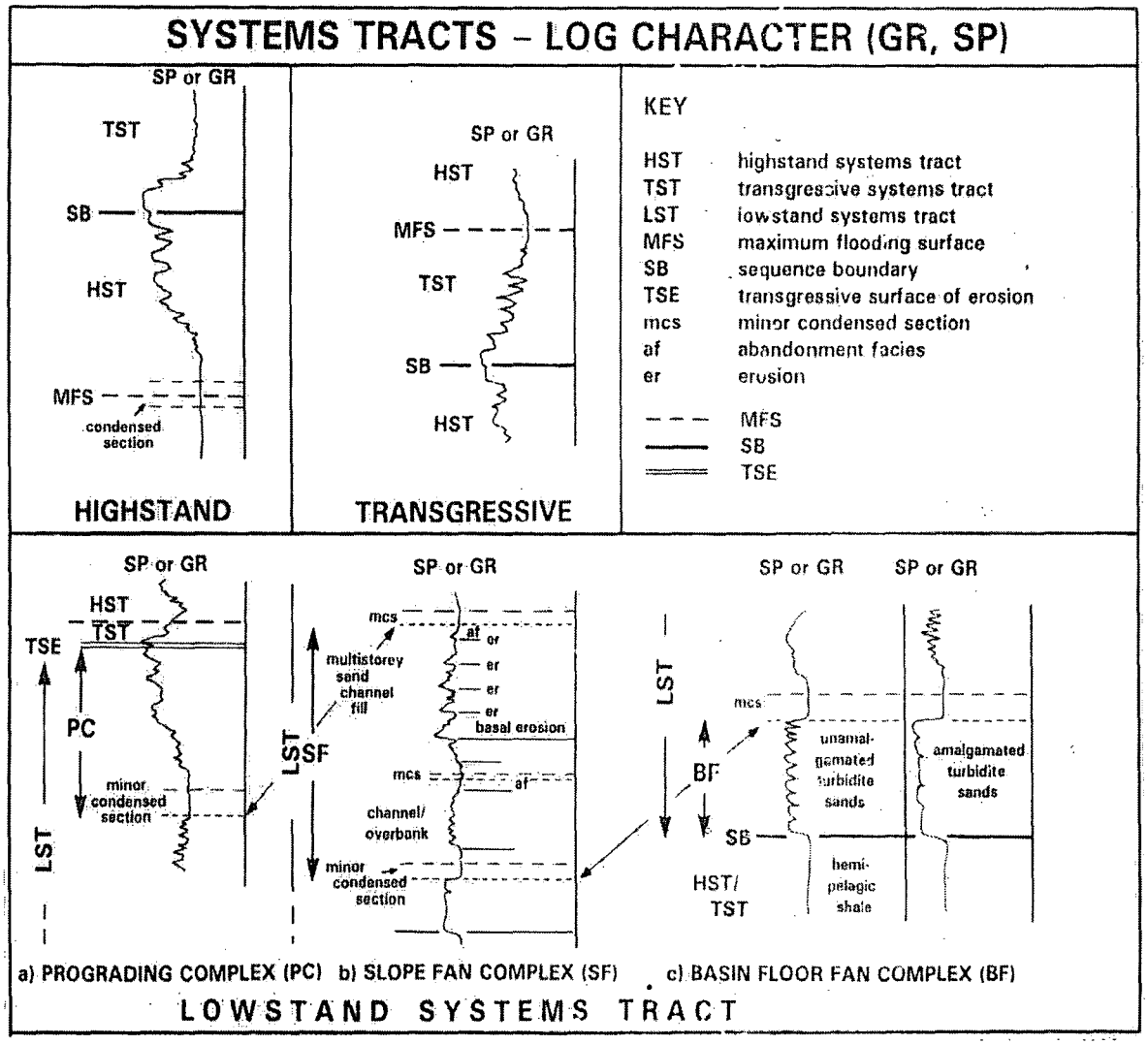

Fig. 6.9. Model log patterns for sequence tracts, with possible sequence stratigraphic interpretation (After Rider, 1996).

A sequence boundary may result from an abrupt change in log response in sandstone units or may be marked by change in shale type in the shale section (Rider, 1996). In the study wells the sequence boundary is characterized by an erosion surface and can be identified by an abrupt change in gamma-ray log signature (for example at depth 4990 ft in H27-NC115, and 4641 ft in A1-NC186) (**Figs. 6.6 and 6.7**).

2) Maximum Flooding surface (MFS):

A maximum flooding surface can be recognized in proximal locations as the surface between a retrograding unit and an overlying prograding unit. Where these are dirtying-up and cleaning-up units respectively, the maximum flooding surface will be a gamma-maximum. Maximum flooding surfaces pass laterally into shelfal condensed intervals (Emery and Myers, 1996). The maximum flooding surface is differentiated from other flooding surfaces because it has the most landward extent. It will also typically be overlain by the thickest shale interval and mark a change in the parasequence stacking pattern from retrogradational to progradational (Coe et al., 2002).

The maximum flooding surfaces are commonly easier to identify than sequence boundaries on well logs because of their relatively widespread distribution within the condensed section and their uniform and distinctive lithologic expression (Posamentire and Allen, 1999).

In the study wells the maximum flooding surface can be recognized in both core and wireline logs. The thin bed of dark-black shale between 4645 and 4668 ft in A1-NC186, and between 4990 and 5032 ft in H27-NC115, represent a condensed section corresponding to a maximum flooding surface (**Figs. 6.6 and 6.7**). This defines the boundary between the highstand systems tract above and the transgressive systems tract below.

3) Marine flooding surface (FS):

The marine flooding surface is a surface that separates younger from older strata, across which there is evidence of an abrupt increase in water depth. This deepening is commonly accompanied by minor submarine erosion and nondeposition, and a minor

hiatus may be indicated (Van Wagoner et al., 1990). When the rate of relative sea-level rise accelerates to a point where the rate of new accommodation space added exceeds the rate of sediment influx, transgression occurs. The transgressive surface marks the boundary between either lowstand or highstand systems tract deposits below and transgressive systems tract deposits above (Posamentier and Allen, 1999).

In A1-NC186 and H27-NC115 flooding surfaces occur within the transgrssive system tract, and these flooding surfaces may be related to ice melting. These flooding surfaces can be correlated between the two wells mentioned.

6.5 Electrosequence analysis of the Hawaz Formation

An electrosequence is an interval defined on wireline logs, through which there are consistent or consistently changing log responses and characteristics, sufficiently distinctive to separate it from other electrosequences (Rider, 1996). The objective of electrosequence analysis is to extract from the logs as much geological information as possible, by identifying vertically continuous, depositional, stratigraphic and eventually sequence stratigraphic units.

In the Hawaz Formation, shapes on the gamma-ray log can be interpreted as grain-size trends and by sedimentological association as facies successions. A fining upward grain-size trend will be represented in increased gamma-ray log values. The coarse grains are represented by low gamma-ray reading, the opposite is true for clay which gives a high gamma-ray log reading. The sedimentological implication of this relationship leads to correlation between facies and log shape. From gamma-ray logs the Hawaz Formation succession may be divided into parasequences, which together form systems tracts, deposited during relative sea-level change.

In this section identifying systems tract from wireline log trend will be discussed.

1) Progradation

In the lowermost part of the cored section in the Hawaz Formation there is a progradational trend, which can be recognized by gamma-ray log values decreasing upward (**Figs. 6.6 and 6.7**). This results from an upward increase in grain-size from siltstone or fine-grained sandstone to medium-grained sandstone (shelf to lower shoreface deposits). Progradation is represented by the funnel trends in the Hawaz formation.

2) Retrogradation

If for each successive marine parasequence the increase in accommodation space is greater than the constant rate of sediment supply, thus the deposits of each successive parasequence will shift landward. Thus a retrogradational stacking pattern occurs when the long-term rate of accommodation space creation is greater than the supply of sediment (Coe et al., 1999). It is indicated by fining-upward stacking patterns, which imply upward deepening; and the gamma-ray values are increasing. In the upper part of the Hawaz Formation retrogradation is represented by a long fining-upward trend (increase of gamma-ray valus) (**Figs. 6.6 and 6.7**).

3) Aggradation

If for each successive parasequence the increase in accommodation space is equal to the rate of sediment supply, the deposits of each depositional zone in the successive parasequence will build out from the same lateral deposition as the previous parasequence. In this case, the shoreline will have stayed in the same position, and the pattern is described as aggradational. A group of parasequences showing this pattern form an aggradational parasequence set (Coe et al., 1999).

The thick shelf deposits in the middle part of the Hawaz Formation (**Figs. 6.6 and 6.7**) reflect an aggradation or facies stacking, with water depths fluctuating within shelf linits. Thick successions of starved-shelf mudstones reflect slow sedimentation during gradual sea-level rise (Galloway and Hobday, 1983).

6.5.1 Transgressive systems tract

A transgressive systems tract (TST) is recognized as a retrogradational parasequence set (Emery and Myers, 1996). In the Hawaz Formation the TST is bounded below by an erosion surface (glaciation) which can be interpreted as a sequence boundary, and above by a maximum flooding surface (base of the Tanezzuft Formation). The high gamma-ray reading displayed at the top of this TST, probably reflect a high content of radioactive shale. This suggests that the clastic source area had moved progressively further away, allowing shale material to accumulate on the sea floor from suspension.

6.5.2 Highstand systems tract

In the Hawaz Formation the HST occurs in two intervals in the lower part of the succession (**Figs. 6.6 and 6.7**) characterized by a decrease in gamma-ray values reflecting a coarsening-upward trend, and a decrease in shale content, suggesting deposition during retrogradation. The upper HST is bounded below by MFS and above sequence boundary (SB), and the lower HST is bounded below by MFS and above by a flooding surface (FS). The HST reflects a slowdown in the rate of relative sea-level rise and thus a decrease in the rate of creation of accommodation space.

6.6 Sequence stratigraphy and relative sea-level curves

6.6.1 Introduction

The interpretation of log trends in terms of relative sea-level change is very important for wireline sequence stratigraphic interpretation. For example, in the upper part of the Hawaz Formation the change from upper shore face to lower shore face reflects a gradual change from sandstone mudstone facies to burrowed sandstone due to a gradual change of sea-level. This change is not easy to pick-up from the gamma-ray log, but in the lower part of the Hawaz Formation the contact between distal shelf and lower shoreface is abrupt in terms of lithology and gamma-ray values. This abrupt change in deposition environment is due to an abrupt change in sea-level, which is easy to pick-up on the log response (at 4990 ft in H27-NC115 and 4641 ft in well A1-NC186).

6.6.2 Relative sea-level curves of the Hawaz Formation

In marine and lacustrine settings, changes in relative sea level result from the interaction between movements of the sea surface (i.e., eustasy) and the sea floor. Therefore, if relative sea level varies cyclically, the rate at which shelf accommodation space is created also varies cyclically. Such cyclic variation of accommodation, and the rate at which accommodation space is created, can have a significant effect on stratal architecture insofar as they can induce transgressoin and regression, and cause the formation of unconformities (Posamentier and Allen, 1999). Relative sea-level is measured between the sea-surface and a local moving datum, such as basement or a surface within the sediment pile (Posamentier et al., 1988).

In the Hawaz Formation the relative sea-level curve can be matched with the values of gamma-ray log trends (**Figs. 6.6** and **6.7**). In A1-NC186 the gamma-ray spikes (at depths 4530 ft, 4560 ft, and 4580 ft) represent flooding surfaces, which occur with a sea-level rise as part of a transgressive system tract. Also the maximum flooding surface (MFS) between the TST and HST at 4670 ft in well A1-NC186 and 5020 ft in well H27-NC115, are interpreted as a sequence boundary, and even though not easy to recognize, they have been put at the maximum gamma-ray reading in both wells. The abrupt change in gamma-ray values can be interpreted as an abrupt rise in sea-level (**Figs. 6.6** and **6.7**).

7. Depositional Model

7.1 Depositional model of the Hawaz Formation in A1-NC186 and H27-NC115

The Hawaz Formation was deposited in wave-dominated shoreface and shelf environments. Evidence of the fan deltas described by Vos (1981) for the Ordovician Hawaz Formation in the western-central Gargaf Arch of western Libya (**Figs. 7.1 and 7.2**), is lacking. Vos recognized six recurring facies types which he interpreted to have originated within a fan delta complex prograding across the Gargaf Arch in a general north and northwestrly direction, with a source terrain to the south (Vos, 1981). The absence of delta deposits in the studied wells may be explained by the fact that the delta was present but has been eroded away by marine processes or that it occurs in the more proximal part of the depositional system outside the study area.

The sedimentological and stratigraphical characteristics of the Hawaz Formation (Chapter 3) in the study area in the Murzuq Basin are attributed to shoreface and shelf facies associations within which some 9 facies have been distinguished (**Fig. 7.3**). The lower part of the cored section of the Hawaz Formation is dominated by the outer and inner shelf facies associations. The outer shelf association is dominated by mudstone whereas the inner shelf association is dominated by siltsone/sandstone. This variation probably corresponds to variations in water depths and energy levels on the shelf. Storm deposits of sand grade are restricted to the inner shelf association. These were deposited immediately below fair-water wave-base and represent shallower water and higher energy than the outer shelf association (**Fig. 7.3**).

In the lower shoreface the wave effect is very weak and, as a consequence of this, fine to medium grain sands dominant in this zone, intercalated with layers of laminated mudstone, both showing abundant bioturbation and trace fossils (**Fig. 7.3**).

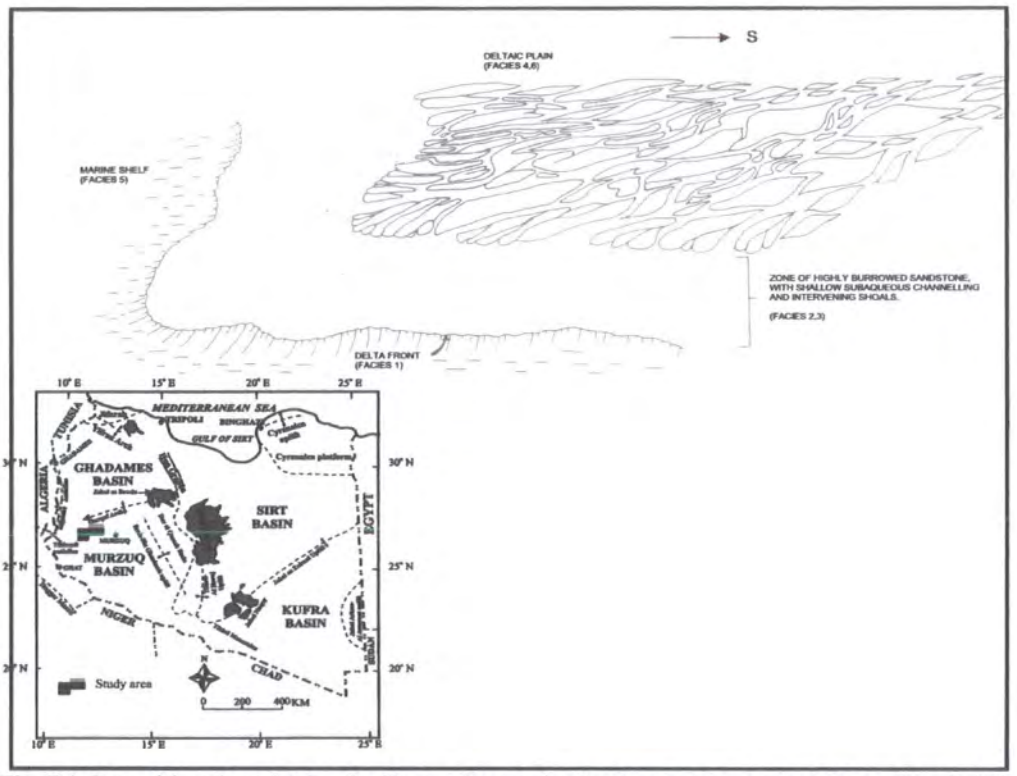

Fig. 7.1. Depositional model for the Hawaz Formation in the western-central Gargaf Arch (After Vos, 1981).

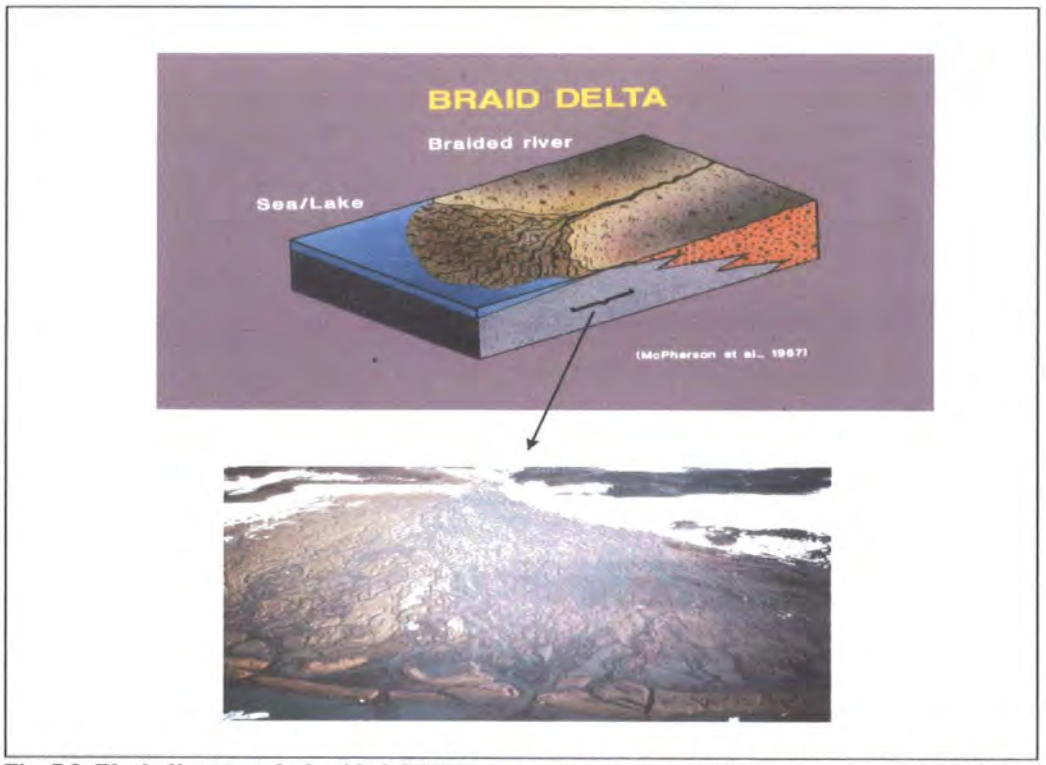

Fig. 7.2. Block diagram of a braided delta system and an example of a modern braid delta from Alaska.

The repetition of similar facies suggests a recurring pattern of similar depositional processes and environments. This is attributed to dynamic intraction between shoreface (upper and lower) and shelf environments (inner and outer) along a NW-SE oriented shoreline, but with the possibility of a contribution from a continental source area as evidenced by a small percentage of the sandstone grain-size samples falling in the fluvial field (see Chapter 2). The rivers are thought to have fed in sediment from the Ghat/Tikiumit Arch to the southwest of the study area (**Fig. 7.5**).

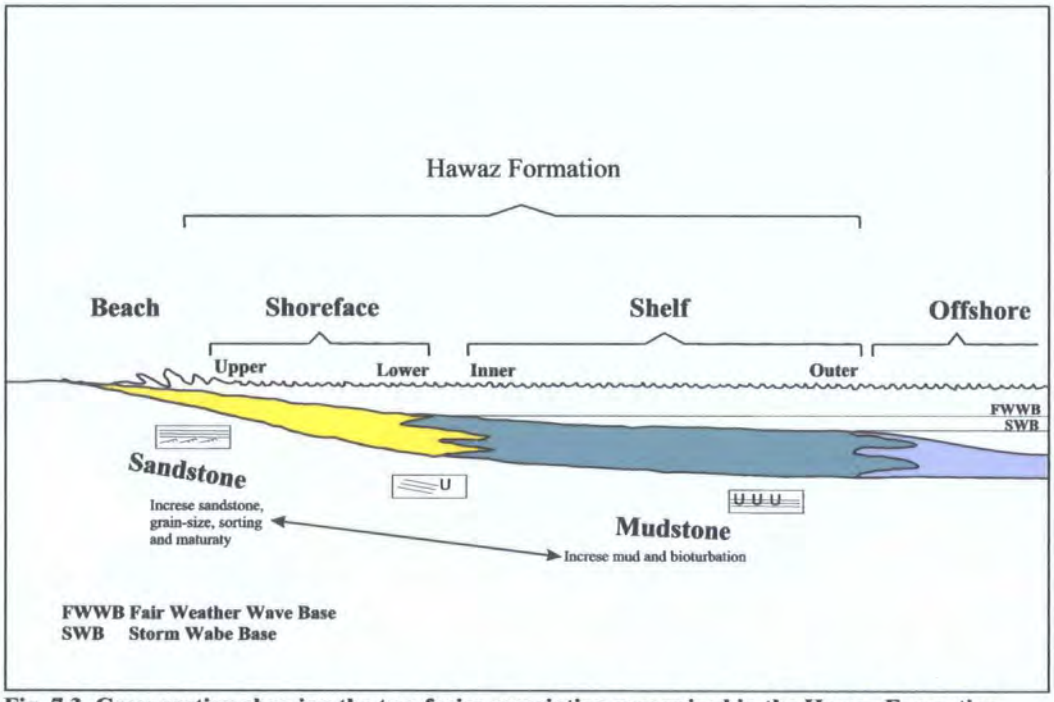

Fig. 7.3. Cross section showing the two facies association recognized in the Hawaz Formation (shoreface and shelf).

The presence of this small percentage of fluvial sand and the braided delta recognized by Vos (1981), suggest that braided stream systems supplied sediment to the shoreline and the adjacent shelf. Bedload in the braided stream system varied from conglomerate to coarse sandstone, but in the study area the dominance of medium to fine-grain sand suggests that sand in the source area supplying the braided stream system was of similar size or sediment by-passing occurred in which the coarser material was deposited in proximal alluvial fans and along the braidplain, and the finer material flushed out along the coastline (**Fig. 7.4**).

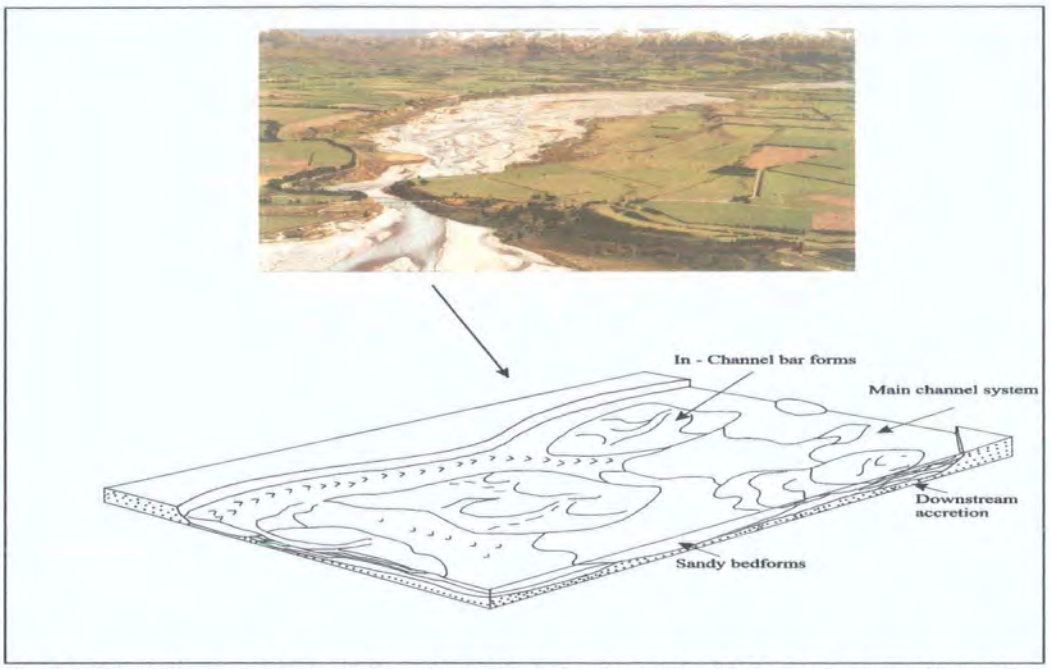

Fig. 7.4. Block diagram of a typical sandy, bedload-dominated braided stream system illustrating bed forms common to these systems.

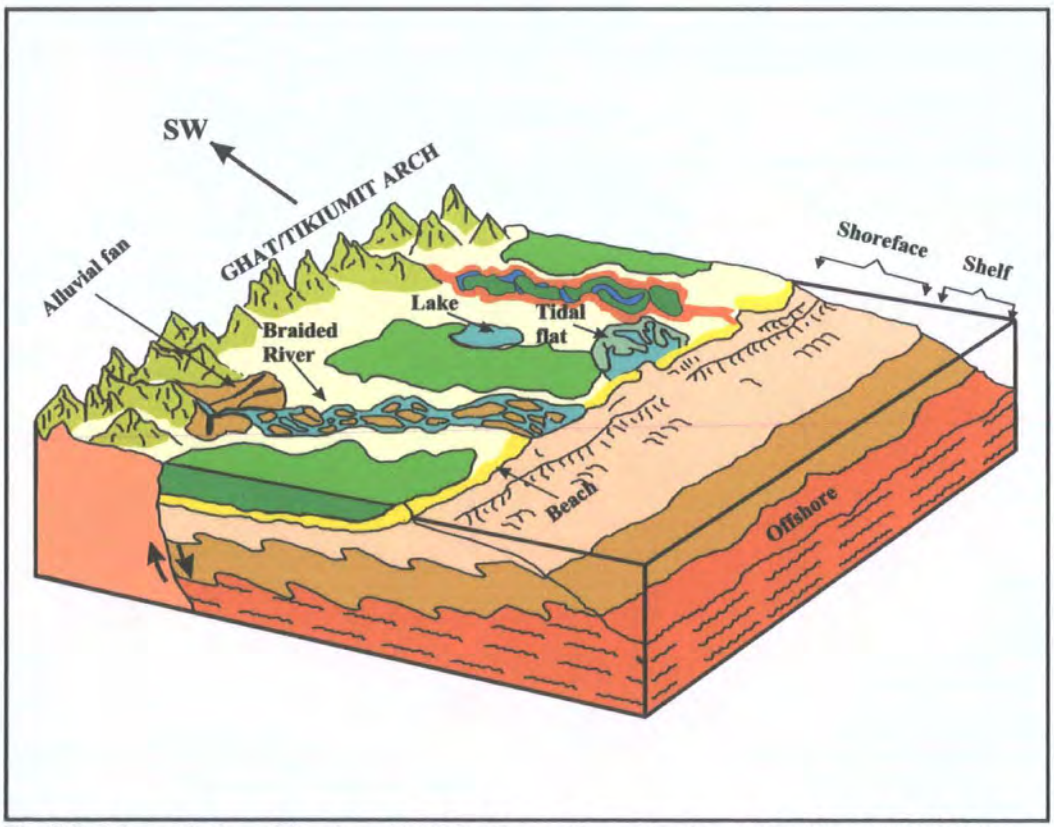

Fig. 7.5. Schematic depositional model of the Hawaz Formation in A1-NC186 and H27-NC115. Note the absence of the fan delta system described by Vos (1981) in the west-central Gargaf Arch, to the W/NW of the study area.

Constant interaction between the shoreface and shelf must have affected the more landward depositional environments to the southwest outside the study area as well. Thus, small-scale relative sea level fluctuations, evidenced by the relatively minor shifts in facies, were the dominant force on the depositional system, and enable sequence stratigraphy to be applied effectively to the succession. The relatively small-scale shifts in facies tracts from shoreface to outer shelf may reflact the very low gradient of the shelf and/or very minor changes in relative sea level.

The Llanviranian-Llandeilian (Middle Ordovician) Hawaz Formation unconformably overlies the lower Ordovician (Tremadocian) Achebyat Formation which in turn overlies the upper Cambrian The Cambrian Period was a long warm interval followed by a major phase of glaciation in Late Ordovician in central northern Africa (Caputo and Crowell, 1985), when ice spread northward from glacial centres in central Africa.

Echikh and Sola (2000) stated that the mid-Ordovician was characterised by tectonic instability, as indicated by the erosional or non-depositional absence of the Hawaz and/or Melaz Shuqran Formations over the Tiririne and Traghan highs. The principal tectonic activity probably took place during the Llandeilo to Caradoc. The resulting faulted topography in the central and eastern parts of the basin was enhanced by glacially-related erosion resulting in the creation of NW-SE directed palaeovalleys which were later filled by Ashgill periglacial coarse clastics of the Mamuniyat Formation. This tectonic phase did not create new fault and fold patterns, but was rather characterised by vertical epeirogenic movements along rejuvenated Pan-African fault systems (Echikh and Sola, 2000). Luning et al. (2000) reviewed the occurrence of anoxic, black shale facies throughout North Africa and the Arabian Peninsula offering a three-system, sequence stratigraphical model characterised by the succession in Libya. They placed the transgressive surface at the base of the black shales (**Fig. 7.12**). Luning et al. (2000) show two different interpretations of the sequence stratigraphy (**Fig. 7.6**).

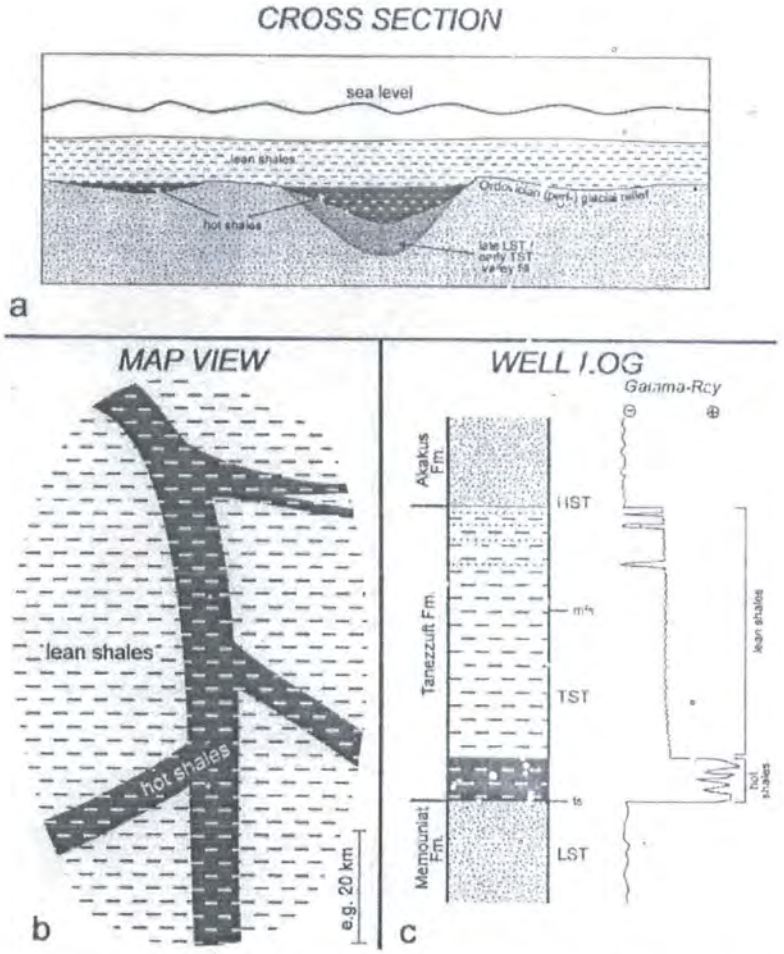

Fig. 7.6 Luning et al. (2000) interpretation for early Silurian hot shale deposition in North Africa and Arabia.

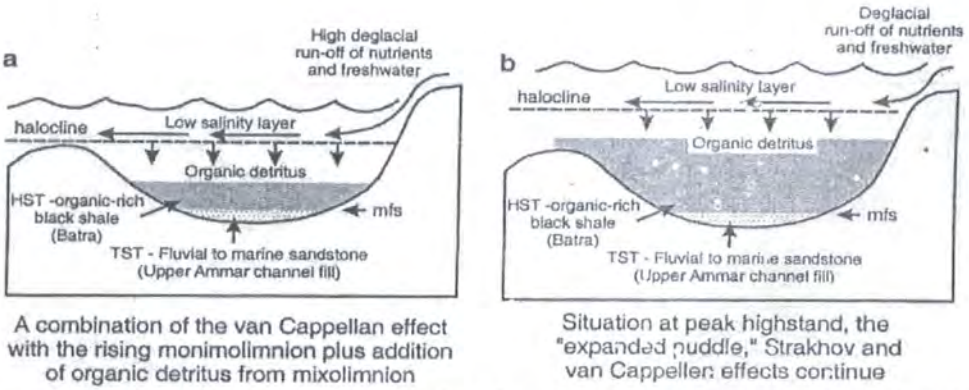

Fig. 7.7. Conceptual model for the upper Ordovician organic-rich "hot" shale in Jordan. (a) Initiation of the anoxic puddle. (b) Expansion of the puddle during the HST (After Armstrong et al., 2005).

In **Fig. 7.6c** they show the base of the Tanezzuft to be a transgressive surface with the maximum flooding surface some distance above. In contrast with **Fig 7.6a** they show a late lowstand and early transgressive system tract beneath the base of the

Tanzzuft, in which case the base of the Tanezzuft must be a maximum flooding surface. Luning et al. (2000) favour the first model and considered it to be applicable throughout North Africa and Arabia.

Luning's et al. (2000) model is inconsistent with Armstrong et al. (2005) based on their field observations in the equivalent Jordanian succession, where black shale lies on the mfs. Initially organic-rich black shale was deposited in glacially incised shelf sub-basins. As the deglacial transgression progressed, sub-basin margins and interfluves were eventually breached producing a rapid increase in accommodation space. Low sedimentation rates meant that this space could not be filled and the basin became starved. The spread of the black shale away from the depocentres within glacially incised shelf depressions or sub-basins was diachronous. Therefore the black shales are interpreted as MF shales and they fulfil the diagnostic criteria for the expanding puddle model (**Fig. 7.7**) (Armstrong et al., 2005). Armstrong et al. (2005) believe that the base of the Silurian black shale in Jordan represents the MFS as the upper Ordovician beneath the black shales is marine, and a similar scenario occurs in the study area in NC115 and NC186 in the Murzuq Basin.

The interpretation of the early post-glacial black shale as Basal Transgressive (BT) shales (Luning et al., 2000) is inconsistent with the Repsol internal report by Ghnia and Chang (2002) (**Fig. 7.8**) who stated that "At the end of Hawaz time, a regional uplift caused by deep heat process resulted in extensive erosion, which removed part or whole of Hawaz section from the middle of the block, forming a "U" shaped valley. This valley generally deepens to the south" and they later said "It is widely believed currently that late Ordovician glaciation also played an important role in this process, a basin-and-range landscape was generated by the beginning of late Ordovician time" (Ghnia and Chang, 2002). Where a glacier flows through a former river valley it usually widens and straightens the valley. Ice erodes both the sides and the bottom of a valley, whereas a river only erodes the bottom. Thus river valleys are commonly V-shaped while glaciated valleys are commonly U-shaped and have steep valley walls, which can be compared with that suggested by Ghnia and Chang (2002) for the Hawaz Formation (Bill, 1932) (**Fig. 7.9**). However, there is no evidence of faulting suggested by Ghnia and Chang, (2002) and Echikh and Sola, (2000), and the unfaulted U shape, which is shown in the seismic data (**Fig. 7.10**), could be explained

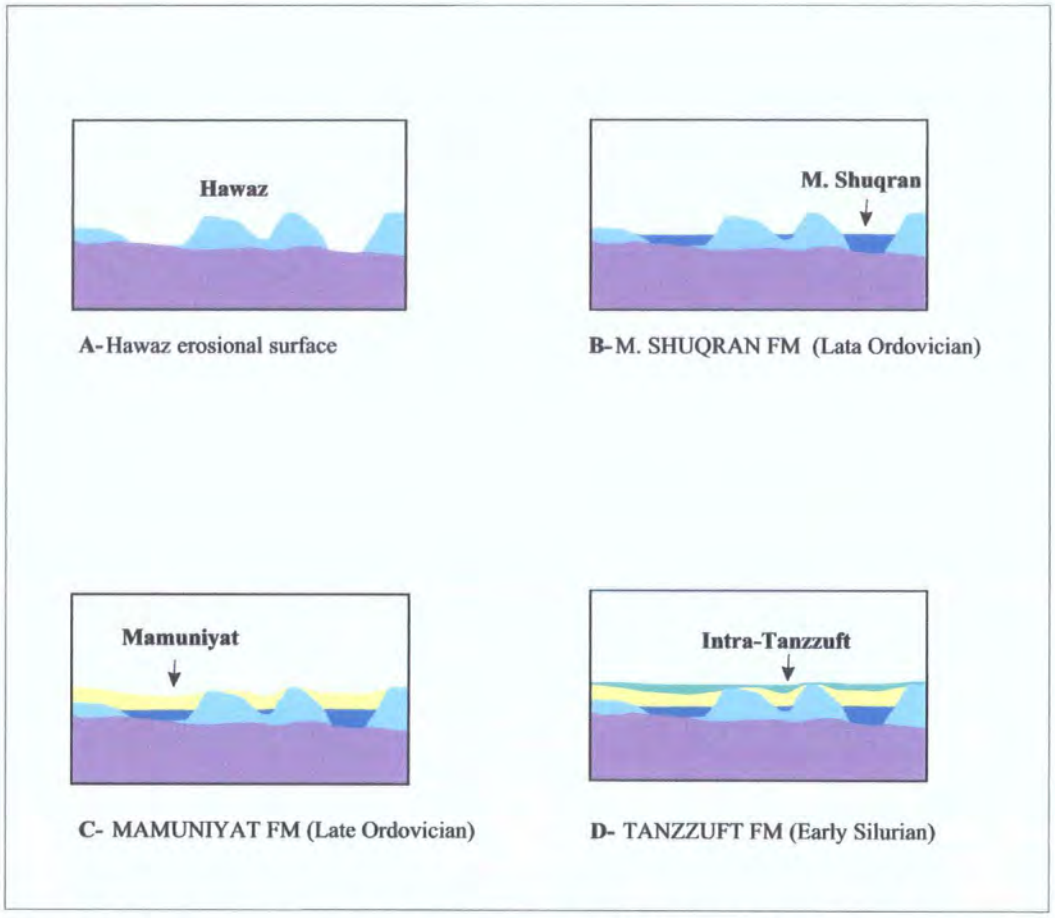

Fig. 7.8. Cartoon showing major evolution stages in NC115 (After Ghnia and Chang, 2002).

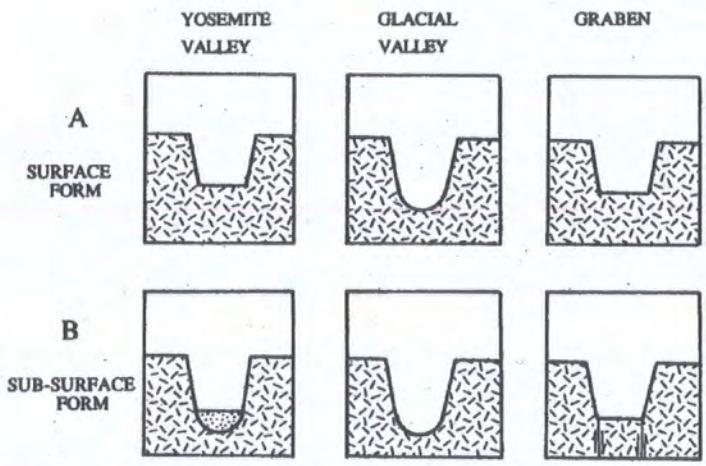

Fig. 7.9. A. In basic surface form, Yosemite Valley resembles a fault-block basin, or graben, more than it does a glacial valley. B. Beneath the thick lake sediments is the rest of a U-shaped glacial valley, note a block of rock that has dropped down between faults (After Bill, 1932).

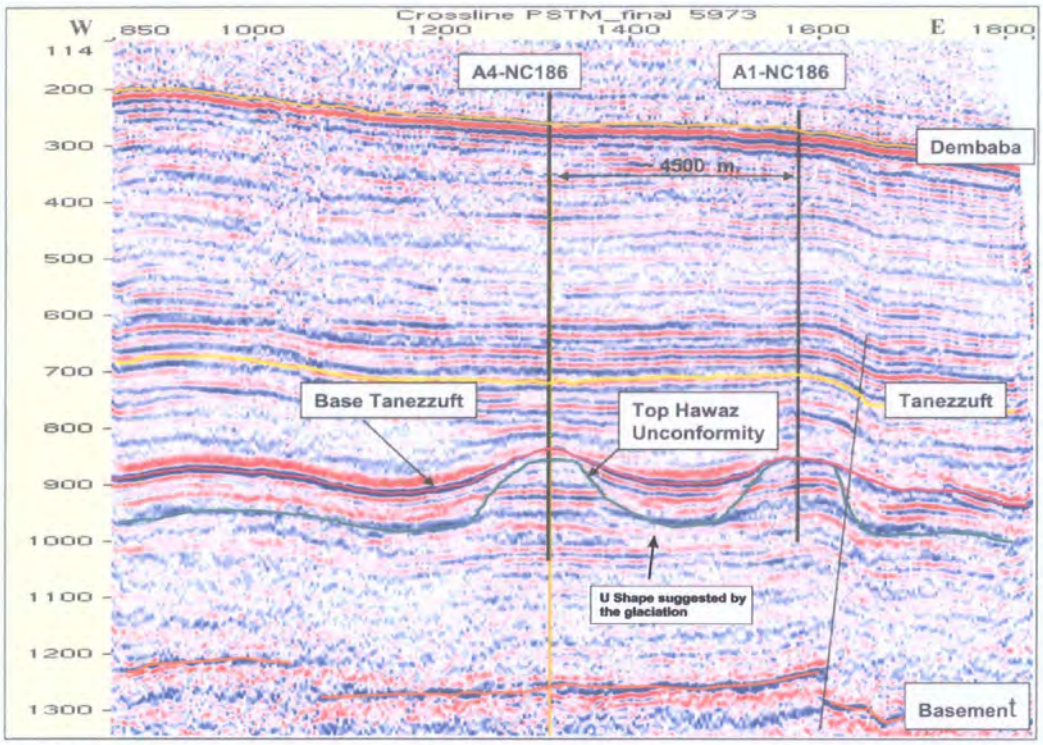

Fig. 7.10. Seismic line showing the U shaped vally in the Hawaz Formation, but without evidence of a fault control suggested by Ghnia and Chang (2002), and Echikh and Sola, (2000). The U shape probably formed by glaciation.

by the erosive action of ice alone (**Fig. 7.9**) which eroded the Mamunuiyat Formation and part of the Hawaz Formation in the study area.

Early post-glacial, transgressive, organic-rich black shales were a ubiquitous feature of the northern Gondwana continental shelf during the late Ordovician to early Silurian. These rocks, which contain up to 10% total organic carbon, have an elevated gamma log response (up to 200 API, Andrew, 1991) due to uranium-enrichment, and constitute one of the world's major hydrocarbon source rocks (Armstrong et al., 2005). Luning et al (2000) stated that "In the earliest stages of the transgression, during the latest Ordovician *persculptus* Zone and the earliest Silurian Rhuddanian Stage, only low-lying areas of the shelf were flooded and shales deposited (**Fig. 7.11B**). There is usually a sharp contact between Ordovician strata and the latest Ordovician–early Silurian shales. The North African and Arabian shelf at that time were characterized by a complex system of flooded intrashelf basins and palaeovalleys which were separated by various tectonic and sedimentary palaeohigh structures "(Luning et al., 2000).

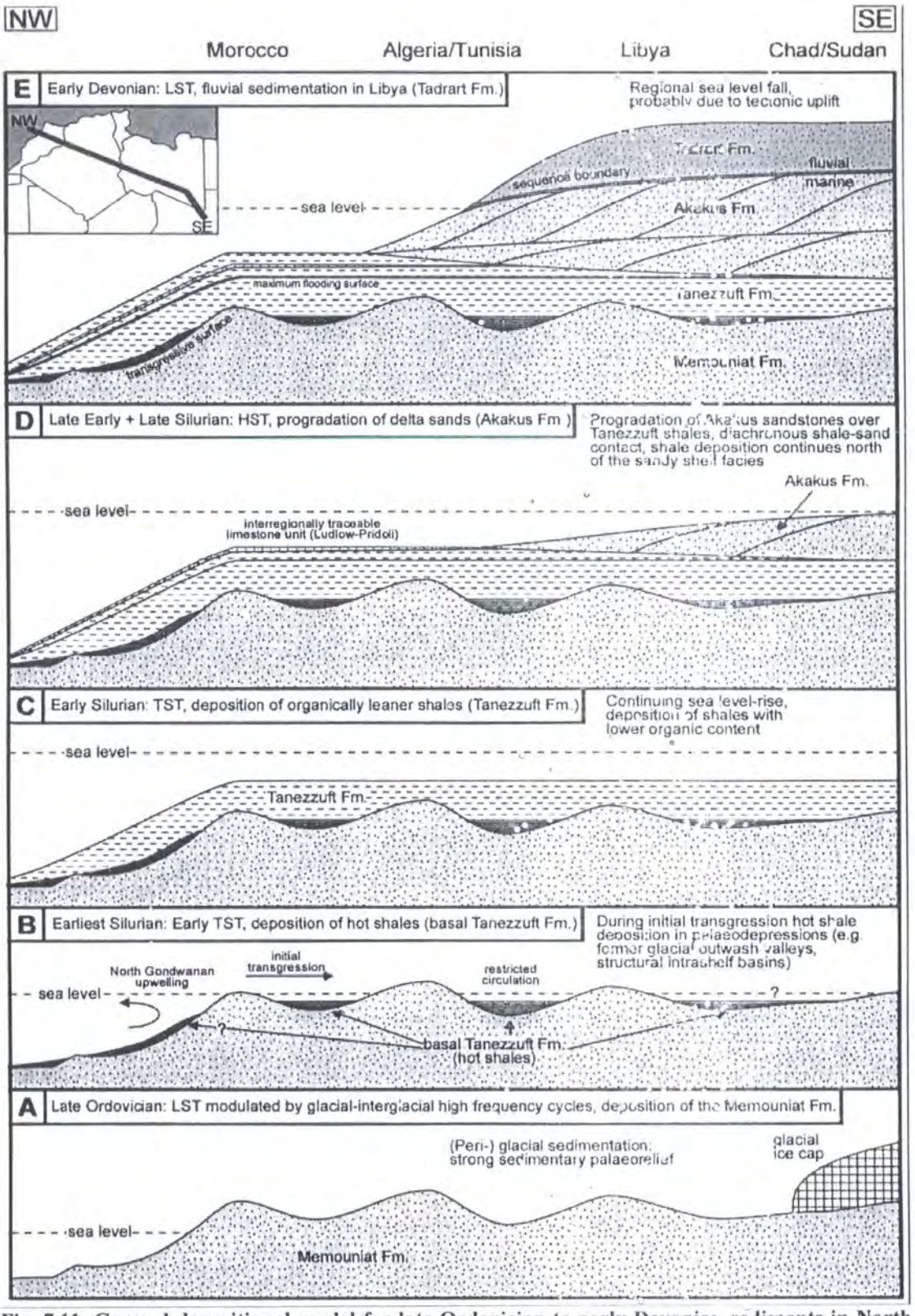

Fig. 7.11. General depositional model for late Ordovician to early Devonian sediments in North Africa with emphasis on the lowermost Silurian hot shales. Systems tracts belong to a second-order sequence (Luning et al., 2000).

8. Conclusions

This study of the Hawaz sandstone shows that

- The Hawaz Formation consists predominantly of alternating fine to medium-grained, well-sorted to moderately well-sorted sandstone.

- The detrital mineral components are monocrystalline quartz with subordinate polycrystalline quartz, rock fragments, heavy minerals, kaolinite and rare feldspar.

- Petrographic data shows that the Hawaz sandstone can be classified mainly as a quartz arenite, with local subarkoses.

- Compositional data indicates that the sandstones in the two studied wells have a similar modal composition and were derived from similar parent rocks.

- Diagenetic cement is mainly in the form of quartz overgrowths, and local calcite and clay matrix, all of which have reduced the porosity.

- The average total porosity of the Hawaz Formation for the two studied wells is 10.3% for A1-NC186 and 11.2% H27-NC115. No permeability analysis of these samples has been carried out.

- The Mid Ordovician deposits of the Hawaz Formation can be subdivided into transgressive and highstand systems tracts.

- The sequence stratigraphy of the Hawaz Formation in the cored section of A1-NC186 and H27-NC115 shows that the contact between the HST and the major TST is defined by an erosion surface which may have been caused by ice action .Evidence of glaciation is seen in the SEM analysis of the grains (see Chapter 4).

- A lowstand system tract may have been present but it has been subsequently eroded, or it may occur in a more landward position.

- The sequence stratigraphy throughout a wide area of H field of NC115 and NC186 concession areas shows that the Hawaz Formation can be correlated using wireline logs.

- The reservoir quality of the Hawaz Formation varies from poor, represented by the upper part of the core section, to good, represented by the lower part of the core section (see Chapter 4).

- Facies analysis shows that the Hawaz Formation was deposited along a marine shoreline in shallow marine shoreface and shelf environments. No evidence of delta facies suggested by Vos (1981) as found in the study area.

References

ABUGARES, Y. I., RAMAEKERS, P., 1993. Short notes and guidebook on the PALAEOZOIC GEOLOGY OF THE Ghat area, SW Libya, Field trip, October 14-17, 1993. Earth Science Society of Libya. Interprint Ltd., Malta. 84 pp.

ALLEN, J. R. L 1982. Sedimentary Structures: Their character and physical basis. Developments in Sedimentology. Vol, 30A, Elsevier, Amesterdam. 593 pp.

ALLEN J. R. L. 1991. The bouma division A and the possible duration of turbidity currents, *Journal Sedimentary Petrology*, Vol. 61, pp. 291-295.

ANDERTON, R., 1976. Tidel-shelf sedimentation: an example from the Scottish Dalradian. *Sedimentology*, Vol. 23, P. 429-459.

ANDREWS, I. J., 1991. Palaeozoic lithostratigraphy in the subsurface of Jordan. Subsurface geology Bulletin, 2.

AOYAGI A, AND KAZAMA T. 1980. Transformational changes of clay minerals, zeolites and silica minerals during diagenesis, *Sedimentology*, Vol. 27, pp.179-188.

ARMSTRONG H. A, TURNER B. R, MAKHLOUF I. M, WEEDON G. P, WILLIAMS M, AL SMADI A, AND ABU SALAH A. 2005. Origin, sequence stratigraphy and depositional environment of an upper Ordovician (Hirnantian) deglacial black shale, Jordan. *Palaeogeography, Palaeoclimatology, Palaeoecology* 220, pp 273-289.

ARNOTT, R. W. C., 1995. The parasequence definition-are transgressive deposits inadequately addressed? *Journal Sedimentary Research*, Vol. B65, No. 1 p. 1-6.

AZIZ, A. 2000. Stratigraphy and hydrocarbon potential of the Lower Palaeozoic succession of License NC-115, Murzuq Basin, SW Libya. In: M. A. Sola and D. Worsley (Eds), Geological Exploration in Murzuq Basin, Elsevier Science, Amsterdam, pp. 349-368.

BANKS, N. L., 1973. Tide dominated offshore sedimentation, Lower Cambrian, north Norway. *Sedimentology*, Vol. 20, P. 213-228.

BARTEK, L., VAIL, P. R., ANDERSON, J. B. AND EMMET, P. A., 1990. The effect of Cenozoic ice sheet fluctuation in Antarctica on the stratigraphic signature of the Neogene. *Journal Geophysical Research*.

BASU A, YOUNG. W. S, SUTTNER L. J, JAMES W. C, AND MACK G H. 1975. Re-evaluation of the use of undulatory extinction and polycrystallinity in detrital quartz for provenance interpretation. *Journal of Sedimentary Petroology*, Vol. 45, No. 4, pp. 873-882.

BELLINI, E., AND MASSA, D. 1980. A stratigraphic Contribution to the Paleozoic of the Southern Basins of Libya. The Geology of Libya, I, 3-56.

BERNER R. A., 1970. Sedimentary pyrite formation. *American journal of science*, Vol. 268, P. 1-23.

BHATTACHARYA, J. P., 1993. The expression and interpretation of marine flooding surfaces and erosional surfaces in core: examples from the Upper Cretaceous Dunvegan Formation, Alberta foreland basin, Canada, in Weimer, P., and Posamentier, H. W., (Eds.). Sequence Stratigraphy and Facies Associations: International Association of Sedimentologist Special Publication 18, p. 125-160.

BLATT, H, 1982. Sedimentary petrology. W. H. Freeman and company, San Francisco, 564 pp.

BLATT H, 1992. Sedimentary petrology. W. H. Freeman New York.

BLATT, H. AND CHRISTIE, J. M. 1963. Undulatry extinction in quartz of igneous and metamorphic rocks and its significance in provenance studies of sedimentary rocks. *Journal of sedimentary Petrology*, Vol.33, pp. 559-579.

BOGGS, S. JR., 1995. Principles of Sedimentology and Stratigraphy. Merrill, Columbus, Ohio,-Hall, Upper Sander River, New Jersey, 2nd edition, 774 pp.

BOKMAN, J. 1952. Clastic quartz particles as indices of provenance. *Journal of Sedimentary Petrology*, Vol, 22. No. 1, pp. 17-24.

BOLES, J. R. 1982. Secondary Porosity Reactions in the stevens Sandstone, San Joaquin valley, California. In: Clastic Diagenesis (EdS) by David A. McDonald and Ronald C. Surdam University of California Santa Barbra, California. pp 217-224.

BORGHI, P. 1939. Fossili devonici del Fezzan. Bolietino de la Sociета Geologica Italiana. Vol. 58, No. 1, pp.186-188. Roma.

BORGHI, P. AND CHIESA, C. 1940. Cenni geologici e paleontologici sul paleozoico dell Egghidi Uan Caza nel deserto di Taita (Fezzan occidentale) Ibid Vol. 2, pp. 123-127. Tripoli.

BOWN, D. G., 2001. Formation Evaluation and Petrophysics. MSc course in Heriot Watt University, Edinburgh, Department of Petroleum Engineering.

BRENCHLEY P. J., MARSHALL. J. D., CARDEN G. A. F., ROBERTSON. D. B. R., LONG. D. G. F., DEIDLA. T., AND ANDERSON. T. F. 1994. Bathymetric and isotopic evidence for a short-lived Late Ordovician glaciation in greenhouse period, *Geology*, Vol. 22, p. 295-298.

BROWN, L. F., JR., AND FISHER, W. L., 1977. Seismic stratigraphic interpretation of depositional systems: examples from Brazilian rift and pull apart basins. In Payton, C E., (Ed.). Seismic Stratigraphy-Application to Hydrocarbon

Exploration: *American Association of Petroleum Geologists Memoir* 26, p. 213-248.

BUCKE. D. P., AND MANKIN C. J, 1971. Clay-mineral diagenesis within interlaminated shales and sandstones, *Journal Sedimentary Petrology*, Vol. 41, P 971-981.

BUROLLET, P. F. 1963. Reconnaissance géologique dans le sud-est du basin de Kufra. Rev. Inst. Fr. Pétrole, 18, 1537-1545.

CAMPBELL, V. C., 1966. Truncated wave-ripple laminae. *Journal Sedimentary Petrology*. Vol, 36. P. 825-828.

CAMPBELL, C. V., 1967. Laminae, lamina set, bed and bed-set. *Sedimentology*, Vol. 8, P. 7-26.

CAMPBELL, V. C., 1971. Depositional model-upper cretaceous gallup beach shoreline, ship rock area, northwestern new mexico. *Journal of Sedimintary Petrology*, Vol. 41, No. 2, P. 395-409.

CAPUTO, M. V. AND CROWELL, J. C. 1985. Migration of glacial centers across Gondwana during Palaeozoic Era, *Geological Society of America Bulletin*, Vol. 96, P. 1020-1036.

CLARK-LOWES. D. D. AND WARD, J. 1991. Palaeoenvironmental evidence from the Palaeozoic 'Nubian sandstones' of the Sahara. *Third Symposium on the Geology of Libya*. Vol. 6 (Eds. M.J. Salem, A.m. Sbeta and M.r. Bakbak.), Elsevier, Amsterdam, p. 2099-2154.

COE A, BOSENCE D, CHURCH K, FLINT S, HOWELL J, AND WILSON C., 2002. The sedimentary record of sea-level change. The open University, Walton Hall, 285 pp.

COLLOMB, G.R. 1962. Étude géologique de Jebel Fezzan et de sa bordure paléozoque. Notes Mém. Comp. Fr. Pétrole, 1, 35 p.

COTTER E., 1985. Graver-topped offshore bar sequences in the Lower Carboniferous of southern Ireland. *Sedimentology*, Vol 32, P. 195-213.

CROXTON, F. E., AND COWDEN, D. J., 1939. Applied general statistics. Prentice-Hall, New York, 944p.

CURT TEICHERT, 1958. Concepts of facies. *American Association of Petrolum Geologist Bulletin*. Vol. 42, P. 2718-2744.

DAPPLES, E. C., KRUMBEIN, W. C., AND SLOSS, L. L., 1953. Petrographic and lithologic attributes of sandstones. *Journal Geology*, Vol. 61, p. 291-317.

DAVID P. BUCKE, 1971. Clay-mineal diagenesis within interlaminated shales and sandstones. *Journal Sedimentary Petrology*. Vol. 41, No. 4, pp. 971-981.

DELLA FAVERA, J. C. 1984. Eventos de sedimentacac episodica nas bacias braslleiras, uma contribulacao para atestar o carater pontuado do registro sedimentar (in Portugese). Anals 33° Brasil. Geol., Rio de Janeiro, 489-501.

DE RAAF, J. F. M., BOERSMA, J. R. AND VAN GELDER, A., 1977. Wave generated structures and sequences from a shallow marine succession, Lower Carboniferous, County Cork, Ireland. *Sedimentology*, Vol. 24, P. 451-483.

DESIO, A., 1936a. Primenotizie sulla presenza del Silurico fossilifero nel Fezzan. *Boll, Soc. Geol. Ital.* Vol. 55, p. 116-120.

DESIO, A., 1936b. Riassunto sulla presenza del Silurico fossilifero nel Fezzan. *Boll. Soc. Geol. Ital.* Vol. 55, p. 319-356.

DICKINSON W. R., 1985. Interpreting provenance relations from detrital modes of sandstones. In: G.G. Zuffa, ed., Provenance of Arenites. NATO ASI series. C148, D.Reidel, Dordrecht, pp. 333-361.

DOYLE J. L, CLEARY W J. AND PILKEY O. H., 1967. Mica: its use in determining shelf-depositional regimes. *Marine Geology*, Vol. 6, pp. 381-389.

DROSER, M. L. AND BOTTJER, D. J. 1989. Ichonofabric of sandstones deposited in high-energy nearshore environments: measurement and utilization. Palaios 4: 598-604 Goldring, R (1996) The sedimentological significance of concentrically laminated burrows from Lower Cretaceous Ca-bentonites, Oxfordshire. Journal of the Geological Society, London 153:255-63.

ECHIKH K. AND M.A. SOLA, 2000. Geology and hydrocarbon occurrences in the Murzuq Basin, SW Libya, In: M. A. Sola and D. Worsley (Eds), Geological Exploration in Murzuq Basin, Elsevier Science, Amsterdam, p. 175-222.

EMERY, D. AND MYERS, K. J., 1996. Sequance stratigraphy. Blackwell Science, 297 pp.

FELLO N. M. 2001. Depositional environments, diagenesis and reservoir modelling of concession NC115, Murzuq Basin, SW Libya. (Ph.D. Thesis, Unpublished).

FISCHER, A.G., 1981. Climatic oscillations in the biosphere, in Nitecki, M. (ed), Biotic crises in ecological and evolutionary time, Academic Press, New York, P. 103-131.

FOLK, R. L. AND WARD, W. C., 1957. Brazos River Bar: A study in the Significance of Grain-size parameters. *Journal of Sedimentary Petrology*, Vol. 27, No. 1, P. 3-26.

FOLK, R. L., 1951. A comparison chart for visual parcentage estimation. *Journal of Sedimentary Petrology*, Vol. 21, No. 1, pp. 32-33.

FOLK, R. L. 1966. A review of grain-size parameters. *Sedimentology*, Vol 6, P. 73-93.

FREULON, J. M. 1954. Sur le dévonien du Sahara oriental (Ajjer et Fezzan). 19th Iternat Geolog. Congrés (Abstract), V. 20, pp. 141. Alger.

FREY, R. W. AND PEMBERTON, S. G., 1984. Trace fossils facies models. In: Facies models: Geoscience Canada, Reprint Series I (Eds) by R. G. Walker), pp. 189-207. Geological Association of Canada, Toronto.

FRIEDMAN, G. M., 1958. determination of sieve-size distribution from thin-section data for sedimentary petrological studies. *Journal Geology*, Vol. 66, P. 394-416.

FRIEDMAN, G. M., 1962. Comparison of moment measures for sieving and thin-section data in sedimentary petrological studies. *Journal of Sedimentary Petrology*, Vol. 32, P. 15-25.

FRIEDMAN, G. M., 1967. Dynamic processes and statistical parameters compared for size frequency distribution of beach and river sands, *Journal of Sedimentary Petrology*, Vol. 37, No. 2, pp.327-354.

FRITZ W. J. AND JOHNINE N. MOOR 1988. Basics of physical stratigraphy and sedimentology. Wiley New York, 371 pp.

FREY, R. W. PEMBERTON. S. G. AND SAUNDERS. T. D. A., 1990. Ichnofacies and bathymetry: a passive relationship: *Journal of Paleontology*, Vol. 64, p. 155-158.

GALLOWAY W, 1974. Deposition and diagenetic Alteration of Sandstone in Northeast Pacific Arc-Related Basins: implications for Graywacke Genesis. *Geological Society of America Bulletin*, Vol. 85, pp. 379-390.

GALLOWAY, W. E. AND HOBDAY, D. K., 1983. Terrigenous clastic depositional system.springer-verlag new york, 423 pp.

GAVINIL. E, RASMUSSEN B, KRAPEZ B AND GROVES. D. I., 2002. Palaeoenvironmental significance of rounded pyrite in siliciclastic sequences of the Late Archaean Witwatersrand Basin: oxygen-deficient atmosphere or hydrothermal alteration? *Sedimentology*, Vol. 49, pp. 1133-1156.

GHNIA, S., AND CHANG, P., 2003. Geological/Geophysical Assessment For Concession NC-115. Repsol Oil Operation Unpublished Report, 72 p.

GRUBIC, A., DIMITRIJEVIC, M., GALECIC, M., JAKOVLJEVIC, Z., KOMARNICKI, S., PROTIC, D., RADULOVIC, P. AND RONCEVIC, G., 1991. Stratigraphy of western Fezzan, SW Libya. In . Salem, M, J. And Belaid, M.N (Eds). The geology of Libya, Academic Press, London, New York, Vol, IV, P. 1529-1565.

HALLAM, A., 1977. Secular changes in marine inundation of USSR and North America through the Phanerozoic. Nature 269, P. 769-772.

HALLAM, A., 1981. Facies interpretation and the Stratigraphic record. W. H. Freeman and Company, Oxford and San Francisco.

HALLETT. D., 2002. Petroleum geology of Libya. Elsevier Amesterdam.

HANCOCK N. J AND TAYLOR A. M. 1978. Clay mineral diagenesis and oil migration in the Middle Jurassic Brent Sand Formation. *Geological Society London*. Vol. 135, pp 69-72.

HAQ, B. U., HARDENBOL, J. AND VAIL, P. R., 1988. Mesozoic and cenozoic chronostratigraphy and cycles of sea-level change. In: C. K. Wilgus, B. S. Hastings, c. g. st sendall, h. w. posamentier, c. a. ross and j. c. van wagoner (Eds.). Sea-level changes: An Integrated Approch. Special publication, society of Economic Palaeontologists and Mineralogistes. Tulsa. 42, P. 40-45.

HARRELL, J. 1984. A visual comparator for degree of sorting in thin and plane sections. *Journal Sedimentary Petrology*, Vol 54. p. 646-650.

HAVLICEK, V. AND MASSA, D., 1973. Brachioposes de l'ordovician superieur de Libya occidental: Implication Stratigrapiques Tegionales. Geobios. 6(4), P. 267-290.

HEALD, M. T. AND LARSES, R. E. 1973. The significance of the solution of feldspar in porosity development. *Journal of Sedimentary Petrology*, Vol. 43, pp. 458-460.

HOEN, E. W. 1968. Geology of the Murzuk Basin. Amoseas Ltd. Unpublished Repor.

HOWEEL, J., AND FITZSIMMONS, R., 1999. An introduction to clastic sequence stratigraphy. A short course for BSRG, December 19th 1999, Stratigraphy Group, University of Liverpool and Conoco, Houston.

HUBERT, F. J., 1963. Textural evidence for deposition of many western north atlantic deep-dea sands by ocean-bottom currents rather than turbidity currents, *Journal Geology*, Vol. 72, pp. 757-785.

INMAN, D. L., 1952. Measures for describing the size distribution of sediments. *Journal of Sedimentary Petrology*, Vol. 22, No. 3, P. 125-145.

INMAN, D. L., AND BAGNOLD, R. A., 1963. Beach and nearshore processes: Part II, Littoral processes, P. 529-553. In Hill, M. N., (Eds). The sea, Vol, 3. the earth beneath the sea. Interscience Publishers, Inc., New York. 963 pp.

JACQUE, M. 1962. Reconnaissance geologique du Fezzan oriental, Notes et Mem, Comp. fran. Pet. No. 5, 44p.

JERVEY, M. T., 1988. Quantitative geological Modelling of siliciclastic rock sequences and their seismic expressions. In: C. K. Wilgus, B. S. Hastings, C. G. St Kendall, H. W. Posamentier, C. A. Ross and J. C. Van Wagoner (Eds.). Sea-level changes: An Integrated Approach. Special Publication, *Society of Economic Palaeontologists and Mineralogists, Tulsa*, 42. P. 47-69.

JOHN F. HUBERT, 1963. Textural evidence for deposition of many western north atlantic deep-sea sands by ocean-bottom currents rather than turbidity currents. *Journal Geology.*, Vol 72. p. 757-785.

JOHNSON, H. D., 1977. Shallow marine sandbars sequence: an example from the late Precambrian of North Norway. *Sedimentology*, Vol 24, P. 245-270.

KLITZSCH, E. 1963. Geology of the North east flank of the Murzuq basin (Djebel Ben Ghnema Dor el Gussa area), *Rev. de l'Inst. Franc. Du Petrole* Vol. 18 No. 10/11, pp.97-118.

KLITZSCH, E. 1965. Ein profil aus dem typusgebiet gotlandischer und devonische schichten der zentralsahara (westrand Murzukbecken, Libyen). *Erdol u. Kohle, Deut.* Vol. 18, p. 605-607.

KLITZSCH, E. 1969. Stratigraphic section from the type areas of Silurian and Devonian strata at western Murzuk Basin (Libya). In: Geology, archaeology and prehistory of the southwestern Fezzan, Libya (ed. Kanes, W.H). Petroloum Exploration Society of Libya. Eleventh Annual Field Conference, p. 83-90.

KLITZSCH, E. 1971. Continental Mesozoic strata of southwestern Libya (Messåk Sandstone) former Nubian Sandstone. 1st Confer. On Afr. Geology, Commonwealth Geolog. Liasion Office, pp. 19. London.

KNELLER B. G. AND BRANNEY, M. J. 1995. Sustained high-density turbidity currents and the deposition of thick massive sands, *Sedimentology*, Vol. 42, pp. 607-616.

KRUMBEIN, W. C. 1934. Size frequency distributions of sediments. *Journal of Sedimentary Petrology* Vol. 4, P. 65-77.

KRUMBEIN, W. C. AND PETTIJOHN, F. J., 1938. Manual of Sedimentary Petrography. D. Appleton-Century Company. New York, London, 549 pp.

LAPPARENT, A. F. AND LELUBRE, M. 1948. Interpretation stratigraphique des séries continentals entra Ohanet et Bourahet (Sahara central). Ibid, vol. 227, pp. 1106-1108. Paris.

LEEDER, M. R., 1982. Sedimentology: Processes and Products, London, P. 35-43.

LELUBRE, M. 1946. Sur le Paléozoique dy Fezzan. C. R. Hebd. Séanc. Acad. Sci., 222, 1403-1404.

LEVELL, B. K., 1980. A late Precambrian tidal shelf deposit, the Lower Sandfjord Formation, Finnmark, North Norway. *Sedimentology*, Vol. 27, P. 539-557.

LOHSE, A. E. 1951. Further discussion of "what is the sedimetology?" *Journal of sedimentary petrology*, Vol. 21, No. 2, p. 121.

LUNING, S., CRAIG, J., LODEL, D. K, STORCH, P., FITCHES, B., 2000. Lower Silurian 'hot shales' in North Africa and Arabia: regional distribution and depositional model. *Earth Science Reviews*, Vol. 49, pp. 121-200.

MACDONALD, D. I. M 1993. Controls on sedimentation at convergent plate margins, In: Frostick, L. E. and Steel, R. J (Eds). Tectonic controls and signature in sedimentary successions. *International Association of sedimentologists Special publication*, No. 20, P. 225-257.

MAMGAIN, V. D. 1980. The pre-Mesozoic (Precambrian to Palaeozoic) Stratigraphy of Libya-A reappraisal. Department of geological researches and mining. Bulletin No. 14.

MASSA, D., AND COLLOMB, G. R. 1960. Observations nouvelles sur la Region d'Aouinet Quenine et du Djebel Fezzan (Libye). Report of the Twenty first Session Norden, 12, 65-73.

MIALL A. D., 1984. Principles of sedimentary basin analysis. 2nd edition. 668 pp.

MIALL A. D., 2005. Testing for eustatic sea-level control in the Precambrian sedimentary record, *Sedimentary Geology*, Vol. 176, pp. 9 –16.

MIDDLTEON. G. V., 1976. Hydraulic interpretation of sand size distributions. *Journal of Geology*, Vol. 84, p. 405-426.

MILTON T. HAKD AND R. E. LARESE, 1973. The significance of the solution of feldspar in porosity development. *Journal of Sedimentary Petrology*, Vol. 43, No. 2, pp. 458-460.

MITCHUM, R. M. JR., VAIL, P. R. AND THOMPSON, S., 1977. Seismic stratigraphy and global changes of sea-level, part 4: Global cycles of relative changes in sea-level. In Payton, C. E. (Ed.): Seismic stratigraphy applications to hydrocarbon exploration. *American Association of Petroleum Geologists Memoir*, 26, P. 83-96.

MUELLER, G., 1967. Methods in Sedimentary Petrology; Hafner publication Company, New York, 283 pp.

NEWTON R. S., 1968. Internal structure of wave-formed ripple marks in the nearshore zone. *Sedimentology*, Vol, 11. P. 275-292.

NICHOLS. G., 1999. Sedimentology and stratigraphy.

NØTTVEDT AND KREISA, 1987. Model for the combined-flow origin of hummocky cross-satification. *Journal Geology*, Vol, 15. P. 357-361.

OTTO, G. H., 1939.A modified logarithmic probability graph for the interpretation of mechanical analysis of sediments. *Journal of Sedimentary Petrology*. Vol. 9, P. 62-76.

OVERWEG, A. 1851. Geognostische Bemerkungen auf der Reise von Philippeville uber Tunis nach Tripoli und von hier nach Murzuc in Fezzan. Zaitschrift Geologischen Ges., Vol, 3, pp. 93-102. Berlin.

PAGE, H. G., 1955. Phi-millimeter conversion table. *Journal of Sedimentary Petrology*, Vol. 25, P. 285-292.

PEDERSEN, G. K., 1985. Thin, fine-grained storm layers in a muddy shelf sequence: an example from lower Jurassic in the Stenlille 1 well, Denmark: *Journal of Geological Society of London*, Vol. 142, P. 357-374.

PELTO, C. R., 1952. The mechanical analysis of sediments from thin-section data: a discussion: *Journal Geology*, Vol. 60, P. 402-406.

PEMBERTON, S. G., MACEACHERN, J. A. AND FREY, R. W., 1992. Trace fossil facies models: environmental and allostratigraphic significance. In: R. G. Walker and N. P. James (Eds.). Facies models: response to sea level change: Geological Association of Canada, St. Johns, Newfoundland, Canada, P. 47-72.

PETTIJOHN, F. J., 1975. Sedimentary Rocks. New York, 3rd edition, 628 pp.

PETTIJOHN, F. J., POTTER, P. E. AND SIEVER, R., 1987. Sand and sandstones, Springer Verlag, 2nd edition, 553 pp.

PIROBON, E. S. T. 1991. Contribution to the stratigraphy of the Murzuq Basin, SW Libya. In: the Geology of Libya, M.J. Salem and M.N. Belaid (Eds). Elsevier, Amesterdam, V, 1767-1783.

PLUMLEY, W. J., 1948. Black Hills terrace gravels: a study in sediment transport: *Journal of Geology,* Vol. 56, p. 526-577.

POSAMENTIER, H. W. AND ALLEN, G. P., 1993. siliciclastic sequence stratigraphic patterns in foreland ramp type basins, *Geology*, V. 21, P. 455-458.

POSAMENTIER H. W., ALLEN G P., 1999. Siliciclastic sequence stratigraphy: concepts and applications, SEMP Concepts in Sedimentology and Paleontology No 7, Tulsa, Oklahoma, U.S.A. 210 pp.

POSAMENTIER H. W., RUFAIDA, D., MEYRICK, R., AND PEMBERTON, S. G., 1998. Stratigraphic analysis of the Main Member of the Upper Cibulakan Formation at E Field, offshore Northwest Java, Indonesia: Indonesian Petroleum Association, 26th Annual Convention Proceedings, P. 129-153.

POSAMENTIER, H. W., JERVEY, M. T. AND VAIL, P. R., 1988. Eustatic controls on clastic deposition II – conceptual framework. In: C.K. Wilgus, B. S. Hastings, C. G. St Kendall, H. W. Posamentier, C. A. Ross and J. C. Van Wagoner (Eds.). Sea-level changes: An Integrated Approach. *Special Publication, Society of Economic Palaeontologists and Mineralogists, Tulsa*, 42, P. 125-154.

POSAMENTIER, H. W., AND JAMES, D. P., 1993. An overview of sequence stratigraphic concepts: uses and abuses. In: Posamentier, H. W. Summerhayes, C. P. Haq, B. U., and Allen, G. P (Eds.). Sequence stratigraphy and facies association. *Special Publications. International Association of Sedimentologyists*. Blackwell Scientific Publications, Oxford, Vol. 18, P. 3-18.

POWERS, M. C., 1953. A new roundness scale for sedimentary particles. *Journal of Sedimentary Petrology*, Vol. 23, P. 117-119.

PROTHERO. D.R., AND FRED SCHWAB 1996. An introduction to sedimentary Rocks and stratigraphy. By W. H. Freeman and company.

RAYMOND, S. 1962. Silica solubility, 0-200C, and the diagenesis of siliceous sediments. *Journal Geology*, Vol. 70, pp. 127-150.

READING, H. G. AND LEVELL, B. K. 1996. Controls on the sedimentary record. In: Reading H. G. Ed.), Sedimentary Environments: Processes, Facies and Stratigraphy Blackwell Science, Oxford. pp.3-36.

REINECK, H. E. AND SINGH, I. B., 1972. Genesis of laminated sand graded rhythmites in storm-sand layers of shelf mud. *Sedimentology*, Vol. 18, P.123-128.

RIDER, M. H., 1996. The geological interpretation of well logs, 2nd edition, 280pp.

ROBERT A. GADIGAN, 1961. Geologic interpretation of grain-size distribution measurements of colorado plateau sedimentary rocks. *The journal Geology*, Vol 69. No. 2, p. 121-143.

RUSSELL, R. D. AND TAYLOR, R. E., 1937. Roundness and shape of Mississippi River sands. *Journal Geology*, Vol. 45, P. 225-267.

RUST B. R. AND NANSON G. C. 1989. Bedload transport of mud as pedogenic aggregates in modern and ancient rivers. *Sedimentology*, Vol. 36, pp. 291-306.

SCHILAGER, W., 1993. Accommodation and supply-a dual control on stratigraphic sequences: *Sedimentary Geology*, Vol. 86, P. 111-136.

SCHMIDT, VICTOR. AND MCDONALD, D. A., 1979. The role of secondary porosity in the course of sandstone diagenesis. In: Scholle, Peter, A. and Schluger, Paul, R (Eds.). Aspects of diagenesis. *Societey Economic Palaentology Mineral Special Puplication*, No. 26, P. 175-207.

SCHOLLE, P. A., 1979. A colour illustrated guide to constituents, textures, cements and porosities of sandstones and associated rocks. *American Association of Petroleum Geologist Memoir*, 28, 201 pp.

SEGONZAC D.G. 1970. The transformation of clay minerals during diagenesis and low-grade metamorphism: a review. *Sedimentology*, Vol. 15, pp. 281-346.

SELLEY, R. C., 1988. Applied Sedimentology. London: A cadmic Press, 446 pp.

SHEPARD, F. P., AND GRANT, U. S., 1947. Wave erosion along the southern California coast. *Geological Society of America Bulletin*, Vol, 58, pp 919-926.

SIEVRE, RAYMOND, 1962. Silica solubility, 0-200C, and the diagenesis of siliceous sediments. *Journal of Geology*, V. 70, P127-150

SINDOWSKI, K. H., 1957. Dia synoptische methode des kornkurven-vergleiches zur ausdeutung fossiler sedimentationstraume: *Geol. Jahrbuch*, Vol. 73, p. 235-275.

SIPPEL, R.F., 1968. Sandstone petrology, evidence from luminescence petrography. *Journal of Sedimentary Petrology*, Vol. 38, p. 530-554.

STRAND, K., 2005. Sequence stratigraphy of the siliciclastic East Puolanka Group, the Palaeoproterozoic Kainuu Belt, Finland, *Sedimentary Geology,* Vol. 176, pp. 149-166.

SUTTNER L.J., AND BASU A. 1981. Climate and the origin of quartz arenies. *Journal of Sedimentary Petrology*, Vol. 51, No. 4, pp. 1235-1246.

TANNER W. F. 1967. Ripple mark indices and their uses. *Sedimentology,* Vol. 9. P. 89-104.

TUCKER, M., 1991. Sedimentary Petrology. An introduction to the origin of sedimentary rocks, Blackwells Scintific, Oxford, 2nd edition, 260 pp.

TUCKER, M., 2001. Sedimentary Petrology. An introduction to the origin of sedimentary rocks, Blackwells Scintific, Oxford, 3rd edition, 262 pp.

TURNER, B.R., 1969. The stratigraphy and sedimentary history of the Molteno Stage in part of the north-east Cape Province. Un published Msc Thesis, University of the Witwatersrand.

TURNER, B. R., 1980. Palaeozoic Sedimentology of the Southeastern Part of Al kufrah Basin, Libya: A model for Oil Exploration. In: Salem M. J. and Busrewil M. T (Eds.). The Geology of Libya, Academic press, London, Vol. II, P. 351-374.

TURNER, B R. 2002. Geological report on the middle to upper Ordovician Succession in the western Gargaf Area. Field report, 27 pp (*Unpublished*).

VAIL, P. R., 1987. sequence stratigraphic workbook. Fundamental of sequence stratigraphy. *American Association of Petroleum Geologists*,. Annual short course Notes, Tulsa.

VAIL P. R., AUDEMART, F., BOWMAN, S. A., EISNER, P. N. AND PEREZ-CRUZ, G., 1991. The stratigraphic signatures of tectones, eustasy and sedimentology-an overview. In G. Einsele, W. Ricken and A. Seilacher (Eds.). Cyclics stratigraphy. Springer-Verlag, NewYork, P. 617-659.

VAIL, P. R., BUBB, J. N., HATLELID, W. G., MITCHUM, R. M., SANGREE, J B., THOMPSON III, S., TODD, R. G. AND WIDMER, J. M., 1977. Seismic stratigraphy and global changes in sea-level, part 1-11 In: Payton, c. e (Ed.). Siesmic stratigraphy applications to hydrocarbon exploration. *American Association of Petroleum Geologist*, Memoir, 26, P. 49-212.

VAIL, P.R., AND TODD, R. G., 1981, North Sea Jurassic unconformities, chronostratigraphy and sea-level changes from seismic stratigraphy: Petroleum Geology of the continental shelf of Northwest Europe, Proccedings, p. 216-235.

VAIL, P. R., HARDENBOL, J. AND TODD, R. G., 1984. Jurassic unconformities, chronostratigraphy and sea-level changes from seismic stratigraphy and biostrtigraphy. In: Schlee, j. s. (Ed.). Interregional unconformities and hydrocarbon exploration. American Association of Petroleum Geologists. Tulsa. Memoir, 33, P 129-144.

VAN WAGONER, J. C., MITCHUM, R. M., JR., CAMPION, K. M. AND RAHMANIAN, V. D., 1990. Siliciclastic sequence stratigraphy in well logs, core and outcrop: Concepts for High Resolution Correlation of Time and Facies. *American Association of Petroleum Geologist Methods in Exploration Tulsa, Series*, Series No. 7, 55 pp.

VISHER, G. S., 1969. Grain-size distribution and depositional processes. *Journal Sedimentary Petrology*, Vol. 39, P. 1074-1106.

VOS, R. G., 1977. Sedimentology of an upper Palaeozoic River, wave and Tide influenced Delta system in southern Morocco. *Journal Sedimentary Petrology*, Vol. 47. P. 1242-1260.

VOS, R. G., 1981. Sedimentology of an Ordovician Fan Complex, Western Libya. *Sedimentary Geology*, Vol. 29, P. 153-170.

WADELL. H., 1932. Volume, Shape and Roundness of rock particles. *Journal Geology*, Vol. 40, pp. 443-451.

WALKER, R. G. AND GAMES, N. P. (Eds), 1992. Facies Models: Response to Sea Level Change, 409 pp. Geological Association of Canada, St Johns, Newfoundland.

WENTWORTH, 1919. A laboratory and field study of cobble abrasion, *Journal of Geology*, Vol. 27, pp. 507-521.

WILGUS, C. K., HASTINGS, B. S., KENDALL, C. G. ST. C., POSAMENTIER, H., ROSS, C. A. AND VAN WAGONER, J. C., 1988. Sea-level changes: An Intergrated Approch. Special Publication, Society of Economic Palaentologists and Mineralogists, Tulsa, 42. 407pp.

WINN JR. R.D., 1991. Storm deposition in marine sheets: wall creek member, frontier formation, powder eiver basin, Wyoming. *Journal of Sedimentary Petrology*, Vol 61, No. 1, PP.86-101.